LCH Laboratoire de Constructions Hydrauliques
Laboratory of Hydraulic Constructions

ÉCOLE POLYTECHNIQUE
FÉDÉRALE DE LAUSANNE

Communication 72

Influence of outlet discharge on the efficiency of turbidity current venting

Sabine Chamoun

Editeur : Prof. Dr A. Schleiss

Lausanne, 2017

Communications du Laboratoire de Constructions Hydrauliques ISSN 1661-1179
Ecole Polytechnique Fédérale de Lausanne
Editeur: Prof. Dr A. Schleiss

PREFACE

Reservoirs created by dams are vital water infrastructures worldwide ensuring not only water, food and energy but also protecting against floods. Sedimentation endangers the sustainable use of these reservoirs. Fine sediments transported as suspension during floods into reservoirs normally represent the most important of the sediment yield. In deep and long reservoirs, the fine sediment laden inflow plunges and travels as a turbidity current along the bottom of the reservoirs downwards to the dam. Thus, during every inflowing flood event, a significant amount of fine sediments is transported by these turbidity currents directly to the dam. Besides the reduction of the useful storage volume, the water release structures as bottom outlets and intakes may be clogged by the fine sediments with time. When opening bottom outlets or low level outlets during the occurrence of turbidity currents, the latter may be vented through the dam before the deposition of the fine sediments in front of the dam. In practice, the question arises on how much sediments can be vented under a certain discharge capacity of the bottom outlet or low level outlet.

By the help of systematic laboratory experiments in a flume and by numerical modeling, Dr. Sabine Chamoun studied for the first time the influence of outlet discharge on the efficiency of turbidity current venting. The effect of the reservoir bed slope as well as the dimensions of the bottom outlet were also highlighted. As another novelty, the timing of venting relatively to the arrival of the turbidity current at the dam and the required duration of venting were investigated. The systematic tests allowed also to quantify the efficiency of venting regarding the amount of sediments evacuated compared to the water used from the reservoir. Finally, Dr. Sabine Chamoun could give some practical recommendations on how turbidity current venting should be performed in order to attain the most optimum release of fine sediments for a certain outflow discharge.

We would like to thank the members of PhD committee Dr. Magali Jodeau from EDF Lyon, France; Prof. Helmut Knoblauch from University TU Graz, Austria and Prof. Alfred Wüest from EPFL, Lausanne, Switzerland for their valuable comments. Finally, we also gratefully thank Swisselectric Research and the Swiss Committee on Dams for their financial support.

Prof. Dr. Anton Schleiss Dr. Giovanni De Cesare

سأصير يوماً شاعراً، والماء رهن بصيرتي.

— محمود درويش، جدارية

One day, I will be a poet. Water will depend on my vision.

— Mahmoud Darwish, Mural

ACKNOWLEDGEMENTS

The funding of this research was provided by Swisselectric Research and complemented by the Swiss Committee on Dams. I would like to thank them for their financial support.

During the last few months of a thesis, it truly feels like a race against time. During this race, there is a thrill, but there is also premature nostalgia. The thrill emanates from the joy of accomplishing, soon, an important step in our life. Nostalgia is due to the fact that we are leaving a pleasant place where development and hard work were combined with enjoyment. Today, I take a break from this long race to look back and value every person who has helped me reach this point.

First and foremost, my greatest gratitude goes to Professor Anton J. Schleiss for trusting me and giving me the opportunity to accomplish this thesis. Thanks to him, the Laboratory of Hydraulic Constructions is not only an enriching source of knowledge and expertise in the field of water but most importantly a pleasant and enjoyable place to work in.

A special thanks goes to my thesis co-director Dr. Giovanni De Cesare who has been my daily scientific and moral support throughout the four years, and with whom I had a very cordial and honest relationship.

The LCH team, you have raised the bar very high, will I ever encounter another team like you? I have wonderful memories and ties with each and every one of you: Fränz, Nicolas, Elena, José Pedro, Irene, Paloma, Alex, Sara, Davide, David F., Panpam, Michel, Cédric, Azin, Carmelo, Dora, Scarlett, Gesualdo, Mario, Severin, Michael, Pierre, Ivan, Stephane, Alain, Ana Clara, Mohammad, Tamara, Matthias, Sebastian G., Pedro, Raphaël. Thank you! Grazie! Choukran! Danke! Gracias! Obrigada! Mamnoun!

Thank you Sebastian Schwindt for translating the abstract, and also, for giving me a ‘’lucky clover’’ at the beginning of this thesis. I will keep it safe Seb.

My lovely office mates, Mona and Jessica, our office was all about hugs, flowers, smiles and support. I am lucky to have spent these years in your company!

To my parents who never hesitated to leave everything behind and travel from Lebanon to Switzerland. How can I thank you enough for your love, care and immense support? Your presence has helped me creating home away from home.

Lastly, Chris, for more than ten years now, you have been my source of strength, energy and laughter (loads of it!). On the verge of a new adventure, and for every new beginning, keep your hand in mine…

ABSTRACT

Sediment yield into reservoirs was underestimated during the design of dams in the past. As a result, today, reservoir sedimentation is endangering the sustainability of dams. Moreover, the obstruction of rivers hinders their capacity to transport sediments and causes the alteration of their morphology and ecosystems. The rate of sedimentation is expected to increase in the future due to climate change. Turbidity currents are one of the main processes transporting sediments into long and deep reservoirs during floods. They are capable of transporting suspended sediments from the plunge point at the delta to the dam. Hence, venting of turbidity currents through bottom outlets is an appealing solution to reduce reservoir sedimentation.

Using a flume of 8.55 m length and 0.27 m width, venting was investigated experimentally and numerically. Governing parameters such as the bottom outlet's discharge, the timing of venting relatively to the arrival of the turbidity current at the dam, the duration of venting, the reservoir's bed slope as well as the outlet's dimensions and level were studied. The efficiency of venting corresponding to the amount of sediments evacuated by the water used from the reservoir could be highlighted by systematic tests.

The efficiency of venting increased with steeper bed slopes since the turbidity current was less reflected at the dam. Therefore, venting should be applied from the very beginning of dam impoundment to keep the cone upstream of the outlets free of sediments and the steepest bed slope possible close to the dam.

The effect of the venting degree -defined as the ratio between outflow and turbidity current discharges- on the efficiency of venting was systematically studied. For turbidity currents reaching the outlet on a horizontal bed in the experimental configuration, a venting degree of about 100% resulted in the highest venting efficiency. For steeper reservoir bed slopes (i.e., 2.4% and 5.0%), the optimum efficiency can be obtained with a venting degree of about 135%.

Venting was the most efficient when synchronized with the arrival of the turbidity current at the dam. Therefore, a gauging station should be placed around 300 m upstream of the low-level outlet to measure parameters such as velocity, indicating the arrival of the turbidity current.

Furthermore, venting should last as long as there is inflow and should be maintained after the end of the flood for a duration that depends on the outflowing sediment concentration. In practice, venting can be stopped when the muddy lake has been evacuated and the vented water

becomes clear again. This also allows cleaning the downstream river from fine sediment deposits after the venting operation.

To optimize venting efficiency and minimize the dead storage, the outlet should be positioned at the lowest level possible. In addition, the height and width of the bottom outlet's entrance should be chosen in a way to create an aspiration cone that corresponds approximately to the dimensions of the body of the turbidity current. In order to keep the size of the low-level outlet reasonable, multiple outlets can be used to create the required aspiration cone.

Keywords: Reservoir sedimentation, turbidity current, sediment management, venting, release efficiency, thalweg slope, outflow discharge, timing, outlet dimensions and level.

RÉSUMÉ

Le transport de sediments vers les réservoirs a été sous-estimé dans le passé, pendant le dimensionnement des barrages. Par conséquent, à présent, la sedimentation des réservoirs menace la durabilité des barrages. De plus, l'obstruction des rivières réduit leur capacité de transport de sédiments et cause l'altération de leur morphologie et écosystème. Le taux de sédimentation augmentera dans le futur dû au changement climatique. Les courants de turbidité représentent un des processus principaux du transport de sédiments dans les réservoirs longs et étroits. Ils sont capables de transporter des sédiments en suspension depuis le point de plongée près de la region du delta jusqu'au barrage. Ainsi, le transit des courants de turbidité à travers les vidanges de fond est une solution attirante pour réduire la sedimentation des réservoirs.

La technique d'évacuation des courants de turbidité a été étudiée expérimentalement et numériquement dans un canal de 8.55 m de long et 0.27 m de large. Des paramètres dominants ont été étudiés tels que le débit de sortie de la vidange de fond, le timing de l'ouverture des vannes, la durée de l'opération, la pente du fond du réservoir, ainsi que les dimensions et la position de la vidange. L'efficacité de l'opération correspondant à la quantité de sédiments évacués par l'eau du reservoir a été évaluée à travers des tests systématiques.

L'efficacité de l'évacuation des courants de turbidité augmente avec l'augmentation de la pente vu que le courant est moins réfléchi au barrage. Par conséquent, le transit des courants de turbidité doit avoir lieu dès le début de l'exploitation du barrage afin de garder libre de sédiments un cône en amont des vidanges et par conséquent d'assurer la pente la plus raide possible auprès du barrage.

L'effet du degré d'évacuation -défini par le rapport entre le débit de sortie et celui du courant de turbidité- sur l'efficacité de l'évacuation a été systématiquement étudié. Lorsque le courant atteint la vidange de fond sur un lit horizontal de la configuration expérimentale, un degré d'évacuation d'environ 100% mène aux plus grandes valeurs d'efficacité. Pour des pentes plus élevées (i.e., 2.4% et 5.0%), l'efficacité optimale est obtenue avec un degré d'évacuation d'environ 135%.

L'évacuation des courants de turbidité est la plus efficace lorsqu'elle est synchronisée avec l'arrivée du courant au barrage. Pour ce, une station de mesure doit être placée à environ 300 m en amont de la vidange de fond afin de mesurer des paramètres tels que la vitesse indiquant l'arrivée du courant.

En outre, le transit des sédiments doit durer tant qu'il y a un afflux de sédiments dans le réservoir et doit être maintenu pendant une durée minimale qui dépend de la concentration en sédiments du courant évacué. En prototype, l'opération de vidange peut être arrêtée lorsque le nuage de sédiments en suspension formé en amont du barrage a été évacué et que le débit sortant est de nouveau clair. Cela permet également de nettoyer la rivière à l'aval des sédiments fins déposés le long de l'opération.

Afin d'optimiser l'efficacité du transit des courants de turbidité et de minimiser le volume ''mort'', la vidange de fond doit être placée au niveau le plus bas possible. La hauteur et la largeur de l'entrée de la structure de vidange doivent être choisies de façon à ce que le cône d'aspiration dans le réservoir ait comme limite les dimensions du corps du courant de turbidité. Dans le but de garder les dimensions des vidanges de fond raisonnables, plusieurs vidanges peuvent être envisagées afin d'assurer un cône d'aspiration suffisamment grand.

Mots clés: Sédimentation des réservoirs, courant de turbidité, gestion de sédiments, vidange de fond, efficacité d'évacuation, pente du thalweg, débit de sortie, timing, dimensions et position des vidanges.

ZUSAMMENFASSUNG

Der Sedimenteintrag in Speicherseen wurde bei der Konzeption von Stauanlagen in der Vergangenheit unterschätzt. Infolgedessen gefährdet die Speicherverlandung heute die Nachhaltigkeit von Stauräumen. Darüber hinaus verringert der Einstau von Flüssen deren Sedimenttransportkapazität und bewirkt tiefgreifende Veränderung der Morphologie und der Ökosysteme. Die Verlandungsraten dürften sich aufgrund des Klimawandels in Zukunft erhöhen. Trübeströme sind einer der Hauptprozesse, welche Sedimente bei Hochwasser in lange und tiefe Speicherseen eintragen. Sie sind in der Lage, Schwebstoffe von der Mündung (Delta) zur Talsperre zu transportieren. Daher ist das Durchleiten von Trübeströmen durch Grundablässe eine vielversprechende Lösung zur Verringerung der Speicherverlandung.

Mittels einer Versuchsrinne mit einer Länge von 8.55 m und einer Breite von 0.27 m wurde das Durchleiten von Trübeströmen experimentell und parallel dazu numerisch untersucht. Massgebende Parameter, wie der Abfluss des Grundablasses, der Zeitpunkt der Durchleitung im Bezug zum Eintreffen des Trübestroms an der Talsperre, die Dauer des Durchleitens, das Längsgefälle des Speichersees sowie die Grösse und die Kote des Auslasses wurden untersucht. Die Effizienz des Durchleitens, welche der Menge der Sedimente entspricht, die mit dem aus dem Speicher abgelassenen Wassers herausgespült wurde, konnten durch systematische Testreihen optimiert werden.

Die Effizienz des Durchleiters nahm mit steilerer Sohlneigung zu, wobei der Trübestrom am Damm weniger reflektiert wurde. Daher sollte das Durchleiten von Beginn des Einstaus an eingesetzt werden, um den Bereich vor den Auslässen (Aspirationstrichter) frei von Sedimenten zu halten und um die steilste Sohlneigung möglichst nahe des Dammes zu erhalten. Die Wirkung des Durchleitungsgrades, definiert als das Verhältnis zwischen Ausfluss und Trübestromabfluss, wurde systematisch auf die Effizienz des Durchleitens untersucht. Für Trübeströme, die den Auslass auf einer horizontalen Sohle im Versuchsaufbau erreichten, ergibt sich bei einem Durchleitungsgrad von etwa 100% die höchste Effizienz. Für steilere Sohlneigungen (d.h. 2.4% und 5.0%) kann der optimale Wirkungsgrad mit einem Durchleitungsgrad von etwa 135% erreicht werden.

Die Durchleitung war am effizientesten, wenn sie mit dem Eintreffen des Trübestroms am Damm synchronisiert wurde. Daher sollte eine Messstation etwa 300 m stromaufwärts des Grundauslasses angeordnet werden, um Parameter wie die Fliessgeschwindigkeit zu messen, wodurch die Ankunft des Trübestroms ermittelt werden kann.

Weiterhin sollte die Durchleitung so lange dauern, wie der Zustrom anhält und nach dem Ende des Hochwassers für eine gewisse Dauer aufrechterhalten werden, dies in Abhängigkeit der Abflusskonzentration. In der Praxis kann die Durchleitung gestoppt werden, wenn der stark suspensionshaltige Tiefenbereich des Sees (Muddy lake) gespült wurde und das ausfliessende Wasser wieder klar wird. Dies ermöglicht auch die Spülung von Feinsedimentablagerungen im Unterstrom nach dem Durchleiten.

Um die Durchleitungseffizienz zu optimieren und den Totraum zu minimieren, sollte der Grundablass so tief wie möglich angeordnet werden. Darüber hinaus sollten die Höhe und Breite des Grundablasses so gewählt werden, dass ein Aspirationstrichter erzeugt wird, der etwa den Abmessungen des Trübestroms entspricht. Um die Grösse der Grundablässe realistisch zu bemessen, können mehrere Grundablässe angeordnet werden, um den erforderlichen Aspirationstrichter zu erzeugen.

Schlüsselwörter: Speicherverlandung, Stauseeverlandung, Trübestrom, Sedimenthaushalt, Durchleitung, Spüleffizienz, Thalweggefälle, Abfluss, Timing, Grundablass Bemessung und Kote.

Translated by Sebastian Schwindt.

CONTENTS

LIST OF FIGURES

LIST OF TABLES

NOMENCLATURE

LATIN CHARACTERS

a	Longitudinal distance between the bottom electrodes of the depositometer	(m)
A	Surface area on which sediments deposit around the measuring bottom electrode of the electrical resistance-based depositometer (ERBD)	(m^2)
B_0	Initial buoyancy flux of the turbidity current	(m^3s^{-3})
C	Volumetric concentration of an element in the numerical mesh	(-)
C_d	Drag coefficient used in the numerical model (Cheng, 1997)	
C_s	Concentration of the turbidity current approaching the wall	(kgm^{-3})
C_{TC}	Turbidity current initial inflow concentration	(kgm^{-3})
C_{VENT}	Outflow concentration	(kgm^{-3})
d	Distance at which the current is located when early venting begins	(m)
d_{10}	Grain diameter for which 10% of sediments have smaller diameters	(m)
d_{50}	Mean grain size diameter	(m)
d_{50*}	Normalized mean diameter as expressed by Zhiyao et al. (2008)	
d_{90}	Grain diameter for which 90% of sediments have smaller diameters	(m)
e	Deposit thickness	(m)
Fr	Densimetric Froude number	(-)
g	Gravitational acceleration	(ms^{-2})
$g_0^{'}$	Initial reduced gravitational acceleration of the turbidity current	(ms^{-2})
g'	Reduced gravitational acceleration of the turbidity current at 4.1 m from the inlet	(ms^{-2})
$g_{app}^{'}$	Reduced gravitational acceleration of the turbidity current approaching the outlet	(ms^{-2})
GVE	Global Venting Efficiency	(%)
H	Characterizing height of the current obtained experimentally	(m)

h_{diff}	Height of the diffusor	(m)
$h_{downwall}$	Height of the downstream wall (numerical)	(m)
H_{flume}	Total height of the experimental flume	(m)
H_{head}	Height of the head of the current	(m)
h_{inlet}	Height of the inlet	(m)
h_L	Height of aspiration of the outlet	(m)
h_{max}	Height of the current corresponding to the maximum velocity U_{max}	(m)
H_{num}	Characterizing height of the current obtained numerically	(m)
h_{outlet}	Height of the outlet	(m)
h_w	Water column between the reference and bottom electrodes of the ERBD	(m)
H_{water}	Water depth on the flume in the case of the horizontal bed	(m)
h_{weir}	Height of the weir (numerical)	(m)
h	Height of the current at a measured point	(m)
k	Turbulent kinetic energy	(m^2s^{-2})
L	Length of the main flume	(m)
L_{flume}	Length of the whole experimental flume	(m)
l_{outlet}	Outlet level above the reservoir's bed	(m)
LVE	Local Venting Efficiency	(%)
m_{dep30}	Total deposited sediment mass at a time step Δt = 30 s	(kg)
$\dot{m}_{dep}$	Deposited sediment mass flow rate	(kgs^{-1})
M_{deptot}	Total mass deposited along the main flume	
M_{TC}	Total inflow sediment mass of the turbidity current	
q_{TC}	Turbidity current specific inflow discharge	(m^2s^{-1})
Q_{TC}	Turbidity current inflow discharge	(m^3s^{-1})

Q_{RES}	Residual discharge (of the diffusor)	(m^3s^{-1})
Q_{VENT}	Venting outflow discharge	(m^3s^{-1})
$Q_{VENTmax}$	Capacity of the bottom outlet	(m^3s^{-1})
R_{dep}	Resistance of the sediment layer deposited	(Ω)
Ri	Richardson number	(-)
Re	Reynolds number	(-)
R_{total}	Total resistance measured by the ERBD	(Ω)
R_{water}	Resistance of the water column between the reference and the bottom electrodes	(Ω)
RVE	Representative Venting Efficiency	(%)
S	Bed slope	(%)
s_{max}	Maximum upstream distance of influence of the outlet	(m)
t	Duration of the test	(s)
T	Temperature	(°C)
$\overline{t}$	Normalized duration of venting	(-)
t_{after}	time at which late venting starts after the arrival of the turbidity current at the outlet	(s)
t_{cut}	duration of venting after which turbidity current inflow is cut	(s)
T_{vf}	Time at which venting is stopped	(s)
T_{vi}	Time at which venting starts	(s)
u	Local velocity of the current at a measured point	(ms^{-1})
U	Characterizing velocity of the current obtained experimentally	(ms^{-1})
U_f	Front velocity of the current	(ms^{-1})
u_{in}	Normal speed imposed numerically at the inlet	(ms^{-1})
U_{max}	Maximum velocity of the current obtained experimentally	(ms^{-1})
U_{num}	Characterizing velocity of the current obtained numerically	(ms^{-1})

V_0	Settling velocity calculated numerically in clear water	(ms^{-1})
VEI	Venting Efficiency Indicator	(%)
v_s	Settling velocity of the polymer powder corresponding to the settling velocity of the d_{50} diameter	(ms^{-1})
V_s	Settling velocity calculated numerically in a volume of suspended sediments having a certain volumetric concentration C	(ms^{-1})
$V_{VENTsed}$	Total volume of sediments vented at a time t	(m^3)
$V_{VENTwat}$	Total volume of water released from the outlet at a time t	(m^3)
w	Width of the flume	(m)
w_{outlet}	Width of the outlet	(m)

GREEK SYMBOLS

ε	Turbulent dissipation rate	(m^2s^{-3})
ϕ	Venting degree	(%)
φ	Diameter of the bottom electrodes used for the ERBD	(m)
λ	Dimensionless concentration parameter (Van Rijn, 1987)	(-)
μ_m	Dynamic viscosity of the water-sediment mixture used numerically (Van Rijn, 1987)	($kgm^{-1}s^{-1}$)
μ_w	Dynamic viscosity of water	($kgm^{-1}s^{-1}$)
ν	Kinematic viscosity of water	(m^2s^{-1})
ρ_s	Particle density of the particles	(kgm^{-3})
ρ_t	Density of the vented turbidity currents	(kgm^{-3})
ρ_w	Water density	(kgm^{-3})
ρ_{t0}	Initial density of the turbidity current	(kgm^{-3})

ABBREVIATIONS

AC	**A**lternative **C**urrent
ERBD	**E**lectrical **R**esistance-**B**ased **D**epositometer
TPU	**T**hermoplastic **P**oly**u**rethane
UVP	**U**ltrasonic **V**elocity **P**rofiler

Chapter 1

INTRODUCTION

1.1 Context

Today, dams are essential water infrastructures providing modern societies with crucial needs such as electricity, water supply for irrigation and households, navigation, flood and drought protection, as well as fish farming. Nevertheless, the construction of new dams is becoming more and more challenging because low-cost sites are not widely available anymore. For this reason, ensuring the sustainability of existing reservoirs and preserving their expected lifetime is fundamental. One of the biggest problems endangering the sustainability of reservoirs is sedimentation (Figure 1.1). In fact, dams hamper sediment transport by obstructing rivers, thus the sediments accumulate inside the reservoirs and fill up their useful storage volume. The loss of reservoir capacity, reduction of flood control as well as the downstream sediment impoverishment are among several consequences of reservoir sedimentation. Hence, sediment management is essential for all reservoirs where large amounts of sediments can be potentially transported from the watershed.

Figure 1.1: Sedimentation of Sufers Reservoir located in Grisons, Switzerland (photo courtesy of Kraftwerke Hinterrhein AG).

During floods, highly concentrated sediment-laden flows can be formed in the watershed and reach the reservoir. Due to the density difference with the clear water, these flows plunge into the reservoir and trigger turbidity currents. Under certain flood conditions, turbidity currents flow along the thalweg of the reservoir until reaching the dam. If no low-level outlet or intake is opened to evacuate the sediments, the turbidity current is blocked and reflected by the dam thus forming a muddy lake that settles with time. In the long term, the deposited sediments may consolidate, clogging the water release structures placed at low levels and leading to the abrasion of hydro-mechanical equipment. Therefore, the evacuation of turbidity currents before their settling is of interest for sediment management in reservoirs.

1.2 Motivation

In many reservoirs, deposited sediments found in the vicinity of the dam are mostly caused by turbidity currents. Therefore, their evacuation through low-level outlets before their settling is highly recommended. Besides, this release operation offers environmental and economic advantages compared to other mitigation techniques. On one hand, due to relatively low outflow discharges used during venting, the loss of water can be minimized. On the other hand, releasing turbidity currents to the downstream river supplies the ecosystem with the required fine sediments. However, dam operators managing reservoirs with sedimentation problems induced by turbidity currents need operational guidelines to maximize the sediment release and minimize the trap efficiency of the reservoir. Comprehensive guidelines are still lacking. Venting of turbidity currents was scarcely studied compared to other sediment removal techniques such as flushing and dredging.

In Switzerland, federal laws (LACE - Loi Fédérale sur l'Aménagement des Cours d'Eau and LEaux - Loi Fédérale sur la protection des Eaux) aim to diminish the impact of possible interventions on water courses. It states that the natural characteristics of a river should be respected and reconstituted in the goal of preserving its diverse fauna and flora. In this context, this study has the objective of systematically investigating the venting of turbidity currents in order to reduce reservoir sedimentation and restore downstream rivers.

The management of sedimentation directly benefits the reservoirs in terms of safety (i.e., improvement of flood control), economy (i.e., conservation of water volumes) and environment (i.e., downstream sediment replenishment).

1.3 Research questions

Based on the review of past research and experience, the most significant questions commonly arising during flood events triggering turbidity currents were selected and addressed. Above all, the effects of outflow discharge, venting timing and duration, reservoir bed slope, outlet dimensions and position relatively to the reservoir's bottom were assessed on the sediment release efficiency of venting. The conditions which maximize the amount of evacuated sediment but minimize water losses are identified. For that purpose, an experimental installation was designed and set up at the Laboratory of Hydraulic Constructions (LCH) of the École Polytechnique Fédérale de Lausanne (EPFL).

The questions can be summarized as such:

- What is the effect of outflow discharge on the sediment release efficiency of venting?
- What is the influence of the slope of the reservoir thalweg on the venting efficiency?
- Upon the arrival of a turbidity current to the outlet, what is the optimal venting timing that would lead to high release efficiency?
- How does the duration of venting affect its release efficiency? Should venting be maintained after the end of the flood and for how long?

In addition, supplementary ranges of parameters are evaluated using a numerical model. These parameters include the outlet's dimensions and level. Moreover, a maximum distance at which the operating outlet can affect the turbidity current is assessed. Venting should not start before the current has reached this maximum distance of influence. Finally, a numerical geometry similar to prototype conditions was simulated.

1.4 Structure of the report

The present report is divided into eight chapters. Chapter 2, 4, 5, 6, and parts of Chapter 3 were prepared based on published or future journal articles. In order to avoid redundancy, the introductions of Chapters 4, 5 and 6 were removed and integrated in Chapter 2 (state of the art). The content of the different chapters is summarized in the following:

Chapter 2 presents an extended literature review, published mostly in the *International Journal of Sediment Research* (Chamoun et al., 2016b), and partially in the *International Journal on Hydropower & Dams* (Chamoun, De Cesare, & Schleiss, 2016c). The problematic of reservoir sediment management is introduced. A theoretical overview on turbidity currents

is presented before discussing the operation of venting and the different parameters affecting its sediment release efficiency. A global summary of venting operations worldwide is then given along with the main challenges and the monitoring instruments needed to reach efficient venting.

In Chapter 3, the experimental set-up, sediment material and testing procedure are presented. The measuring instruments are described, followed by a dimensional analysis leading to the main parameters to be tested. Finally, the list of experimental tests performed in this study are presented. This chapter was partially published in the *Journal of Flow Measurement and Instrumentation* (Chamoun, Zordan et al., 2016).

Chapter 4 discusses the operation of venting for turbidity currents flowing over a horizontal bed. The definition of venting efficiency is provided and serves as a basis for most of the analysis applied in the experimental investigation. The turbidity currents generated are then characterized based on different parameters such as the turbulence rate and front velocity. The influence of outflow discharge as well as the duration of venting on the release efficiency of the operation is systematically assessed. This chapter was accepted for publication in the *Journal of Hydraulic Research* (Chamoun et al., 2017a).

The bed slope of the reservoir is varied in Chapter 5. Three different slopes including the horizontal position are compared and their effect on the efficiency of venting is discussed. The turbidity currents triggered during these tests are described and characterized. This chapter served as a basis for a publication in the *Journal of Environmental Management* (Chamoun et al., 2017b).

In Chapter 6, the timing of venting is varied relatively to the arrival time of the turbidity current at the outlet. Two different bed slopes are used and the influence of the timing on venting efficiencies is evaluated. Also, the duration of venting after the end of the flood (i.e., the end of the turbidity current inflow into the reservoir) is analyzed. This chapter served as a basis for a publication in the *Journal of Hydraulic Engineering* (Chamoun et al., 2017c).

Chapter 7 introduces the numerical model which was built and calibrated based on the experimental model and data. The numerical model is described and the validation procedure explained. The parametric study is then extended to additional variables compared to the experimental tests such as the outlet's dimensions and level. Other features of venting (e.g., upstream distance of influence of the outlet) were also investigated, offering better insight on the phenomena occurring during venting.

Finally, Chapter 8 offers a conclusion along with practical recommendations and proposes further developments for future research related to turbidity-current venting.

An Appendix presents supplementary information and data that could enhance the reader's understanding of the manuscript and serve for further research.

Note that the tables, figures and equations are numbered incrementally while referring to each chapter.

Chapter 2

STATE OF THE ART AND THEORETICAL BACKGROUND[1]

Reservoir sedimentation is a problem that dam operators are increasingly facing as dams are aging. Not only does it reduce the reservoir's capacity but it also affects its outlet structures such as bottom outlets and powerhouse intakes. Sedimentation may also impoverish downstream ecosystems. For these reasons, several strategies for sediment management are being investigated and applied in reservoirs worldwide. Among these methods, venting of turbidity currents reaching the dam can be very beneficial and economical. This measure helps in preserving a certain continuity of sediment transport in rivers obstructed by dams. However, several practical but also theoretical challenges hamper this technique, rendering its use less common and its aspects relatively unknown. The present chapter resumes the actual state of the art concerning turbidity-currents venting and presents an outlook for future development and research in this field.

[1] Chapter 2 is based on the scientific article ‘’Managing reservoir sedimentation by venting turbidity currents: A review’’ by S. Chamoun, G. De Cesare and A. J. Schleiss published in 2016 in the International Journal of Sediment Research and on the journal article ‘’Venting turbidity currents for the sustainable use of reservoirs” by the same authors published in 2016 in the Journal on Hydropower & Dams. The review work presented hereafter is original and was performed by the author.

2.1 Reservoir sedimentation

Reservoir sedimentation is a worldwide problem causing the loss of reservoir capacity of existing dams and thus the reduction of their useful and economic life (Sloff, 1991). The global annual reservoir capacity is decreasing, and the construction of new reservoirs is not sufficient to compensate this loss (Oehy & Schleiss, 2007). The global annual cost of lost reservoir capacity due to sedimentation was estimated by The World Bank at $6 billion ((Fan, 1999) as cited by Heidarnejad et al. (2006)). In the United States for instance, addressing sedimentation by providing extra reservoir capacity, dredging the sediments or replacing the lost storage by new storage costs $690 million annually (Crowder, 1987). Depending on the type and use of the reservoir, the effects of storage loss is summarized in Table 2.1 (Brown (1958) as cited by Sloff (1991)):

Table 2.1: Consequences of storage loss depending on the reservoir's use (according to Brown (1950) as cited by Sloff (1991)).

Reservoir use	Sedimentation consequence
Hydropower	Loss of required storage for peak power production
Irrigation	Loss of storage and water required for food production
Flood control	Increase of magnitude and frequency of floods in the downstream river
Water supply	Additional costs due to the loss of service values
Recreation	Development of delta regions causes health hazards and unfavorable conditions for fish life and boating
Navigation	Shoaling and loss of the flow regulating capacity for low water

However, the loss of storage capacity is not the only consequence of sedimentation. Other problems are faced, such as the obstruction of intakes and the abrasion of hydraulic machinery (e.g., Mauvoisin dam in Switzerland (Boillat et al., 2000b)), downstream starvation for sediments (termed *hungry water* by Kondolf (1997)) and its ecological implications (Wüest, 2010), aggregation of backwater region (e.g., Sanmenxia and Guanting reservoirs in China

(Fan & Morris, 1992a)) and chocking of bottom outlets (e.g., Rempen dam in Switzerland (Boillat & Pougatsch, 2000)).

Even reservoirs located in regions with moderate surface erosion, like part of the Alps, face sedimentation (Schleiss et al., 2008). Nevertheless, the rate of sedimentation in the Alpine region is relatively low (Schleiss & Oehy, 2002). In Switzerland, for instance, the average annual loss in reservoir capacity is 0.2% only (Beyer Portner & Schleiss, 1998), while in China, it is of 2.3% (Wang & Hu, 2009). A record sedimentation occurred in China when the Laoying Reservoir of Shanxi province was completely filled up with sediments during a flood before the completion of its construction (Ren & Ning, 1985). Japan's reservoirs also face severe sedimentation: 100 million m^3 of sediments out of the 200 million m^3 produced from mountain areas are deposited each year in reservoirs (Kantoush & Sumi, 2010). Another example is the Sefid Rud reservoir in Iran, where the useful life was estimated to more than 100 years during the design phase. Unfortunately, the amount of inflowing sediments was underestimated and the actual useful life turned out to be not more than 30 years (Pazwash (1982) as cited by Sloff (1991)). Also in Iran, the Dez Dam faces high sedimentation rates of more than 1 m per year and flushing tunnels are proposed to vent the sediment-laden flood inflow (Schlegel & Dietler, 2010). Finally, one of the most extreme sedimentation cases is at Tarbela Dam where studies showed that due to the high sedimentation rates, the reservoir's storage will be completely filled by 2030 (Attewill et al., 1998).

In the goal of projecting and predicting the sedimentation rate in a given reservoir, Cheng and Zhao (1992) proposed the following relationship:

$$V_{st} = V_0(1 - e^{kt}) \tag{2.1}$$

where V_{st} is the volume of deposits, V_0 is the initial volume of storage, t is the number of years after which the sedimentation is estimated, and k is a constant determined from field measurements.

2.2 Management of reservoir sedimentation

Balancing sediment inflow and outflow in reservoirs is a key challenge for sustainable reservoir management. In the past, increasing the storage volume was considered as a way to halt the consequences of sedimentation. However, the cost of a m^3 of stored water is continuously increasing not only due to the rising construction costs but mainly because low-cost sites for dams are gradually decreasing (Vanoni, 2006). Therefore, different techniques are applied and optimized to mitigate sediments from reservoirs and ensure the sustainability of their capacity,

(e.g., Fan & Morris, 1992a, 1992b; Lowe & Fox, 1995; Basson & Rooseboom, 1997, 1999; Boillat et al., 2000a; Brandt, 2000; Chang et al., 2003; Li et al., 2005; De Cesare & Lafitte, 2007; De Cesare et al., 2009; Khan & Tingsanchali, 2009; Wang & Hu, 2009; Kantoush & Sumi, 2010; Althaus, 2011; Schleiss, 2013; Schleiss et al., 2016). An overview of the various methods is given in Figure 2.1.

Selecting the appropriate method depends on the reservoir's size and mode of operation, the type of dam (e.g., gate structure dams or large dams) and also on the region where it is located, which highly impacts the quantity and size of sediments transported. Each method has its limitations and impacts regarding ecological, economic, and practical issues.

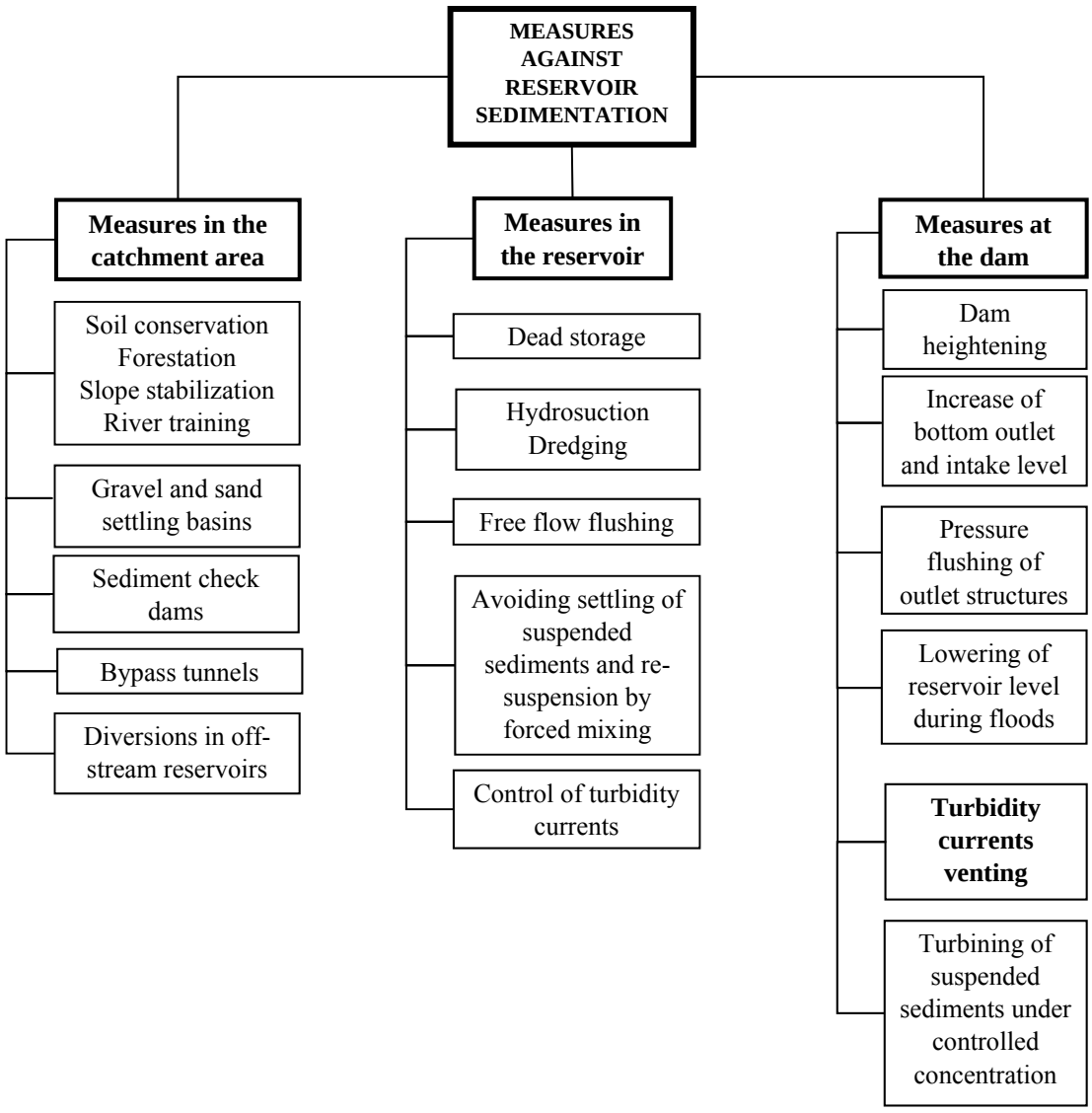

Figure 2.1: Overview of the sediment management methods used to deal with reservoir sedimentation (according to Schleiss & Oehy, 2002).

Figure 2.2 below illustrates the most common operations for sediment removal. Among these measures, turbidity current venting can be, in many cases, very effective and economical (Wan et al., 2010), especially since suspended sediments often count for the major part of sediments in reservoirs. Venting is generally preferred to other sediment mitigation techniques such as airlift, dredging (Basson & Rooseboom, 1999) and flushing (Antoine et al., 2013; Espa et al., 2016), mainly because it is less harmful for the downstream environment but also for economic reasons. Nonetheless, most research studies that mentioned venting of turbidity currents are rather qualitative. Venting was scarcely discussed compared to other sediment removal techniques (e.g., flushing, dredging). Systematic experimental, numerical as well as prototype investigations are still lacking.

Venting is an operation that requires not only good knowledge of the dynamics of turbidity currents but also adequate and in-time bottom outlet operations. Therefore, the main focus of this review is on the venting process itself rather than the dynamics of the turbidity currents. However, numerous studies have addressed turbidity currents: Fan, 1986; Altinakar et al., 1990, 1996; Garcia, 1992; Fan & Morris, 1992a, b; Middleton, 1993; Morris & Fan, 1997; De Cesare, 1998; Simpson, 1999; Oehy & Schleiss, 2007; Wang & Hu, 2009; Georgoulas et al., 2010; Meiburg & Kneller, 2010; Nogueira et al., 2014 among others, all described their formation, dynamics and evolution. Nevertheless, a concise description of the physical features of these currents is given in the following.

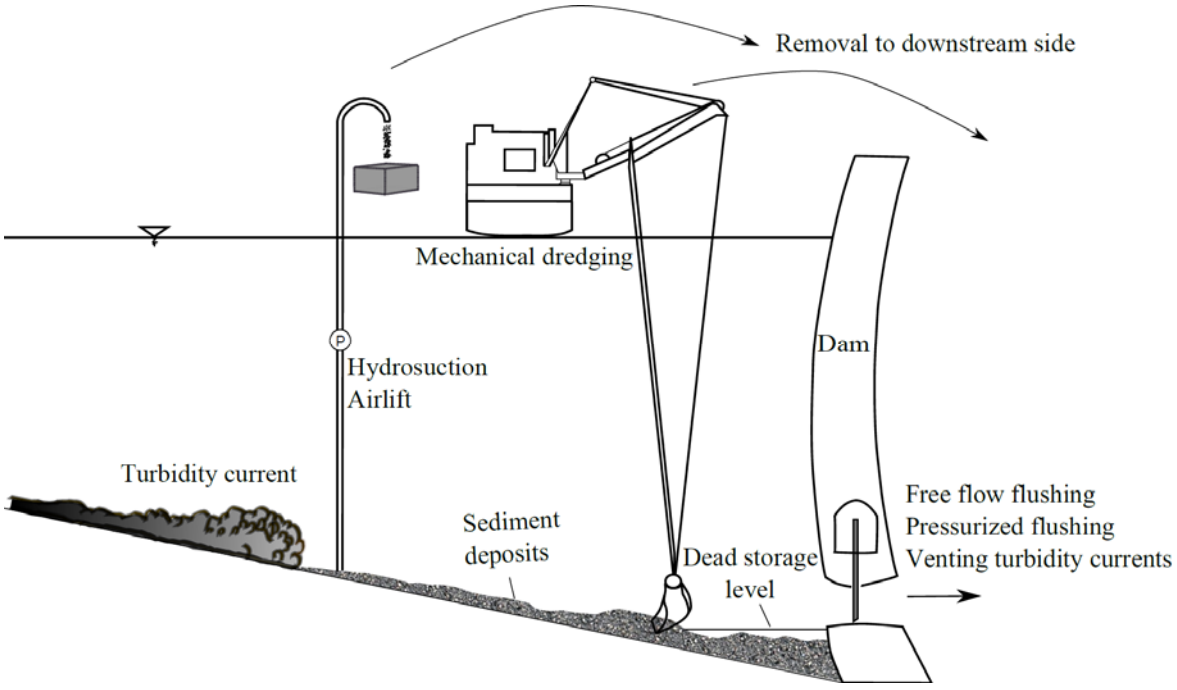

Figure 2.2: Illustration of the most common sediment evacuation techniques (Chamoun et al., 2016b).

2.3 Overview of turbidity currents

Turbidity currents lie in a much wider category called density currents. The latter are driven by density differences in one single fluid or between two or more fluids. Differences in the density can be due to many factors (e.g., difference in temperature, salinity, presence of suspended particles). Depending on the scale of the difference, the density current may move as an overflow, interflow, or underflow (Middleton, 1993). These types of currents are called respectively hypopycnal, homopycnal, and hyperpycnal currents by Georgoulas et al. (2010). In the case of turbidity currents, the presence of suspended sediments is what causes the density difference with the ambient clear water of the reservoir and triggers the plunging of the current. The plunge point occurs when the sediment-laden current has the minimum specific energy corresponding to the minimum depth and the minimum velocity (Ren & Ning, 1985). In the present research, the considered currents are the most common ones, flowing at the bottom of the reservoir after their plunging due to their high densities (Figure 2.3).

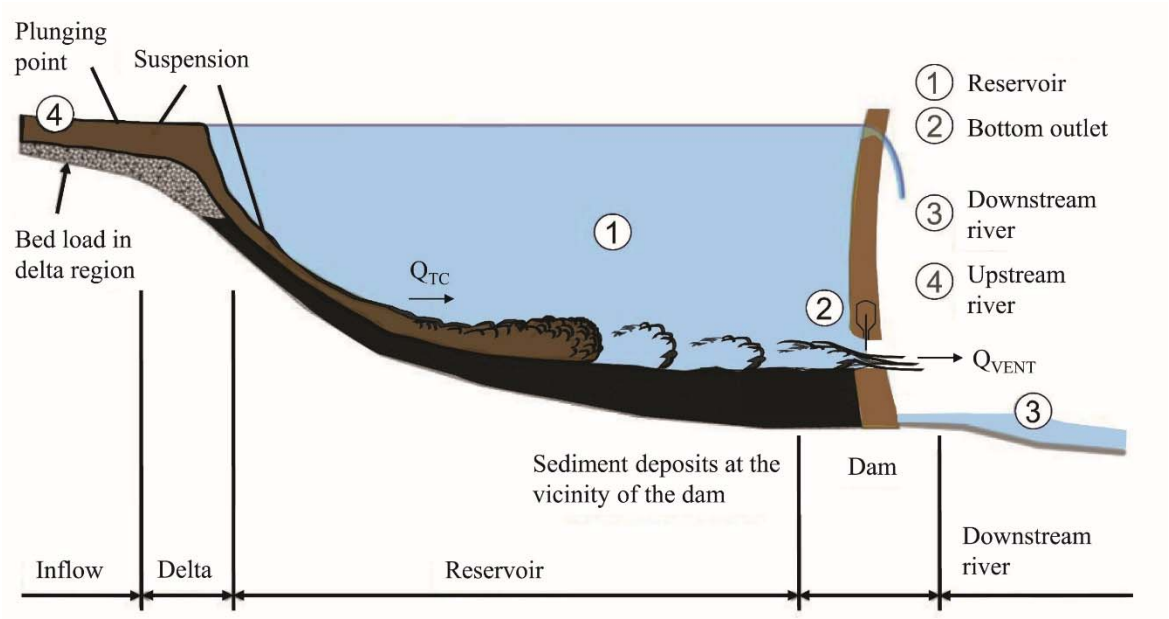

Figure 2.3: Turbidity current traveling along the bed of the reservoir with a projection of its venting through the bottom outlet (adapted from De Cesare (1998)).

2.3.1 Characteristics of turbidity currents

Turbidity currents are generally formed during floods, avalanches, landslides or even particular events such as reservoir drawdown or flushing operations (e.g., Luzzone dam) where the lowering of water can cause the collapse of deposits triggering turbidity currents (Richard et

al., 1999; De Cesare et al., 2015). A turbidity current consists of three consecutive parts: the head, the body, and the tail (Kneller & Buckee, 2000). The head of the current is kept in movement by density differences (causing a pressure gradient) while the body and tail dynamics are due to gravitational forces.

Dynamics and shapes differ when passing from the head to the body and tail. The height of the head is always larger than that of the body and tail. This is due to the resistance that the head faces from both the ambient fluid and the bed (friction) which induces a bigger height than the rest of the current where only bed friction is present (Middleton, 1993). Additionally, Figure 2.4 shows that there is energy loss at the head of the current in the form of eddies. This loss is compensated by a higher velocity in the body ensuring a constant rate of advance (Middleton, 1993).

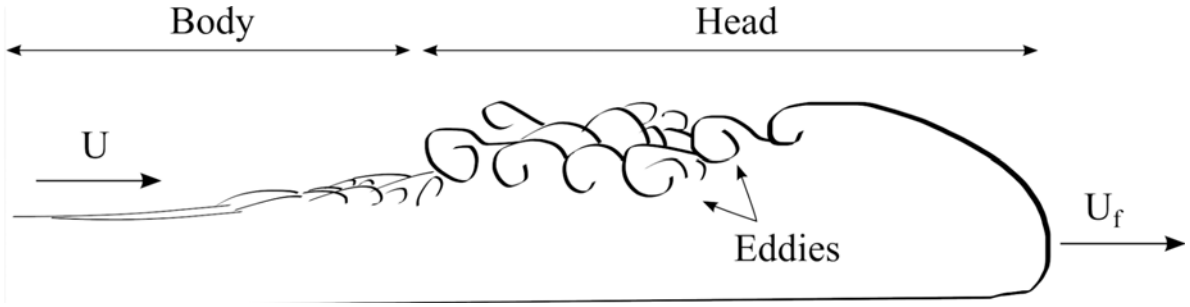

Figure 2.4: General structure of the turbidity current's head and body emphasizing the turbulent eddies at the head.

Turbidity currents have a reduced gravitational acceleration *g'* expressed by (Graf & Altinakar, 1995):

$$g' = g\left(\frac{\rho_t - \rho_w}{\rho_w}\right) = g\left(\frac{\Delta\rho}{\rho_w}\right) \tag{2.2}$$

where ρ_t and ρ_w are the densities of the turbidity current and the ambient fluid respectively. The former can be expressed by $\rho_t = C_s \rho_s + (1\text{-}C_s)\rho_w$ where C_s is the sediment mean volumetric concentration and ρ_s the sediment's particle density. In prototype turbidity currents, typical values of $\Delta\rho$ are between 30 and 200 kg/m^3.

In order to characterize the flow regime of turbidity currents, densimetric Froude number Fr_D is used (Graf & Altinakar, 1991):

$$Fr_D = \frac{U}{\sqrt{g'h\cos\alpha}} \tag{2.3}$$

where h is the height of the current, α the slope of the bed, and U the depth-averaged velocity of the turbidity current (Figure 2.5). However, Richardson number Ri is commonly used instead of Fr_D and is expressed by (Turner, 1973):

$$Ri = \frac{1}{Fr_D^2} = \frac{g'h\cos\alpha}{U^2} \tag{2.4}$$

When $Ri > 1$, the current is subcritical and in the opposite case it is supercritical.

Another important characteristic of turbidity current is its buoyancy B, which is the sediment flux by unit width (Graf & Altinakar, 1995). It represents the capacity of the current to maintain sediments in suspension:

$$B = g'hU = g'q \tag{2.5}$$

where q is the turbidity current's specific discharge. The variation of buoyancy along the reservoir indicates whether the current is conservative or not. If the variation is null, the current is conservative meaning that no sediment exchange (deposition/erosion) occurs between the current and the bed. In the opposite case, the current is able to react with the bed.

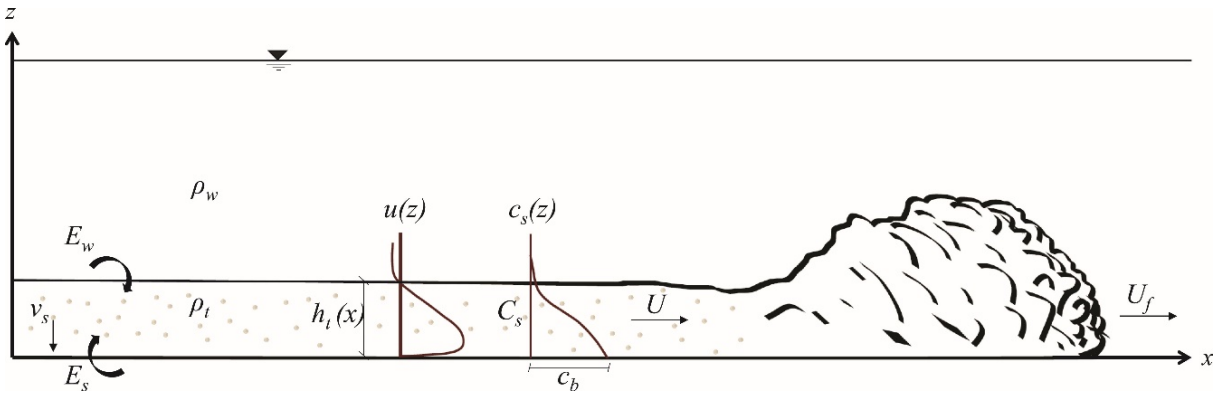

Figure 2.5: Parametric representation of a turbidity current flowing on a horizontal bed.

The characterizing height h, mean velocity U, as well as the sediment mean volumetric concentration C_s can be determined by an integration along the height of the current, using the following formulae (Ellison & Turner, 1959):

$$Uh = \int_0^{\infty} udz = \int_0^{h_t} udz = \bar{U}h_t = q \tag{2.6}$$

$$U^2 h = \int_0^{\infty} u^2 dz = \int_0^{h_t} u^2 \, dz \tag{2.7}$$

$$C_s U h = \int_0^{\infty} (u c_s) \, dz = \int_0^{h_t} (u c_s) \, dz \tag{2.8}$$

where $u(z)$ and $c_s(z)$ are the local velocity and volumetric concentration at a certain point z above the bed, h_t is the height at which u equals zero, and U is the mean velocity of the current.

In order to auto-suspend sediments, the turbidity current should satisfy Bagnold's auto-suspension criterion (Bagnold, 1962):

$$\frac{U \sin\alpha}{v_s} > 1 \tag{2.9}$$

where v_s is the settling velocity of the sediments suspended by the current.

2.3.2 Hydrodynamic equations of turbidity currents

The governing equations of a well-established turbidity current in steady state are the mass balance for water and for the suspended particles as well as the momentum conservation for the mixed flow. The depth-averaged one-dimensional equations are briefly presented in the following:

- Mass balance for water (Graf & Altinakar, 1995):

$$\frac{d}{dx}(Uh) = E_w U \tag{2.10}$$

where E_w is an entrainment coefficient of the ambient fluid into the turbidity current (Figure 2.5). The latter is linked to Richardson number Ri by an empirical relationship (Parker et al., 1987):

$$E_w = \frac{0.075}{\left(1 + 718\, Ri^{2.4}\right)^{0.5}} \tag{2.11}$$

When Ri gets larger (subcritical flows), less mixing with ambient water occurs at the interface.

- Mass balance for the suspended particles (Graf & Altinakar, 1995):

$$\frac{d}{dx}(C_s U h) = v_s (E_S - c_b) \tag{2.12}$$

where E_s is an entrainment coefficient of bed sediments and c_b the sediment concentration at the bed. Empirical relationships for E_s and c_b are proposed by Garcia & Parker (1993) and Parker (1982). In the case of conservative currents, the right component of equation (2.12) is equal to zero since there is neither sediment deposition ($v_s = 0$) nor erosion ($E_s = 0$). In such currents, the sediment transport rate $\psi = UC_sh$ remains constant (Parker et al., 1987).

- Momentum conservation for the mixed flow (Graf & Altinakar, 1995):

$$\frac{d}{dx}\left(U^2 h\right) = -\frac{1}{2} gR\cos\alpha \frac{d}{dx}\left(C_s h^2\right) + \left(gRC_s h\right)\sin\alpha - u_{*b}^2 \tag{2.13}$$

where R is the specific density of the submerged granular material and u_{*b} is the friction velocity at the bed and is expressed by (Graf & Altinakar, 1995):

$$u_{*b}^2 = \left(\frac{f}{8}\right) U^2 \tag{2.14}$$

In the above equation, f is the Weisbach-Darcy friction coefficient. It depends on the Reynolds number and the relative roughness (Graf & Altinakar, 2000).

A deep study of the above equations and relationships helps in determining the main parameters to be considered in processes including turbidity currents.

2.4 Venting of turbidity currents

Venting of turbidity currents consists of opening bottom or low-level outlets as soon as the current reaches the dam in order to pass it downstream. Ideally, the goal is to vent all the sediments contained in the turbidity current if possible and feasible. Globally, venting of turbidity currents is not systematically applied, though the earliest data of releasing such currents from a reservoir were recorded already in 1919 at the Elephant Butte Reservoir in the United States (Lee et al., 2014). According to Batuca and Jordaan (2000), the first researcher that suggested that venting of turbidity currents can be an effective technique to avoid sediment deposition was Bell (1942).

During venting operations, the loss of water is minimized due to relatively small outflow discharges, which consequently limits ecological and economic impacts. Therefore, one major advantage of venting turbidity currents through bottom or low-level outlets is the possibility to reduce sediment accumulation without drawing down the water level of reservoir (Sahnaz & Aras, 2012). For this reason, venting is widely used in arid regions where water is in shortage (Brandt, 2000).

2.4.1 Conditions for successful venting

Before opting for venting as a means for sediment management, four main conditions must be fulfilled:

- The formation of turbidity currents: Forel (1885) was the first to report turbidity currents when observed during their plunging at Lake Constance and Lake Geneva in the 1880s (Figure 2.6). Many indicators of the presence of turbidity currents in a reservoir are commonly known (Morris & Fan, 1997) and include the emergence and disappearance of a muddy flow at the upstream part of the reservoir, sampling of highly concentrated water with sediments and velocity profiling of reservoir sections suggesting the existence of a bottom flow. Field data from Shaver Lake (U.S.) show that a turbidity current forms if the difference between its sediment concentration and that of the reservoir's clear water is around 1.28 kg/m^3 (Chien & Wan, 1999). Oehy et al. (2000) stated that favorable conditions for the formation of turbidity currents existed in narrow and deep Alpine reservoirs. However, this condition shall be completed by the following.

Figure 2.6: Aerial photo of the turbid waters of Rhone River plunging beneath Lake Geneva.

- The plunging current must reach the dam. Turbidity currents which dissipate before reaching the dam result in very low venting efficiencies (Fan & Morris, 1992a). For sediment-laden currents to be maintained, a minimum initial sediment concentration as well as a continuous inflow into the reservoir are required (Chien & Wan, 1999). In Lake Mead for instance, an inflow concentration of less than 0.1 kg/m^3 is not sufficient enough for density currents to reach the dam (Ren & Ning, 1985). In the Guanting Reservoir, a

minimum sediment concentration of 20 kg/m^3 is required (Chien & Wan, 1999). This condition is fulfilled in Groβsölk reservoir in Austria. In the latter, turbidity currents follow the thalweg until reaching the dam, even if the turbine intake (placed upstream of the outlet) was operating and the bottom outlet closed (Schneider et al., 2007). This is quite promising for venting operations in this reservoir. On the other hand, the progression of a turbidity current is linked to the inflow; as long as there is an inflow, the current progresses, but once the inflow is cut, the current decelerates and settles. The settled portion of the current is not vented (Morris & Fan, 1997). Wang and Hu (2009) also highlighted the importance of the particle distribution showing that turbidity currents having finer sediments tend to reach the dam with lower concentrations and inflow discharges compared to turbidity currents having coarser sediments.

- The presence of bottom or low-level outlets with a certain capacity and which can be used to evacuate sediment-laden currents. Outlets can have many different functions and therefore require a minimum capacity depending on the reservoir size. Besides the control of the first filling of the reservoir, the bottom outlet is also used for preventive and emergency emptying, flood control, and sediment evacuation (Boillat et al., 2000a).
- Turbidity current venting sometimes requires long outlet opening depending on the duration of the inflowing event. For this reason, another condition is to have enough downstream river capacity to evacuate both water and sediments released during such operations.

2.5 Venting efficiency

Venting of turbidity currents is most efficient when performed regularly during yearly floods entering the reservoir since they are responsible for the entrainment of most of the sediments. However, if venting is adopted, it is recommended to perform it since the beginning of the dam's operation for two main reasons (Bell, 1942): (1) Lake Arthur Reservoir in South Africa showed that once the "turbid underflow" -as named by Bell (1942)- settles, its venting cannot be postponed and the deposits then require costly mechanical means of removal (2) when a turbidity current deposits, it decreases the slope of the reservoir's thalweg. A smaller slope renders future turbidity currents more and more subcritical, and thus reduces the size and quantity of sediments they are able to transport. As a result, they tend to dissipate more easily before reaching the dam.

The efficiency of turbidity current venting is defined as the sediment mass ratio between outflow and inflow. In the following, when referring to inflow parameters with the ''*TC*'' index (i.e., discharge, concentration, mass), the latter are not related to the flood itself but to the turbidity current after its plunging and when arriving at the dam.

In literature, the venting efficiency is expressed by (Lee et al., 2014; Morris & Fan, 1997):

$$VE = \frac{M_{VENT}}{M_{TC}} = \frac{\int_{t=0}^{t=T} C_{VENT} Q_{VENT} \mathrm{d}t}{\int_{t=0}^{t=T} C_{TC} Q_{TC} \mathrm{d}t} \tag{2.15}$$

where M_{VENT} and M_{TC} represent the sum of outflow and inflow masses of sediments respectively, C_{VENT} and C_{TC} are the respective suspended sediment concentrations of outflow and turbidity current inflow at time t, Q_{VENT} and Q_{TC} are the respective outflow and inflow discharges at time t and T is the total duration of the turbidity current inflow close to the dam site. Venting efficiencies generally range from 23% to 65% (Fan & Morris, 1992b). Nevertheless, in some reservoirs, the efficiency can reach values higher than 100%. This is explained by the erosive character of some turbidity currents that provoke drag and friction on the bed and thus entrain already settled sediments. However, during field investigations in particular, the method for estimating venting efficiencies is not always explicitly stated and depends on the monitored parameters. For this reason, care should be taken when comparing venting efficiencies that were estimated on different basis and in different reservoirs.

Basson and Rooseboom (1997) mentioned some favorable conditions for an efficient venting: a steep slope of the reservoir thalweg, a long duration of incoming flood (at least longer than the travel time from the plunge point to the dam), a high concentration of fine particles in the density current, a well-chosen outflow discharge, and of course, a correct timing for the opening of low-level outlets. Sloff (1991) stated that more sediments are vented when: the reservoir is short and has large incoming discharge, the outlets are at low levels and large and the outflow is high. In the following, the main parameters affecting venting efficiencies are discussed.

2.6 Main venting parameters

2.6.1 Outflow discharge

A good example of venting sediment-laden currents is the Sanmenxia reservoir (China) located on the Yellow River which is the river that carries the largest sediment load (Morris & Fan,

1997). Data from this reservoir among others showed that venting efficiencies decreased with an increasing length of the reservoir and a decreasing ratio of average outflow to inflow discharges Q_{VENTav}/Q_{TCav} (Morris & Fan, 1997). However, the effect of Q_{VENTav}/Q_{TCav} revealed to be different by Lee et al. (2014). The latter investigated the venting operation of a turbid density current by providing a formula to estimate outflow concentration and therefore venting efficiencies through reservoir outlets. The study was based on a combination of numerical, theoretical and experimental works as well as field measurements. The experimental model had two circular outlets placed vertically at 6 cm and 18 cm above the bed of the flume. Only two outflow conditions were tested, $Q_{VENT}/Q_{TC} = 1$ and $Q_{VENT}/Q_{TC} = 0.5$. Concentration measurements were made by collecting samples and oven drying them. For $Q_{VENT}/Q_{TC} = 1$, venting efficiency was around 49% for the lower outlet and 11% for the higher outlet. A decrease in outflow $Q_{VENT}/Q_{TC} = 0.5$ induced an increase in venting efficiency for the lower outlet (60%) while it showed a slight decrease for the higher outlet (8%). Another study was done by Yu et al. (2004) on the selective withdrawal of saline currents. Turbidity currents could not be used since deposition was unavoidable on a horizontal bed and could not be measured.

Summarily, it is of high interest to optimize venting based on the normalized parameter Q_{VENT}/Q_{TC} particularly for cases where outflow discharges are lower than inflow discharges. The capacity of the bottom outlet has a very important role in this optimization. Commonly, Q_{VENT} is known to be low compared to Q_{TC} and venting is usually performed under restrained outflow discharges. In fact, Q_{TC} is a parameter that is difficult to measure and is usually related to the flood discharge measured upstream of the reservoir.

In the goal of estimating the range of magnitude of Q_{VENT}/Q_{TC}, a analysis was performed on 22 Swiss dams.

Table 2.2 below provides, for 22 large Swiss reservoirs, the capacity of the outlets $Q_{VENTmax}$, the direct watershed surface A, the 2 and 10 years return period inflow flood discharges Q_2 and Q_{10} respectively, and the maximum venting discharge ratio for each flood case $Q_{VENTmax}/Q_2$ and $Q_{VENTmax}/Q_{10}$. Note that for the estimation of Q_2 and Q_{10}, Francou coefficients k_2 and k_{10} (Francou & Rodier, 1967), were calculated for a 2 and 10-years flood discharge based on discharge and watershed data of 22 hydrometric stations (source: hydrodaten.ch) in Switzerland. The values obtained are $k_2 = 2.9$ and $k_{10} = 3.2$. It was then possible to calculate Q_2 and Q_{10} for the 22 chosen Swiss reservoirs knowing their direct watershed surface.

Table 2.2: The outlet capacity, watershed area, two and ten-year flood discharges, and corresponding outflow to inflow discharge ratios of 22 Swiss dams.

Dam	$Q_{VENTmax}$ **(m^3/s)**	A **(km^2)**	Q_2 **(m^3/s)**	Q_{10} **(m^3/s)**	$Q_{VENTmax}/Q_2$ **(%)**	$Q_{VENTmax}/Q_{10}$ **(%)**
Schiffenen (3 outlets, each)	133	1400	358	500	37	27
Moiry	55	245	104	153	53	36
Rossens (2 outlets each)	150	908	263	373	57	40
Grande Dixence (direct)	35	46	32	49	110	71
Emosson	95	183	84	125	112	75
Mattmark	57	88	50	76	114	75
Rossinière (2 outlets each)	193	398	146	213	131	90
Oberaar	26	21	18	29	143	90
Nalps	91	102	56	84	163	108
Mauvoisin	100	114	60	91	166	110
Zervreila	150	200	90	133	167	112
Punt dal Gall	200	295	118	174	169	115
Valle di Lei	123	137	69	103	179	119
Luzzone (direct)	52	37	27	42	193	123
Palagnedra	140	138	69	103	203	135
Santa Maria	124	102	56	84	223	147
Sambuco (direct)	53	30	23	36	228	145
Mapragg	214	159	76	114	280	188
Contra	340	233	100	148	339	230
Gebidem	250	150	73	110	342	228
Gigerwald	129	52	34	53	373	242
Rempen	192	83	48	73	400	263

In

Table 2.2, reservoirs are sorted starting from the lowest to the highest $Q_{VENTmax}/Q_2$. Results shows that in case of venting in reservoirs such as Schiffenen, Moiry, and Rossens, $Q_{VENTmax}/Q_2$ and $Q_{VENTmax}/Q_{10} < 100\%$ and outflow discharges are restrained compared to inflow discharges. For the remaining reservoirs, $Q_{VENTmax}/Q_2$ and $Q_{VENTmax}/Q_{10} > 100\%$, meaning that the capacity

of the outlet is higher than the 2 and 10 years flood discharges. Nevertheless, the full capacity of outlets is rarely used, even during flushing operations. The main reason for this discharge limit is that the downstream river capacity may not be high enough to contain the maximum discharge of the outlet for long periods of time. High discharges can lead to risks of flooding and environmental disasters in the downstream river. For example, in the Luzzone reservoir, even if the $Q_{VENTmax}$ = 52 m^3/s, the highest flushing discharge that was used is 40 m^3/s while the most frequently used discharge is around 30 m^3/s (OFIBLE, 1992, 1993, 1994). This, for instance, leads to $Q_{VENTmax}/Q_2$ = 110% instead of $Q_{VENTmax}/Q_2$ = 193% in case of the Luzzone reservoir.

On a different note, as previously mentioned, the discharge of the turbidity current reaching the dam Q_{TC} is usually larger than the flood discharge measured upstream. This is due to clear water entrainment into the turbidity current while flowing in the reservoir before reaching the dam. Therefore, the calculated Q_2 and Q_{10} below might underestimate Q_{TC}. Thus, it can be concluded that during operations of venting turbidity currents through bottom outlets, outlet discharges are most of the times smaller than the discharge of the turbidity current.

2.6.2 Venting timing

Another important parameter is the timing of the outlet opening. Annandale (2005) and Wan et al. (2010) stated that it is possible to vent high sediment loads carried by turbidity currents by timing the opening of the gates correctly. Chen and Zhao (1992) revealed that the timing of gate opening/closing as well as the amount of the opening (outlet discharge) are crucial. In fact, if the operation is too late or the opening of the outlet is too small, smaller amounts of sediments will be evacuated. If the gate is opened too early or the opening is too large, however, valuable water will be lost and strong velocity fields of clear water can be formed in front of the outlet (Chen & Zhao, 1992). Additionally, venting a turbidity current at the right time is important since the less time sediments are detained in the reservoir the lower the trap efficiency becomes (Brune, 1953). Wen Shen (1999) mentioned that during a flood or high inflow discharges, the peak of sediment inflow generally appears before the peak of flow discharge. In fact, upon reaching the peak flood conditions, sediment concentrations decrease by a factor of ten even though water discharges remain high (Mulder & Syvitski, 1995). De Cesare et al. (2001) quantified this relationship by elaborating a formula based on field measurements in the Luzzone Reservoir (Switzerland), relating the time to peak of suspended load to that of water discharge:

$$\frac{t_{sp}}{t_p} = 0.85 \pm 0.16 \tag{2.16}$$

where t_{sp} is the time at which the suspended sediment load reaches its peak during a rainfall event, while t_p is the time at which the water discharge hydrograph reaches its peak. Schneider et al. (2007) also confirmed this behavior by field measurements at the Groβsölk reservoir.

In Heisonglin reservoir in China, sediment management is a combination of seasonal drawdown, flushing, and venting of turbidity currents (Morris & Fan, 1997). The latter is applied only during dry periods. The characteristics of three main venting operations are shown in Table 2.3 below. The fact that the events of July 1964 and August 1966 have lower efficiencies can be explained by two reasons: (1) the opening of the outlets was done after the inflow peak has reached the dam and the muddy lake has been formed and settled, (2) initial outflow discharges for these two events were very low and could not erode the already settled muddy lake. On the opposite, during the August 1964 event, outlets were opened before the arrival of the inflow to the dam and with higher outflow discharges compared to the other two events. The high efficiency obtained can also be due to the scouring of sediments that settled less than one month before in the vicinity of the dam (during the July 1964 event). These results suggest that the difference in opening timing of outlets might have had an effect on the venting efficiency values.

Note that for this reservoir, and based on the data presented by Morris and Fan (1997), applying the formula in equation (2.15) did not always result in the same values of the efficiencies provided. Unfortunately, not enough details were given concerning the calculations behind the efficiencies given. This, as mentioned in section 2.5, renders the comparison between venting operations more complicated.

Table 2.3: Characteristics of three venting operations in Heisonglin Reservoir (Morris & Fan 1997).

Reservoir	**Aug. 1 1964 event**	**Jul. 11 1964 event**	**Aug. 9 1966 event**
Q_{TCmax} **(m^3/s)**	135	132	23.2
$Q_{VENTmax}$ **(m^3/s)**	7	4.8	4.6
C_{TCmax} **(g/l)**	731	534	472
$C_{VENTmax}$ **(g/l)**	749	582	340
VE **(%)**	91	38	50
Timing of outlet	Before inflow	After inflow peak	After inflow peak

2.6.3 Outlet level

Outlets used to vent turbidity currents can be placed at the bottom of a reservoir and called ‘’bottom outlets’’ or at higher elevations, called ‘’low-level outlets’’. In 1942, Bell was the first to mention, though qualitatively, the importance of the height of outlets on the aspiration of turbidity currents during their withdrawal.

The height or position of an outlet relatively to the bottom of the reservoir is one of the most crucial parameters in terms of venting. Its importance is directly linked to the critical height of aspiration h_L which characterizes an outlet operating with a certain discharge and facing a turbidity current with a certain density. The critical height of aspiration is a concept that was developed by Gariel (1949) and Craya (1949) using experimental and theoretical approaches respectively. This height has upper and lower limits relatively to the central axis of the outlet. When the interphase between clear and turbid water is at higher levels than the upper limit, then only turbid water is vented and no clear water is discharged. In the opposite case, if the interphase of the current reaching the dam is at a lower level than the lower limit of the height of aspiration, then only clear water is vented and thus venting is not efficient. This height of aspiration with its upper and lower limits is illustrated in Figure 2.7.

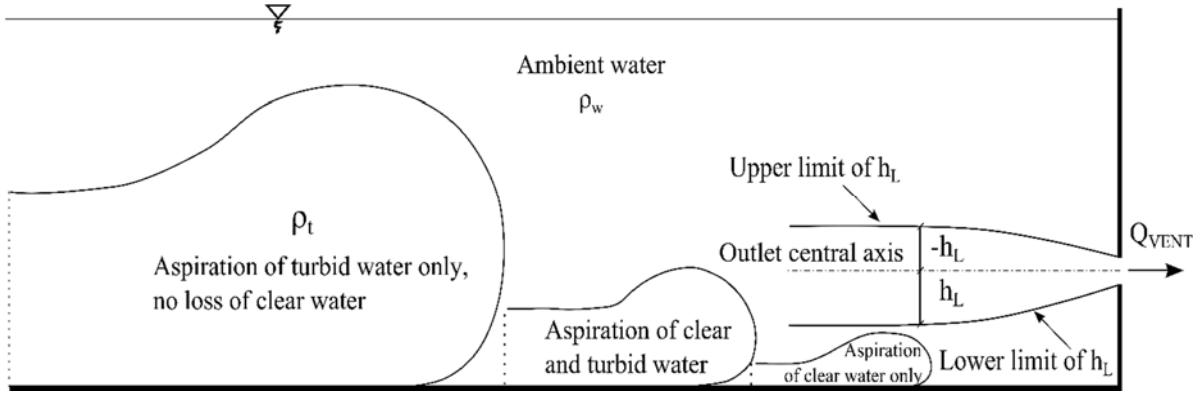

Figure 2.7: Illustration of the height of aspiration of an outlet during venting.

Gariel (1949) and Craya (1949) developed this concept for saline current. Fan (1960) adapted the results for turbidity currents by performing flume tests. The general form of the relationship links the density of clear water ρ_w, the density difference between the turbidity current and the clear water $\Delta\rho = \rho_t - \rho_w$, the outflow discharge Q_{VENT} and the critical height of aspiration h_L. It is shown in equation (2.17) below (Craya, 1949; Gariel, 1949; Fan, 1960; Fan, 2008):

$$\left[\frac{\Delta\rho}{\rho_w}\frac{g(\pm h_L)^5}{Q_{VENT}^2}\right]^{1/5} = K \tag{2.17}$$

In the above formula, K is a constant that depends on the height and geometry (i.e., slot or orifice) of the outlet and on the type of the stratified current (e.g., linearly stratified, saline, turbid).

Based on this concept of critical height, Fan (2008) deals with the selective withdrawal of stratified or two-layer flows using outlets located at different heights. Distinction between 2D (slots) and 3D outlets (orifices) as well as bottom and low-level outlets are presented and discussed. One of the main results of Fan (2008) is the elaboration of a method that allows the estimation of outflow concentrations in discharged currents under various conditions.

Generally, the lower the outlet, the higher the venting efficiency. With bottom outlets, the height of aspiration always includes part or even all of the turbidity current. For higher outlets, venting efficiencies start increasing once the gap between the bed of the reservoir and the lower sill of the outlet is filled with sediment deposits.

2.6.4 Secondary parameters

Other parameters can influence the venting process. Morphological and topographical parameters such as the soil type and the slope of the thalweg have a direct effect on the characteristics (e.g., concentration and grain size distribution) and dynamics (e.g., subcritical or supercritical) of a turbidity current. Also, the intensity and duration of the flood event impact the inflow duration of the turbidity current and consequently affects venting duration. Finally, legal, economic and downstream environmental aspects affect decisions concerning venting of turbidity currents (Althaus & De Cesare, 2006; Palmieri et al., 2001).

2.7 Overview of venting applications

Many reservoirs worldwide use venting operations as their main evacuation technique (Figure 2.8). In the following, a discussion of these reservoirs is structured geographically.

2.7.1 Venting in Taiwan

- In Taiwan, typhoon events lead to the formation of turbidity currents transporting large amounts of fine sediments. At the Shihmen Reservoir, one of the hydro-power turbines and its runner was transformed to a sediment sluice to release the sediments. A numerical study

was conducted and showed that the efficiency of venting turbidity currents in this reservoir increased from 21% to 40% by adding an extra sluicing tunnel (Sloff et al., 2016).

- At the Tsengwen reservoir, Lee et al. (2014) used a combined experimental, theoretical and numerical approach to investigate the operation of venting. Efficiencies measured in the field for two different typhoon events did not exceed 1% when performed through the intake or the bottom outlet while the spillway could release sediments with an efficiency of 17% (Lee et al., 2014).

2.7.2 Venting in China

- The Bajiazui Dam is a very successful application of the venting operation. The average sediment release ratio is 46% (Sahnaz & Aras, 2012).
- At the Xiaolangdi Reservoir, venting turbidity currents have become the main sedimentation control strategy (Wang & Hu, 2009). Venting efficiencies are around 20% on average.
- Another illustrative example of venting is the Nanqin Reservoir where, in August 1985, outflow sediment concentration was 1.5 times higher than the inflow concentration. Additionally, the ratio of water outflow to water inflow was smaller than the ratio of sediment outflow to sediment inflow, which means that there was no loss of ‘’useful’’ water and that the venting efficiency was considerably high (Chen & Zhao, 1992).
- In Sanmenxia Reservoir, Wan et al. (2010) mentioned that venting efficiencies ranged from 18% to 36% with no backwater in the density currents and no rising pool water during flood periods.
- In the Fengjiashan Reservoir, venting was considered during the design stage due to the topographical and morphological conditions favoring the formation of turbidity currents. Between 1976 and 1980, around 14 density current events were detected at this reservoir and suspended sediment concentrations exceeded 30 kg/m^3 (Batuca & Jordaan, 2000). A number of bottom and low-level outlets were placed at the right and left banks of the river (Batuca & Jordaan, 2000) and venting efficiencies ranged between 23% and 65% (Ren & Ning, 1985).
- In the Guanting Reservoir, during 1956 and 1957, sediments released from the reservoir resulted entirely from vented density currents (Ren & Ning, 1985).
- Other reservoirs such as the Liujiaxia reservoirs in China where many events of density currents were observed also apply venting.

Figure 2.8: Location and density of reservoirs where turbidity currents were observed and venting is applied.

2.7.3 Venting in Switzerland

- The Mapragg and Gigerwald reservoirs receive high amounts of sediments. In 2009, the average yearly volume loss in the former was estimated to 0.4% and 0.2% in the latter (Müller & De Cesare, 2009). In Mapragg, turbidity currents are associated with large sediment inflows and venting is applied. These operations are applied with respect to the Swiss regulations concerning downstream discharges and capacity (between 5 and 25 m^3/s) as well as venting frequencies (once per year). Venting in this reservoir is economically optimized. In fact, alarm systems are triggered only when a turbidity current is reaching the dam with a concentration high enough (2 g/l) for venting operations to become more beneficial than a future dredging of the sediments.
- In the Livigno Reservoir, the downstream environment witnessed a sudden drought and bottom outlets were immediately opened, releasing considerably large amounts of fine sediments (De Cesare et al., 2015). In fact, an involuntary turbidity current venting took place during the outlet opening.

2.7.4 Venting in Iran

- Releasing turbid density currents is one of the main techniques used to reduce sedimentation in the Sefid-Rud Reservoir in Manjil. In this reservoir, venting operations using power intakes alone were compared to cases where both power intakes and one bottom outlet were open. Results showed that efficiencies increased from a maximum of 2.3% to 35% when using the bottom outlet (Morris & Fan, 1997). This shows that releasing sediment by venting through outlets is an adequate choice for this reservoir.
- In Dez Dam, Southwest of Iran, the yearly sedimentation rate is around 0.5% of its storage capacity. Turbidity currents were shown to be the main reason behind sedimentation in this reservoir (Schleiss et al., 2010) and venting is highly recommended.

2.7.5 Venting in the United States

- Hoover Dam, the largest reservoir by volume in the United States, impounds Lake Mead Reservoir. Turbidity currents are the main mechanism for transporting sediments within this reservoir (Smith et al., 1960). In fact, the longest recorded travel distance (129 km) for a turbidity current was observed in Lake Mead (Morris & Fan, 1997). At the construction phase, a cofferdam was built 214 m upstream of the dam. During the first 5 years of operation, before its inundation, this cofferdam obstructed all sediments that moved along the bed of the reservoir towards the dam (Smith et al., 1960). Once it was possible to apply venting, efficiencies ranged from 18% to 39% (Ren & Ning, 1985).
- The Elephant Butte Reservoir is built on the Rio Grande River in New Mexico, which is known to have a high sediment load. Consequently, sedimentation in this reservoir was extensively studied and was part of the design phase (Lane & Koelzer, 1943). Venting efficiencies in this reservoir range from 9% to 23% (Lara, 1960).

2.7.6 Venting in North Africa

- From 1953 to 1958, venting efficiencies were between 45% and 60% in the Iril Emda Reservoir in Algeria. During the first year of operation, the efficiency was much lower (25%) mainly because the sill of the outlets was 7 m above the bed (Raud, 1958).
- In Tunisia, at the Nebeur Reservoir, venting is also applied through two different valves: Neyrpic and Bafour. The former has a discharge of 12.5 m^3/s and the latter of 1 m^3/s and operating the valves depends on the concentrations of the density currents that reach the dam. If the density of the current relative to water (ρ_t/ρ_w) is below 1.02, venting operations

are stopped. Efficiencies of venting in this reservoir ranged between 59% and 64% ((Abid (1980) as cited by Ren and Ning (1985)).

- In Oued Neckar reservoir in Morocco, density currents are directed towards the bottom outlets by putting in place 3 submersible dikes and 2 submersible guide embankments (Batuca & Jordaan, 2000; C. J. Sloff, 1991).

2.7.7 Venting in other countries

In France, at Sautet dam, turbidity currents frequently occur in the reservoir and deposit sediments close to the dam (Nizery et al., 1952). In this case, venting should be considered as the main strategy to avoid sedimentation. Examples of reservoirs where turbidity currents are observed and venting is recommended - or applied with no published data yet - include the small reservoirs of Daesti, Valcea and Raureni in Romania (Rosca et al. (1982) as cited by Batuca and Jordaan (2000)) and the Ciudsko-Pskovskoe Reservoir in Russia (Filatova & Kalejarv, 1973). Sloff (1991) also mentioned the Bhatgarh Dam in India where the major part of the annual sediment load is carried through the reservoir as suspended sediments.

Table 2.4 below provides a list of the above mentioned reservoirs along with some of their characteristics. In some of the shown reservoirs, the wide range of venting efficiencies is mainly due to different venting conditions. In other words, for the same reservoir, some venting conditions (e.g., outflow discharge, level of bed deposits) vary from one event to another. For instance, in the Sefid Rud reservoir, venting was first applied while turbidity currents did not yet reach the lower limit of the outlet. The efficiency drastically increased once this gap was filled with deposited sediments and turbidity currents flowed directly at the level of the outlets. The same was observed in the Xiaolangdi Reservoir (Wang & Hu, 2009).

Figure 2.9 was initially prepared by Palmieri et al. (2003) based on data from Basson and Rooseboom (1997) and is adapted in this research work to include reservoirs applying venting of turbidity currents. The graph delimits zones where it is optimal to flush, store or sluice sediments from reservoirs. The horizontal axis represents the residence time of water inflow in reservoir. The vertical axis compares volumes of water stored with mean annual sediment loads. One can see that all of the points added are located outside of the flushing zone (Figure 2.9). Reservoirs applying venting are situated between the zones corresponding to sluicing operation and storage. The different sizes of the points used in this graph correspond to different ranges of venting efficiency values. Each category has a range of 20 percentage points starting at 0% (the smallest symbol) and ending at 80% (the largest symbol). As depicted in the graph, no obvious trend exists for venting efficiencies. This result is consistent with the fact that

several parameters, cited and developed in the previous sections, influence the outcome of venting turbidity currents.

Table 2.4: Overview of worldwide venting applications.

Reservoir	Storage capacity (10^6 m^3)	Annual runoff (10^6 m^3)	Annual average siltation rate (%)	Annual average sediment load (10^6 t)	Venting efficiency (%)	References
Tsengwen	748	1740	-	-	1-17	Lee et al. (2014)
Iril Emda (Algeria)	160	210	1.1	3.38×10^6 (m^3)	25 - 60	Raud (1958); Batuca & Jordaan (2000)
Fengjiashan (China)	398	485	-	-	23 - 65	Ren & Ning, (1985)
Guanting (China)	2270	1'400	15.7	57.22	20 – 34	Ren & Ning, (1985); Batuca & Jordaan (2000)
Mapragg (Switzerland)	5	167	0.4	0.058	10	Axpo Power and Kraftwerke Sarganserland (2013); Müller & De Cesare (2009)
Sanmenxia (China)	9640	43200	26	1605	1.2 – 21	Ren & Ning, (1985); Morris & Fan (1997)
Sefid Rud (Iran)	1760	5008	2.1	50.4	0.9 – 36	Morris & Fan (1997)
Heisonglin (China)	8.6	14.2	6	0.71	36 – 92	Morris & Fan, (1997); Wang & Lin (2004)
Nanqin (China)	10.19	121	5.8	0.533	64	Chen & Zhao (1992)
Elephant Butte (U.S.A.)	3250	1238	0.53	12.8	9 – 23	Lara (1960); Lane (1943)
Bajiazui (China)	495	-	-	-	46 – 100	Sahnaz & Aras (2011); Wang & Lin (2004); Pan & He (2000)
Xiaolangdi (China)	12650	40550	-	23.33	6 – 36	Wang & Hu (2009); Morris & Fan (1997)
Liujiaxia (China)	5720	27300	1	15	52 – 87	Wang & Lin (2004); Pan & He (2000); Fan & Morris (1992); Batuca & Jordaan (2000)

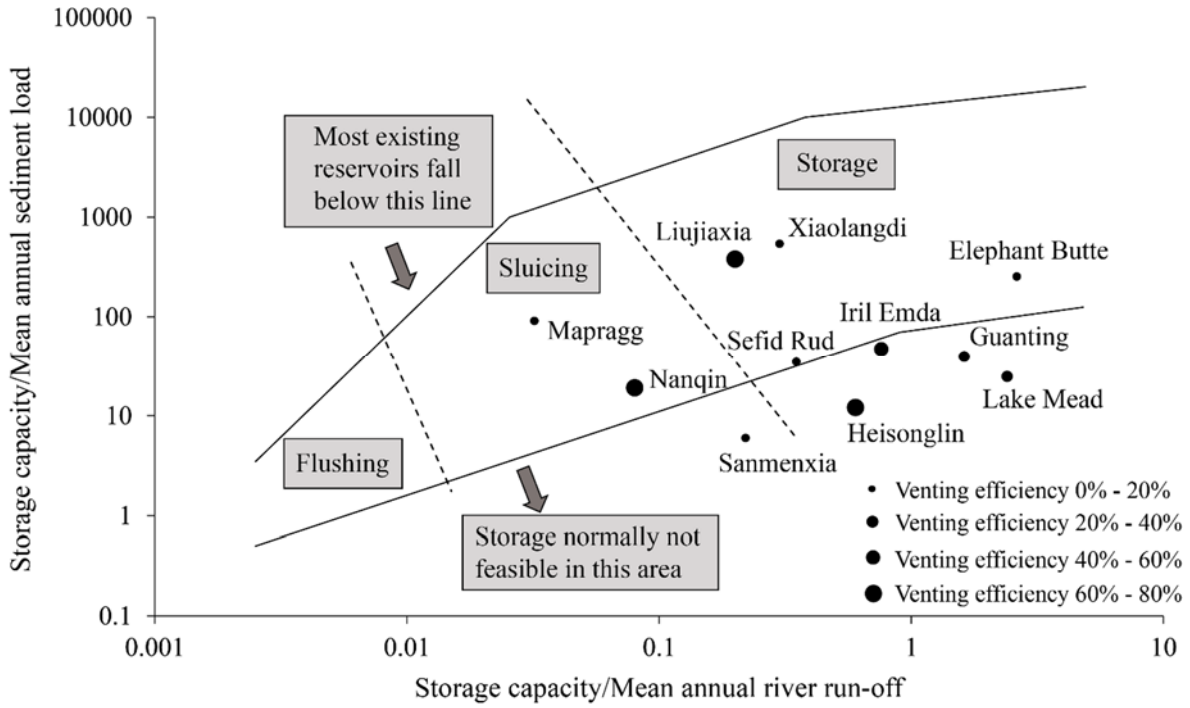

Figure 2.9: Position of the main reservoirs applying venting of turbidity currents relatively to different operation types (Graph adapted from Palmieri et al. (2003)).

2.8 Monitoring instruments and challenges

In order to apply venting in optimized conditions, good monitoring is required. The latter allows in-time and efficient evacuation of the turbidity current. Despite the complexity of the conditions, the monitoring of turbidity currents in reservoirs is developing. Many variables should be monitored on the site. Optimally, measurements should be performed upstream, downstream, and in the vicinity of the dam. Going from the visual observation to specific and detailed measurements, different techniques are used. Some of the most important parameters to be checked are: the plunge point (can be done through visual observation), velocity and concentration profiles and erosion and deposition (bedforms) rates. Table 2.5 gives an overview of the most known instruments available for field measurement of turbidity currents. In order to apply venting in an optimized way, information on turbidity currents and their dynamics is necessary. Consequently, information on the watershed and sediment grain sizes entrained is necessary.

Turbidity currents entraining the largest part of sediments are usually triggered during yearly floods or even during earthquakes. Thus, their monitoring can sometimes be quite complicated from a practical point of view. Such underflows are so powerful that they dislodged equipment and even destroyed it. Paull et al. (2003) describes difficulties encountered during the

monitoring of the powerful sediment gravity flow that occurred at the Monterey Canyon (California) on the 20th of December 2001. Instruments were dislodged and found completely buried under thick sediment deposits. Xu et al. (2004) measured velocity profiles during four turbidity current events on this same Canyon and also mentioned considerable damage to the instruments used. Likewise, during measurements in the Zaire submarine valley (Congo), Khripounoff et al. (2003) described damage of various degrees with the material used: a sediment trap exploded, a current meter was broken and a turbidity probe was lost. During a study performed at Lake Lugano in Switzerland (De Cesare et al., 2006), instruments mounted at a measurement chain were also lost and broken during the measurements. Therefore, one of the main challenges of venting is that it requires real-time discharge hydrographs in the reservoir and special remote techniques (e.g., radars, aerial photography) to detect the plunging of a current.

Table 2.5: Overview of instruments to measure turbidity currents in a reservoir.

Instrument	Measured parameter
Multibeam echosounder	Image of the turbidity currents and bathymetry (Czuba et al., 2011; Hage et al., 2016)
Acoustic Doppler Current Profiler (ADCP)	Vertical velocity and concentration profiles in time (Hage et al., 2016; Haun & Lizano, 2016); Bathymetry (Dinehart & Burau, 2005)
Chirp profiles	Image of the dense near-bed zone (Hage et al., 2016; Schock et al., 1989)
Time Domain Reflectometry (TDR) probes	Sediment concentration (Sloff et al., 2016)
Laser or electrical-resistance based instruments	Bathymetry (Chamoun, Zordan et al., 2016)
LISST (Sequoi Scientific Inc., 2011)	Suspended sediment concentration point measurement, particle size distribution and temperature (Haun & Lizano, 2016)
Vibrating-Tube Density Meters (VTDMs); Coriolis Flow Density Meters (CFDMs)	Suspended sediment concentration point measurement and temperature (Felix et al., 2016)
Single-frequency acoustic attenuation method	Sediment concentration profile (Felix et al., 2016)
Turbidimeters	Turbidity and suspended sediment concentration point measurement (M. Müller, 2012; Rai & Kumar, 2015)

Economically, field measurements of turbidity currents can be considerably expensive (Lee et al., 2014). Despite the fact that, in long term, venting operations may be more beneficial than other sediment management techniques, it requires higher initial investments. On another hand, financial benefits more than 50 years in the future are low when reduced to a net present value. This is why, capital costs related to sedimentation generally (e.g., construction of large low-level outlets) are often considered as not ‘’economically justified’’ (Kondolf et al., 2014). Nevertheless, in most of the cases, posteriorly adding a low-level outlet for existing dams is nearly impossible, which endangers the sustainability of the reservoir.

Other challenges include the readiness for venting operations. A management plan is needed to open the outlets at the right time and with the adequate discharge. For instance, automatic alarms can be set and triggered based on the turbidity currents' discharges and concentrations.

2.9 Discussion

Favorable conditions for high venting efficiencies can be predicted: steep slope, short reservoir length, high outflow discharge, large amount and high concentrations of incoming fine sediments as well as low and large outlets (i.e., enough to contain the turbidity current momentum). However, quantified conclusions and recommendations are hardly possible since systematic investigation of venting has not yet been performed. Research regarding venting should optimize efficiencies based on the systematic testing of some crucial and unstudied parameters such as outflow discharge, outlet height, and timing of opening. This optimization is particularly interesting for venting operations through outlets with limited discharge capacities where it is needed to understand how much sediments can be released by partial/suboptimal venting.

Fan (2008) reported a need for further work in the field of venting stratified flows such as turbidity currents while for instance, saline currents are much more investigated. Namely, turbidity current venting efficiencies are supposed to increase with increasing outflow discharges, but this relationship is expected to be log-shaped. Also, depending on the reservoir length, the number of outlets can be optimized. The smaller the reservoir length the higher the energy levels of the turbidity current reaching the dam site. This means that larger or multiple outlets might be needed for such reservoirs. Furthermore, the optimal opening timing cannot be predicted easily. Determining the most adequate height of the outlet is also essential. Outlets are preferably placed at the bottom for better venting results. However, one disadvantage of such a position can be the fast clogging of the outlet especially in case the turbidity current has a higher momentum than the outlet capacity. Outlets placed at higher levels do not have this

disadvantage but should operate in a way that the lower limit of the height of aspiration at least reaches the inflowing current.

On a different note, some more basic questions remain unclear and should be treated carefully: Wan et al. (2010) stated that reservoir operations related to water and sediments relied mainly on the rates observed at the hydrometric station at the entrance of the reservoir. These measured values can be largely different than the real rates of the turbidity current reaching the dam. This fact was proven by Oehy et al. (2000) based on data from the Luzzone Reservoir. It leads to the need to link reservoir operations to conditions observed the closest possible to the dam site rather than at the entrance of the reservoir. Fortunately, research on turbidity currents is developing and is able to offer better insight on the current's progression and characteristics from plunging until reaching the dam. Another interesting question concerns the frequency of turbidity currents observed at a specific reservoir: will they always and regularly form? In the Elephant Butte Reservoir for instance 13 currents entered the reservoir during the first 20 years and only one in the second 20 years. According to Lara (1960), this is probably due to a variety of causes, among which the growth of vegetation in the watershed. Another example is the Mapragg Reservoir in Switzerland where turbidity currents were observed once per year between 2007 and 2012 but did not appear again since 2012 (Axpo Power and Kraftwerke Sarganserland, 2013). This means that a good understanding of the watershed soil erosion and transport mechanisms is crucial.

2.10 Conclusions

Turbidity currents, known to be one of the main causes of sedimentation in many reservoirs, can become a means to prolong a reservoir's life only if their venting is applied in an optimal way. Generally, it is advised to vent regularly and from the very beginning of a reservoir's lifetime. Besides the advantages in terms of sedimentation, venting of turbidity currents offers an ecological favor to the downstream environment by transiting fine sediments. However, for good river revitalization, fine sediments are essential but not enough for the downstream environment and bed load sediment transport is also crucial.

Past research and field measurements showed that venting had varying efficiencies depending on many factors and one can always predict a better scenario of higher efficiency for each venting operation. However, quantified recommendations based on systematic research works related to venting of turbidity currents do not exist.

For this reason, the present research study aims at determining the conditions under which the most influential parameters result in efficient venting. In this goal, parameters such as

outflow discharge, venting timing, thalweg slope and duration of venting are experimentally investigated and their effect on venting efficiency is assessed for the first time. The study is also extended numerically and a wider range of parameters are tested including the outlet's dimensions and its vertical position above the reservoir's bottom.

Chapter 3

EXPERIMENTAL SET-UP AND PROCEDURE[2]

[2] Section 3.3.4 of Chapter 3 is based on the scientific article ‘’Measurement of the deposition of fine sediments in a channel bed’’ by S. Chamoun, J. Zordan, G. De Cesare and M. J. Franca, published in 2016 in the Journal of Flow Measurement and Instrumentation. The experimental work presented is original and was performed by the author.

3.1 Experimental set-up

Experimental tests were carried out in a flume characterized by a total length L_{flume} = 8.55 m, width w = 0.27 m, and total height H_{flume} = 1 m. It can be tilted from a horizontal position (0%) to a 5% slope. The flume (Figure 3.1, Figure 3.3(a), Figure 3.3(b)) is divided into three elements going from upstream to downstream: the head tank (0.8 × 0.27 × 1 m^3) (number 6), the main flume (6.7 × 0.27 × 1 m^3) (number 7) and the downstream compartment (1.05 × 0.27 × 1 m^3) (number 8). A downstream tank (number 9) and a mixing tank (number 5) are located below the flume at the downstream and upstream sides respectively. The mixing tank serves for the preparation of the water-sediment mixture (~0.7 m^3). It is equipped with a submerged pump allowing for internal recirculation of the mixture before and during the test. This process keeps the sediments in suspension inside the tank and ensures steady concentrations throughout the tests.

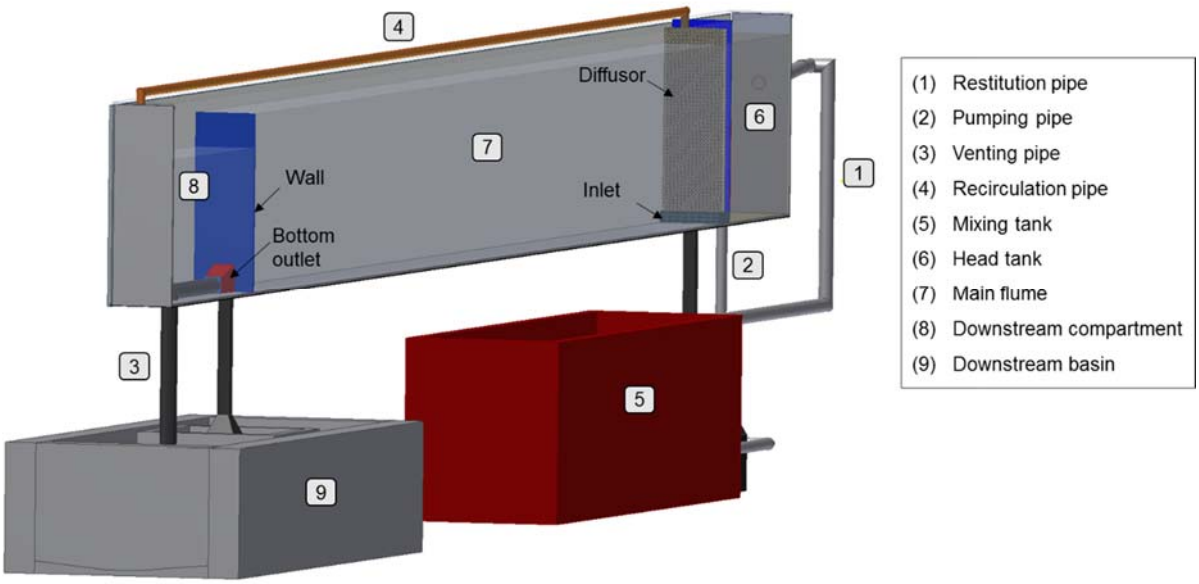

Figure 3.1: 3D schematic illustration of the experimental model showing its different components.

The head tank receives the water-sediment mixture from the mixing tank through the pumping pipe (number 2). The mixture can also flow in the opposite direction through a restitution pipe (number 1). A sliding gate, controlled by a lever, separates the head tank and the main flume. The two compartments are linked through a tranquilizer (the inlet) which has an opening height h_{inlet} = 4.5 cm (Figure 3.2). The latter regulates the scale of turbulence of the released current and gives a uniform distribution to the velocity field of the current. Note that

the head tank is equipped with a propeller mixer that allows mixing throughout the test to avoid deposition of the sediments and to maintain a steady concentration.

Figure 3.2: (a) The upstream system linking the mixing tank to the head tank, highlighting the restitution and pumping pipes; (b) the mixing tank with the water-sediment mixture inside being mixed by the recirculating pump; (c) system linking the downstream compartment of the flume to the main flume through the recirculation pipe along with the corresponding pump, also showing the lever used to open/close the sliding gate; (d) the inlet and the diffusor above it.

The main flume represents the reservoir in which the turbidity current flows. At the end of the main flume, a wall is fixed with a height $h_{downwall}$ = 0.8 m for the horizontal bed and the 2.4% slope and $h_{downwall}$ = 92 cm for the 5.0% slope. It simulates the dam and serves as a weir to maintain a constant water level in the main flume. A rectangular bottom outlet ($h_{outlet} \times w_{outlet}$ = 12 × 9 cm^2) is placed at the wall and centered on the width of the flume (Figure 3.3b).

The bottom outlet is linked to the downstream tank by the venting pipe (number 3), where a valve and an electromagnetic flowmeter are placed to control the outflow discharge. After venting the current, the released flow reaches a small container where continuous concentration measurements are performed, before spilling into the downstream tank (Figure 3.3).

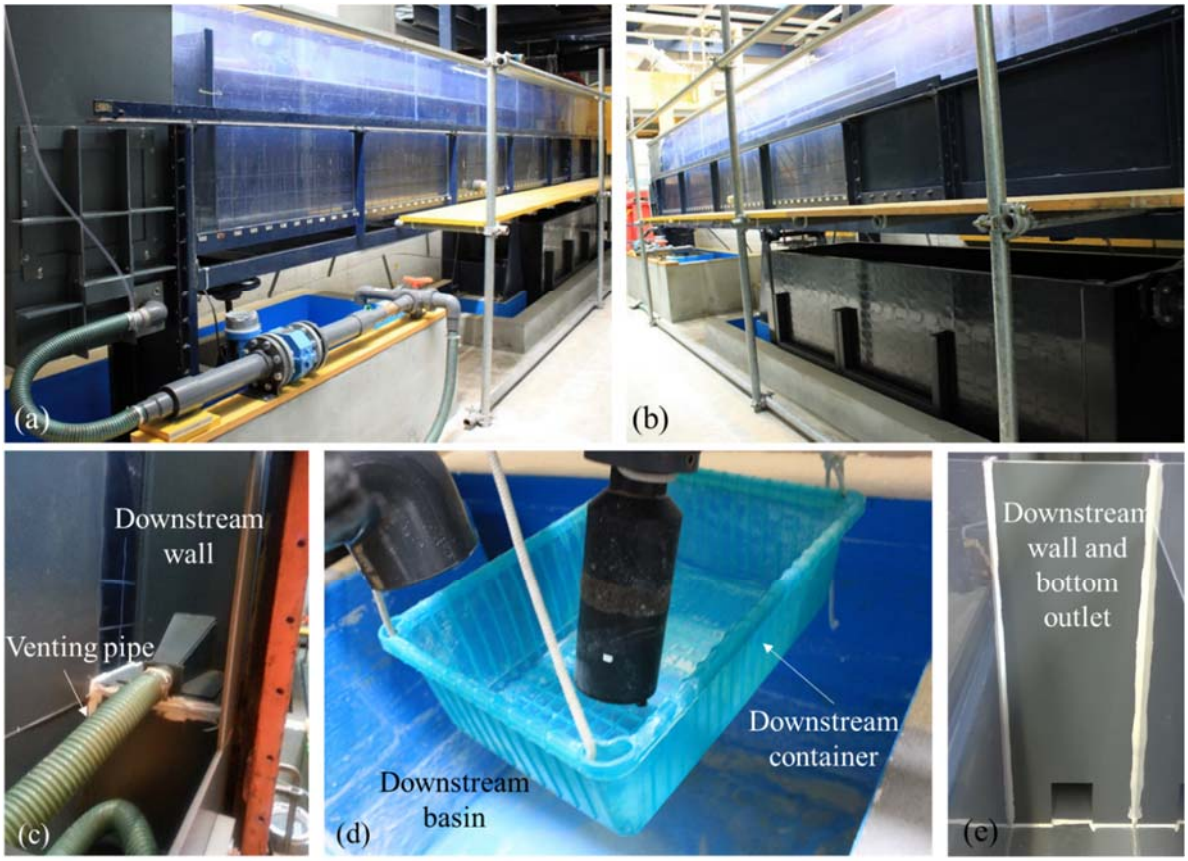

Figure 3.3: (a) view of the experimental model from the downstream side; (b) view of the experimental model from the upstream side; (c) Outlet seen from downstream side along with the venting pipe; (d) the downstream turbidity probe placed in the downstream container where concentration measurements are performed during venting before spilling into the downstream basin; (e) the downstream wall and the bottom outlet.

During the turbidity current flow, the water level in the reservoir is kept constant due to the spilling of clear water into the downstream compartment (number 8). However, in the case where the outflow discharge is larger than the inflow discharge, part of the spilled clear water of the downstream compartment is pumped back into the main flume through a recirculation pipe (number 4). A diffusor placed above the inlet receives the residual clear water and distributes it over its height. Thus, the water level of the main flume is prevented from decreasing.

3.2 Sediment material

Different materials can be used for the simulation of turbidity currents. Fine sediments that correctly scale settling velocities such as clay, chalk or silica flour present high electrostatic and capillary forces particularly when they settle (Kneller & Buckee, 2000). To solve this problem, larger grain sizes should be used, but in this case, significantly higher flow velocities are needed to keep the sediments in suspension, which can be a limiting condition for laboratory tests. A compromising solution consists of using fine sediments with a reduced density (such as the present case) as stated by Kneller and Buckee (2000). However, reducing the bulk density means that higher sediment concentrations should be used to obtain representative turbidity current densities. The increase of concentrations might affect the behavior of the sediment particles, namely the settling velocity, when compared with prototype turbidity currents that suspend sediments having similar diameters. Nevertheless, this type of material lowers scale effects to an acceptable extent relatively to the other options.

In the present work, a fine polymer powder was chosen and mixed with the water to simulate the sediments contained in turbidity currents. The fine sediments are a high performance thermoplastic polyurethane (TPU). The grain size distribution of the material was determined using a Malvern Mastersizer (Particle Size Analyzer by laser refraction) (Figure 3.4). The characteristic diameters obtained are d_{10} = 66.5 µm, d_{50} = 140 µm and d_{90} = 214 µm where d_x represents the grain size diameter for which x% of the sediments has smaller diameters. The density of the sediment material is ρ_s = 1160 kg/m^3.

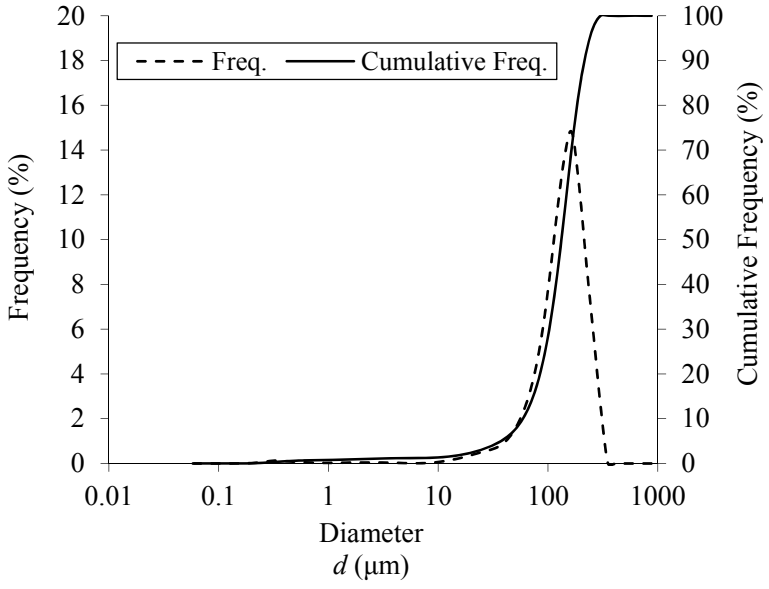

Figure 3.4: Grain size distribution of the sediments.

The mean diameter d_{50} was used for the estimation of the representative settling velocity of the material v_s. To calculate the settling velocity, two different equations were used. Stokes' Law was firstly applied:

$$v_s = g \frac{\rho_s - \rho_w}{\rho_w} \frac{1}{18\nu} d_{50}^2 \tag{3.1}$$

where g is the gravitational acceleration, ρ_w is the density of clear water, and ν the kinematic viscosity of water. The value obtained using Stokes' Law is v_s = 1.7 mm/s.

However, a microscopic photograph of the particles was taken (Figure 3.5) and showed that grain particles are angular. Since Stokes' Law is more adequate for spherical particles, a formula adapted for natural sediments (Cheng, 1997) was applied:

$$v_s = \frac{\nu}{d_{50}} (\sqrt{25 + 1.2 d_*^2} - 5)^{1.5} \tag{3.2}$$

where,

$$d_* = \left(\frac{\rho_s - \rho_w}{\rho_w} \frac{g}{\nu^2} \right)^{(1/3)} d_{50} \tag{3.3}$$

The output of this equation is v_s = 1.2 mm/s. In the following, an average value of v_s = 1.5 mm/s will be adopted.

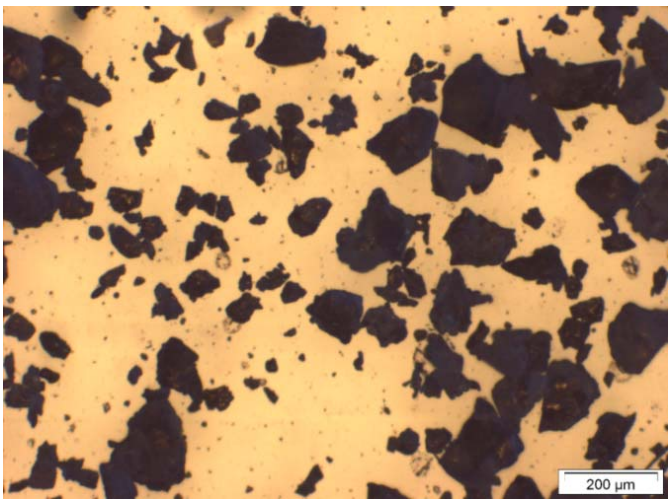

Figure 3.5: Microscopic photo of the sediment material.

One of the challenges encountered during the preparatory phase of the tests was the wetting of the sediment material. The preparation of the water-sediment mixture required initial wetting

of the material. Due to the fine grain sizes, an automatic mixer led to the formation of foam and the loss of substantial part of the wetted sediments. Therefore, the initial wetting was done in a small container where the sediments were manually kneaded with the water before being added to the mixing tank.

3.3 Measuring instruments

During the tests, different parameters were measured continuously. In Figure 3.6, the parameters as well as the measuring instruments described in the following section are illustrated on the experimental installation.

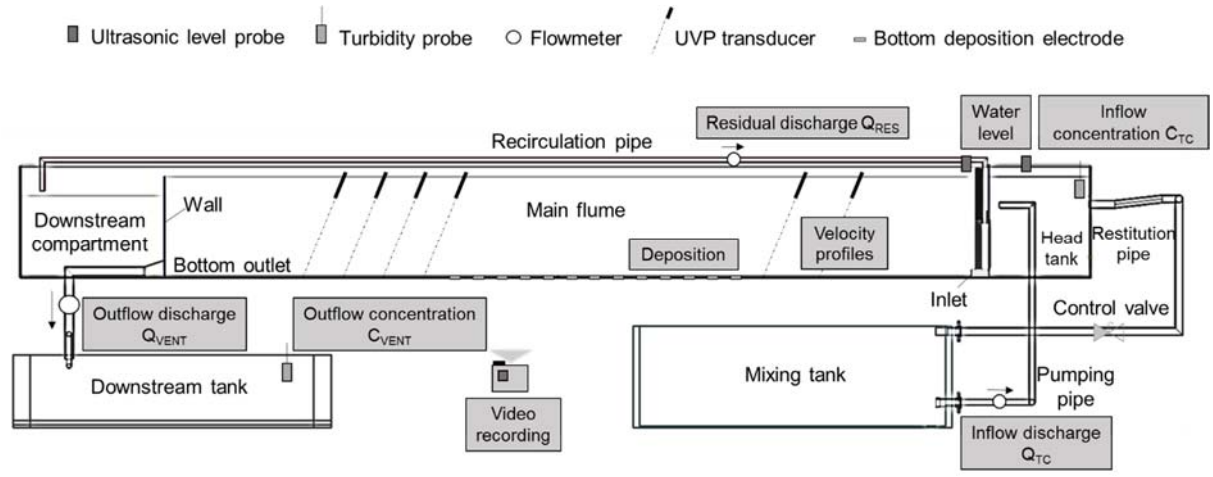

Figure 3.6: Diagram showing the different measuring instruments as well as the measured parameters (in grey frames).

3.3.1 Electromagnetic flowmeter

Three electromagnetic flowmeters (Endress+Hauser, Switzerland) were used to measure discharges. One is placed at the pumping pipe to monitor the inflowing discharge of the turbidity current Q_{TC}. A second flowmeter is placed at the venting pipe to measure the outflowing discharge Q_{VENT}. The third flowmeter is placed at the recirculation pipe situated between the downstream compartment and the main flume.

3.3.2 Ultrasonic level probes

Two ultrasonic level probes (Baumer, Switzerland) were placed in the head tank and in the main flume, upstream and downstream the sliding gate respectively. Water levels should be

kept constant and equal to avoid fluxes between the clear water in the flume and the mixture in the head tank. This would affect the mixture's concentration and the inflow discharge.

3.3.3 Turbidity probes

Two SOLITAX sc turbidity probes (HACH LANGE, Germany) were used. The measurement of the turbidity (in FNU) is converted to sediment concentrations (in g/l) using the calibration curve shown in Figure 3.7. One of the probes is placed in the head tank and measures the inflowing sediment concentration C_{TC}. The second is placed in the downstream container and measures the outflowing sediment concentration C_{VENT} of the evacuated water-sediment mixture.

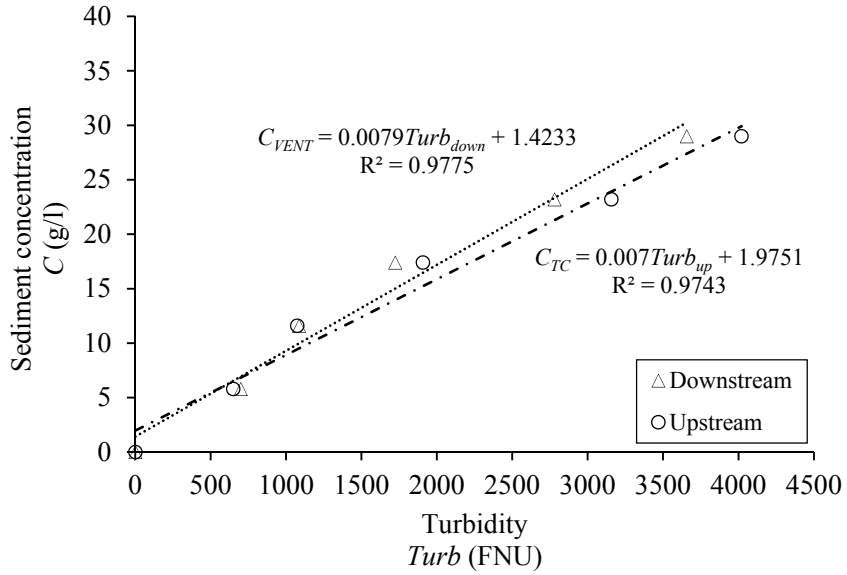

Figure 3.7: Calibration curves of the turbidity probes.

3.3.4 Electrical resistance-based depositometer ERBD

This instrument was developed by De Rooij et al. (1999) and measures the sediment deposit mass at the bottom of the flume. The calibration procedure of this instrument is complex and was combined with the calibration of a pulsed red laser diode (Chamoun, Zordan, et al., 2016). Parts of the article are used in the following.

This system is based on a technique developed by De Rooij et al. (1999). Its main principle relies on the fact that the electrical resistance of a deposited layer can be linked to its thickness or mass. In order to measure this resistance, two electrodes are used: (1) a stainless steel reference electrode placed inside the fluid above the deposited layer and (2) a bottom electrode

implemented in the bed where deposition takes place. A schematic illustration of the system is presented in Figure 3.8 where a common reference electrode is installed in the upper part of the channel and several bottom electrodes are installed along the channel bed. As shown, the two types of electrodes are connected to a Wheatstone Bridge which is in turn connected to an alternative current (AC) electrical source. The AC and a capacitor are used to avoid electrolysis of the water (Oehy, 2003). Using the bridge, the variation of the total resistance between the two electrodes can be measured. The latter is the sum of the resistance of the water above the layer and that of the layer. The water resistance depends on its temperature T as well as the height of the water column h_w - e. However, the temperature was shown to be the predominant parameter during the calibration process.

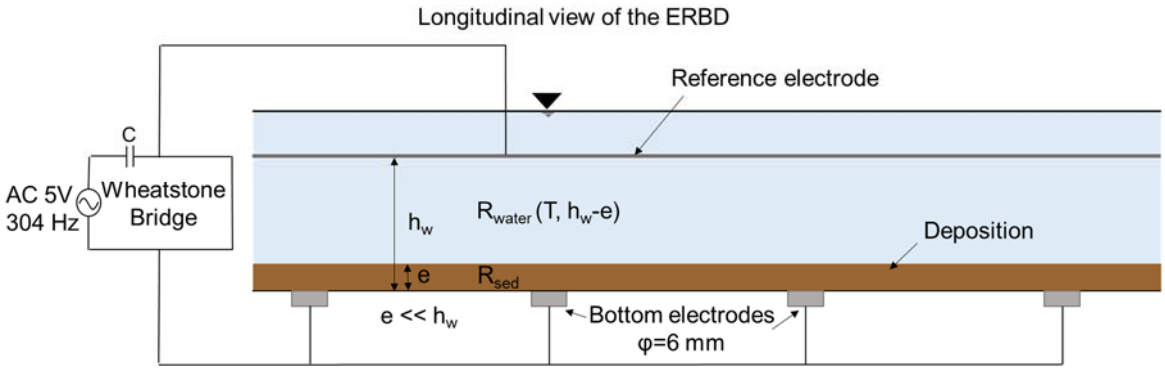

Figure 3.8: Schematic illustration of the ERBD system (longitudinal view of the flume).

More information, particularly on the electrical scheme, can be found in De Rooij et al. (1999) and Oehy (2003). Note that in the tests discussed here, the electrical characteristics used for the Wheatstone Bridge are similar to those used by Oehy (2003) i.e., AC electrical source frequency = 304 Hz, supply voltage = 5 V, lower resistance of the Bridge = 2.2 kΩ, upper resistance of the Bridge = 10 kΩ, Capacitance C = 470 nF.

Calibration apparatus and procedure

Measurements for the calibration took place in the main flume where the ERBD bottom electrodes (total of 62 bottom electrodes with a diameter of 6 mm each) have been implemented in the bed. Since all implemented electrodes are expected to have the same electrical behaviour -in terms of resistance- with the same depositional mass (De Rooij et al., 1999), one random bottom electrode was chosen to be calibrated. The calibration curve obtained can then be adopted for the whole system of electrodes.

The installation used for the calibration consisted of a Plexiglas cylinder of 15 cm diameter and 100 cm height. Plexiglas was chosen due to its transparency that allows to visually control the settling process. A stainless steel rod was inserted and welded in the cylinder at a distance of 10 cm from the bottom (Figure 3.9a). The cylinder was placed on an impermeable foam tape (Figure 3.9b) glued on the bottom of the channel. Weights were placed on the cylinder in order to maintain it in equilibrium when filled with water and to avoid leaks during the measurements. Additionally, a valve was placed above the rod (20 cm from the bottom) in order to subtract clear water from the column without causing any disturbances to the deposited layer.

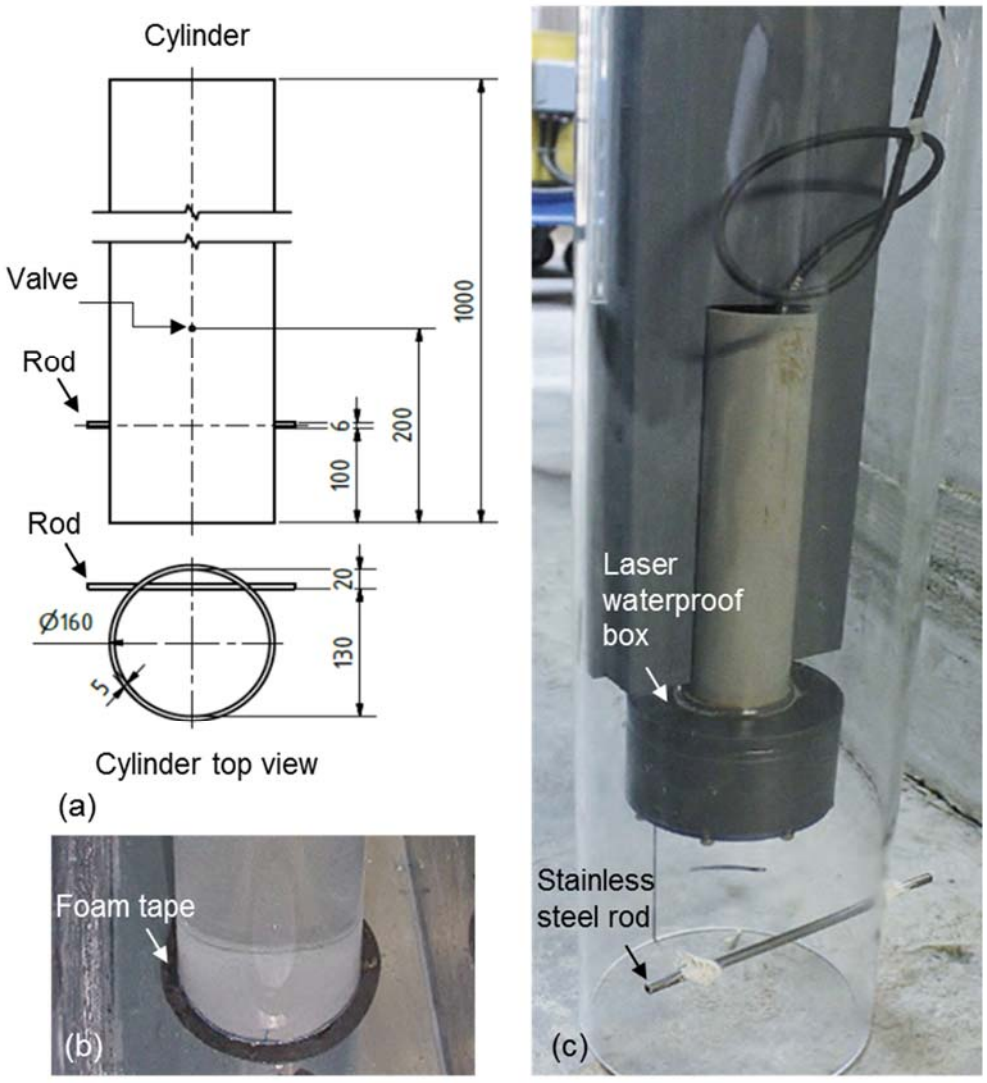

Figure 3.9: Experimental set-up showing (a) the dimensions of the Plexiglas cylinder (unit: mm) in a lateral ant top view, (b) the cylinder on the impermeable foam tape during the settling process of the powder and (c) the laser (calibrated simultaneously) waterproof box placed inside the cylinder (Chamoun et al., 2016).

A first phase of the calibration aimed to find the relationship between the water resistance and the temperature, without the introduction of any particles. For this goal, the cylinder was firstly filled with 32 cm of clear water at a very low temperature (5.5°C), and it was left to warm up until reaching the ambient temperature. Measurements of the resistance using the ERBD were made for different temperatures, which provided a relationship between water resistance and temperature (Figure 3.10).

A second phase consisted of measuring the resistance when adding amounts of the polymer powder to deposit. First of all, the temperature of the water and the clear water resistance were measured. Once the reference measurement (water only) was achieved, the cylinder's tap was opened and around one liter of clear water was withdrawn. This amount of water was used for wetting the sediments to be injected to ensure that the initial water column remains the same. 12 g of sediments were added and the mixture was dropped into the cylinder using a funnel to make sure the dispersion of the mixture in the column of water is as homogeneous as possible. This allowed a uniform settling process on the bed surface so that the local resistance measurements taken could be representative.

Once all the powder deposited and the water column became clear again (visual assessment), resistance measurements were taken. Thus, for a known amount of deposited powder corresponds a resistance given by the ERBD. Temperatures were also measured and taken into account for the calculation of the layer's resistance. After recording the needed values, another liter of clear water was withdrawn from the cylinder using the tap, and the same procedure was repeated.

Calibration curves

The calibration of the ERBD should be done for the particular material in use. The resistance measured depends on the packing density of the material and thus on its grain size as well as on the conductivity of the sediments. As mentioned previously, the total resistance measured at the Wheatstone Bridge (R_{total} in Ω) corresponds to the sum of the water resistance above the sediment layer (R_{water}) and the resistance of the layer (R_{dep}). Equation (3.4) summarizes this relationship as such (Oehy, 2003):

$$R_{total} = R_{water} + R_{dep} \tag{3.4}$$

The water resistance depends mainly on the temperature of the ambient water but also on the water column (h_w-e in Figure 3.8). However, in the present work, the initial water column h_w (before the injection of the mixture) is considered constant during and after the settling of

the sediments. In fact, the variations of this column are only due to the development of the deposition thickness *e*. Therefore, the reduction of the water column is considered negligible in the present experimental conditions ($h_w >> e$ in Figure 3.8).

The validity of this hypothesis, another cylinder was used during the first phase of the calibration procedure, with a rod placed 60 cm higher compared to the main cylinder. As such, the effect of the water column on the water resistance is evaluated. The new cylinder was filled with clear water at very low temperatures and was left to attain the ambient temperature. Therefore, similarly to the calibration procedure performed using the first cylinder, a relationship between clear water resistance and temperature was obtained for the second cylinder and can be seen in Figure 3.10 below.

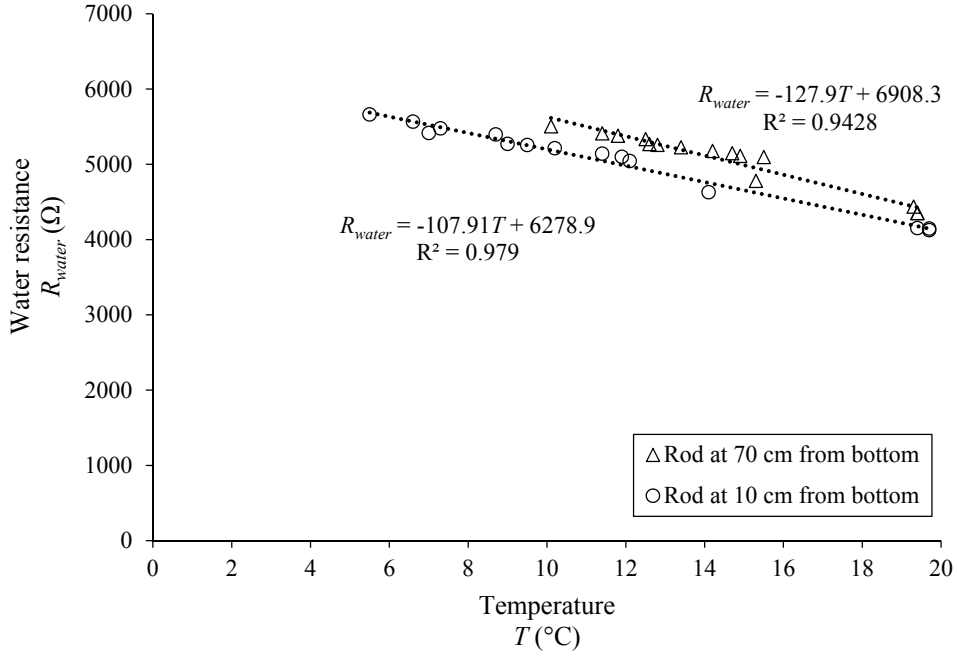

Figure 3.10: Relationship between the resistance of water and temperature for two different rod positions.

In fact, both cylinders gave relationships with very similar tendencies but with a small shift. Comparing the effect of a temperature unit (1°C) and that of the water column unit (1 cm), we conclude that the effect that the variation of the water column has on the water resistance represents only 5.4% of the effect that the temperature variation induces. These results validate the assumption of a constant water column before and after the addition of sediment masses under the experimental conditions. Therefore, the temperature will be the only parameter considered for the calculation of water resistance during the tests.

Once the relationship between clear water resistance and temperature found, the total resistance was measured by the ERBD while adding incremented sediment layers. Hence, the relationship between the added mass of sediments from one side and the resistance of the layer from the other was obtained by subtracting the water resistance R_{water} from the total resistance R_{total} (Figure 3.11). In order to convert masses into thicknesses, the bulk density of the sediment ρ_{bulk} = 1050.1 kg/m^3 determined using the laser instrument can be used. This bulk density can be measured by other means (e.g., settling funnel) but by using the mass-thickness relationship extracted from the laser, the precision is accurate.

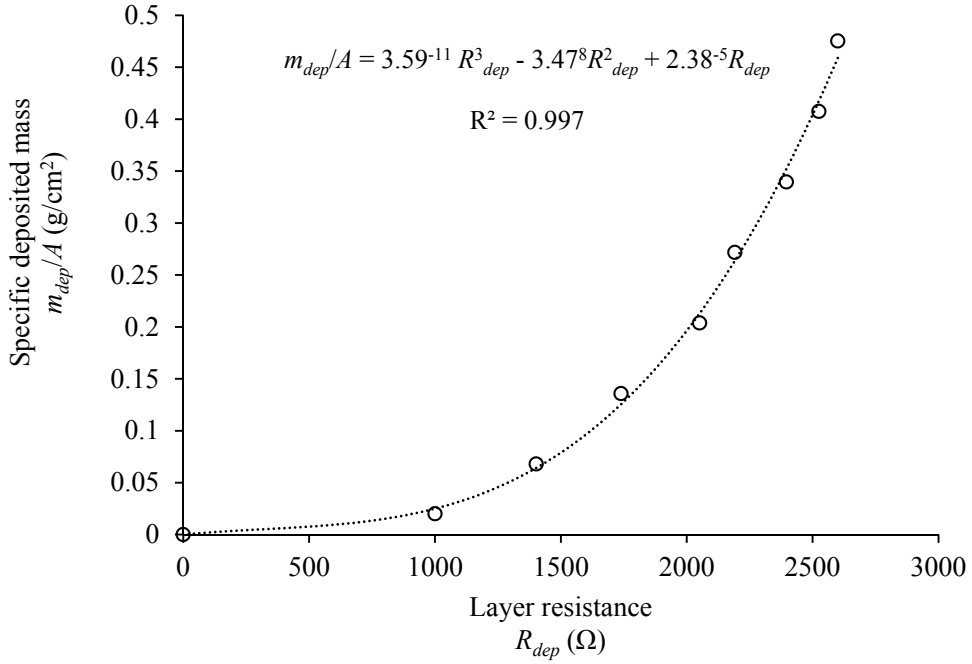

Figure 3.11: The sediment layer specific mass (surface area $A \approx 180$ cm^2) as a function of the resistance of the deposited layer. The dotted line represents a cubic polynomial curve adjusted to the empirical data with an $R^2 = 0.997$.

3.3.5 Thermometer

A thermometer was used to measure temperatures upstream (head tank) and downstream (main flume) of the sliding gate for two main reasons:

- Temperatures in the head tank and in the main flume should be close enough to keep the density difference solely due to the presence of suspended particles. The average temperature difference of the considered tests is 2.5 °C, which corresponds to a density difference of 0.00025 g/cm^3, equivalent to 7% of that due to the suspended sediments.

- The value of the resistance of water subtracted from the total measured resistance of the ERBD also depends on the water temperature.

3.3.6 UVP (Ultrasonic Velocity Profilers)

Six Ultrasonic Velocity Profilers (UVP, Metflow, Switzerland) are mounted 2.8 m, 4.1 m, 5.5 m, 5.8 m, 6.0 m, and 6.2 m from the inlet. The angle of inclination is 25° directed downstream with respect to the vertical. The emitting frequency is 4 MHz. The sampling period of the UVP is 38 ms per profile. Note that the use of a single UVP probe placed in the direction of the stream gives the streamwise component of the velocity. However, mixing occurs at the interface between the turbidity current and the ambient fluid creating a 3D velocity field, particularly at the head of the current. Therefore, only velocity profiles measured in the body of the current are used to characterize it.

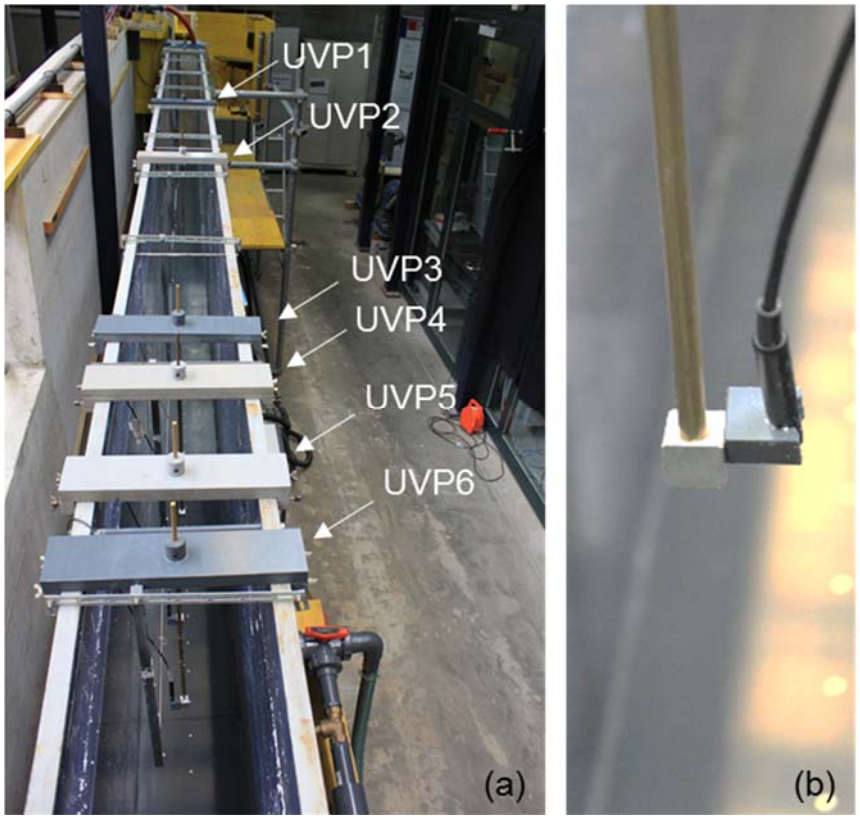

Figure 3.12: (a) UVP transducers positioned in the main flume and (b) UVP mount holding the transducer.

3.3.7 Camera recordings

A major key for understanding physical phenomena comes from observation. A camera was positioned in front of the channel to record the tests and capture photos every 5 seconds (the resolution of the video recordings is 1080p = 1980 × 1080 pixels).

Acquisition system:

All the measuring instruments were connected and controlled by one computer. A LabVIEW interface was created to run and stop the measurements simultaneously. The acquisition frequency of the flowmeters, level probes, turbidity probes, and the ERBD was around 2.75 Hz, which means that data was recorded each 0.36 s on average.

Figure 3.13: Apparatus of the acquisition system.

3.4 Experimental procedure

The experimental procedure of all the tests respect the following main steps:

1) The main flume was filled with clear water up to the height of the downstream wall (80 cm for the horizontal bed and the 2.4% bed slope and 92 cm for the 5.0% bed slope). Simultaneously, the mixture of water and sediments was prepared in the mixing tank.

2) Once the mixture in the mixing tank was ready (the needed volumetric concentration was reached), it was pumped into the head tank through the pumping pipe and restituted to the mixing tank through the restitution pipe. This recirculation ensured that the mixture is homogeneous between the mixing tank and the head tank. It also helped to establish adequate inflow discharge of the pump and lasted until reaching the expected concentration of the test in the head tank. Before starting the test, care was taken to have equal levels in the head tank and the main flume.
3) Once the concentration and water level conditions were fulfilled in the head tank, the valve placed on the restitution pipe was closed and the sliding gate opened. This procedure triggers a turbidity current inside the main flume due to the density difference between the mixture and the clear water. The current then formed in the main flume and traveled along the bed until reaching the bottom outlet. The same inflow discharge was maintained throughout the test, and the current was continuously-fed. The turbidity current flowed along the channel over a distance of 6.7 m and was monitored by the instruments described in section 3.3 throughout the test.
4) Depending on the timing tested, the bottom outlet was opened and venting started with a preset outflow discharge. The evacuated part of the current then reached the downstream tank where sediment concentrations were continuously measured. In the case where the outflow discharge Q_{VENT} > turbidity current Q_{TC}, the residual discharge $Q_{RES} = Q_{VENT} - Q_{TC}$ is ejected from the downstream compartment into the main flume through the recirculation pipe. Note that for each test, the duration was as long as possible. However, some constraints such as the capacity of the downstream tank and the total volume of the mixture used for a specific test shortened the duration for some tests more than others.
5) In two cases, the inflow was cut during venting. The upstream pump was stopped and the sliding gate was closed while venting was maintained.

3.5 Instrumentation accuracy

- The accuracy of the flowmeters, in the range of the discharge values used is ±0.6% (Endress+Hauser, Switzerland).
- The ultrasonic level probes have an accuracy around ±0.5 mm (Baumer, Switzerland).
- The accuracy of the turbidity probes is around ±1% of the measured value (HACH LANGE, Germany).

- In the case of the ERBD, three main sources of error exist. It can be due to the measured temperature used in the calculation of the water resistance. In fact, the local temperature measured might not be representative of the temperature of the whole water column and consequently causes over/underestimation of the water resistance. Using the data in Figure 3.10, an estimation of the generated error due to 1°C higher or lower than the actual temperature affects by ± 0.02 mm. In order to minimize this error, the measurement of temperature should be done at different points in the water column between the two electrodes. On another hand, the fluctuation of the total resistance measured can be caused by electrical noise. The mean standard error electrically generated in the present study is estimated by ±0.04 mm. Finally, as the deposition develops, the water column above continuously varies. However, as explained in section 3.3.4, this error is negligible and is estimated at 1.2×10^{-3} mm. To sum up, the total error that can affect the measured thickness of the deposit can be around 0.061 mm. This error depends on the value of the temperature difference between the water column and measuring point, the variation of the water column, and the stability of the electrical installation.

The main source of error using the UVP can be due to a misalignment of the transducers. The error in the inclination was estimated by Oehy (2003) as less than 0.5° (using the same type of UVP mount which corresponds to ±3% velocity error.

3.6 Dimensional analysis

Based on the theoretical background and literature review presented in Chapter 2, an assessment of the parameters governing the operations of venting turbidity currents through outlets was performed. Summarily, two categories of parameters can be distinguished: (1) parameters affecting the dynamics of the turbidity currents and (2) operational parameters related to the manipulation of the gates during/before venting. The first category includes parameters such as the **grain size distribution** of the sediments and their **density** which in turn depend on the **morphology** of the basin. In addition, the **geometry of the reservoir** (e.g., narrow, wide, steep), the **flood duration** and **discharge** also affect the dynamics and development of the currents. The second category concerns parameters related to the manipulation and characteristics of the gates during venting. Namely, the **outflow discharge**, the **timing** and **duration** of venting and **outlet's dimensions** and **position**. The parameters selected to be experimentally investigated in the present research are:

- Three different bed slopes *S*: a horizontal bed, a 2.4% slope and a 5% slope.

- For each slope, the outflow discharge Q_{VENT} normalized by the turbidity current's discharge Q_{TC} was systematically varied and evaluated. The ratio is called the venting degree $\phi = Q_{VENT}/Q_{TC}$.
- The timing of the outlet opening was varied relatively to the arrival of the turbidity current to the wall. Four different timing were tested: (1) an early venting timed before the arrival of the turbidity current to the wall/outlet at a distance $d/h_{outlet} = 5$, (2) an in-time venting synchronized with the arrival of the turbidity current to the wall, (3) a 30-s late venting and (4) a 60-s late venting.
- The duration of venting was assessed due to the high acquisition frequency of the measurements throughout the tests.
- Two tests were performed where the turbidity current inflow was interrupted before the end of venting, simulating the end of the flood.

The main criterion used for the evaluation of the chosen parameters is the release efficiency of venting.

3.7 Experimental tests

Before performing the systematic tests, some preliminary tests were performed, which allowed to establish an adequate experimental procedure and to make sure that all instruments are properly functional and well connected. Also, during preliminary tests, different concentrations were tested as well as different inflow discharges in order to find adequate conditions for the current to form and be sustained until reaching the outlet. Moreover, the initial conditions should not shorten the tests' duration. For instance, very high inflow discharges can keep all sediments suspended but result in short tests. Therefore, a compromise had to be reached. Once the procedure and boundary conditions were set, the series of tests began. A few tests were repeated and the results led to closely similar outputs, and most importantly, to the same conclusions and trends. Table 3.1 below presents the systematic tests performed.

Table 3.1: Overview of all performed experimental tests.

Test Number No.	Slope S (%)	Venting degree ϕ (%)	Opening timing d/h_{outlet} (-) or t_{after} (s)	Turbidity current inflow
E0.0	0	0	In-time	Continuous
E0.1		30		
E0.2		50		
E0.3		65		
E0.4		80		
E0.5		100		
E0.6		115		
E0.7		125		
E1.0	2.4	0	In-time	
E1.1		30		
E1.2		50		
E1.3		65		
E1.4		100		
E1.5		135		
E1.6		155		
E1.7		200		
E1.8		115	d/h_{outlet} = 5	Continuous
E1.9		115	t_{after} = 30 s	
E1.10		115	t_{after} = 60 s	
E2.0	5.0	0	In-time	Continuous
E2.1		50		
E2.2		100		
E2.3		115		
E2.4		135		
E2.5		155		
E2.6		200		
E2.7		115	d/h_{outlet} = 5	
E2.8		115	t_{after} = 30 s	
E2.9		115	t_{after} = 60 s	
E2.10		30	In-time	Stopped
E2.11		65	In-time	Stopped

Chapter 4

VENTING OF TURBIDITY CURRENTS APPROACHING A RECTANGULAR OPENING ON A HORIZONTAL BED[3]

The sediment release efficiency associated with venting turbidity currents on a horizontal bed is experimentally investigated in this chapter. In fact, in reservoirs where sedimentation in the dead storage has already occurred, the thalweg close to the dam tends to approach horizontal. This is due to the settling of suspended sediments that were not evacuated during past sedimentation events. The outflow discharge and duration of venting are the main parameters assessed. Venting efficiency is studied based on three different concepts: (1) a representative venting efficiency based on the average values of inflow and outflow sediment fluxes, (2) a global venting efficiency comparing integral values of inflow and outflow sediment fluxes during a certain duration of venting and (3) a local venting efficiency comparing masses starting at the arrival of the turbidity current to the outlet and taking into account deposited sediment masses. An efficiency indicator accounting for water losses is also introduced.

[3]Chapter 4 is based on the scientific article ‘’Venting of turbidity currents through a rectangular opening’’ by S. Chamoun, G. De Cesare and A. J. Schleiss accepted for publication in 2017 in the Journal of Hydraulic Research and on the conference article ‘’Experimental investigation on turbidity current venting under restrained outflow discharges’’ by the same authors, presented in the 8th International Conference on Fluvial Hydraulics, River Flow 2016. The experimental work presented hereafter is original and was performed by the author.

4.1 Test conditions

All the tests considered in the present chapter are performed using a horizontal bed (S = 0%), and venting is synchronized with the arrival of the current at the outlet. Additionally, initial conditions (i.e., inflow concentration and discharge) are not varied in order to assess the effects of operational parameters related to venting. Therefore, the steadiness of inflow concentrations, discharges and water levels upstream and downstream of the main flume were checked:

- The average initial turbidity current concentration of the considered tests (Table 4.1) is C_{TC} = 27 g/l corresponding to a volumetric concentration of 2.3%. The average standard deviation of the inflow concentration for a single test is 2.3 g/l, and the standard deviation of the concentration between the tests is 2 g/l. Thus, turbidity current initial concentrations were considered sufficiently constant throughout the tests.
- The average initial turbidity current discharge for all the tests is 1 l/s. For a single test, the average standard deviation of the turbidity current discharge is Q_{TC} = 5.10^{-3} l/s, and the standard deviation between the tests is 0.02 l/s. Quasi-steady conditions were also ensured at the inlet in terms of discharge.
- The average standard deviation of the outflow discharge for all the tests is 0.009 l/s, representing only 3% of the smallest tested outflow discharge (0.3 l/s). Thus, constant outflow conditions were accomplished during the tests.
- Differences between water levels measured at the head tank and the main flume during the tests are within 4 mm on average, representing 0.5% of the total water depth.

More information on the initial conditions concerning temperature and water depths measured at the head tank and in the main flume are provided in Appendix A2. In Table 4.1, the main initial conditions of the tests discussed in the present chapter are given. C_{TC} is the initial concentration of the turbidity current, ρ_{t0} is the initial density of the turbidity current, $g_0' = gC_{TC}\left((\rho_S-\rho_w)/\rho_w\right)$ (in which g is the gravitational acceleration and ρ_w the density of the clear water above the turbidity current) is the initial reduced gravity, $B_0 = g_0' q_{TC}$ (in which q_{TC} is the initial discharge of the current per unit width) is the initial buoyancy flux of the turbidity current (Graf & Altinakar, 1995), and $\Phi = Q_{VENT}/Q_{TC}$ is the venting degree where Q_{VENT} is the outflow discharge at which the outlet operates, normalized by the turbidity current's inflow discharge Q_{TC}.

Table 4.1: Inflow and outflow test conditions.

	Inflowing turbidity current					Venting degree Φ
Test No.	S **(%)**	C_{TC} **(g/l)**	ρ_{t0} **(kg/m^3)**	g'_0 **(cm/s^2)**	B_0 **(cm^3/s^3)**	Q_{VENT}/Q_{TC} **(%)**
E0.1	0.0	27.6	1003.5	3.74	143.1	30
E0.2	0.0	26.0	1003.3	3.53	130.8	50
E0.3	0.0	28.4	1003.6	3.86	139.2	65
E0.4	0.0	27.0	1003.4	3.66	139.0	80
E0.5	0.0	29.4	1003.7	3.99	151.3	100
E0.6	0.0	25.5	1003.2	3.46	127.1	115
E0.7	0.0	23.0	1002.9	3.12	115.8	125

4.2 Definition of venting efficiency

In the field, the definition of venting efficiency depends on the monitored parameters and their locations. Since venting operations take place mostly during flood conditions, measurements are more difficult than in normal flow conditions. In past experiences, instruments were dislodged, buried under thick sediment deposits or damaged by powerful turbidity currents (De Cesare et al., 2006; Khripounoff et al., 2003; Paull et al., 2003; Xu et al., 2004). In the laboratory, measurements are better controlled, which allows systematic investigations of venting efficiency and a better understanding of the physical phenomenon.

4.2.1 Venting efficiency in literature

To date, the discussion of venting efficiency (VE) has been largely based on a definition that can be easily applied using field measurements. Efficiencies are calculated through the ratio of the total evacuated sediment mass to the total inflowing sediment mass of the turbidity current in the reservoir during a flood event (Morris & Fan, 1997; Lee et al., 2014):

$$VE = \frac{M_{VENT}}{M_{TC}} = \frac{\int_{t=0}^{t=T} C_{VENT} Q_{VENT} \mathrm{d}t}{\int_{t=0}^{t=T} C_{TC} Q_{TC} \mathrm{d}t} \tag{4.1}$$

where M_{VENT} and M_{TC} represent the total masses of outflowing and inflowing sediments, respectively; C_{VENT} and C_{TC} are the sediment concentrations of outflow and inflow turbidity current, respectively, at time t; Q_{VENT} and Q_{TC} are the outflow and turbidity current discharges, respectively, at time t; and T is the total duration of the flood event (Lee et al., 2014).

However, it is hard to compare venting efficiencies based on field data from different reservoirs. In fact, measurements of discharges and concentrations, particularly related to inflow, can be located at different locations of the upstream river/reservoir. Nonetheless, before, during, and after plunging, the concentrations and discharges of the sediment-laden flow are highly variable. In the field, in most cases, the reservoir represents a type of black box, in which depositional and erosional fluxes are rarely known. Thus, the amount of suspended sediments of the turbidity current in the vicinity of the dam can be very different from what is measured in the river or at the entrance of the reservoir. Hence, different approaches are proposed in this chapter to improve the calculation of venting efficiency.

4.2.2 Discussion of the definition of venting efficiency

In their experimental work, Lee et al. (2014) used steady inflow (i.e., concentration and discharge) and outflow (i.e., discharge) conditions and observed a quasi-steady outflow concentration during venting. To calculate the efficiency of venting, Lee et al. (2014) considered the steady values of inflow and outflow concentrations and discharges to calculate a representative value of efficiency. This definition is firstly applied in this chapter and called the *''representative venting efficiency (RVE)''*.

On another hand, equation (4.1) provides a global comparison, for the whole duration of a venting operation, between masses of sediments flowing into the reservoir and out of it. This definition is easy to apply in the field, as measurements are generally performed at the entry of the reservoir (or in the river upstream of the reservoir), and at the outlets. However, it does not account for what happens in the reservoir.

Experimental studies offer the possibility to investigate these processes further because measuring instruments can be mounted more easily in the laboratory than in the field. Furthermore, test runs can be repeated. The definition of venting efficiency can be refined with the help of experiments to account for only the most influential parameters in terms of time and sediment masses. Equation (4.1) is firstly re-written by separating the inflow duration into two parts, those before and those after the moment at which venting has started. The times corresponding to the beginning and end of venting are called T_{vi} and T_{vf}, respectively. The output of this equation is called the *''global venting efficiency (GVE)''*:

$$GVE = \frac{M_{VENT}}{M_{TC}} = \frac{\int_{t=T_{vi}}^{T_{vf}} C_{VENT}\, Q_{VENT}\, dt}{\int_{t=0}^{T_{vi}} C_{TC}\, Q_{TC}\, dt + \int_{t=T_{vi}}^{T_{vf}} C_{TC}\, Q_{TC}\, dt} \tag{4.2}$$

During venting, the outlet discharges are generally small and depend on the turbidity current discharge. This results in a localized zone of aspiration at the outlet. Thus, it is reasonable to assume that the potential for eroding and evacuating sediments that have already deposited before venting has started is negligible. Therefore, in the denominator of Equation (4.2), the mass of sediments inflowing into the reservoir before venting has started (from $t = 0$ to $t = T_{vi}$) will not be considered. This hypothesis is especially acceptable in the case of this work where the tests are achieved on a smooth bed, and the outlet can only evacuate sediments transported by the turbidity current.

In addition, because the outlet discharges are relatively low, venting does not normally cause any drawdown in the reservoir level. Therefore, unlike flushing operations, venting does not induce retrogressive erosion. Thus, sediments that deposit in the reservoir before and during venting can hardly be eroded. The deposited mass cannot be vented and will ‘’artificially’’ reduce the value of the efficiency. For this reason, to reach a more ‘’localized’’ experimental view of the venting operation, deposition will be subtracted from the turbidity current inflow mass. Consequently, a new definition is proposed for the venting efficiency. It is called the *‘’local venting efficiency (LVE)’’*:

$$LVE = \frac{M_{VENT}}{M_{TC}} = \frac{\int_{t=T_{vi}}^{T_{vf}} C_{VENT}\, Q_{VENT}\, dt}{\int_{t=T_{vi}}^{T_{vf}} C_{TC}\, Q_{TC}\, dt - \int_{t=T_{vi}}^{T_{vf}} \dot{m}_{dep}\, dt} \tag{4.3}$$

where $\dot{m}_{dep}$ is the deposited sediment mass flow rate. Yu et al. (2004) noted the complications encountered when experimentally dealing with the selective withdrawal of sediment-laden currents. In fact, the deposition occurring throughout the test renders the analysis more complex. For this reason, Yu et al. (2004) produced saline currents. In the present work, the turbidity currents were simulated with suspended sediments and the deposition problem was solved by measuring deposition in time and space throughout the tests using the ERBD (Chapter 3, section 3.3.4).

4.3 Results

4.3.1 Experimental observations

During each test, the turbidity current is released from the inlet and flows through the flume (Figure 4.1). As it advances, the velocity of the front of the current decreases. Consequently, the height of its head increases. This height increase is accompanied by a slight lift in the position of the current's nose. The latter observation is consistent with the theoretical model developed by Simpson and Britter (1979) based on gravity currents advancing along horizontal boundaries with no-slip conditions. The clear water immediately fills up the space below the risen nose.

When the current reaches the outlet, the height of its head is 40 cm on average, corresponding to 3.3 times the height of the bottom outlet (12 cm).When the front of the current reaches the bottom outlet, the latter is opened. The current rebounds and slowly climbs up the wall (Figure 4.2). At the moment when it reaches the water surface, it begins reflecting upstream. The reflected part of the current is denser than the clear water above and lighter than the continuously inflowing turbidity current below it. Therefore, at the beginning of the reflection, an interflow is temporarily formed. The latter is less and less visible in time as the reflected current gets progressively diluted due to clear water entrainment and spreads on the whole water column. The reflection slowly progresses upstream and lasts as long as there is a continuous inflow. Because the turbidity current can climb to the top of the downstream wall in most cases, some losses of suspended sediments were noted over the weir. However, the turbidity of the spilled water was visually much lower than the one observed at the muddy lake and the effect on the venting process and efficiency was considered to be negligible.

Figure 4.1: Turbidity current advancing in the flume at three different positions towards the outlet. The position and corresponding time of the test are also given (test E0.5).

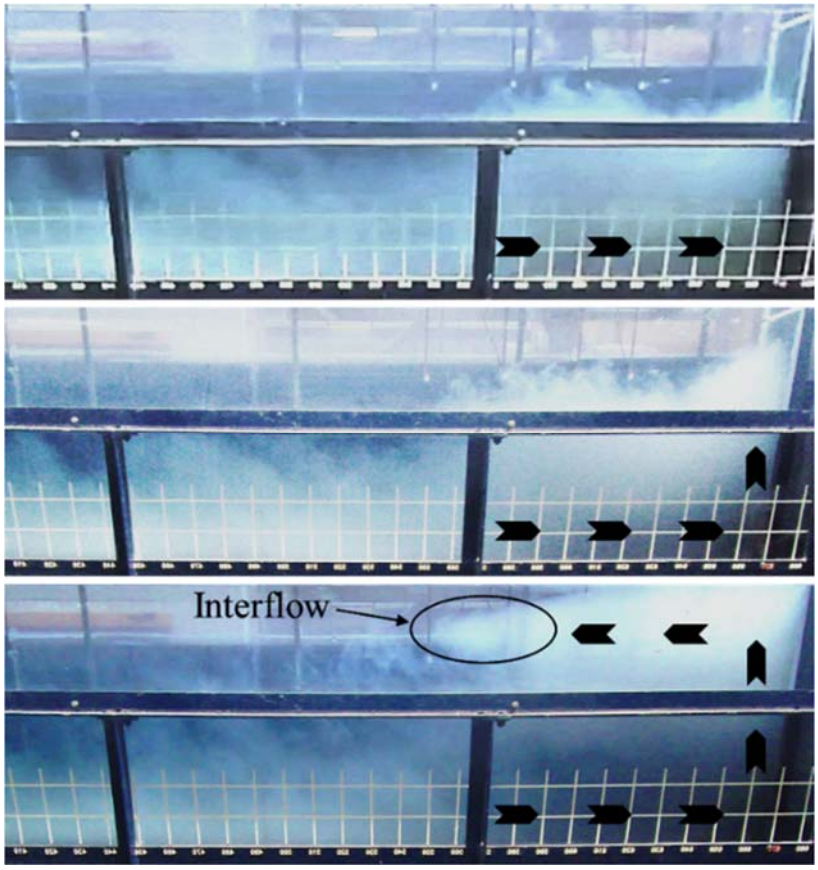

Figure 4.2: Turbidity current after its arrival at the outlet and the reflection of the part of the flow that is not vented (test E0.5).

4.3.2 Front velocities

Front velocities are evaluated by observing the position of the front of the current based on videos taken throughout the tests. The front velocity, which is normalized using the representative settling velocity (of the d_{50}) of the material, at different positions x/L from the inlet is shown in Figure 4.3. The observations begin around $x/L \approx 0.44$ (2.9 m from the inlet) because the first part of the flume is hidden by a metallic structure; thus, the current cannot be observed. In all the tests, the front of the current decelerates from an average velocity of 4.1 cm/s to 2.1 cm/s over the distance from $x/L = 0.44$ to $x/L = 1$. This is because the current is depositing and g' is therefore decreasing as the current moves down the flume. The deceleration is linear and exhibits a closely similar trend between the different tests. In fact, this deceleration is expected on a horizontal slope and was observed and discussed in literature. In Figure 4.3, the results from the present work are compared with other data from Altinakar et al. (1990), who worked with gravity currents on small slopes. The data in Figure 4.3 are of turbidity currents with two different types of sediment material advancing on a horizontal slope. The

goal of this comparison is to confirm that with different sediment material used experimentally, and thus different settling velocities, a horizontal bed results in a front deceleration. Differences in the trends are mainly due to different initial buoyancy fluxes and sediment material types.

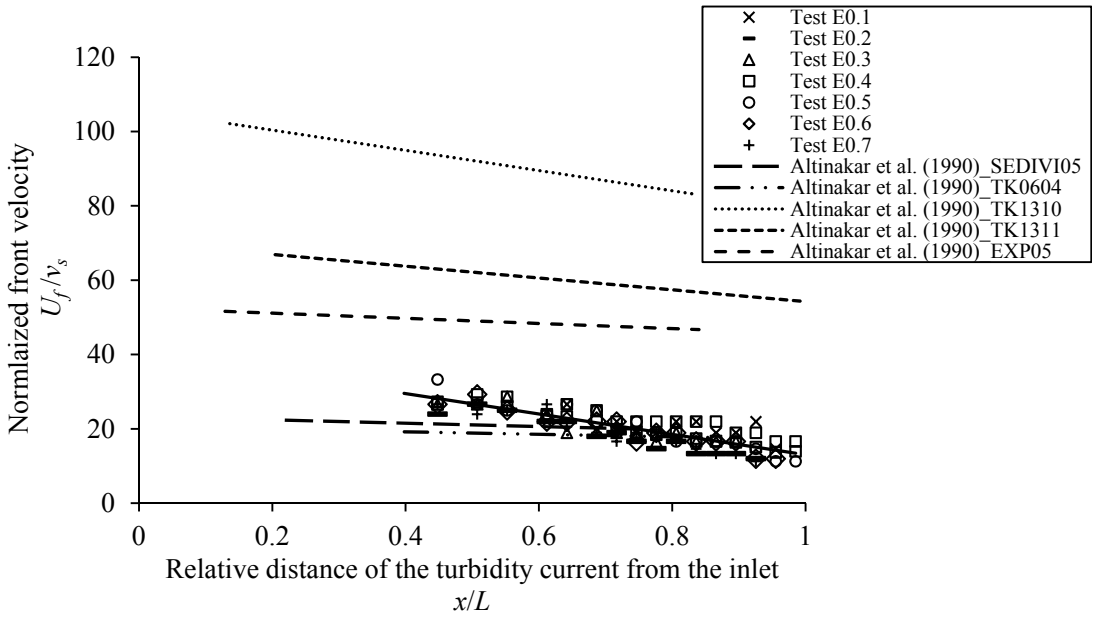

Figure 4.3: Deceleration of the front velocity for tests E0.1 to E0.7 based on turbidity currents advancing on a horizontal bed. Data from the present study and from Altinakar et al. (1990) are presented. All considered tests from Altinakar et al. (1990) were performed on a horizontal bed. TK0604 and SEDIVI05 use coarser material (d_{50} = 32 µm), while TK1310, TK1311 and EXP05 use finer material (d_{50} = 14 µm). All tests shown in this graph are continuously-fed.

Britter and Linden (1980) also found that for bed slopes of $0° \leq \alpha \leq 0.5°$, the heads of saline currents decelerated away from the source. This deceleration is explained by the fact that the buoyancy force component down the slope does not exist for horizontal beds; thus, it does not counterbalance the bed friction, unlike the case where a slope exists. However, Bagnold's auto-suspension criterion (Bagnold, 1962), ensured for $v_s/U_f < \sin\alpha$, is systematically not satisfied for a horizontal slope (Altinakar et al., 1990) because $v_s/U_f > \sin\alpha$, which is 0 in this case. In the case of the horizontal bed, $0.035 < v_s/U_f < 0.088$.

4.3.3 Head velocity

Velocity profiles close to the outlet (i.e., placed at x = 5.5, 5.8, 6.0 and 6.2 m from the inlet while x_{outlet} = 6.7 m) are used to characterize the velocity profiles in the head of the turbidity currents. In fact, the latter are reflected as soon as they reach the wall, before the arrival of their

body below the UVP transducers. Figure 4.4 shows the measuring axis (dashed lines) of the UVP transducers relatively to the current at the moment of reaching the dam.

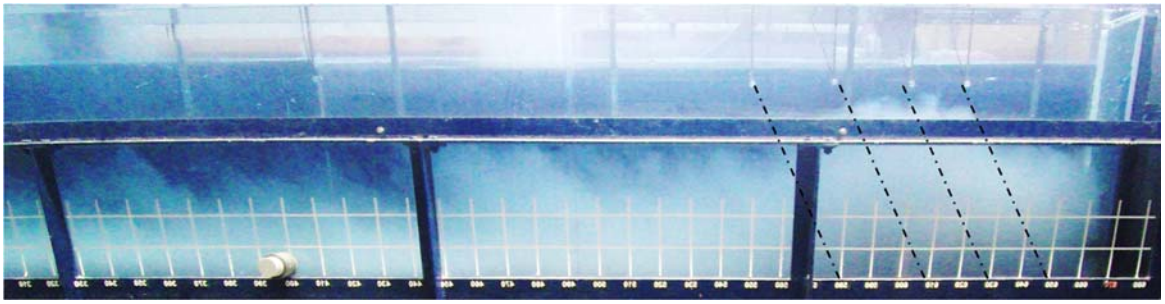

Figure 4.4: The measurement axis (dashed lines) of the UVP transducers placed in the vicinity of the outlet relatively to the turbidity current reaching the outlet.

Figure 4.5 shows average velocity profiles measured at different positions (i.e., UVP2, UVP3, UVP4, UVP5 in Figure 3.12 of Chapter 3). As concluded through the observation of front velocities, it can be seen that the current decelerates. Moreover, Figure 4.5 shows the lift of the nose as observed previously (section 4.3.1).

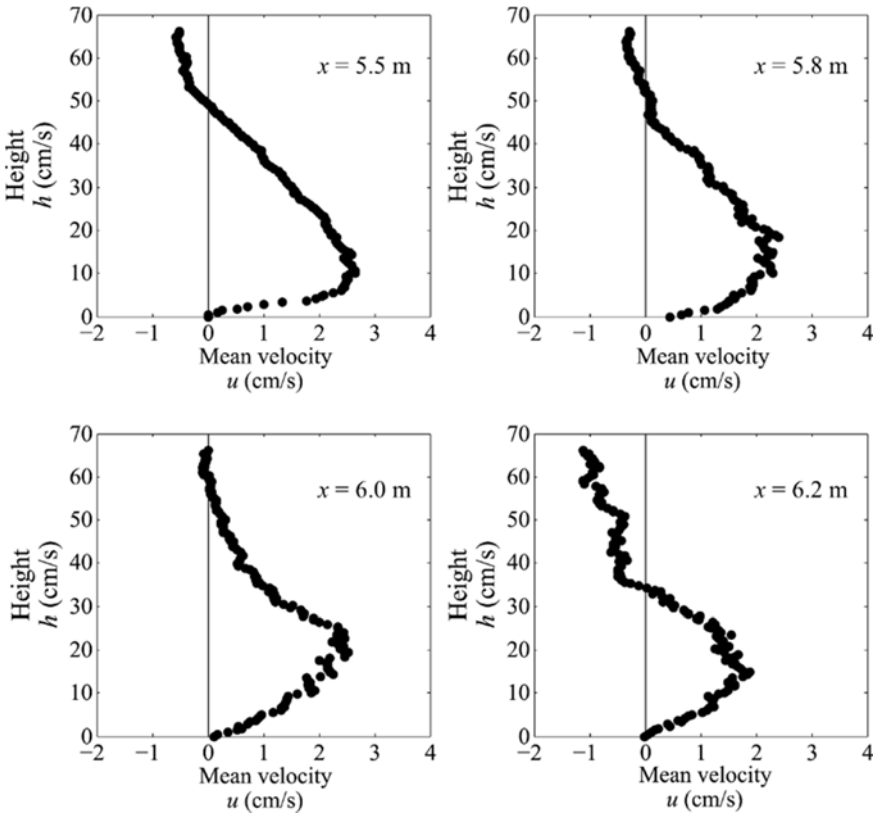

Figure 4.5: Averaged head velocity profiles of the turbidity current at x = 5.5, 5.8, 6.0, and 6.2 m (UVP2, UVP3, UVP4, UVP5) from the inlet.

It should be stated that the head of a turbidity current is highly turbulent, and thus velocities in this region can be two or three-dimensional. In the case of this narrow flume, lateral velocities can be neglected but vertical velocities exist, particularly in the head, and can be seen visually. Therefore, these 1D velocity profiles provide part of the information on the behavior of the current in terms of velocities. Note that the profiles shown in Figure 4.5 below are the average of 85, 36, 25, and 10 instantaneous profiles (obtained every 38 ms) respectively, belonging to the head of the current.

4.3.4 Turbulence rate

The level of turbulence is evaluated using the Reynolds number *Re*. Because all the tests have very similar initial conditions, an average $Re = UH/v$ is calculated and is approximately 5×10^3. In the latter equation, U and H are the characterizing velocity and height of the current, respectively, and v is the kinematic viscosity of water. U and H are calculated by applying the equations proposed by Ellison and Turner (1959) (Chapter 2, Equations (2.6) and (2.7)) using the UVP velocity profiles acquired 4.1 m from the inlet. The profiles at this location were selected by discarding the profiles taken in the head and keeping the ones taken in the body of the current. Figure 4.6 shows the mean velocity profile normalized by the maximum velocity (U_{max}) as a function of the measured height h normalized by h_{max} (corresponding to U_{max}). The characterizing height obtained is $H = 23.9$ cm and the characterizing velocity $U = 2.2$ cm/s.

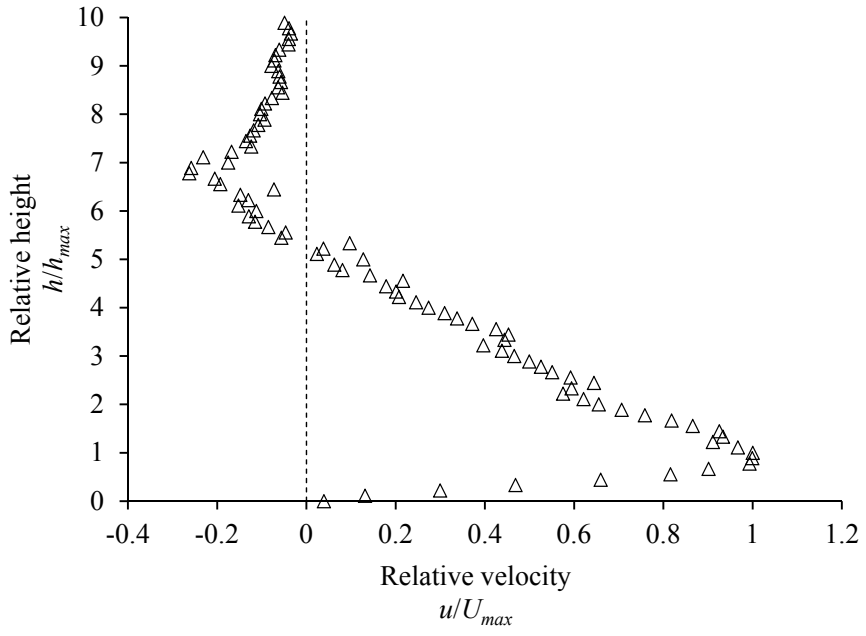

Figure 4.6: Average velocity profile of the turbidity currents flowing on the horizontal bed, 4.1 m from the inlet.

4.3.5 Deposition

The measured value provided by the ERBD is a mass by surface area. Therefore, the total mass deposited calculated at each probe corresponds to the measured value of mass by surface area multiplied by the distance a (= 10 cm) between two probes and the width of the channel w. It is thereby assumed that the deposition is linearly distributed between the probes. The variation of the deposited sediment mass m_{dep30} measured with a time step Δt = 30 s is plotted in Figure 4.7. The curve corresponding to the timing of the opening of the bottom outlet (T_{vi}) is highlighted in gray.

The rate of deposition Δm_{dep30} starts decreasing from t = 90 s and becomes more or less steady around t = 210 s. Spatially, the turbidity current deposits more sediment close to the inlet, and deposition decreases and becomes less variable farther from the inlet. Exceptionally, the first bottom electrode measures no or slight deposition due to the high erosion occurring at this location where the turbulent current is released. Similar trends were also observed by Oehy (2003), Oehy and Schleiss (2007), and Oehy et al. (2010).

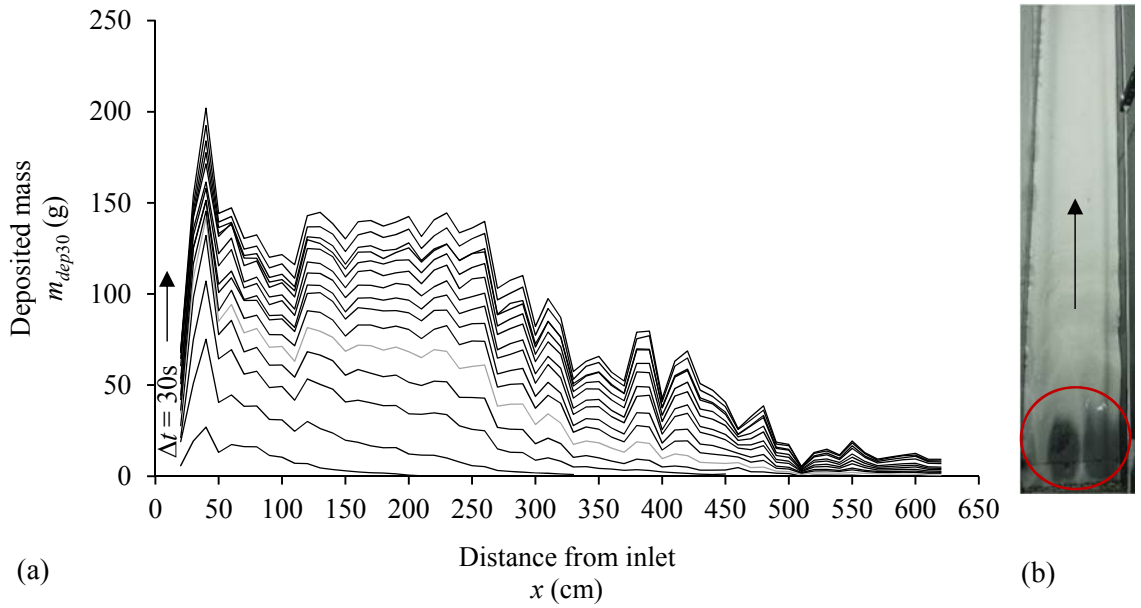

Figure 4.7: (a) cumulative mass of deposited sediments (over $a \times w$ = 270 cm^2) plotted in space and time along the flume (test E0.4), (b) top view of the main flume after the test showing the deposited sediments in the vicinity of the inlet; the red circle highlights the erosion immediately downstream of the inlet.

4.3.6 Outflow concentration

Values of outflow concentrations are plotted every 0.36 s (measurement frequency), allowing a detailed assessment of their variations. However, in the following, data was plotted every 1.8 s for a clearer assessment. In all cases, a quasi-steady value of concentration is reached after approximately $t\text{-}T_{vi}$ = 100 s (Figure 4.8 and Figure 4.9). Yu et al. (2004) theoretically demonstrated that outflow concentrations reach a steady state corresponding to the concentration of the body of the vented density current. However, the quasi-steady state is reached in different ways. For small venting degrees such as the cases of Φ = 30% and Φ = 50%, a steady state is reached progressively after the opening of the outlet. For the higher venting degrees such as the cases of Φ = 80% and Φ = 115%, high concentrations are observed at the beginning of venting, followed by a decrease towards the steady state. In Figure 4.8 and Figure 4.9, two examples of each case are shown (outflow concentrations corresponding to all the tests are provided in Appendix A3). These trends can be explained by the ability of higher venting degrees to withdraw suspended sediments from the muddy lake formed close to the outlet. The muddy lake is formed once the turbidity current reaches the wall and its concentration increases with the duration of the inflow. It has a higher sediment concentration compared to the turbidity currents reaching the wall. Thus, withdrawing from it results in high concentrations in the vented fluid which decrease when the current starts reflecting upstream.

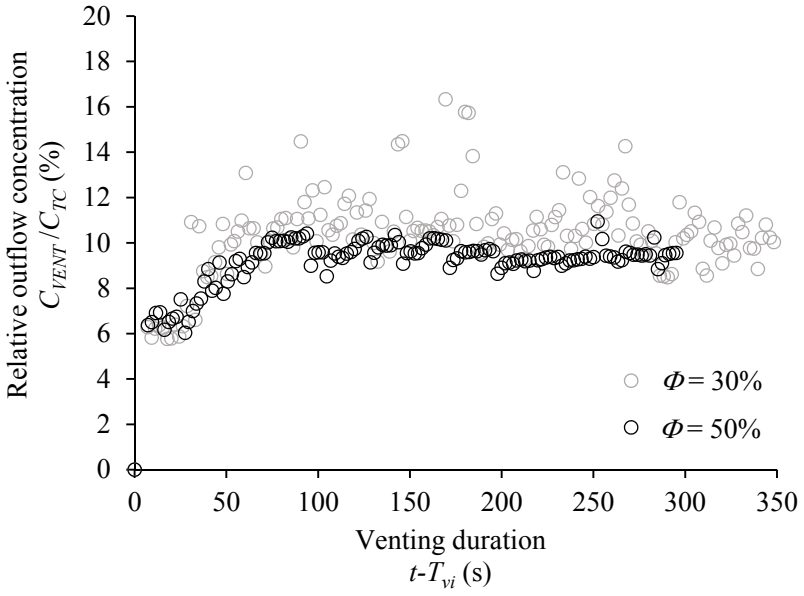

Figure 4.8: The relative outflow sediment concentrations at venting degrees of Φ = 30% (test E0.1) and Φ = 50% (test E0.2).

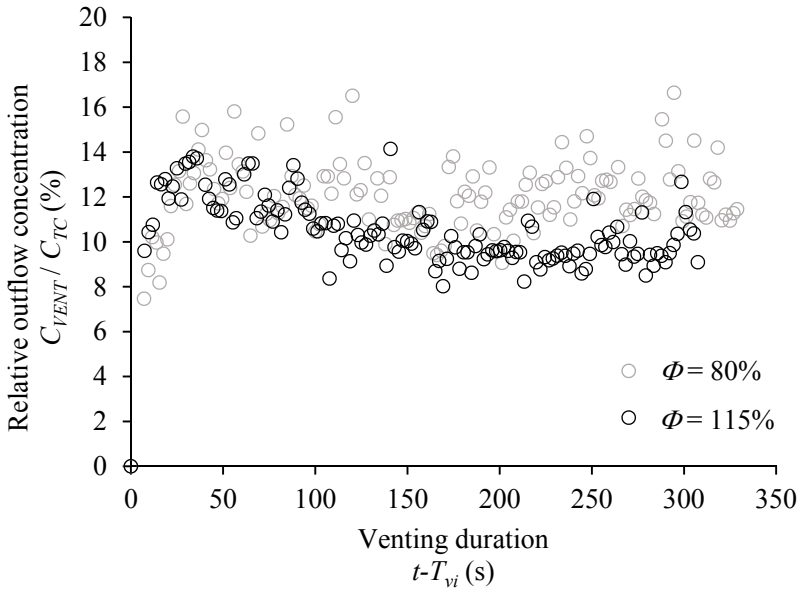

Figure 4.9: The relative outflow sediment concentrations at venting degrees of Φ = 80% (test E0.4) and Φ = 115% (test E0.6).

Figure 4.8 and Figure 4.9 show that the steady state of C_{VENT}/C_{TC} is approximately 10% to 12%. This is explained by substantial dilution of the turbidity current that reaches the outlet compared to the initial concentration of the turbidity current C_{TC}. This result is directly linked to high deposition as well as the entrainment of ambient clear water.

To improve the analysis, the duration of the test is normalized. One of the parameters used for this normalization is the limiting height of aspiration, defined in Chapter 2, section 2.6.3. Fan (1960) suggested the following equation to calculate the height of aspiration h_L when venting a sediment-laden flow through an orifice:

$$\left[\frac{\Delta\rho}{\rho_w}\frac{g(-h_L)^5}{Q_{VENT}^2}\right]^{1/5} = -1.2 \tag{4.4}$$

where $\Delta\rho = \rho_t - \rho_w$ represents the density difference between the vented turbidity current ρ_t and the clear water ρ_w above the current. h_L is the height of aspiration, and g is the gravitational acceleration. According to Graf and Altinakar (1995), ρ_t can be expressed as follows:

$$\rho_t = C_s\rho_s + (1-C_s)\rho_w \tag{4.5}$$

Because no concentration measurements are available close to the outlet, the concentration C_s of the turbidity current approaching the outlet right before its venting will correspond to the average of the steady state of C_{VENT}.

The aspiration heights obtained in all tests using Equation (4.4) are shown in Figure 4.10 below. The height of the central axis of the outlet (6 cm above the bed) was used as the 0 level in the graph below. Note that for Φ = 125%, h_L = 27 cm is still lower than the height of the head of the current approaching the bottom outlet (section 4.3.1).

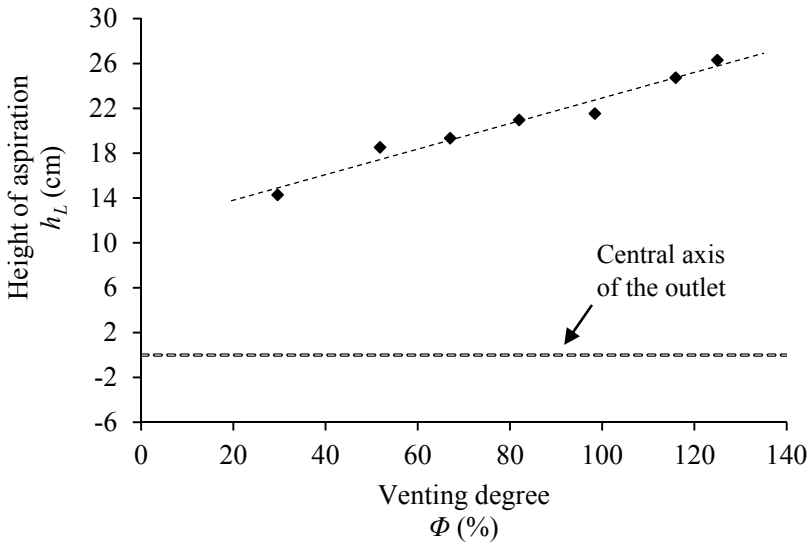

Figure 4.10: Aspiration heights calculated using equation (4.4) for different venting degrees $\Phi = Q_{VENT}/Q_{TC}$. The relationship between the two parameters is linear.

Additionally, using C_s, the reduced gravity g'_{app} of the current approaching the dam can be estimated.

$$g'_{app} = g\left(\frac{\rho_s - \rho_w}{\rho_w}\right)C_s \tag{4.6}$$

Using the two parameters h_L and g'_{app}, the venting duration can be normalized as follows: $\bar{t} = (t - T_{vi})^2 g'_{app} / h_L$.

4.3.7 Venting efficiency

Representative venting efficiency

Because a steady state outflow concentration is reached during turbidity current venting, a representative venting efficiency (*RVE*) (section 4.2.2) can be computed. It is defined as the ratio between the averaged value of the outflow mass (of the steady state) to the inflow mass (of the steady state). In other words, instantaneous masses of the steady state are averaged and used. This efficiency is thus independent of the duration of venting.

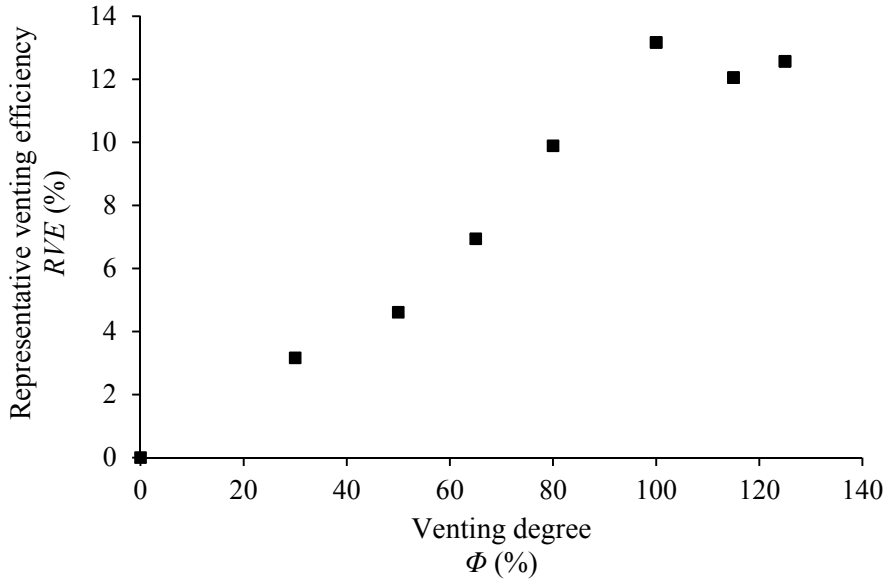

Figure 4.11: *RVE* as a function of the venting degree Φ (modified from Chamoun et al. (2016a)).

Lee et al. (2014) used this type of efficiency in their analysis of venting efficiencies. The results of the present work revealed a peak in the representative venting efficiency at $\Phi = 100\%$. A slight decrease in the efficiency was observed at higher venting degrees (Figure 4.11). Lee et al. (2014) tested two venting degrees (i.e., 50% and 100%). However, in their case, they observed a decrease in the efficiency when venting degrees are increased from 50% to 100%. This can be explained by different operating conditions, such as using two outlets at different elevations and a bed slope of 2%.

Global venting efficiency

By applying Equation (4.2), a *GVE* is calculated for each time step. In other words, at each time step t, venting is considered to be stopped ($= T_{vf}$) and the value of the global efficiency is calculated. This allowed the assessment of the effect of the duration of venting on the efficiency.

In Figure 4.12, the *GVE* is shown as a function of the normalized venting duration for all the tests with different venting degrees. A log-shaped curve is obtained for all the cases. Additionally, increasing the venting degree from 65% to 80% shows the highest gains in efficiency. However, for $\Phi \geq 100\%$, the values of venting efficiencies are almost similar, suggesting that the increase of venting degree may be causing more water loss than sediment release. In the case of $\Phi = 100\%$, the total mass of vented sediments during the whole test is

around 8% of the total mass of sediments transported by the turbidity current, and the total mass of deposited sediments is 40% of the same mass.

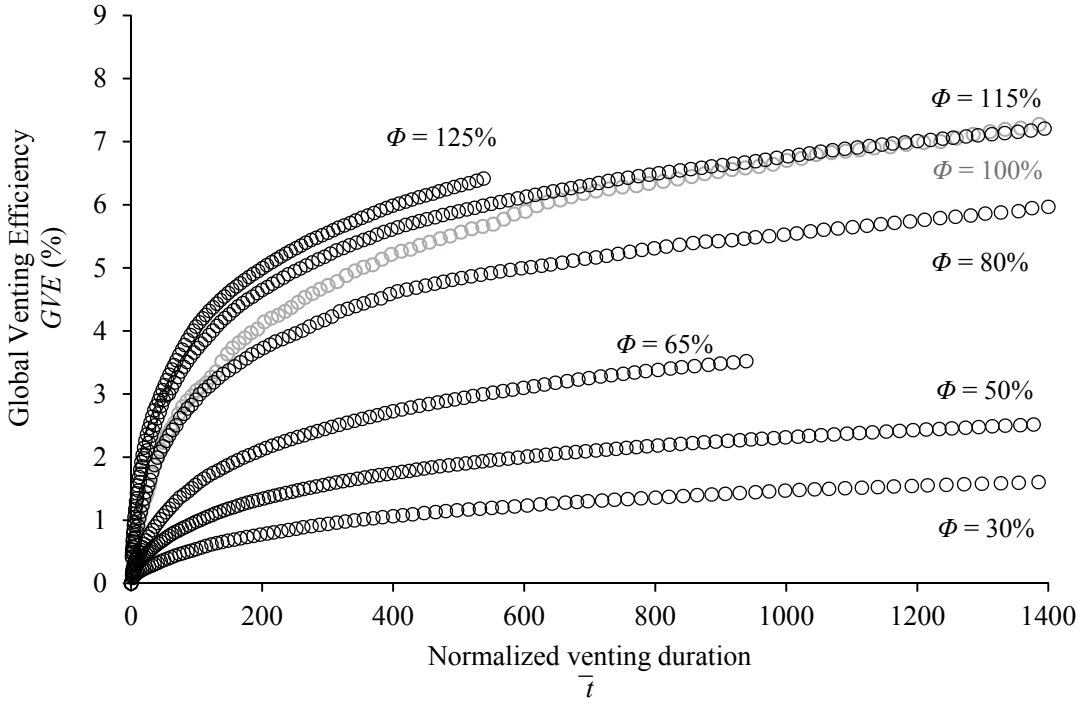

Figure 4.12: The *GVE* as a function of the normalized venting duration at different venting degrees (grey is used to distinguish neighbouring curves).

Local venting efficiency

In this section, equation (4.3), which represents the proposed *LVE*, is applied. At $\Phi = 30\%$, 50% and 65%, the efficiency increases until a steady state is reached (Figure 4.13). At $\Phi = 80\%$, 100%, 115%, and 125%, a different trend is observed and can be divided into three phases: (1) the *LVE* increases at approximately $0 < \bar{t} \leq 30$, corresponding to the high concentrations formed in the muddy lake; (2) the *LVE* decreases at approximately $30 < \bar{t} \leq 500$, corresponding to the reflection of the turbidity current and hence the decrease in the concentration in front of the outlet; and (3) the outflow conditions and venting efficiencies stabilize at $\bar{t} > 500$, corresponding to the venting of the body of the current reaching the dam. For $\Phi = 125\%$, the duration of venting was not long enough to reach the steady state. But given the trend of the curve, efficiencies are expected to reach values below or equal to the efficiencies at $\Phi = 100\%$ and 115%.

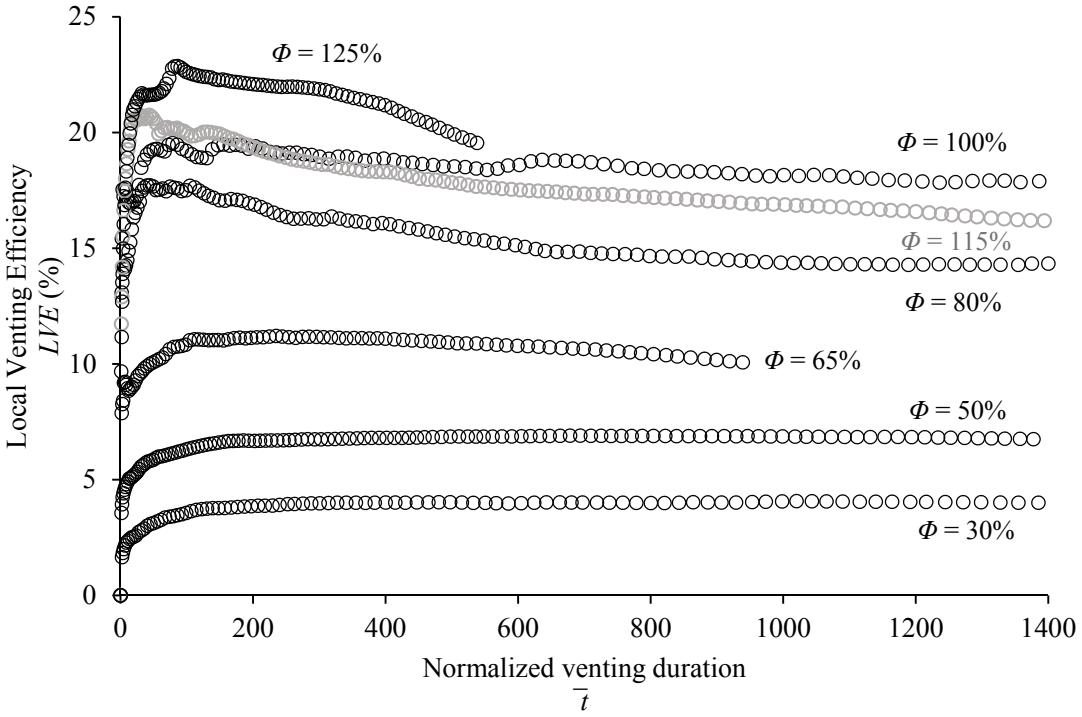

Figure 4.13: *LVE* as a function of the normalized venting duration at different venting degrees (grey is used to distinguish neighbouring curves).

The quasi-steady state at $\Phi = 115\%$ has a venting efficiency lower than at $\Phi = 100\%$. Thus, starting at a venting degree of $\Phi = 100\%$, the benefit of venting at higher venting degrees is mainly during phase (1) of venting. After this phase, the efficiency at $\Phi > 100\%$ becomes lower or approximately equal to that at $\Phi = 100\%$. This fact is linked to the water losses which increase with increasing outflow discharges.

Venting efficiency and water losses

To include water losses in the definition of the efficiency, a venting efficiency indicator (*VEI*) is proposed. It takes into account the water volumes vented by computing a global volumetric concentration of the outflow at every time step and multiplying it by the *LVE* (Equation (4.7)).

$$VEI = LVE \frac{\int_{t=T_{vi}}^{T_{vf}} V_{VENTsed} \mathrm{d}t}{\int_{t=T_{vi}}^{T_{vf}} V_{VENTwat} \mathrm{d}t} \tag{4.7}$$

As shown in Figure 4.14, the curves of *VEI* corresponding to $\Phi = 115\%$ and $\Phi = 125\%$ are shifted below the curve at $\Phi = 100\%$ compared to the *LVE* curves. The former curves almost

overlie the curve at Φ = 80%. Thus, by taking into account not only sediment quantities but also vented water volumes, venting at Φ = 115% or 125% is less efficient than at Φ = 100% and almost as efficient as at Φ = 80%. Therefore, as explained previously, in terms of sediment quantities, higher outflows yield higher efficiencies, particularly during phase (1) of venting. However, when considering water losses, it is clear that the most efficient venting is obtained at Φ = 100%. Thus, operating at a venting degree of 100% is recommended when the approach thalweg tends to horizontal.

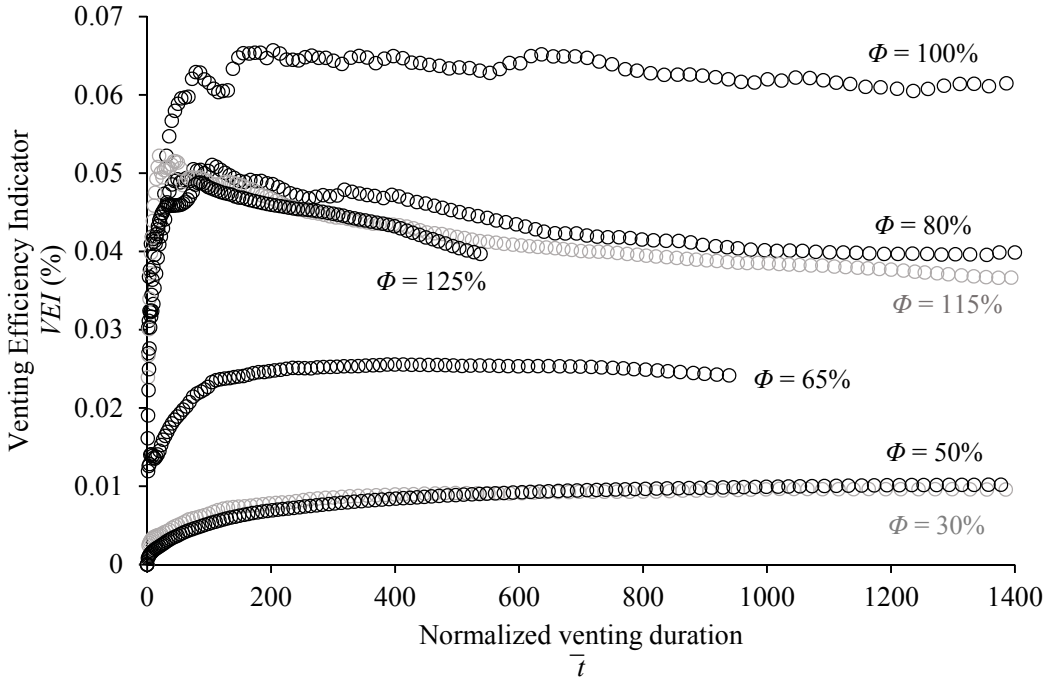

Figure 4.14: *VEI* as a function of the normalized venting duration at different venting degrees (grey is used to distinguish neighbouring curves).

4.4 Conclusions

A better understanding of the venting operation of turbidity currents flowing over a horizontal bed could be achieved. Venting degrees, defined as the ratio between outflow and inflow turbidity current discharges, are varied from Φ = 30% to 125% and the beginning of venting is synchronized with the arrival of the turbidity current at the outlet. The studied turbidity currents are not conservative; thus, they deposit on the flume bed.

The venting efficiency is evaluated based on three definitions: (1) the representative venting efficiency based on the steady values of inflow and outflow concentrations and discharges (2) the global venting efficiency *GVE*, which considers only the turbidity current's inflowing and outflowing sediment masses and (3) the local venting efficiency *LVE*, which takes into account

the deposited mass in the flume. It subtracts the deposited mass from the total inflowing sediment mass carried by the turbidity current, as these deposited masses have no potential to be entirely removed from the system before and during venting. The latter definition results in more significant values and trends of venting efficiency. Furthermore, the venting efficiency indicator *VEI* is defined. It considers not only the sediment masses but also the water losses during venting operations.

The analysis of the results of *GVE*, *LVE*, and *VEI* as a function of venting duration suggest that at venting degrees of Φ = 80%, 100%, 115%, and 125%, the efficiency of venting is the highest at the beginning of the venting operation (i.e., phase (1)). It then decreases before reaching a more or less steady state. However, Φ = 100% corresponding to an outflow discharge equal to the inflow discharge results in the highest efficiency when water losses are taken into account. Therefore, for venting turbidity currents flowing on a flat bed and with a time-synchronized opening based on the arrival of the current to the bottom outlet, venting is recommended at a venting degree of 100%.

In the discussed results, values of efficiencies obtained are relatively small. In fact, when reaching the bottom outlet, the current's head height is approximately 3.3 times higher than the height of the outlet. This renders the aspiration capacity of the outlet relatively small, and the reflected part of the current considerable. Increasing the height of the outlet is a parameter that may affect efficiency values. Moreover, the outlet is centered based on the width of the flume, creating a three-dimensional flow in its vicinity. However, the flowing turbidity current spreads across the width of the flume. Replacing the rectangular orifice with an outlet across the whole width of the channel may potentially increase efficiency values. In the case of this chapter, only subcritical turbidity currents are generated on the horizontal slope. Different dynamics of the currents approaching the outlet may also affect the evacuation process during venting. In summary, several parameters can play a role in this process and remain to be tested, of which the bed slope might be among the most significant.

Chapter 5

MANAGEMENT OF TURBIDITY CURRENT VENTING UNDER DIFFERENT THALWEG SLOPES[4]

The present chapter evaluates the efficiency of venting turbidity currents by varying the bed slope. Three different slopes are tested and the combined effect of outflow discharge and bed slope on the sediment release efficiency of venting is studied based on the different criteria previously described (i.e., *GVE*, *LVE*, *VEI*). The results show that the steeper the slope, the higher the release efficiency of venting will be. The favorable venting conditions which result in the highest sediment release efficiency and the lowest water losses from the reservoir could be highlighted.

[4] Chapter 5 is the basis of the scientific article ‘’Management of turbidity-current venting in reservoirs under different thalweg slopes’’ by S. Chamoun, G. De Cesare and A. J. Schleiss under revision in the Journal of Environmental Management. The experimental work presented hereafter is original and was performed by the author.

5.1 Test conditions

In the present chapter, three different bed slopes are tested: the horizontal bed (0%), the 2.4% (1.4°) and 5.0% (2.9°) slopes. For all the slopes, the timing of venting was synchronized with the arrival of the turbidity current to the wall. The venting degree $\Phi = Q_{VENT}/Q_{TC}$ was varied for each slope (Table 5.1). The venting duration was indirectly assessed because measurements are taken throughout the tests with sufficiently high frequency. Table 5.1 provides the inflow and outflow boundary conditions of the tests. S is the bed slope, C_{TC} is the initial concentration of the inflowing turbidity current, ρ_{t0} is the initial density of the turbidity current, $g'_0 = g\, C_{TC}\, ((\rho_s-\rho_w)/\rho_w)$ (where g is the gravitational acceleration and ρ_w the density of the clear water) is the initial reduced gravity of the current, and $B_0=g'_0 q_{TC}$ (where q_{TC} is the initial specific discharge of the current) is the initial buoyancy flux of the turbidity current (Graf & Altinakar, 1995). The tests discussed in Chapter 4 were also considered in order to compare the difference between venting on the horizontal bed and on the two other bed slopes.

Similarly to Chapter 4, the turbidity currents' inflow concentration and discharge are not varied. In the following, the steadiness of inflow is checked for the 2.4% and 5.0% slopes:

- On average, the initial concentration of the turbidity currents (Table 5.1) is $C_{TC} = 25$ g/l (volumetric concentration of 2.1%). For a single test, the average standard deviation of inflow concentration is 1.9 g/l while the standard deviation of the concentrations between the tests is 2.6 g/l. The initial concentration of turbidity currents was thus sufficiently steady throughout the tests.
- The initial turbidity current discharge is of 1 l/s on average for all the tests. For a single test, the average standard deviation of the turbidity current discharge is $Q_{TC} = 6\times10^{-3}$ l/s, and the standard deviation between the tests is 9×10^{-3} l/s. Thus, steady inflow discharges were also ensured at the inlet.
- The standard deviation of the outflow discharge averaged on all the tests is 0.01 l/s, representing only 3.6% of the smallest tested outflow discharge (0.3 l/s). Constant outflow conditions were accomplished during the tests.
- Water level differences between the head tank and the main flume during the tests are of 9 mm on average, representing 0.8% of the maximum water depth (the latter is 80 cm for the 2.4% slope and 92 cm for the 5.0% slope).

More information on the initial conditions concerning temperature and water depths measured at the head tank and in the main flume are provided in Appendix A2.

Table 5.1: Characteristics of the inflow and outflow boundary conditions of the generated turbidity currents.

		Inflowing turbidity current				Venting degree Φ
Test No.	S **(%)**	C_{TC} **(g/l)**	ρ_{t0} **(kg/m^3)**	g'_0 **(cm/s^2)**	B_0 **(cm^3/s^3)**	Q_{VENT}/Q_{TC} **(%)**
E0.1	0.0	27.6	1003.5	3.74	143.1	30
E0.2	0.0	26.0	1003.3	3.53	130.8	50
E0.3	0.0	28.4	1003.6	3.86	139.2	65
E0.4	0.0	27.0	1003.4	3.66	139.0	80
E0.5	0.0	29.4	1003.7	3.99	151.3	100
E0.6	0.0	25.5	1003.2	3.46	127.1	115
E0.7	0.0	23.0	1002.9	3.12	115.8	125
E1.0	2.4	26.1	1003.3	3.54	130.6	0
E1.1	2.4	21.1	1002.6	2.86	103.4	30
E1.2	2.4	28.4	1003.6	3.86	142.8	50
E1.3	2.4	28.4	1003.6	3.86	142.1	65
E1.4	2.4	22.1	1002.7	3.00	110.0	100
E1.5	2.4	25.1	1003.1	3.40	123.7	135
E1.6	2.4	26.0	1003.3	3.53	130.0	155
E1.7	2.4	25.1	1003.2	3.41	124.6	200
E2.0	5.0	22.8	1002.8	3.09	113.2	0
E2.1	5.0	28.7	1003.6	3.89	143.3	50
E2.2	5.0	26.2	1003.3	3.56	132.8	100
E2.3	5.0	27.5	1003.5	3.74	137.5	115
E2.4	5.0	25.0	1003.1	3.39	123.0	135
E2.5	5.0	23.5	1002.9	3.19	119.9	155
E2.6	5.0	21.8	1002.7	3.0	108.1	200

5.2 Results

5.2.1 Experimental observations

Using the video recordings, the size of the head was assessed for each of the three slopes. Figure 5.1 shows the development of the head size of the current H_{head}, normalized by the

height of the inlet h_{inlet} = 0.045 m plotted relatively to the position x of the current's head from the inlet, normalized by the length of the main flume L = 6.7 m. Note that the observations start only at $x/L \approx 0.44$ because of the presence of a metallic wall as part of the flume's structure before that distance.

The head of the turbidity current increases with distance and with increasing slopes. In fact, the higher the slope, the higher the clear water entrainment, which causes the increase of the size of the head. However, with a horizontal bed, the head increases more or less linearly with distance from the inlet. For the 2.4% and 5.0% slopes, starting $x/L \approx 0.8$, the current's head seems to develop exponentially while approaching the wall.

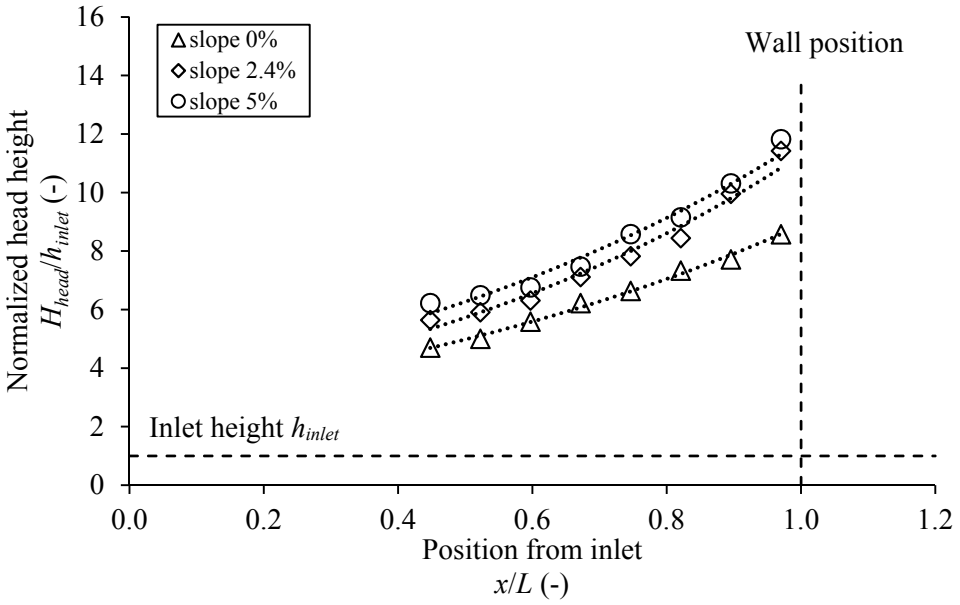

Figure 5.1: Evolution of the normalized head height H_{head}/h_{inlet} of the turbidity current as a function of the relative position x/L of the current in the flume for the different bed slopes.

The increase of the size of the head was previously observed by Britter and Linden (1980) for saline currents and by Altinakar, et al. (1990) for turbidity currents. The latter extrapolated the former's data and concluded that $dH_{head}/dx = 0.23\alpha$ (in radian) for saline currents and for $5° \leq \alpha \leq 90°$. However, Altinakar et al. (1990) concluded based on their data that turbidity currents' head grow faster than that of saline currents. A comparison between the data of Britter and Linden (1980) and those of the present study also lead to the conclusion that H_{head} increases with a faster rate for turbidity currents (Figure 5.2). Also, on a horizontal bed ($\alpha = 0°$), $dH_{head}/dx \neq 0$ for turbidity currents, unlike for saline currents where the head's size does not increase in distance on a horizontal bed. This explains the shift between the two lines.

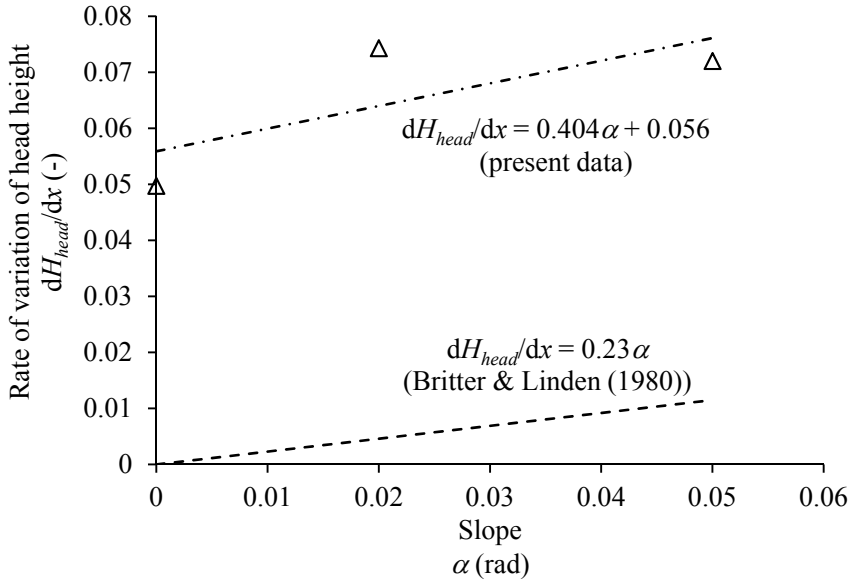

Figure 5.2: Increase rate of the head height of a turbidity current dH_{head}/dx as a function of the slope compared to that of a saline current as found by Britter and Linden (1980).

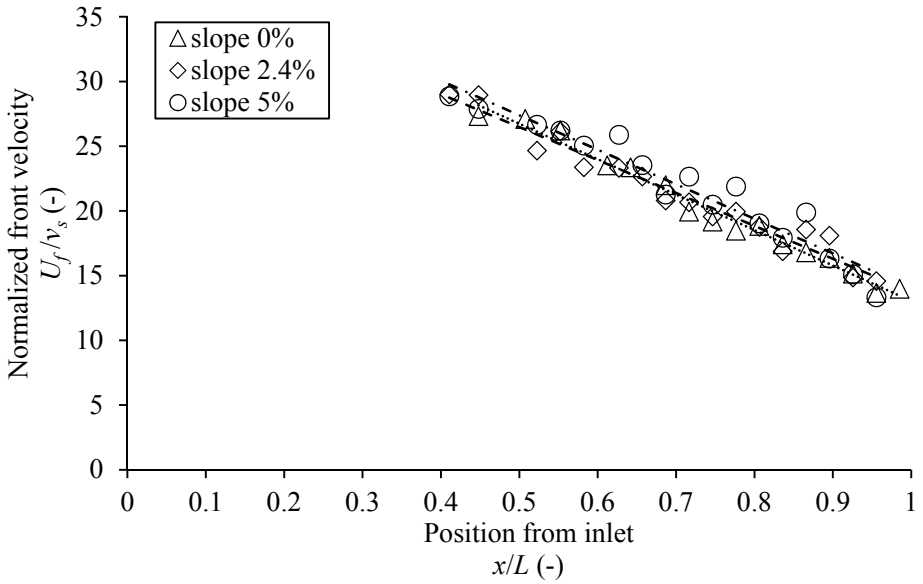

Figure 5.3: Normalized front velocity U_f/v_s of the turbidity currents as a function of the relative position x/L of the current in the flume for the different bed slopes.

In Figure 5.3, the front velocity U_f normalized by the settling velocity of the material v_s is plotted for the different slopes. For each slope, all the corresponding tests were considered and an average front velocity was calculated at a specific location. In the three cases, turbidity currents are decelerating with more or less the same rate. The gravity component parallel to the slope increases with the slope and is expected to accelerate the current. However, high water

entrainment counterbalances this component and leads to similar front velocities for the three slopes.

Figure 5.3 shows the trendlines corresponding to the data from the different slopes. The average equation obtained from the three very similar trendlines is $U_f/v_s = -26.5(x/L) + 40.1$. This leads to an average rate of decrease of the front velocity $dU_f/dx = -5.9\times10^{-3}$.

5.2.2 Turbulence rate

Using the UVP transducers, velocity profiles of the turbidity currents are obtained at different positions in the main flume (i.e., 2.8 m, 4.1 m, 5.5 m, 5.8 m, 6.0 m, and 6.2 m from the inlet). For all the cases, the profiles taken in the head of the current (3D velocity fields) are discarded and only the profiles in the body are considered. The profiles at 4.1 m from the inlet were chosen to represent the turbidity current's velocity (Figure 5.4).

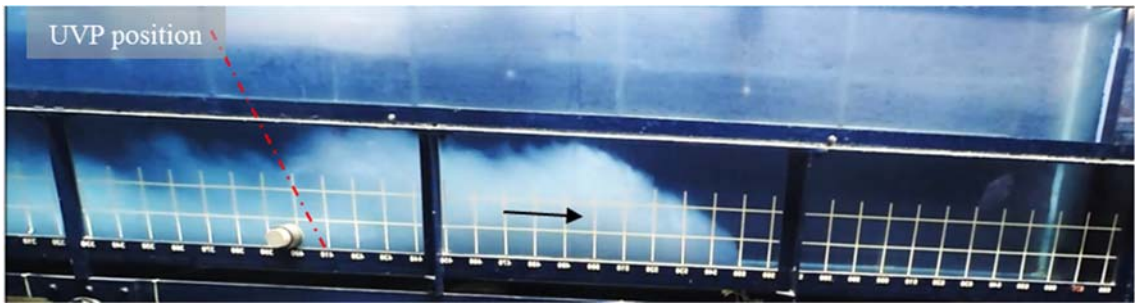

Figure 5.4: Turbidity current flowing on the 5.0% slope, highlighting the part of the current where the velocity plots are considered. The grid on the channel is 10 × 10 cm^2 (test E2.6)

Average profiles were calculated for the different slopes. Figure 5.5 shows the velocity u normalized by the maximum velocity of each profile (U_{max}) along the measuring height h normalized by h_{max} corresponding to U_{max}. Using Turner's equations (Ellison & Turner, 1959), the representative velocity U and height H of the currents are calculated for the three slopes. Based on these data, the bulk Richardson number $Ri = (g'H\cos\alpha)/U^2$ can be concluded (similarly to Chapter 4 section 4.3.4). Consequently, the Froude number $Fr = 1/Ri^{0.5}$ could be estimated.

The currents are found to be subcritical on the horizontal bed and 2.4% slope and slightly supercritical on the 5.0% slope (Table 5.2). Additionally, the Reynolds number was calculated as $Re = UH/v$ where v is the kinematic viscosity of water. Table 5.2 provides a summary of the above mentioned parameters. The turbidity currents encountered in reservoirs are commonly highly turbulent; similar Reynolds numbers are hardly achievable in laboratory. However, for

all the cases, $Re > 2000$ suggesting that all the turbidity currents generated are fully turbulent (Kneller & Buckee, 2000). Thus, the Froude number similarity can be applied and the results can be scaled up to prototype.

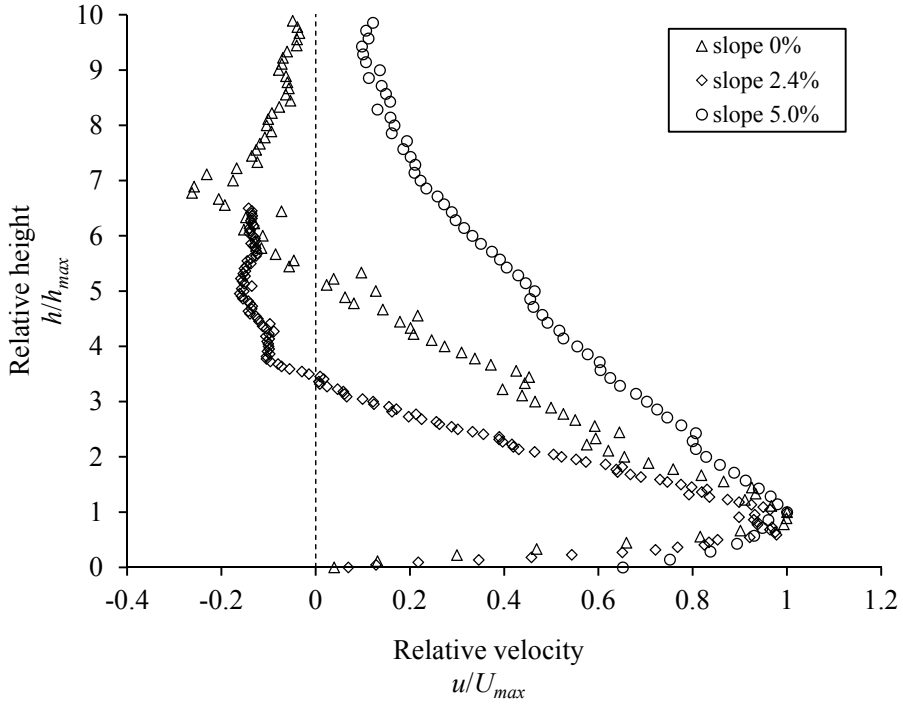

Figure 5.5: Average velocity profiles of the turbidity currents u/U_{max} at $x = 4.1$ m from the inlet for the different slopes.

Table 5.2: Characteristics of turbidity currents on different slopes: velocity U and height H, Richardson number Ri, Froude number Fr and Reynolds number Re.

***S* (%)**	***U* (cm/s)**	***H* (cm)**	***Ri***	***Fr***	***Re* (10^3)**
0.0	2.23	23.89	11.51	0.29	4.87
2.4	3.52	18.77	2.73	0.60	6.60
5.0	5.08	13.91	0.97	1.02	7.07

5.2.3 Deposition

Deposition in time and space showed similar trends for the three slopes tested. Spatially, the highest deposition occurs close to the inlet due to the development of the current where the coarse sediments settle. While the current advances, the deposition mass decreases because the sediments contained in the current become finer. Temporally, a first phase of high depositional rate is observed which is explained by the phase of development of the current. This is followed

by a decrease in the deposition rate, approaching a steady rate of deposition. This is probably linked to the arrival of the current to the wall and the formation of the muddy lake. At this stage, the depositional rate decreases and more sediments are suspended.

A better assessment of the temporal variation of the deposition is done by plotting the integral of the sediment mass in time. Figure 5.7 shows the variation of the total deposited mass M_{deptot}, normalized by the total inflow mass M_{TC} relatively to test duration t and using the 5.0% slope. Three different common cases of venting degrees were chosen ($\Phi = 0\%$; 50% and 100%). Reference lines were added at the time when venting began $t = T_{vi}$ with $\Phi = 50\%$ and $\Phi = 100\%$.

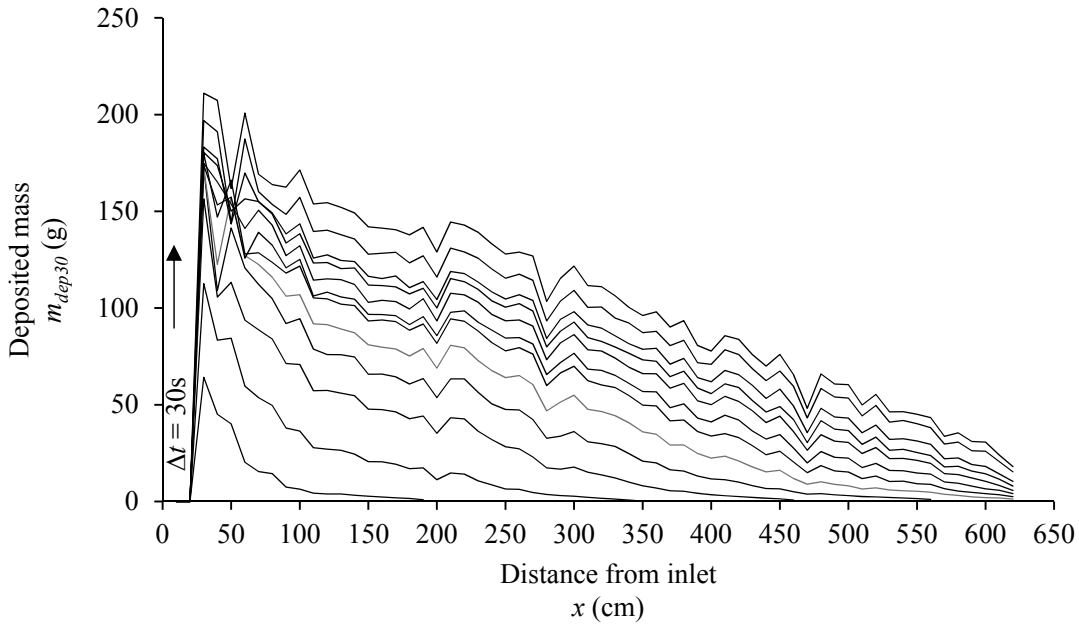

Figure 5.6: Variation of deposition in time and space obtained on the 2.4% bed slope using a venting degree $\Phi = 50\%$ (test E1.2).

Deposition increases the most during the phase before the arrival of the current at the wall. Then, around the time where the current reaches the wall, a slow decrease in deposition is observed. Additionally, the variation of the relative total deposition is very similar when comparing the reference test where no venting was applied ($\Phi = 0\%$), with the tests where venting was applied with $\Phi = 50\%$ and $\Phi = 100\%$. This proves that the venting operation does not induce an effect on the deposition and unlike flushing for instance, does not cause a retrogressive erosion. However, one shall note that deposition is measured until 620 cm from the inlet while the wall is located at 670 cm. The effect on deposition might be present in the closer vicinity of the wall where deposition is not measured.

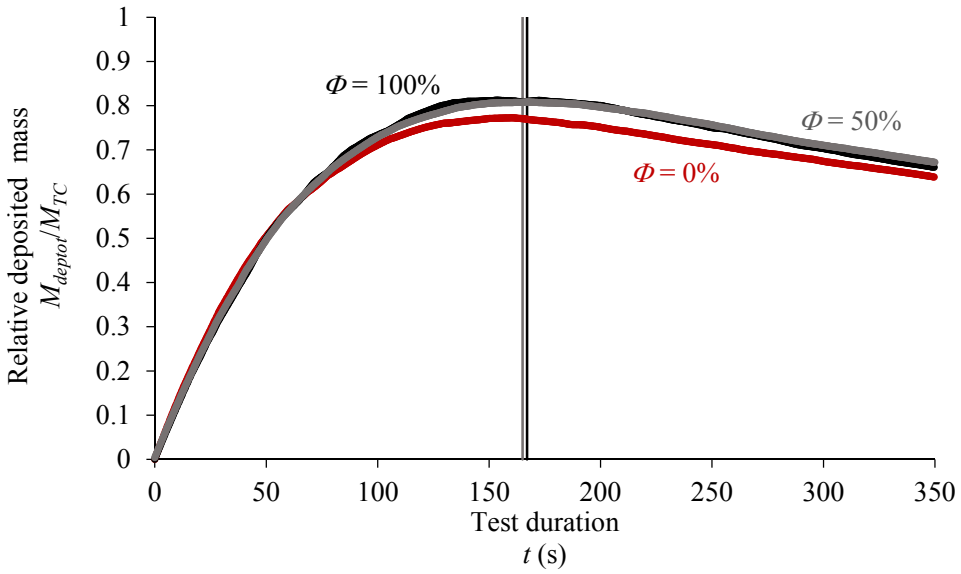

Figure 5.7: Variation of the relative deposited mass in time for S = 5.0% slope (tests E2.0, E2.1 and E2.2).

In the following, the total mass deposited along the flume M_{deptot} right before opening the outlet at $t = T_{vi-}$ is compared with the total inflow sediment mass M_{TC} at this same time for the three different slopes. Table 5.3 shows a slight increase of the deposited mass with increasing slopes. In fact, as mentioned previously, higher slopes yield a higher water entrainment which results in a higher dilution of the current, thus the decrease of the density difference $\Delta\rho = \rho_t - \rho_w$ between the turbidity current (ρ_t) and the clear water (ρ_w). Consequently, the reduced gravitational acceleration $g' = g\,(\Delta\rho/\rho_w)$ becomes lower leading to the decrease of the buoyancy of the current. The latter represents the ability of the current to keep sediments in suspension. All this results in similar or slightly higher deposition when increasing slopes from the horizontal position. As a conclusion, the tested slopes seem to be too small to impose a sustainable increase in the buoyancy of the currents. The type and settling velocity of the sediments used are most probably the main reason for this behavior.

Table 5.3: Percentage of deposited mass compared to inflowing mass for the different slopes at $t = T_{vi}$.

S (%)	M_{deptot}/M_{TC} (%)
0.0	68
2.4	71
5.0	80

5.2.4 Outflow concentration

For all the slopes, a progressive increase of the concentration precedes a more or less steady state. In the following, Figure 5.8 shows an example of the variation of the normalized outflow concentration as a function of duration of venting, for the case of $\phi = 50\%$. Increasing slopes generally resulted in higher outflow concentrations. However, this variation is much clearer when passing from the horizontal bed to the 2.4% slope than the case where the slope is increased from 2.4% to 5.0%. C_{VENT}/C_{TC} is around 9% for the horizontal bed and between 11% and 12% for the 2.4% and 5.0% slopes. Thus, for all the cases, there is a dilution of the current before reaching the bottom outlet, due to deposition and clear water entrainment.

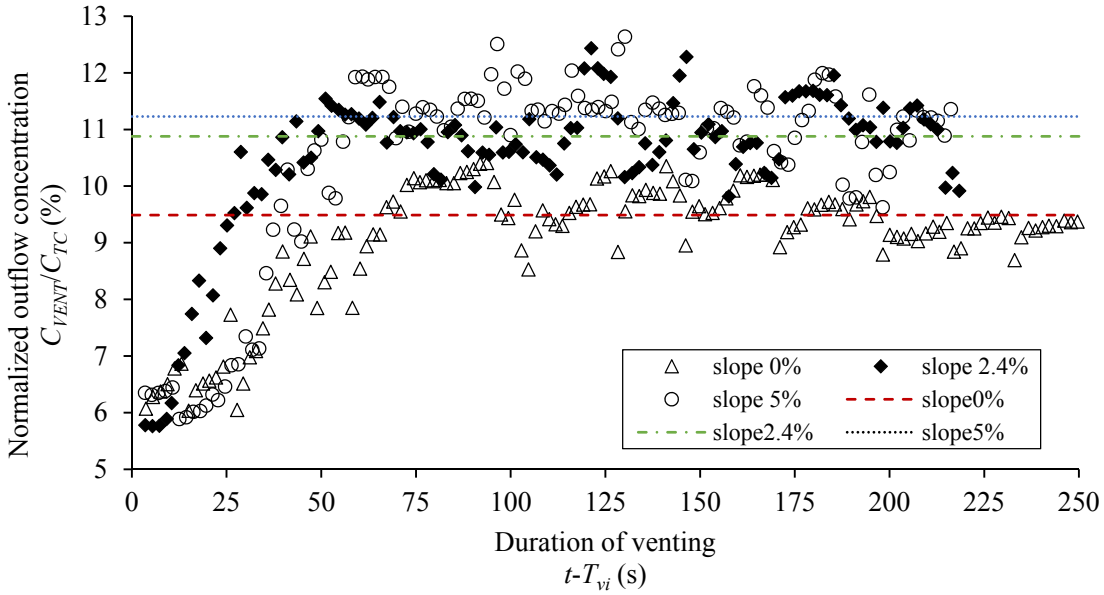

Figure 5.8: Variation of the normalized outflow concentration C_{VENT}/C_{TC} as a function of the duration of venting t-T_{vi} for a venting degree $\phi = 50\%$ for the different slopes (tests E0.2, E1.2 and E2.1). The horizontal lines represent the average value of the steady-state region of outflow concentration.

The photos in Figure 5.9 show that by increasing the bed slope, the part of the turbidity current that is not vented is less reflected upstream. Thus, the muddy lake that is formed and from which sediments are evacuated during venting is more concentrated with steeper slopes. With a horizontal bed, the reflected turbidity current could reach large distances upstream while for the 5.0% slope, the suspended sediments did not spread much further than around 2 m from the wall. Figure 5.9 shows the muddy lake at t-$T_{vi} = 260$s for the horizontal bed and for the 5.0% slope.

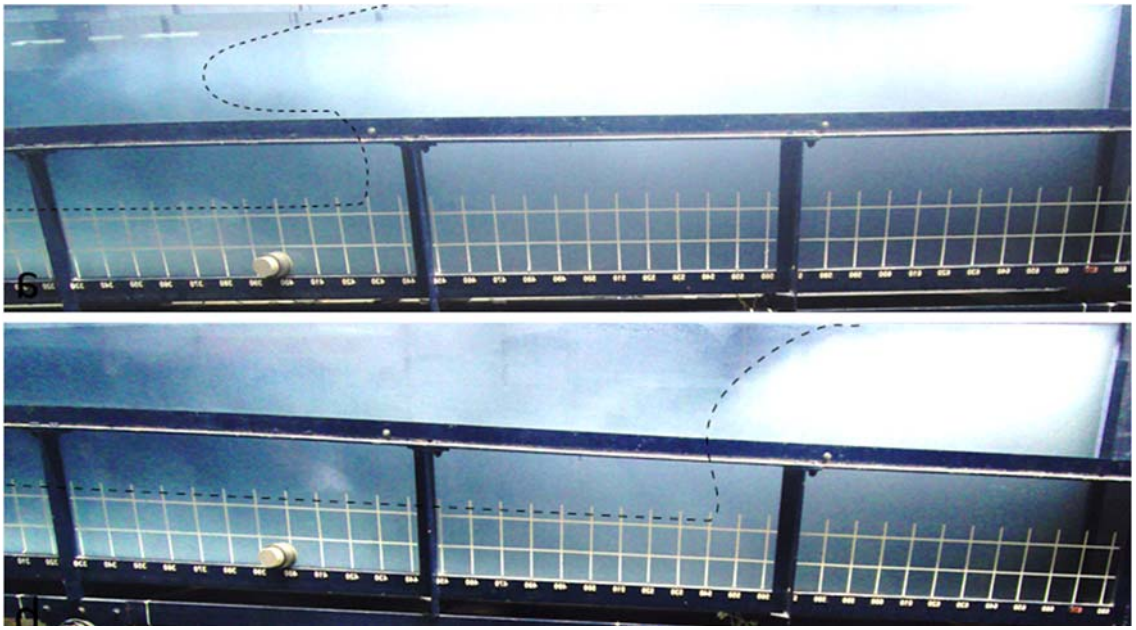

Figure 5.9: Reflected turbidity current at t-T_{vi} = 260 s for (a) the horizontal bed (test E0.5) and (b) the 5.0% slope (test E2.6).

5.2.5 Venting efficiency

Based on the different measurements, the efficiency of venting is analyzed based on the definitions of local venting efficiency (*LVE*) and venting efficiency indicator (*VEI*) described in Chapter 4, section 4.2. As a first analysis, the efficiency of venting was evaluated based on the *LVE* calculated at one specific time step for each slope (Figure 5.11). This time step corresponds to the maximum common duration of venting for the different venting degrees Φ tested with a certain slope (i.e., tests with different Φ using the same slope did not always have the same duration): t-T_{vi} = 212s for S = 0%, t-T_{vi} = 190s for S = 2.4% and t-T_{vi} = 127s for S = 5.0%. The *LVE* values were firstly plotted for the case of restrained outflow discharges ($\Phi \leq 100\%$), which represents most of the time, the case of Alpine reservoirs. A second degree polynomial was obtained for the three different cases.

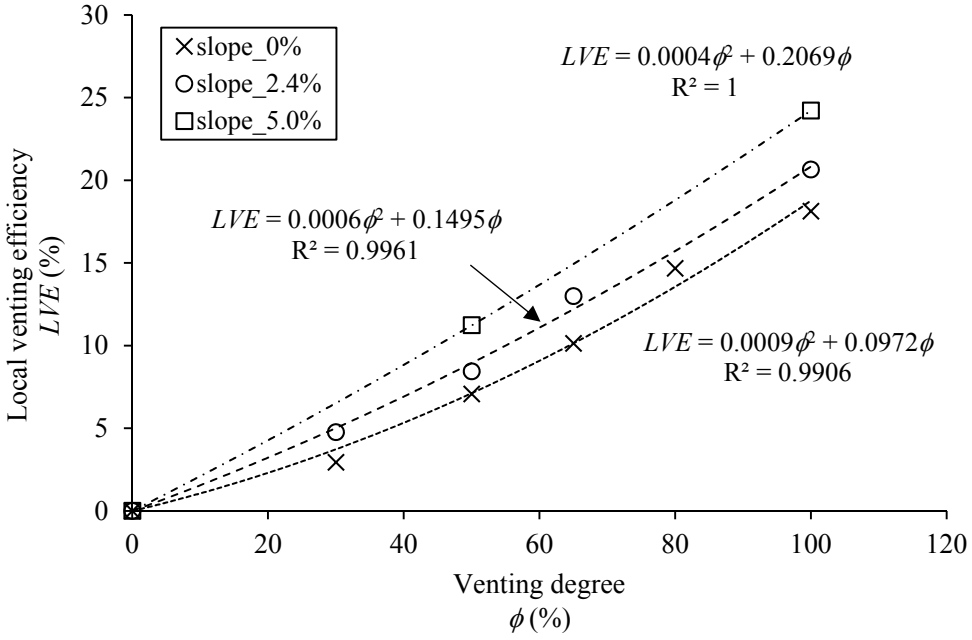

Figure 5.10: Local venting efficiency *LVE* as a function of the venting degree Φ for a specific duration of venting fixed for each bed slope, limited to the cases of restrained outflow discharges.

Next, the whole range of the tested venting degrees was considered. The *LVE* values were highlighted for cases where an increase of the venting degree is the least efficient. For the horizontal bed, $\phi = 100\%$ and $\phi = 115\%$ result in closely similar values of efficiency. For the 2.4% and 5.0% slopes, the efficiencies obtained with $\phi = 135\%$ and $\phi = 155\%$ have very similar values. However, the variation of *LVE* as a function of the venting duration is evaluated in the following to verify whether the tendencies in Figure 5.11 are only ‘’local in time’’ or dependent on the duration of venting.

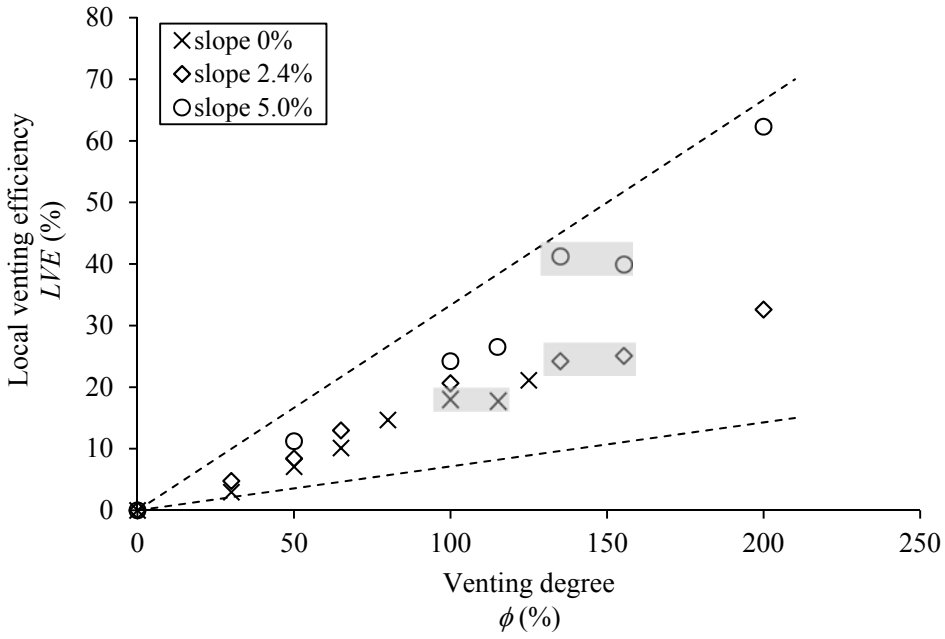

Figure 5.11: Local venting efficiency *LVE* as a function of the venting degree Φ for a specific duration of venting fixed for each bed slope.

Local venting efficiency with different venting degrees

In the following, efficiencies are plotted relatively to the normalized duration of venting defined in Chapter 4, section 4.3.6. Venting turbidity currents on a flat bed showed the highest efficiency for $\Phi = 100\%$ based on the *LVE* and the *VEI* results (Chamoun et al., 2017a). However, venting with $\Phi > 100\%$ is still efficient for the 2.4% or 5.0% slopes (Figure 5.12 and Figure 5.13).

Figure 5.12 and Figure 5.13 show very similar *LVE* when venting with $\Phi = 135\%$ and $\Phi = 155\%$. This suggests that with an outlet capacity approaching 155% of the turbidity current's discharge, venting turbidity currents on a 2.4% or 5.0% slope can be limited to $\Phi = 135\%$ and leads to similar sediment release efficiencies. Additionally, venting efficiencies obtained with the 5.0% slope show a high peak at the beginning of venting due to the highly concentrated muddy lake, before decreasing and reaching the quasi-steady state. However, if venting is applied with $\Phi = 200\%$, the efficiency increases again compared to that obtained with $\Phi = 135\%$. However, the analysis in Chapter 2, section 2.6.1 (Chamoun et al., 2016c) based on data from 22 Swiss dams showed that the capacity of bottom outlets is generally small compared to the potential flood-induced discharge of the approaching turbidity current to be vented (< 200%). Therefore, it is assumed that the increased efficiency obtained for the case of

$\Phi = 200\%$ is due to venting combined with sluicing or flushing conditions, especially in the quasi 2D conditions of the experimental set-up.

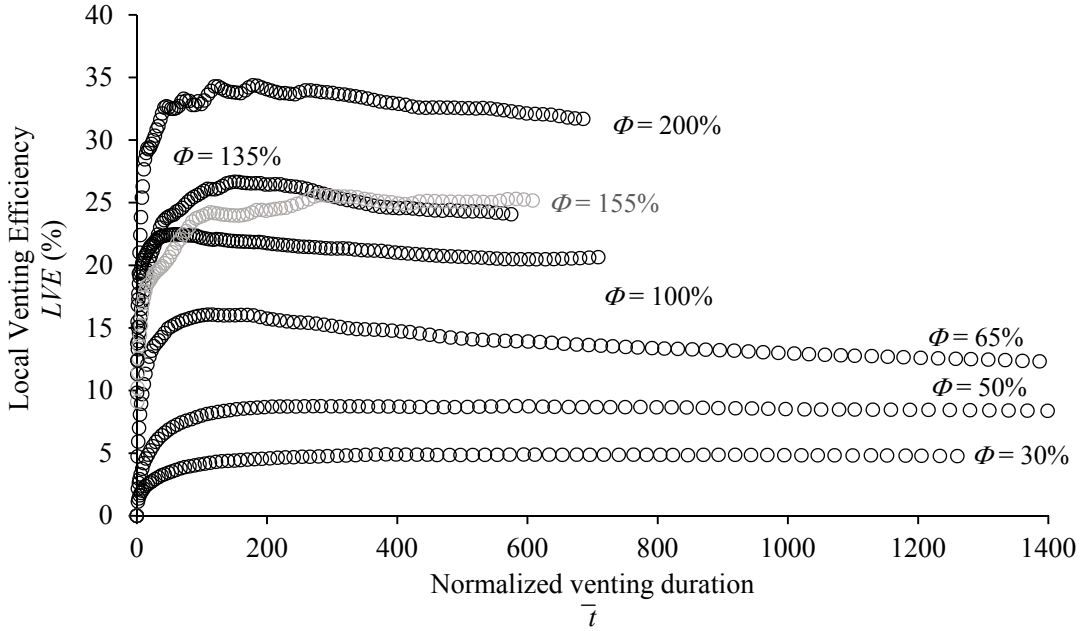

Figure 5.12: Local venting efficiency *LVE* as a function of the normalized venting duration for the different venting degrees Φ on a 2.4% bed slope.

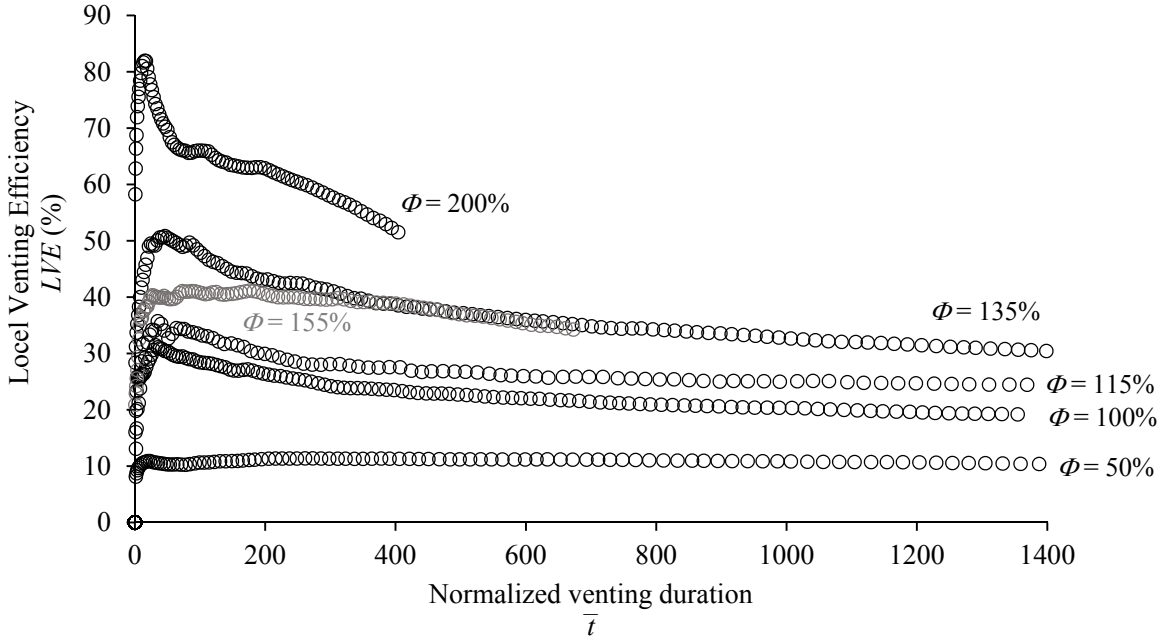

Figure 5.13: Local venting efficiency *LVE* as a function of the normalized venting duration for the different venting degrees Φ on a 5.0% bed slope.

Venting efficiency indicator

In most of the cases where venting is applied, water is in shortage and drawdown of the reservoir's water level should be avoided. In the following, the variation in time of the *VEI* is evaluated for the two upper slopes. The results (Figure 5.14 and Figure 5.15) confirm the conclusions obtained with the *LVE* results: by considering water losses, the curves corresponding to $\Phi = 155\%$ slightly drop below the ones corresponding to $\Phi = 135\%$. Additionally, using the 5.0% slope, the *VEI* values for $\Phi = 135\%$ and $\Phi = 200\%$ get closer. These results suggest that an optimal venting is obtained with $\Phi = 135\%$ when using bottom outlets having a capacity up to 155% of the turbidity current's discharge Q_{TC}. However, in the case where the capacity of the outlet reaches 200% of the turbidity current's discharge, which is not very common, results showed that the efficiency in terms of both sediment release and water losses is the highest with $\Phi = 200\%$. This might be due to some relatively higher local erosion and the higher height of aspiration of the outlet that forces the muddy lake to stay close to the outlet.

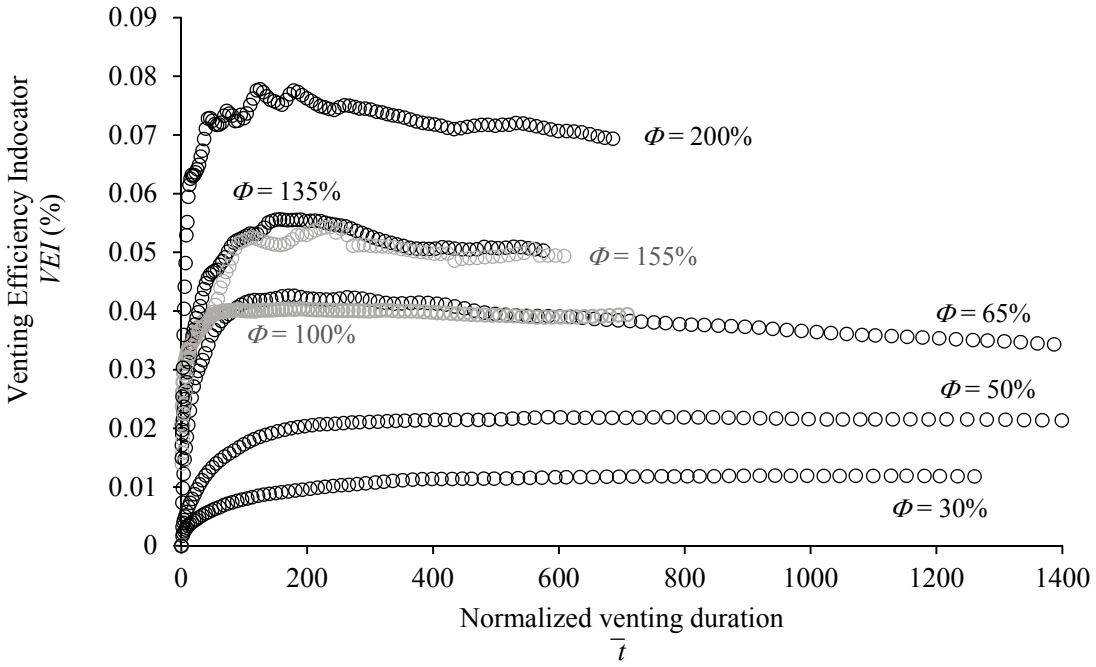

Figure 5.14: Venting efficiency indicator *VEI* as a function of the normalized venting duration for the different venting degrees Φ on a 2.4% bed slope.

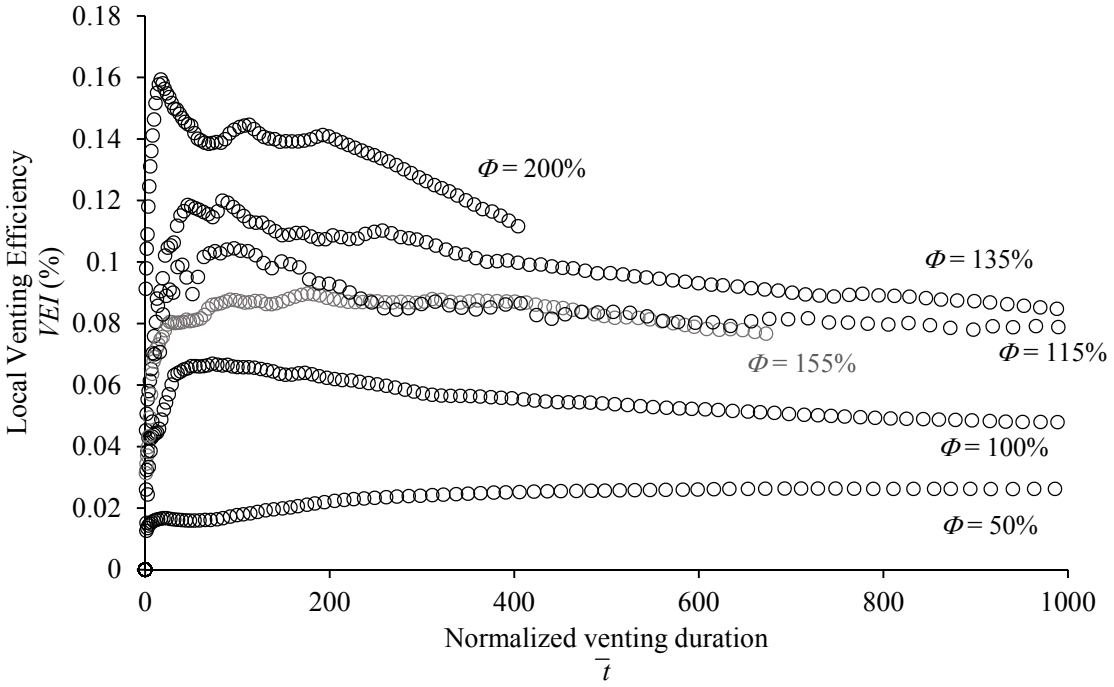

Figure 5.15: Venting efficiency indicator *VEI* as a function of the normalized venting duration for the different venting degrees Φ on a 5.0% bed slope.

Local venting efficiency with different slopes

The variation of the local venting efficiency in time for the different slopes studied is compared hereafter. It can be seen in Figure 5.16 and Figure 5.17 that for the same venting degree (ϕ = 50% and ϕ = 100% respectively), the *LVE* increases with increasing slopes. It is mainly due to the behavior of the muddy lake (affecting outflow concentrations) as well as the deposition, discussed in sections 5.2.3 and 5.2.4. Therefore, in the range of the slopes studied in this research, one can conclude that a higher slope yields a higher venting efficiency. Venting is recommended starting directly after the commissioning of the dam, in order to maintain the formation of a cone in front of the low-level outlets and avoid the flattening of the bed and blockage of the outlets. It is also suggested to combine venting with other techniques such as airlift, hydro-suction or dredging upstream of the dam.

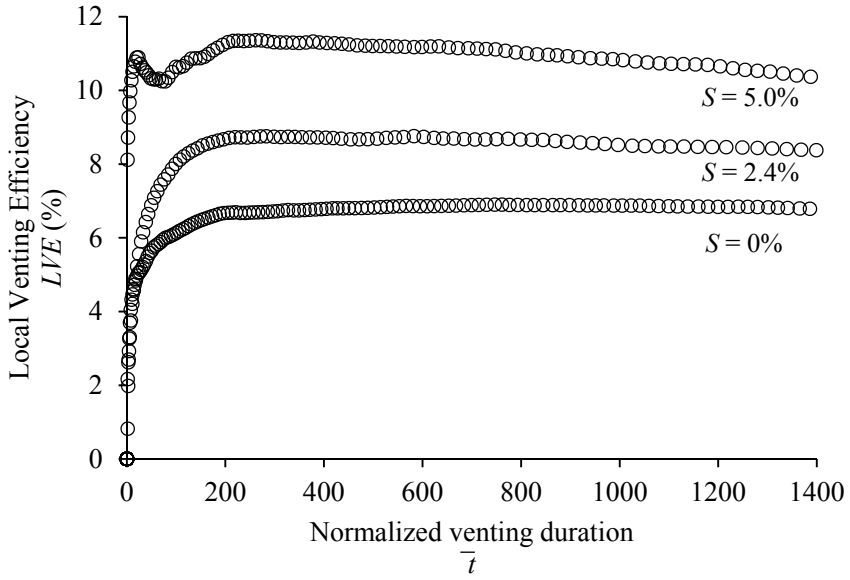

Figure 5.16: Local venting efficiency *LVE* as a function of the venting duration for a venting degree $\phi = 50\%$ for the different slopes.

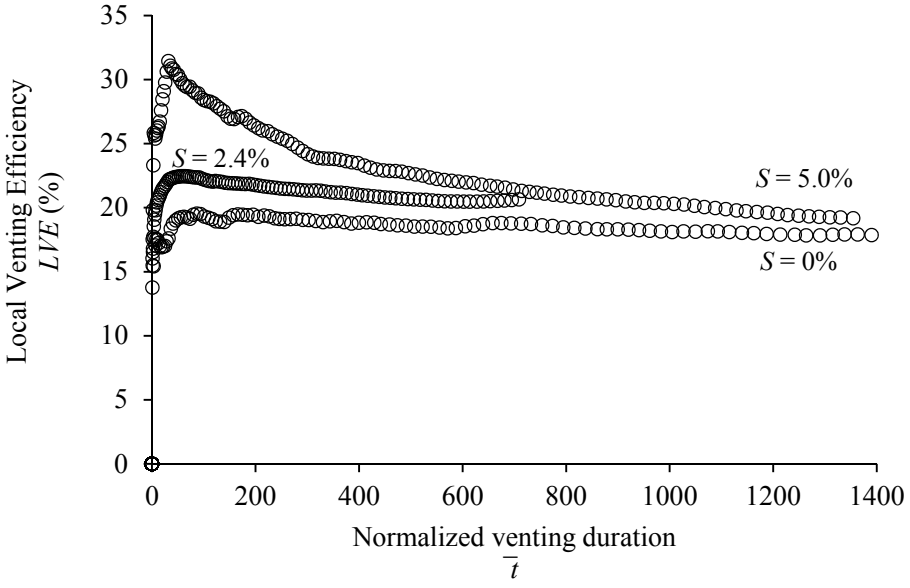

Figure 5.17: Local venting efficiency *LVE* as a function of the venting duration for a venting degree $\phi = 100\%$ for the different slopes.

5.3 Conclusions

Venting of turbidity currents through a bottom outlet was experimentally investigated using three different thalweg slopes (i.e., 0%, 2.4% and 5.0%) and applying various venting degrees defined as the ratio between outlet discharge and turbidity current discharge. The experimental

results are evaluated based on a defined local venting efficiency (*LVE*) and the venting efficiency indicator (*VEI*).

The tests revealed that unlike the case of a horizontal bed where a venting degree ϕ = 100% led to the highest efficiency, for the two higher slopes (i.e., 2.4% and 5.0%) and with an outlet capacity of 155% of the turbidity current discharge, the highest release efficiency was obtained with ϕ = 135%. This is mainly due to the fact that with higher slopes, the muddy lake formed once the turbidity current reaches the wall, is less extended upstream. The muddy lake from which the outlet vents is thus more concentrated for a longer duration of venting. Nevertheless, venting with ϕ = 200% yielded the highest efficiencies, probably because of reaching flushing conditions during venting. Additionally, venting with higher slopes led to higher venting efficiencies for the same venting degree. Therefore, the steeper the thalweg upstream of the dam, the better the efficiencies that can be reached during venting.

Chapter 6

INFLUENCE OF OPERATIONAL TIMING ON THE EFFICIENCY OF VENTING TURBIDITY CURRENTS[5]

In the present chapter, the venting operation is experimentally investigated using two reservoir bed slopes (i.e., 2.4% and 5.0%). The main research questions concern the opening timing of bottom outlets and the duration of venting. The timings tested are relative to the arrival of the current to the outlet. The results showed that in-time venting, synchronized with the arrival of the turbidity current at the outlet, is more efficient than early or late venting. It is recommended to start opening the gates when the turbidity current is around 300 m upstream of the outlet, so that the operation can be synchronized with the arrival of the current at the dam. Additionally, venting should not be stopped immediately after the end of the flood but should instead last for a certain length of time, shown to be dependent on the outflow discharge.

[5] Chapter 6 is the basis of the scientific article ‘’Influence of operational timing on the efficiency of venting turbidity currents’’ by S. Chamoun, G. De Cesare and A. J. Schleiss under review in the Journal of Hydraulic Engineering. The experimental work presented hereafter is original and was performed by the author.

6.1 Test conditions

The tests performed in the present chapter investigate the influence of two of the most important operational parameters related to venting on the efficiency of the operation. Therefore, identically to the tests discussed in the previous chapters, an important aspect was to ensure relatively similar turbidity currents while varying the operational parameters. Initial inflow concentration C_{TC} and discharge Q_{TC} were kept as steady as possible from one test to another and during the same test. Moreover, water level in the head tank and in the main flume were kept as equal and steady as possible during the tests. Temperature differences between the two compartments were also checked to be the lowest possible to ensure that density differences were mostly due to the suspended sediments.

Table 6.1: Characteristics of the turbidity currents generated and venting conditions.

Inflowing turbidity current						Venting degree Φ	Timing of opening	Inflow
Test No.	S **(%)**	C_{TC} **(g/l)**	ρ_{t0} **(kg/m^3)**	g'_0 **(cm/s^2)**	B_0 **(cm^3/s^3)**	Q_{VENT}/Q_{TC} **(%)**	d/h_{outlet} **or** t_{after} **(s)**	**Type**
E1.8	2.4	19.4	1002.4	2.63	97.8	115	$d/h_{outlet} = 5$	Continuous
E1.4	2.4	22.1	1002.7	3.00	110.0	100	$d/h_{outlet} = 0$	Continuous
E1.5	2.4	25.1	1003.1	3.40	123.7	135	$d/h_{outlet} = 0$	Continuous
E1.9	2.4	27.4	1003.4	3.71	130.7	115	$t_{after} = 30$ s	Continuous
E1.10	2.4	28.0	1003.5	3.80	138.3	115	$t_{after} = 60$ s	Continuous
E2.7	5.0	27.8	1003.5	3.77	138.1	115	$d/h_{outlet} = 5$	Continuous
E2.2	5.0	26.2	1003.3	3.56	132.8	100	$d/h_{outlet} = 0$	Continuous
E2.3	5.0	27.5	1003.5	3.74	137.5	115	$d/h_{outlet} = 0$	Continuous
E2.4	5.0	25.0	1003.1	3.39	123.0	135	$d/h_{outlet} = 0$	Continuous
E2.8	5.0	26.0	1003.2	3.53	128.7	115	$t_{after} = 30$ s	Continuous
E2.9	5.0	26.2	1003.3	3.56	132.8	115	$t_{after} = 60$ s	Continuous
E2.10	5.0	22.0	1002.7	3.0	110.3	30	$d/h_{outlet} = 0$	Interrupted
E2.11	5.0	21.0	1002.6	2.83	105.2	65	$d/h_{outlet} = 0$	Interrupted

Hereafter are the main parameters discussed in this chapter:

- Two bed slopes S were tested: 2.4% and 5.0%.

- Four different venting timings (Figure 6.1 and Figure 6.2) were investigated relative to the arrival of the turbidity current's head to the wall: (1) the outlet is opened before the arrival of the current at the outlet (early venting) at a distance $d/h_{outlet} = 5$ where $h_{outlet} = 12$ cm is the height of the bottom outlet; (2) the outlet's opening is synchronized with the arrival of the turbidity current's head at the outlet (in-time venting); (3) the outlet is opened at $t_{after} = 30$ s after the arrival of the current at the wall, once it has reached its top (30-s late venting); (4) the outlet is opened at $t_{after} = 60$ s after the arrival of the current at the wall and the beginning of the retrogressive reflection of the muddy lake (60-s late venting).
- Turbidity current inflow: the inflow was interrupted for two tests during venting (tests E2.9 and E2.10 in Table 6.1). The upstream pump was stopped and the sliding gate closed while venting was maintained. The inflow interruption was timed nearly 130 s after the beginning of venting. For the rest of the tests, the inflow was continuous throughout the test.

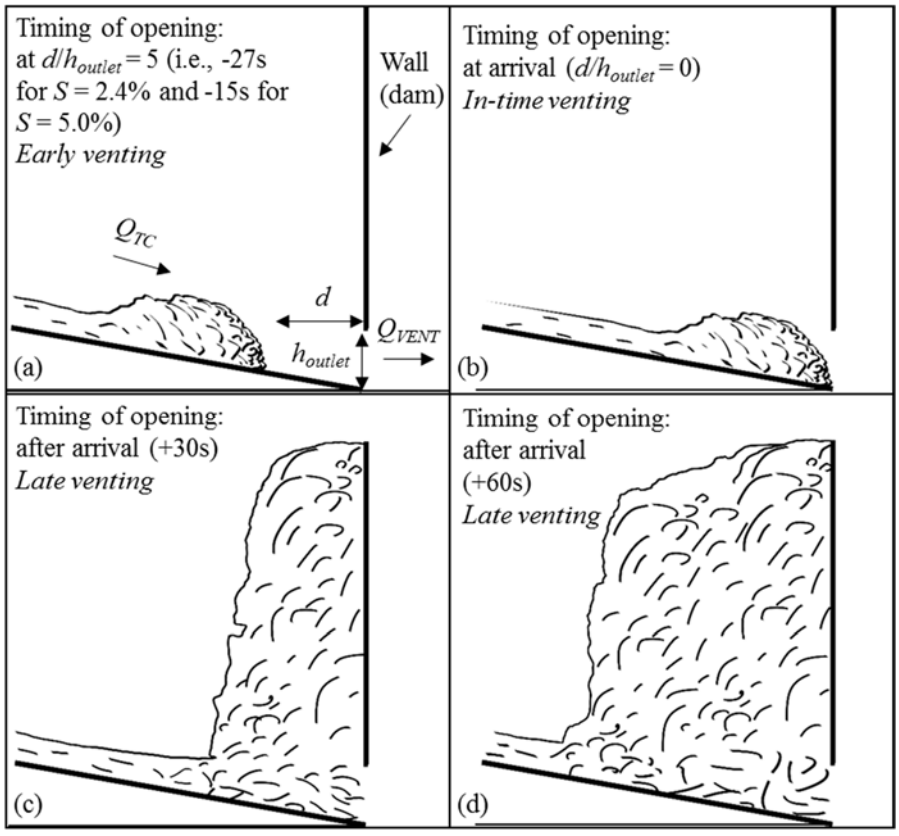

Figure 6.1: Illustration of the four venting timings (a) early venting; (b) in-time venting; (c) 30-s late venting; and (d) 60-s late venting.

More information on the initial conditions concerning temperature and water depths measured at the head tank and in the main flume are provided in Appendix A2. Details of the different tests are shown in Table 6.1. The same $\Phi = 115\%$ was used for early and late venting.

For in-time venting, two venting degrees $\Phi = 100\%$ and $\Phi = 135\%$ were tested. Other characteristics of the currents are also presented in Table 6.1: ρ_{t0} is the initial density of the turbidity current, $g'_0 = gC_{TC}((\rho_s-\rho_w)/\rho_w)$ is the reduced gravity of the inflowing turbidity current where g is the gravitational acceleration and ρ_w the density of the clear water. Finally, B_0 is the initial buoyancy flux of the current expressed by $B_0=g'_0 q_{TC}$ (q_{TC} is the initial specific discharge of the current) (Graf & Altinakar, 1995).

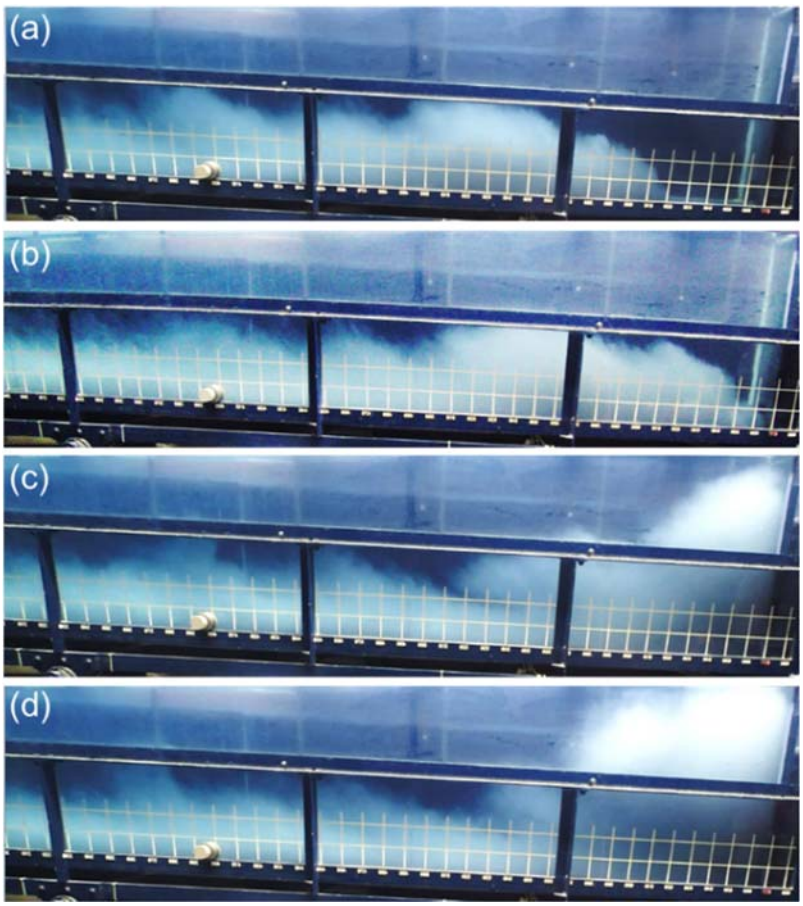

Figure 6.2: The four different timings tested: (a) early venting; (b) in-time venting; (c) 30-s late venting; and (d) 60-s late venting (test E2.6).

6.2 Results

6.2.1 Local venting efficiency

Early venting versus late venting

Sediment release efficiency was firstly evaluated based on local venting efficiency *LVE* (Chamoun et al., 2017a). In the following, the tests with early and late venting are compared

based on the *LVE* (Figure 6.3). *LVE* is plotted as a function of the normalized duration of venting: $\bar{t} = [(t-T_{vi})^2 g'_{app}]/h_L$ defined in Chapter 4.

For both slopes, the *LVE* reached higher values when venting started before the arrival of the turbidity current at the outlet/wall. On the other hand, the *LVE* value obtained when venting was timed after 60 s was slightly higher than the *LVE* value obtained when venting after 30 s for $S = 2.4\%$. The opposite trends for late venting were obtained with the 5.0% slope. Therefore, the *LVE* for late venting might be slope-dependent. In any case, venting after the arrival of the turbidity current and the formation of the muddy lake should be avoided.

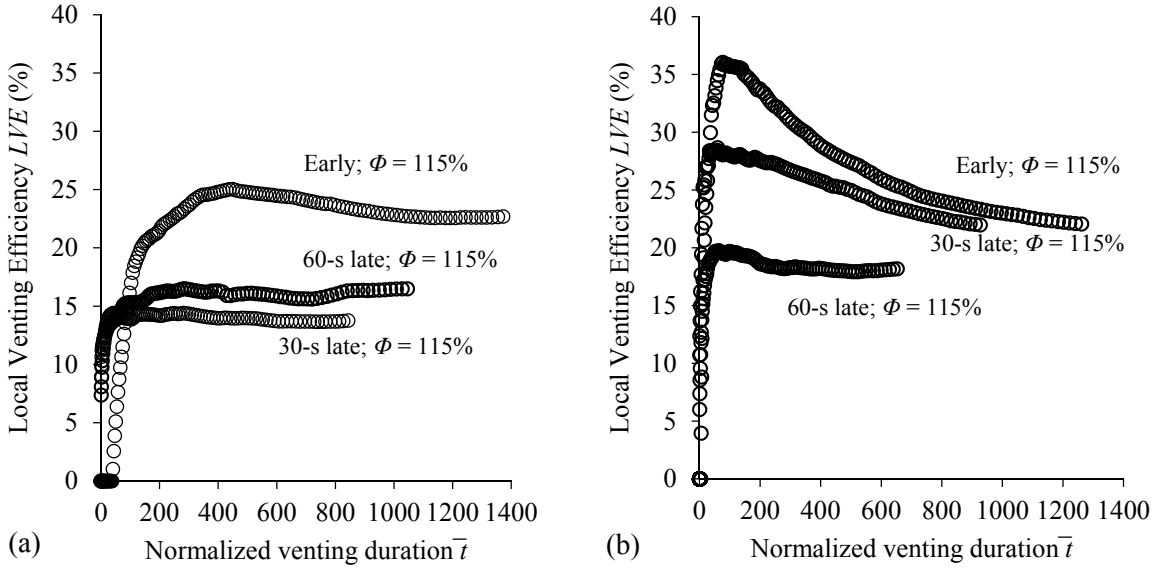

Figure 6.3: Local venting efficiency *LVE* for the case of early and late venting operations for (a) $S = 2.4\%$ (tests E1.8, E1.9 and E1.10) and (b) $S = 5.0\%$ (tests E2.6, E2.7 and E2.8).

Venting before the arrival of the cu60-s60rrent resulted in higher *LVE* values probably because the streamlines upstream of the outlet are sufficiently developed to ensure good suction of the current during their evacuation. Features such as streamlines and volumetric concentration were later investigated using the numerical model. More details can be found in Appendix A4. In fact, the countercurrent that is commonly formed above the turbidity current is reduced because the outlet's discharge acts in the opposite direction. The current therefore encounters less interface shear stress and the water entrainment into the turbidity current decreases (Cao et al. 2015). Although no visible acceleration of the current is observed when the outlet is opened at $d/h_{outlet} = 5$ (i.e., −27 s for $S = 2.4\%$ and −15 s for $S = 5.0\%$), the head of the current is drawn toward the outlet. At the moment of entering the bottom outlet, the nose of the turbidity current is triangular instead of the typical curved form (Figure 6.4). It is slightly

detached from the remaining parts of the current, which then follows into the bottom outlet. Note that this is observed around 15–20 cm upstream of the outlet, which correspond to more or less $1.5h_{outlet}$, suggesting that the outlet's zone of influence (highlighted by the red circle in Figure 6.4) is very local.

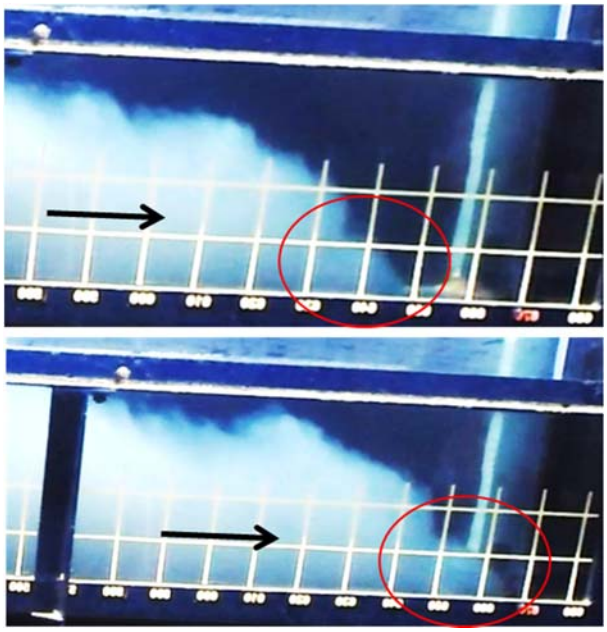

Figure 6.4: The head of the turbidity current while approaching the outlet to be vented (Δt = 5s) (test E2.6). Red circles highlight the moment at which the current is visually seen to be drawn and sucked by the outlet.

Even though early venting was shown to be more efficient than late venting, opening should not be too early. The earlier the opening, the higher the water loss. In Chapter 7, a numerical model was calibrated based on the experimental data. It showed that the maximum distance of aspiration s_{max} at which the current is influenced by the flow field of the outlet depends on the outflow discharge, up to a venting degree of $\phi = 80\%$, where $s_{max} = (s_{max})_{\phi=80\%} = 1$ m. For $\phi > 80\%$, the aspiration distance reached by the outlet's flow field also equaled $(s_{max})_{\phi=80\%}$. This distance was normalized by the aspiration height $(h_L)_{\phi=80\%}$ corresponding to $\phi = 80\%$. h_L is a function of the outflow discharge and the density difference between the approaching current and the reservoir's clear water. A relationship $s_{max}/(h_L)_{\phi=80\%} = 5$ was found. The latter represents a simple means for the calculation of the maximum distance upstream of the dam at which early venting can be performed.

Early venting versus in-time venting

In the following, the *LVE* obtained with the early venting with Φ = 115% is compared with that of the in-time venting with Φ = 100% and Φ = 135%. The case of Φ = 100% corresponds to the optimal venting degree when venting takes place on a horizontal bed (Chapter 4; Chamoun et al. 2017a), and Φ = 135% represents the optimal venting degree on the 2.4% and 5.0% slopes (Chapter 5; Chamoun et al. 2017b). Additionally, the *LVE* values for in-time venting with Φ = 115% were linearly interpolated for S = 2.4% (dashed curve in Figure 6.5).

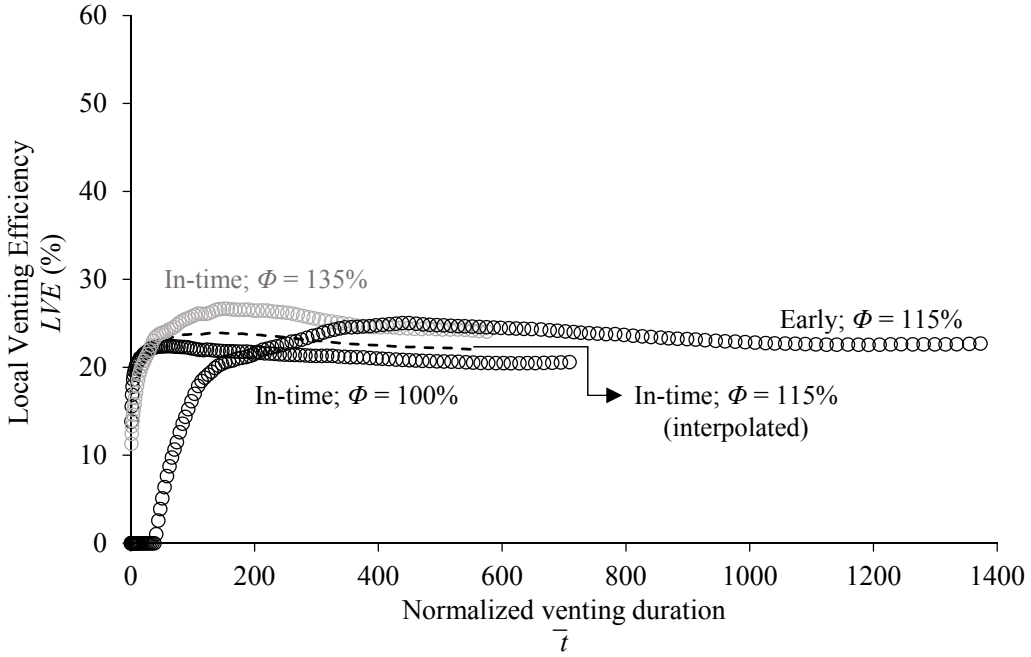

Figure 6.5: Local venting efficiency *LVE* for early venting and in-time venting for S = 2.4% (tests E1.8, E1.4 and E1.5). The dashed curve corresponds to the linear interpolation for in-time venting with Φ = 115%.

Figure 6.5 and Figure 6.6 show that early venting was not efficient at the beginning of the operation (before the current reached the outlet) since the outlet's streamlines could not accelerate the current and clear water was lost. In other words, no sediments were vented before the current closely approached the bottom outlet. This is more notable for the 2.4% slope where the approaching current was slightly slower than with the 5.0% slope and therefore the time between the opening of the outlet and the arrival of the current to the outlet was longer. This resulted in greater water loss at the beginning of the operation. However, over the longer term, although the current was not accelerated, the efficiency values obtained with early venting and in-time venting became similar for both slopes.

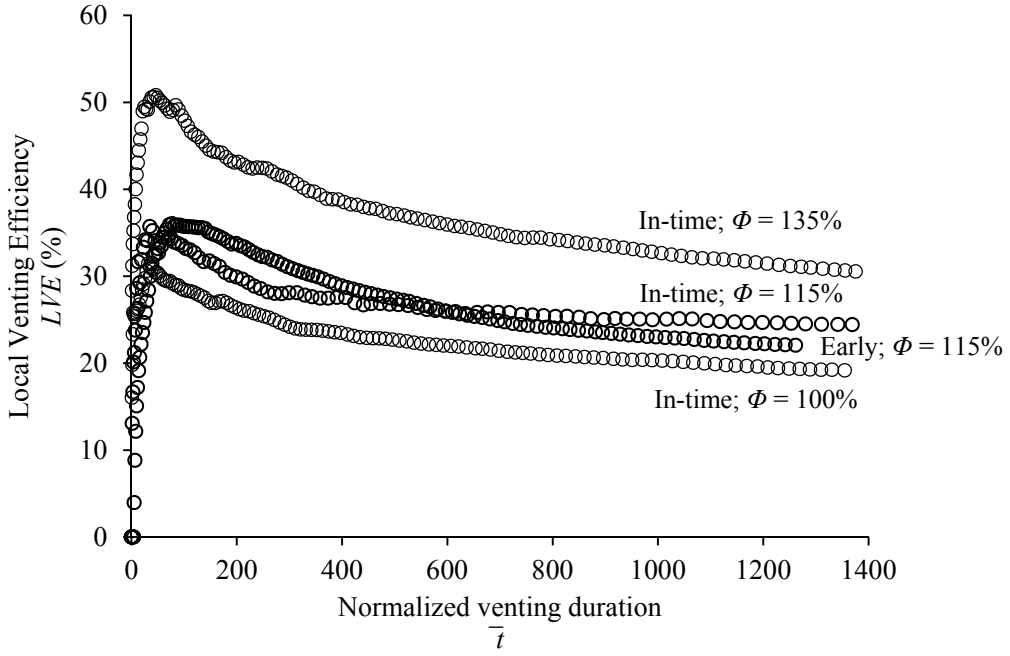

Figure 6.6: Local venting efficiency *LVE* for early venting and in-time venting for $S = 5.0\%$ (tests E2.7, E2.2, E2.3 and E2.4).

Based on these results, and since the influence of the outlet's flow field during venting is local, it can be expected that starting venting much earlier than the arrival of the current at the dam would result in high water loss. The earlier the opening, the longer the duration at the beginning of venting where the *LVE* is low or null. Therefore, venting should be timed as close as possible to the arrival of the current at the dam if possible, in order to ensure high efficiency at the beginning and throughout venting.

After a certain venting duration, flow conditions tend toward steadiness since inflow and outflow are steady and the muddy lake formed is partially evacuated and partially reflected upstream (before settling). Therefore, the quasi-steady values of *LVE* reached before the end of these tests can be considered as a reference state when projecting to longer venting durations. The long-term change that might affect this steadiness could be due to the sediments slowly settling in the upstream vicinity of the outlet, which can cause its partial clogging.

6.2.2 Venting efficiency indicator

The venting efficiency indicator (*VEI*) (Chamoun et al., 2017a) previously described as a criterion to assess sediment release and water loss (Chapter 4 and 5) is evaluated for each slope. Results are shown in Figure 6.7 and Figure 6.8.

In both cases, an early venting at d/h_{outlet} = 5 upstream of the outlet resulted in higher efficiency than late venting in terms of sediments released and water loss. For S = 5.0%, early venting produced a higher *VEI* just a few seconds after the beginning of the operation (the time needed for the current to reach the dam). With S = 2.4%, the current was slightly slower and therefore the *VEI* corresponding to the early venting required more time to surpass the *VEI* curves corresponding to late venting. The *VEI* results confirm the *LVE* results.

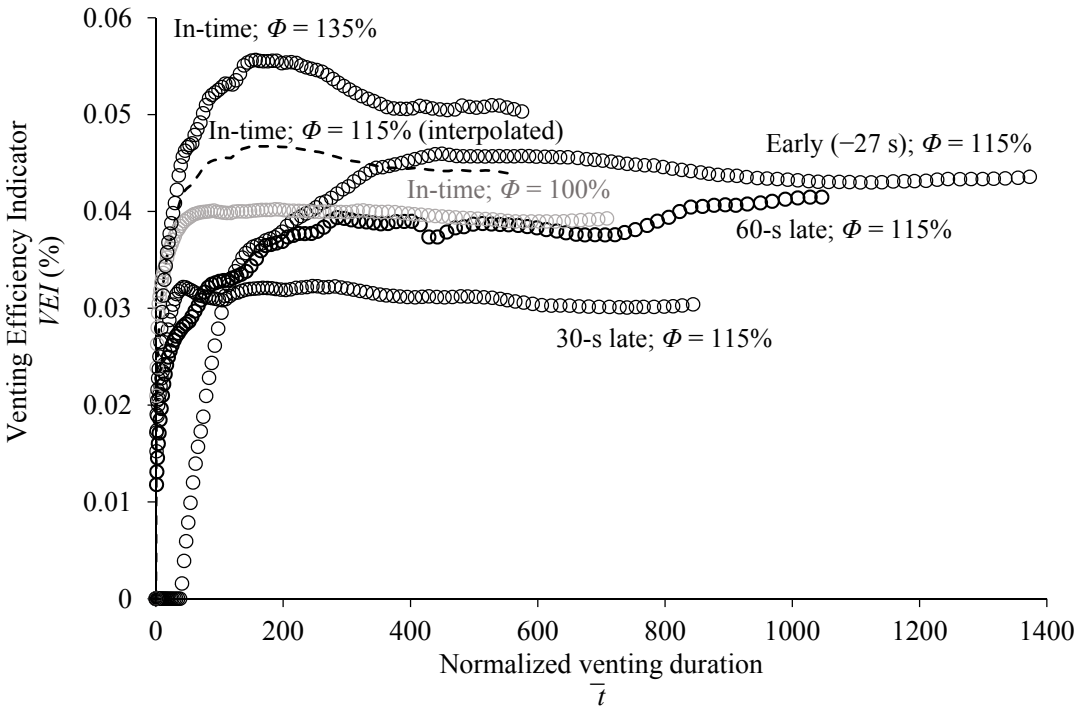

Figure 6.7: Venting efficiency indicator *VEI* for the different venting timings and venting degrees and a bed slope S = 2.4% (the dashed curve corresponds to the linear interpolation for in-time venting with Φ = 115%).

Furthermore, linear interpolation of the *VEI* (dashed curves in Figure 6.7 and Figure 6.8) shows that venting in-time with Φ = 115% leads to a closely similar or slightly higher efficiency than venting before the arrival of the current. Moreover, in-time venting has the advantage of directly releasing sediments from the very beginning. In contrast, early venting is not efficient before the current has reached the outlet, as concluded from both *LVE* and *VEI* values. Thus, the optimal timing for venting turbidity currents in terms of sediments and water loss is when the turbidity current arrives at the outlet.

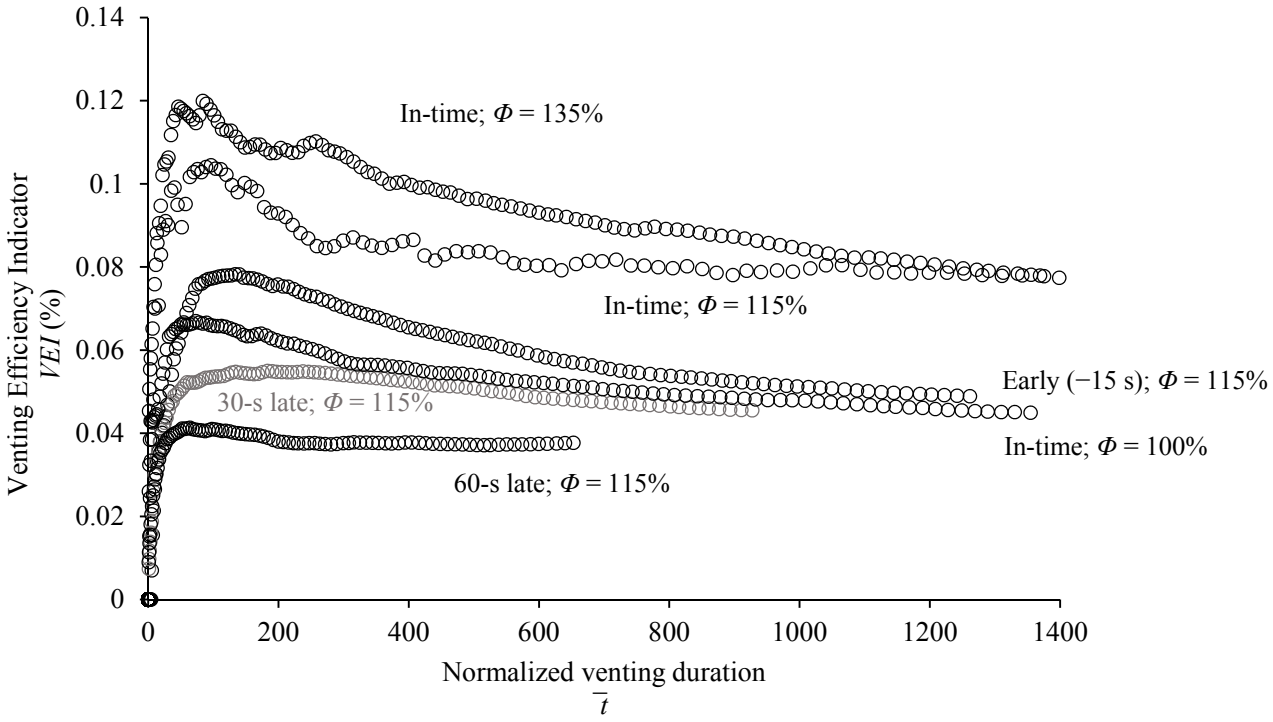

Figure 6.8: Venting efficiency indicator *VEI* for the different venting timings and venting degrees and a bed slope $S = 5.0\%$.

6.2.3 Required venting duration after the end of the flood

In the possibility of venting, operators not only wonder when to start the operation, but also when to stop it in order to avoid high water loss. Venting should last at least as long as the flood duration. However, once the flood ends, the suspended muddy lake formed upstream of the dam does not instantaneously settle. Therefore, to avoid sedimentation and clogging of the outlet over the long term, venting should not be immediately stopped after the end of the flood. To examine the maximum duration of venting after the flood ending, the latter was experimentally simulated by interrupting inflow during the two tests described hereafter.

In all the previous tests discussed up to this point, the turbidity currents were continuously fed. In past research, the typical behavior of outflow concentrations was experimentally evaluated when venting continuously-fed turbidity currents (e.g., Chamoun et al. 2017a; Chamoun et al. 2017b; Lee et al. 2014). It is characterized by a first phase of increasing concentration followed by a quasi-steady state. An example is shown in Figure 6.9 using a venting degree $\Phi = 135\%$ for the two slopes $S = 2.4\%$ and $S = 5.0\%$, where venting was started as soon as the current reached the dam.

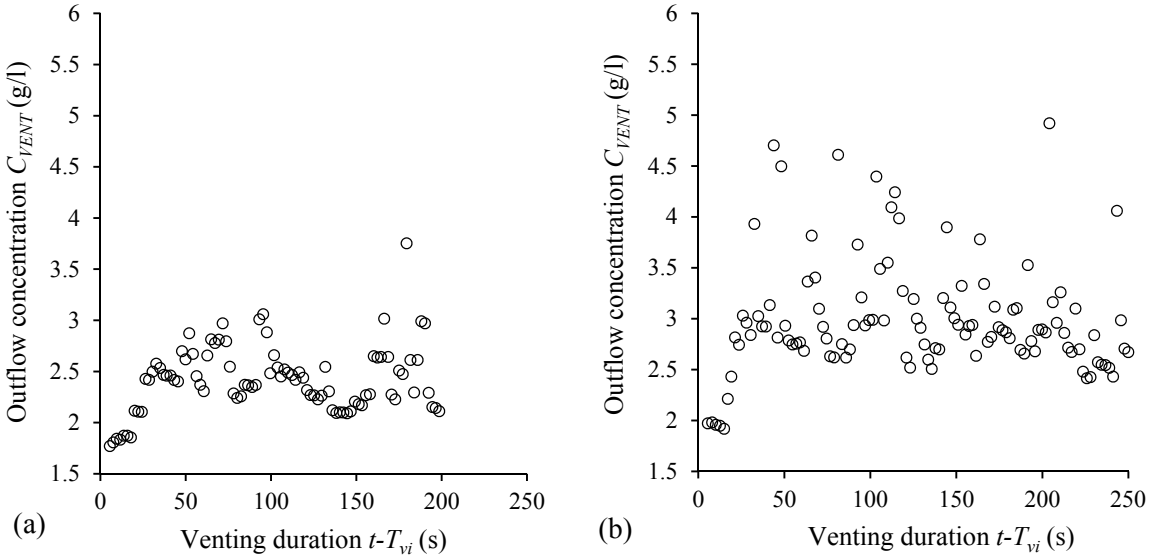

Figure 6.9: Outflow concentration as a function of venting duration for a venting degree Φ = 135% and for bed slopes (a) S = 2.4% and (b) S = 5.0% for a continuously-fed turbidity current and in-time venting.

In the following, two tests were performed where the turbidity current inflow discharge was stopped after around t_{cut} = 130 s of venting. Two venting degrees were tested: Φ = 30% and Φ = 65%. Relatively long venting durations were tested due to the low venting degrees chosen. In both cases, the concentration was observed to decrease once the inflow was interrupted (Figure 6.10 and Figure 6.11). In fact, the muddy lake formed in the vicinity of the outlet died out due to sediment settling as well as sediment evacuation through the outlet. Nevertheless, based on the trend lines in Figure 6.10 and Figure 6.11, the rate of outflow concentration decay after the interruption of the inflow was higher for Φ = 65% (8‰) than for Φ = 30% (4‰). The intercept values of the trend lines represent the maximum outflow concentration reached before the inflow was cut off.

Table 6.2: Time required for outflow concentrations to decrease after the inflow interruption.

Test No.	t_{cut} (s)	Time to lowest concentration value after flood end (s)
E2.9	130	1272
E2.10	130	923

This result can be explained by the fact that with Φ = 65%, larger amounts of sediment are released from the muddy lake than with Φ = 30%. Therefore, the muddy lake tends to fade away faster. In Figure 6.10 and Figure 6.11, the linear trend lines of outflow concentrations after the inflow interruption are extrapolated. The time needed for the outflow concentration to

decrease again to the lowest value measured at the beginning of venting (1.7 g/l in the tests; the reservoir's natural concentration in the prototype) can be concluded for each case (Table 6.2). Compared with Φ = 65%, the test with Φ = 30% requires more or less double the time for the concentration to decrease.

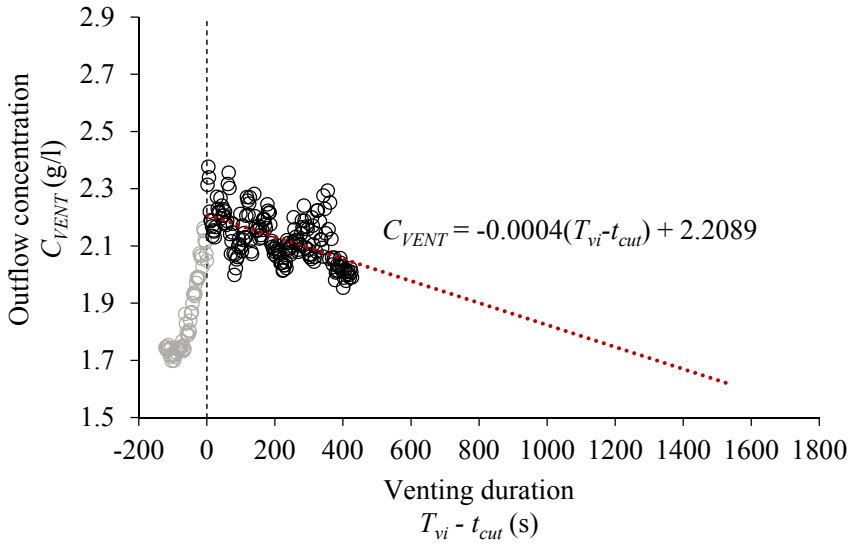

Figure 6.10: Outflow concentrations for a venting degree Φ = 30% on a 5.0% slope over time. The gray circles represent the outflow concentrations before the inflow discharge was stopped. The black circles show the outflow concentrations after the turbidity current inflow was stopped.

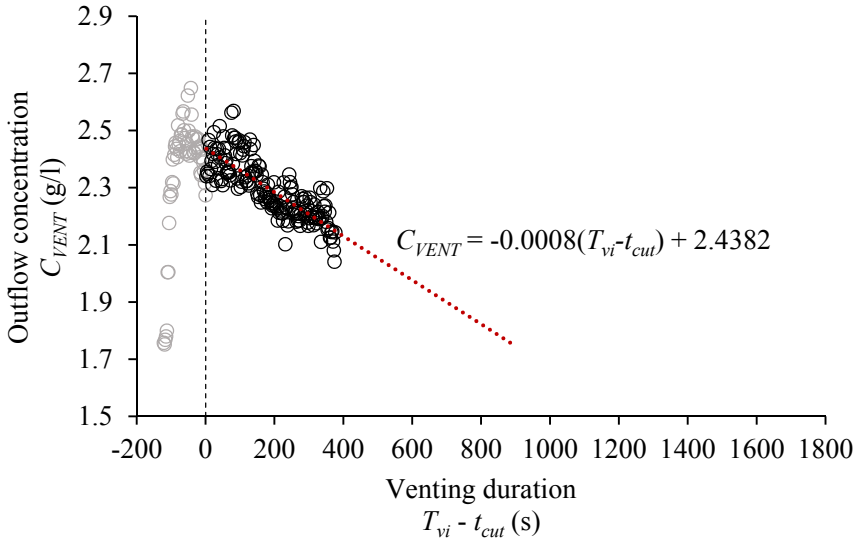

Figure 6.11: Outflow concentrations for a venting degree Φ = 65% on a 5.0% slope. The gray circles represent the outflow concentrations before the inflow discharge was stopped. The black circles show the outflow concentrations after the turbidity current inflow was stopped.

For practical applications, the inflow interruption corresponds to the end of a flood generating a turbidity current. The results in Figure 6.10 and Figure 6.11 show that the muddy lake upstream of the outlet can still be vented for a certain time after the end of the inflow. Comparing Figure 6.10 ($\Phi = 30\%$) with Figure 6.11 ($\Phi = 65\%$), it can be seen that this time depends on the venting degree Φ.

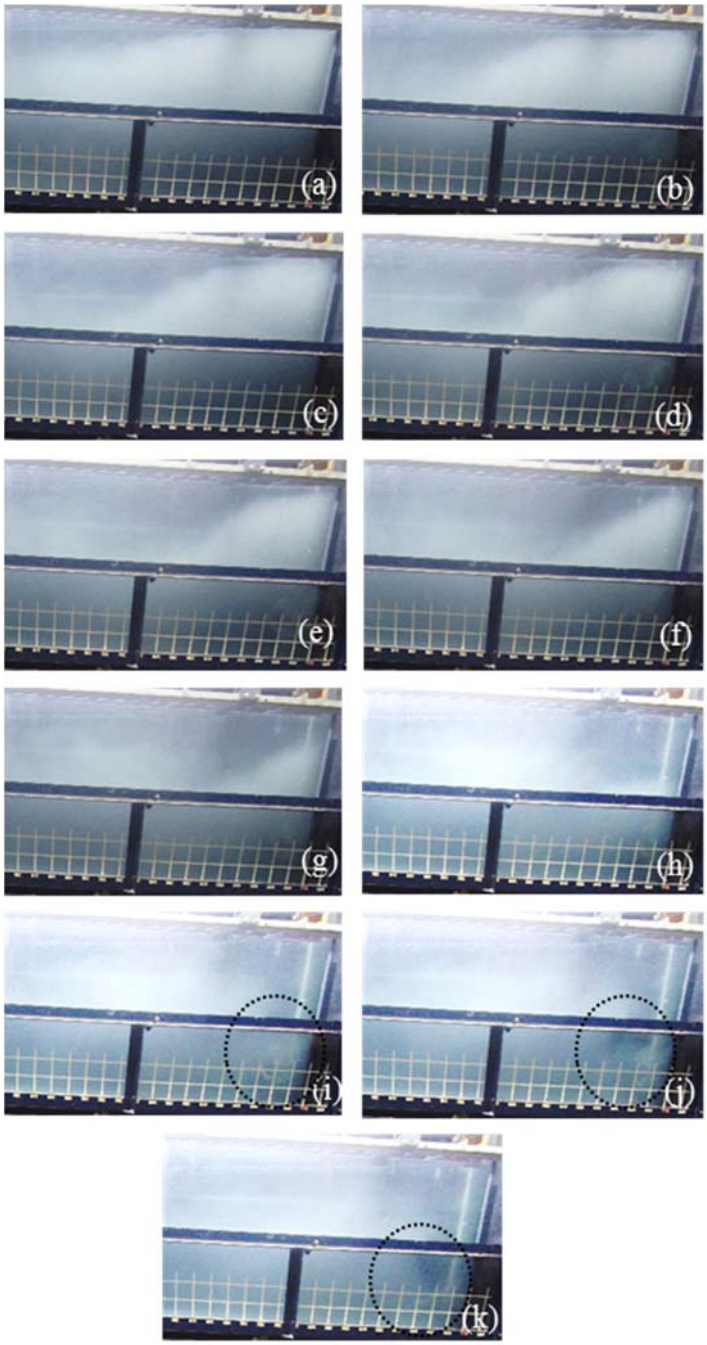

Figure 6.12: The muddy lake disappearing after cutting off the inflow (corresponding to Figure 14(a)). $\Delta t = 125$ s between Figure 14(a) and Figure 14(b) and $\Delta t = 5$ s between the remaining figures. Black circles highlight the location where the muddy lake can be seen to die out (test E2.10).

In the opposite case where inflow is not limited in time, the muddy lake slowly increases in size and expands upstream of the outlet (more or less, depending on the slope of the flume). However, in the case where the inflow is limited in time, the muddy lake slowly disappears. Part of its sediment is settling and another part is vented after the inflow ceases. The development of the muddy lake at different time steps after the inflow stopped is shown in Figure 6.12. Figure 6.12(a) corresponds to the time at which the inflow was interrupted. The time step between Figure 6.12(a) and Figure 6.12(b) is $\Delta t = 125$ s. Before that, no visual changes can be detected. For the rest of the sub-figures, $\Delta t = 5$ s.

Sediment deposition

The depositometer provides the total deposit at each bottom electrode. The deposition M_{deptot} measured at all bottom electrodes is summed up at each time step and shown as a function of the test duration in Figure 6.13. One of the cases where the inflow is stopped (E2.9) is compared to one of the cases where inflow is continuous during venting (E2.2).

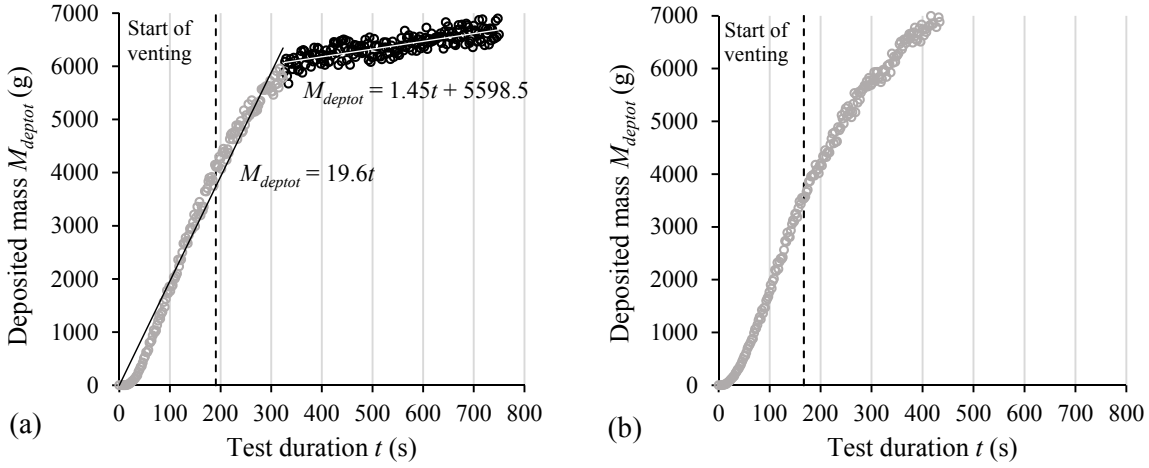

Figure 6.13: Mass of sediments deposited as a function of the duration of the test for a slope $S = 5.0\%$: (a) $\Phi = 30\%$ with inflow limited in time (test E2.9) and (b) $\Phi = 100\%$ with continuous inflow (test E2.2). The gray circles represent the deposited mass before the inflow was stopped. The black circles show the deposited mass after the inflow ceased. The dashed line corresponds to the start of venting.

The time during which the inflow is stopped corresponds to the black circles in Figure 6.13(a). As soon as the inflow stopped, the rate of deposition decreases, the curve flattens, revealing that the remaining suspended sediments deposit faster. The rate of deposition drops from 19.6 g/s to 1.45 g/s, decreasing 13.5 times. The dissipation of the current is also visually

seen through the transparent walls of the experiment flume once the inflow stopped. In the opposite case where the turbidity current is continuously fed, the deposition keeps increasing following more or less the same trend (Figure 6.13(b)).

After the inflow discharge is stopped, turbidity currents tend to die out. The currents produced in the present research all decelerate (Chamoun et al. 2017a). The front velocity U_f estimated using the video recordings decreases over time for both slopes. This is due to high rates of deposition rendering the currents less and less buoyant and unable to suspend the sediments they contain. This capacity of the turbidity currents to suspend the sediments can be assessed by Bagnold's auto-suspension criterion (Bagnold, 1962), expressed by $v_s/U_f < \sin\alpha$ (where α is the slope angle). Table 6.3 summarizes the values of v_s/U_f for each bed slope. The minimum and maximum values of v_s/U_f correspond to the maximum and minimum values of U_f, respectively. It can be concluded that $v_s/U_f > \sin\alpha$ most of the time, which explains the high deposition behavior of the turbidity currents.

Table 6.3: Settling velocity relative to front velocity v_s/U_f for each bed slope compared with $\sin\alpha$.

Bed slope S **(%)**	**Slope angle** α **(°)**	v_s/U_f		$\sin\alpha$
		Min	**Max**	
2.4	1.4	0.030 (> 0.02)	0.070 (> 0.02)	0.02
5.0	2.9	0.034 (< 0.05)	0.075 (> 0.05)	0.05

6.3 Conclusions

The opening timing of the bottom outlet during a venting operation was experimentally investigated for two different reservoir bed slopes S. Four different timings were tested: (1) early venting corresponding to opening the outlet when the current was at a distance $d/h_{outlet} = 5$ from the outlet (i.e., −27 s for $S = 2.4\%$ and −15 s for $S = 5.0\%$), (2) in-time venting synchronized with the arrival of the turbidity current at the outlet, (3) late venting timed 30 s after the current has arrived at the outlet and (4) late venting timed 60 s after the arrival of the current. The cases of late venting are directly linked to physical conditions: 30 s corresponds to the time at which the current starts being reflected upstream of the wall or the dam and 60 s corresponds to the time at which the muddy lake is formed and the current has already started reflecting upstream.

Based on the analysis of the local venting efficiency (*LVE*) and the venting efficiency indicator (*VEI*), considering sediments evacuated and water loss, venting should ideally begin

as soon as the turbidity current reaches the vicinity of the bottom outlet. Early venting was more efficient than late venting. When the outlet was opened before the arrival of the current, even though no acceleration of the current can be observed, the potential flow field upstream of the operating outlet was better developed. This renders the venting of the current smoother and thus the transit of the sediments more efficient. In the case of the late opening, the sediments in the muddy lake start to settle before venting has started, rendering their release almost impossible.

In contrast, the duration of venting should last after the end of inflow and before outflow concentrations decrease to the initial reservoir concentration values, which depends on the venting degree. For a 65% venting degree for example, this duration was almost twice as short as for a 30% degree where the muddy lake could last longer before settling out or being evacuated. Additionally, the increased rate of the total sediment deposition immediately dropped 13.5 times after the end of the turbidity current inflow. After a certain time, the cumulated mass of sediment deposit is expected to reach a constant value because no sediments will be available to settle. The time it takes for the total deposition to reach this steady state is directly linked to the settling velocity of the material. In future research, it would be useful to test other parameters that might potentially influence the optimal duration of venting after the end of inflow. These parameters include the geometry of the reservoir and the thalweg's slope close to the outlet.

The optimal timing of venting with minimized loss of useful clear water strongly depends on the estimation of the travel duration of the turbidity current along the reservoir, from the plunge point to the dam. For instance, in the Rio Grande Reservoir, Fiock (1934) stated that given the size of the reservoir, silty water is detected in the outflow 2–5 days after the density current has entered the reservoir. An underestimation of this relatively long traveling time can generate significant water losses. However, the exact time at which the turbidity current reaches the dam is rarely measured in reservoirs where venting is applied. To obtain better information on the dam site, it is highly recommended to take velocity or concentration profile measurements over the reservoir's depth near the dam, particularly during yearly flood events that may trigger turbidity currents. Possible mounting procedures and settings were mentioned by Müller (2012) and Schneider et al. (2007). Considering that the time required to open the gate and for the flow field to establish is around 5–10 minutes, and that the common turbidity current velocities are between 30 cm/s and 100 cm/s (De Cesare 1998; Khripounoff et al. 2003; Lambert and Giovanoli 1988; Xu 2010), the distance at which the measurements should be taken is around 300 m upstream of the dam. In other words, once the turbidity current is

detected at this distance, the gate should be opened to allow in-time venting, leading to high sediment release efficiency. The travel time of the turbidity current can also be estimated using a numerical model calibrated based on field data. Summarily, venting should be preferably performed when the turbidity current is at a minimum distance of $s_{min} \approx 300$ m and a maximum distance of $s_{max} = 5(h_L)_{\phi=80\%}$. If $5(h_L)_{\phi=80\%} < 300$ m then $s_{max} = s_{min} \approx 300$ m.

Finally, if performed under controlled conditions, venting of turbidity currents is an economical and environmentally friendly technique of sediment mitigation in reservoirs. Well-timed venting operations applying adequate outflow discharges for an optimized duration helps minimize water loss while reducing sedimentation in reservoirs and providing necessary sediments to the downstream river.

Chapter 7

NUMERICAL MODELING OF TURBIDITY-CURRENT VENTING

Despite the numerous advantages of experimental testing, numerical modeling offers easiness of geometrical variation and a wide range of monitored parameters among other appealing features. When properly calibrated with experimental or field data, a numerical model is a convenient means for extending experimental results. In the present chapter a numerical model is used to investigate several parameters among which the outlet's dimensions, position and approach slope. Additionally, the zone of influence of the bottom outlet during venting was defined and determined.

7.1 Introduction

Numerical modeling of turbidity currents offers great insight on the various parameters and aspects of these complex sediment-laden currents. Turbidity currents occur in flood conditions; therefore their observation and measurement in the field is complicated and has been rarely performed in the past. The experimental triggering and monitoring of turbidity currents is relatively convenient. However, numerical models, when adequately calibrated with field and experimental data allow better geometrical and parametrical flexibility.

A wide range of theoretical, empirical and analytical studies has been performed on turbidity currents in the past (Altinakar et al., 1990; Garcia, 1992; Parker et al., 1987; Parker et al., 1986; Stow & Bowen, 1980), which allowed the development and improvement of robust numerical codes properly representing the dynamics of turbidity currents. Several numerical studies were undertaken on turbidity currents studying their dynamics, deposits, effects on structures, and triggering conditions. Georgoulas et al. (2010) proposed a multiphase model to reproduce 3D turbidity currents from laboratory experiments by Gladstone et al. (1998) and Baas et al. (2004) using the CFD code Fluent of ANSYS Inc. Jiang et al. (2014) also used Fluent to simulate the deposits of turbidity currents in the Qiongdongnan Basin (China). Lee et al. (2014) performed numerical modeling to investigate venting of turbidity currents using the CFX solver of ANSYS Inc. De Cesare et al. (2001, 2006) used the CFX solver to simulate turbid density current movement at Luzzone Reservoir and at Lake Lugano. Huang et al. (2008) performed numerical simulations comparing turbidity currents generated by sudden-release (lock-exchange) and those generated by continuous inflow. The work also highlighted the considerable scale effect induced by sudden-release experiments when compared with large-scale field cases. Khan et al., (2005) investigated the hyperpycnal plumes (turbidity currents) generated by the plunging of River Tronto into the Adriatic shelf using a 2D depth-integrated finite volume model and focused particularly on the depositional pattern of the currents. Cao et al., (2015) proposed a 2D double layer-averaged model to reproduce the whole process of turbidity currents in reservoirs starting from the open-channel flow (subaerial) preceding plunging to the formation and flow (subaqueous) in the reservoir. They also considered the case of Xiaolangdi Reservoir and revisited one turbidity current venting event. A similar study was conducted by Wang et al. (2017) using a 1D model to simulate the whole process along with an application on the Sanmenxia Reservoir case. Finally, a review on the computational modeling of turbidity currents was performed by Meiburg (2015).

Generally, literature showed that CFX solvers proved to be very effective in representing the two-phase flow characteristics of turbidity currents and generated satisfying results when compared with laboratory and field measurements (Lee et al., 2014).

7.2 Description of the numerical model

At the beginning of the numerical work, a 2D model was built given that the flume is relatively narrow and the flow can be considered as two-dimensional. However, since the outlet is positioned on part of the flume's width, the model was extended to a 3D model, which gave more accurate results. The software ANSYS Inc. was used and the CFX 17.1 solver was chosen.

7.2.1 Geometry

The geometry of the numerical model is built based on the experimental set-up. The horizontal approach bed is chosen for the numerical investigation. Figure 7.1 shows the geometry along with the dimensions of the different elements: L is the length of the main flume, H_{water} the clear water depth in the case of the horizontal bed ($S = 0\%$), w and w_{outlet} are the widths of the flume and that of the bottom outlet respectively, h_{inlet}, h_{diff}, h_{outlet}, h_{weir} and $h_{downwall}$ are the heights of the inlet, diffusor, outlet, weir and downstream wall respectively.

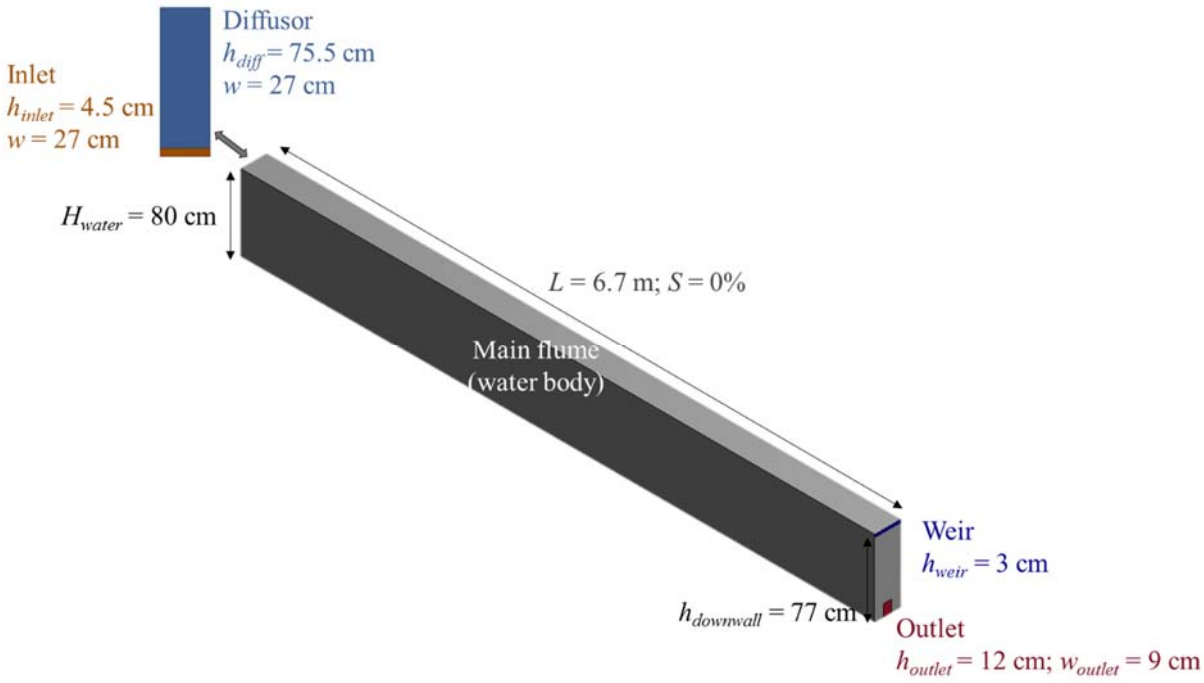

Figure 7.1: Geometrical characteristics of the numerical model.

7.2.2 Mesh

The mesh is tetrahedral except for the region where an inflation is applied between the bed and the water body (main flume). The inflation option applied is the ‘’first layer thickness’’. The first layer height is fixed at 1 mm with a growth rate of 1.2. The maximum layers on which inflation is applied is 11. This means that the inflation starts from the bed up to a layer of 32 mm (Figure 7.2). The inflation allowed good modeling of the lower layer of the current particularly at the near-bed region. This region is of great importance especially when modeling non-conservative gravity currents. In the present case, turbidity currents are depositive (non-conservative) and sediment concentrations near the bed gradually increase during the flow, affecting the dynamics of the currents. The mesh consists of some 524’393 elements (depending on the configuration tested, e.g., outlet dimensions).

Additionally, edge sizing is applied on the different edges of the model. The details are summarized in Table 7.1. However, the mesh is automatically generated, adapting as much as possible to the imposed conditions. Therefore, some elements might be differently sized compared with the dimensions presented in Table 7.1.

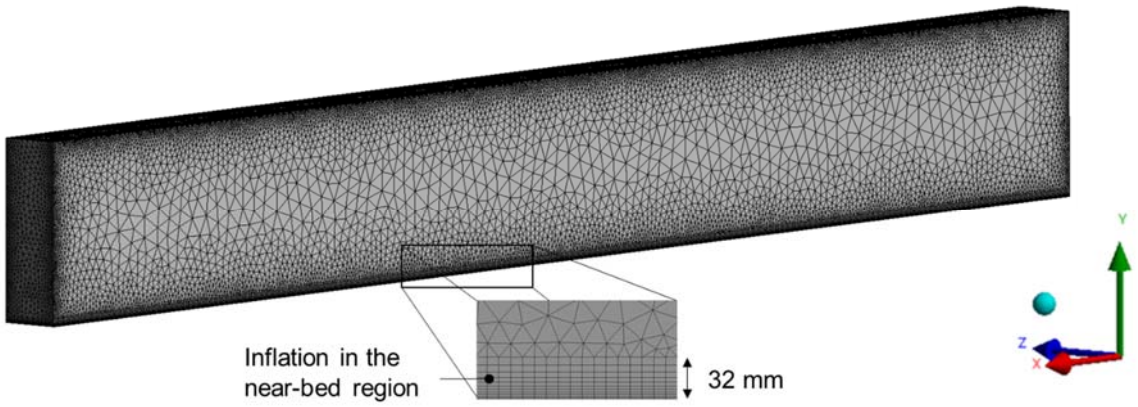

Figure 7.2: View of the mesh of the 3D model with a zoom on the bed inflation.

Table 7.1: Characteristics of the different edge sizing applied for the mesh.

Edge	Element size (mm)	Element number
L	9	745
w	50	6
w_{outlet}	20	5
h_{inlet}	9	84
h_{diff}	9	84
$h_{downwall}$	9	86
h_{weir}	9	4

7.2.3 Model setup

An inhomogeneous Eulerian-Eulerian multiphase model is used with the Shear Stress Transport (SST) turbulence model. The Particle Model is used to model the interfacial area density and transfer terms between the two phases. The Density Difference Model is used to represent the fluid's buoyancy. The process is isothermal; no heat transfer is considered and thus no thermal energy balance is solved. The density of the fluid is set through the sediment volumetric concentration and the computation is based on the Reynolds-averaged Navier-Stokes equations. All details concerning the equations solved for momentum, continuity, volume conservation and interphase transfer can be found in the ANSYS Inc (2013) user's guide.

The CFX solver offers the possibility for users to gain better control of the code through the insertion of CEL (CFX Expression Language) expressions. Hereafter are the CEL expressions implemented in the CFX solver and which improved the representativeness of the model in the present case:

- The settling velocity V_s is a function of the concentration of the suspension (Richardson & Zaki, 1997) and is expressed by:

$$\frac{V_s}{V_0} = (1-C)^m \tag{7.1}$$

where V_s is the settling velocity of the particle in a suspension having a volumetric concentration C, V_0 is the settling velocity of the particle in clear water, m is a coefficient that depends on Reynolds number. Several values of m ranging from 2.25 to 7 were proposed in literature as summarized by Chien and Wan (1999). However, a sensibility analysis was performed and showed that varying this coefficient had very little effect on the results in the present conditions. A value of 2.5 was given to m. On another hand, the following formula of the settling velocity of natural sediment particles in clear water V_0 is used (Zhiyao et al., 2008):

$$V_0 = \frac{\nu}{d_{50}} d_{50*}^3 [38.1 + 0.93 d_{50*}^{12/7}]^{-7/8} \tag{7.2}$$

where,

$$d_{50*} = \left[\frac{\rho_s - \rho_w}{\rho_w} \frac{g}{\nu^2} \right]^{1/3} d_{50} \tag{7.3}$$

and ρ_s is the particle density, ρ_w the clear water density, g the gravity acceleration and ν the kinematic viscosity of water.

- The drag coefficient was introduced as (Cheng, 1997):

$$C_d = \frac{4}{3}\frac{\rho_s - \rho_w}{\rho_w}\frac{gd_{50}}{V_s^2} \tag{7.4}$$

- The deposition process of the sediments is not represented by the CFX solver and therefore had to be imposed indirectly through a relationship between the mixture's dynamic viscosity and the concentration of the current *C*. The dynamic viscosity μ_m of the mixture is computed based on the equation of the kinematic viscosity of a sediment-laden flow proposed by Van Rijn (1987). The latter relates the viscosity to the volumetric sediment concentration. The equation was adapted to suit numerical conditions (notably when the sediment concentration of a mesh element is $C = 0$ or $C = 0.74$) and is presented as such:

$$\mu_m = \min(\mu_w(1+\lambda)(1+0.5\lambda), 5) \tag{7.5}$$

where,

$$\lambda = ((0.74/(0.73998C + 0.0001)^{1/3} - 1)^{-1} \tag{7.6}$$

and $\mu_w = 0.89 \times 10^{-3}$ kg/m.s (at 25 °C) is the dynamic viscosity of clear water. The output of this relationship is shown in Figure 7.3. Thus, starting a certain concentration, the viscosity of the current becomes too high for the buoyancy of the current to keep the sediments in suspension. Consequently, sediments in such regions with high concentration act like deposited sediments. These high concentrations are especially located in the near-bed region where deposition occurs.

The two phases are water and sediments (as dispersed solid). Experimentally, the sediments are angular and the mean diameter d_{50} measured by the MasterSizer ranged between 130 µm and 144 µm (Chapter 3 section 3.2). Nonetheless, the particles in the numerical model were considered as spherical particles with a mean diameter set to 120 µm and $\rho_s = 1160$ kg/m^3. In fact, in the numerical model, a $d_{50} = 130 - 140$ µm could not represent the dynamics of the current well enough; the currents were slower compared to the experimental tests and less sediments reached the dam. However, representing the shape and characteristics of the sediments with higher exactitude requires more information on the shape of the particles and induces heavy computational capacities and time.

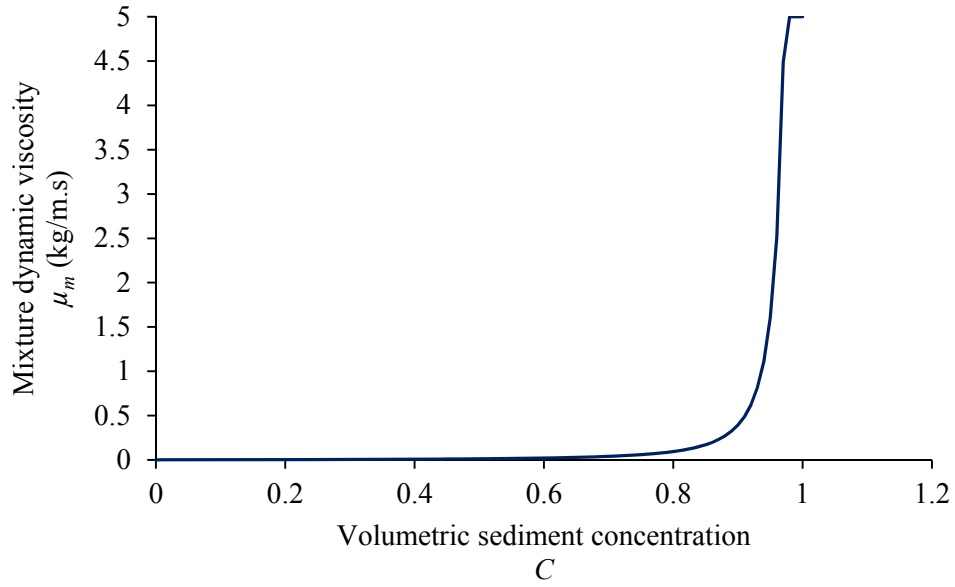

Figure 7.3: Relationship between the dynamic viscosity of the mixture μ_m and the volumetric sediment concentration C.

7.2.4 Initial and boundary conditions

At the initial state, the volume fraction of water in the whole body is set to 1 and that of the sediments to 0. The velocity is set to 0 m/s. Seven different boundary conditions were created in the highlighted regions of Figure 7.4 below:

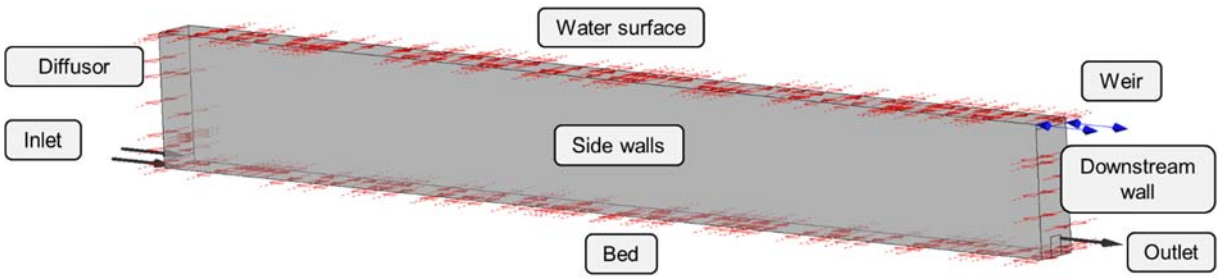

Figure 7.4: Location of boundary conditions of the numerical model.

- Inlet: an ‘’inlet’’ boundary condition is used with a specified normal speed of $u_{inlet} = 0.0817$ m/s, corresponding to $Q_{TC} = 1$ l/s used experimentally. The k and ε turbulence model is used with the turbulence kinetic energy $k = 1.5(Iu_{in})^2$ and the turbulence eddy dissipation $\varepsilon = k^{3/2}/h_{inlet}$ where $I = 0.037$ is the standard turbulence intensity value (ANSYS, 2013) and $h_{inlet} = 0.045$ m is the dissipation length chosen. The

sediment volume fraction at the inlet is 0.025 corresponding to the average value tested experimentally. Consequently, the water volume fraction is 0.975.

- Outlet: an ‘’outlet’’ boundary condition is imposed at the outlet with a specified normal speed u_{VENT} depending on the outlet discharge tested. A function is created to control the timing of the outlet opening.
- Diffusor: a ‘’no-slip wall’’ condition is used when $Q_{VENT} < Q_{TC}$ and the discharge through the diffusor $Q_{RES} = 0$ l/s (defined in Chapter 3, section 3.4). In the opposite case ($Q_{VENT} > Q_{TC}$), an ‘’inlet’’ condition is applied to the diffusor with a normal speed u_{RES} corresponding to a discharge $Q_{RES} = Q_{VENT} - Q_{TC}$.
- Bed and downstream wall: a ‘’no-slip wall’’ condition is set in these regions.
- Side walls: a ‘’symmetry’’ plane condition is used.
- Weir: an ‘’opening’’ is applied at this location with the relative static pressure used as the Mass and Momentum law.
- Water surface: a ‘’free slip’’ boundary condition is used.

7.3 Calibration of the numerical model

Before reaching satisfying numerical results, numerous sensitivity tests were done. Parameters were varied (i.e., different expressions for the drag coefficient, boundary conditions, sediment characteristics, turbulence models). The numerical model was calibrated based on the experimental data obtained with the horizontal bed. Different venting degrees ϕ were simulated. The main comparative criteria considered was the outflow concentration C_{VENT}. Examples of the cases of $\phi = 80\%$ and $\phi = 115\%$ are shown in Figure 7.5 and Figure 7.6.

The highest deviation was observed at the beginning of venting. This is essentially due to the fact that in the numerical model, the values are obtained right at the exit of the outlet, while in the experimental model, the evacuated flow passes through the venting pipe (≈ 300 cm) before reaching the downstream basin where it is measured. However, the steady phase of the outflow discharge is well represented and the deviation of the numerical values from the experimental values ranged between 14% and 20%. This deviation is acceptable considering the complexity of the simulated phenomenon, particularly in the vicinity of the outlet where the muddy lake forms.

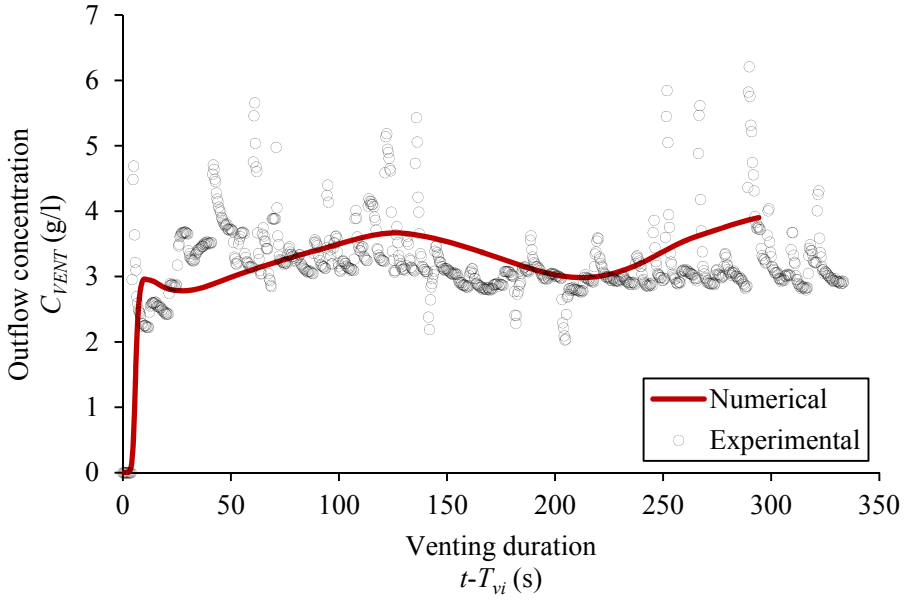

Figure 7.5: Outflow concentrations obtained experimentally and numerically for a venting degree $\phi = 80\%$, a horizontal bed, and an opening timing synchronized with the arrival of the current at the wall.

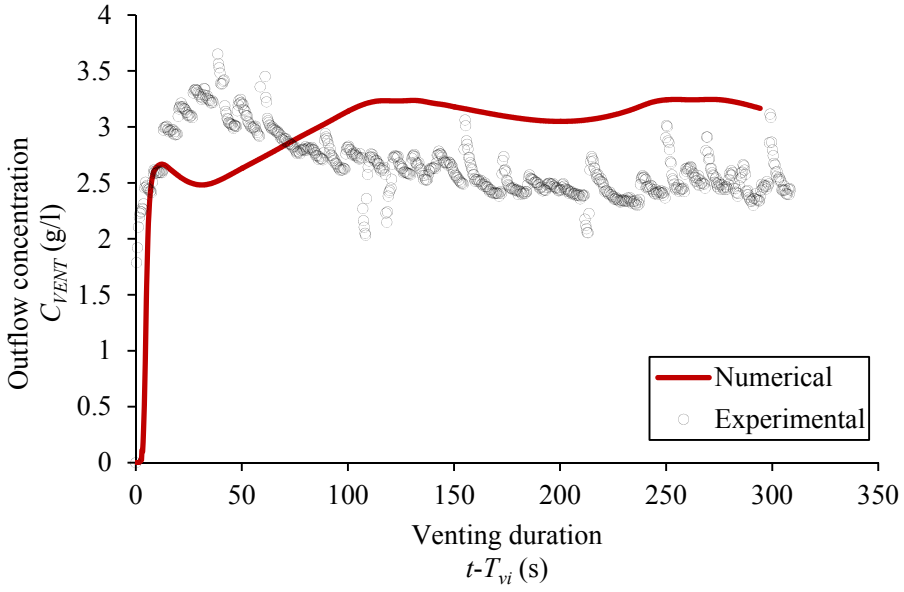

Figure 7.6: Outflow concentrations obtained experimentally and numerically for a venting degree $\phi = 115\%$, a horizontal bed, and an opening timing synchronized with the arrival of the current at the wall.

The representative venting efficiency *RVE* (Chapter 4, Figure 4.11) was also used to verify the numerical model. The results obtained numerically deviate by only 9.6% from the experimental efficiency values (Figure 7.7).

On another hand, the velocity profile measured experimentally by the UVP at 4.1 m from the inlet is compared with the velocity profile obtained numerically at the same location (Figure 7.8). The velocity is globally well reproduced, despite the fact that the counter current above the turbidity current could not be well simulated. Similarly to the experimental analysis (Chapter 4, section 4.3.4), the characterizing height H_{num} and velocity U_{num} were determined using the equations of Turner (Chapter 2, Equations (2.6) and (2.7)). The numerical values obtained are $U_{num} = 2.7$ cm/s and $H_{num} = 22.5$ cm, a divergence of 20% and 5% with the experimental U and H respectively.

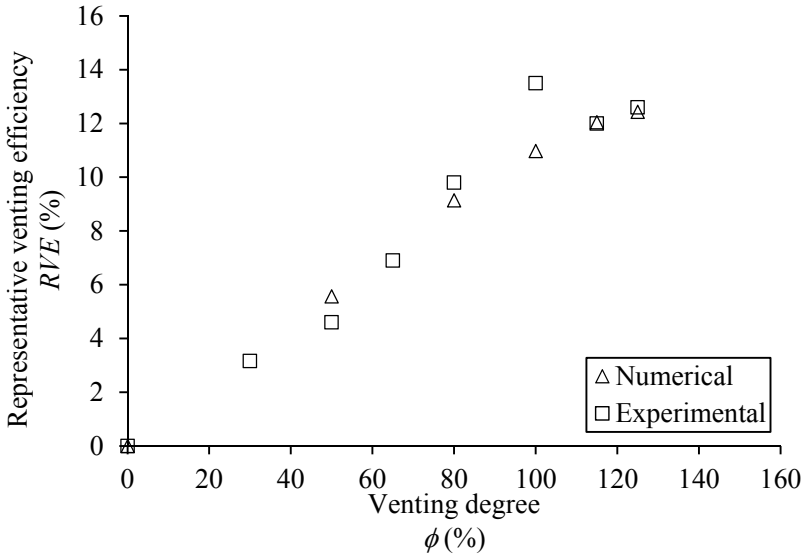

Figure 7.7: Numerical and experimental representative venting efficiency RVE as a function of the venting degree ϕ.

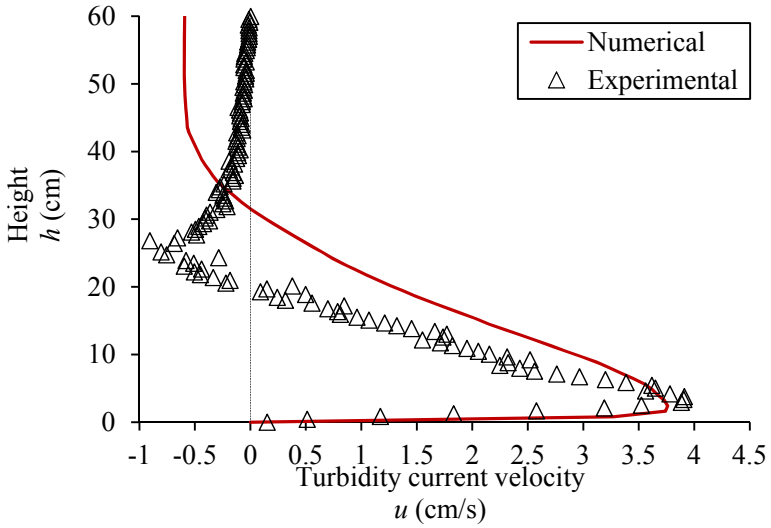

Figure 7.8: Experimental and numerical longitudinal velocity profiles obtained at 4.1 m from the inlet.

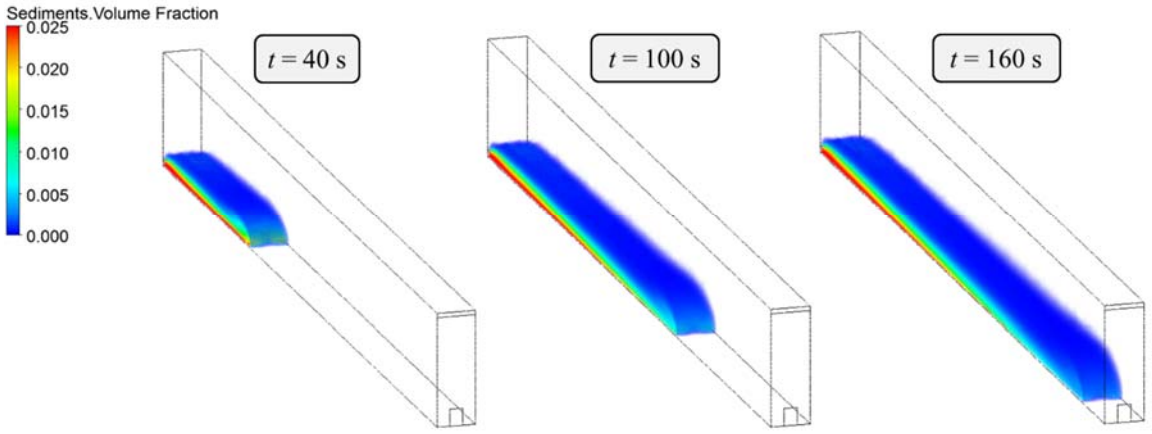

Figure 7.9: Turbidity current progressing in the flume at t = 40 s, 100 s and 160 s.

The average front velocity of the turbidity currents obtained experimentally for a horizontal bed is 3.72 cm/s and the average numerical front velocity is 3.80 cm/s. An error of only 2%. The deceleration of the current is successfully simulated, meaning that the hydro-dynamics of the currents are well represented numerically (Figure 7.9).The numerical and experimental front velocities as a function of the longitudinal position of the turbidity current from the inlet are compared in Figure 7.10.

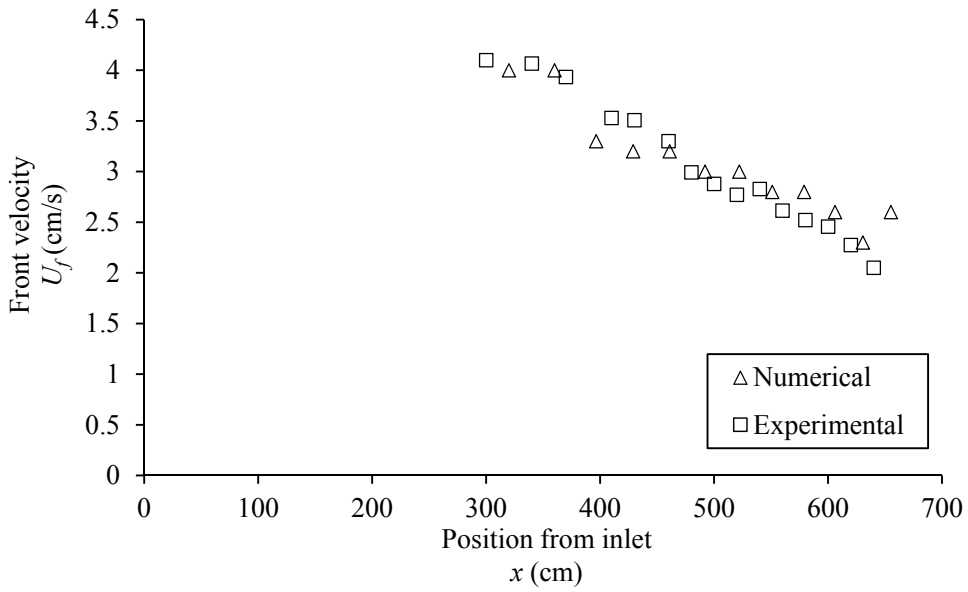

Figure 7.10: Numerical and experimental front velocities U_f as a function of the current's position from the inlet.

7.4 Numerical simulations

Table 7.2 presents the numerical simulations that will be discussed in this chapter. The different parameters varied are: the outlet's height h_{outlet}, width w_{outlet}, level l_{outlet} and the venting degree ϕ. Cases of early venting were also tested in the goal of determining the maximum distance of influence of the outlet. Additionally, a geometrical variation resembling prototype conditions was simulated.

Table 7.2: Overview of the numerical simulations.

Simulation Number No.	Outlet height h_{outlet} (cm)	Outlet width w_{outlet} (cm)	Outlet level l_{outlet} (cm)	Bed slope S (%)	Venting degree ϕ (%)	Timing
N0.1	3	9	0	0	100	In-time
N0.2	6				100	
N0.3	24				100	
N0.4	12	27			100	
N0.5		3			100	
N0.6		1			100	
N0.7		9	12		100	
N0.8			24		100	
N0.9			0		50	
N0.10					80	
N0.11					115	
N0.12					125	
N0.13					150	
N0.14					165	
N0.15					185	
N0.16					200	
N0.17					0	Early
N0.18					10	
N0.19					30	
N0.20					50	
N0.21					65	
N0.22						

Simulation Number No.	Outlet height h_{outlet} (cm)	Outlet width w_{outlet} (cm)	Outlet level l_{outlet} (cm)	Bed slope S (%)	Venting degree ϕ (%)	Timing
N0.23	12	9	0	0	80	Early
N0.24					90	
N0.25					100	
N0.26	6	9	0	0	100	
N0.27	12					
N0.28	24					
N1.1	12	9	0	Combined	100	In-time
N1.2				5	100	In-time
N1.3					115	Early
N1.4					115	60-s late

7.5 Numerical results

The total time of the simulations is $t = 470$ s on average with a time step of 0.25 s. This time step was optimized in order to reach convergence of the solution and satisfying Courant Number stability criterion (ANSYS 15.0, 2013). Venting starts at $t = T_{vi} = 176$ s, the time at which the turbidity current reaches the outlet. Numerical simulations converged well: only one iteration was needed most of the times and the Courant Number was always < 1.

Unlike experimental conditions, numerical simulations ensure a full steadiness of boundary conditions, particularly at the inlet, between different simulations and throughout the same simulation. The currents simulated numerically are similar in terms of dynamics (particularly deposition) and the amount of sediments reaching the outlet is the same during the different simulations (using the same bed slope). Hence, the criterion that will be used numerically for the assessment of the efficiency of venting operations under the different conditions is the outflow concentration. The parameters tested numerically are discussed hereafter.

7.5.1 Outlet level

The level of the lower sill of the outlet having the experimental dimensions (i.e., h_{outlet} and w_{outlet}) is fixed at three different vertical positions: at the bottom, 12 cm and 24 cm above the bed level. Results show that the higher the outlet, the lower the outflow concentrations and thus the less efficient venting becomes (Figure 7.11). One of the reasons for this behavior is that the

higher the outlet, the more the turbidity current will be reflected. As shown in Figure 7.12, a reflected turbidity current forms for the cases where the outlet is placed above the bottom. The reflected current reaches larger distances upstream when the outlet is placed at higher levels from the bottom.

Another reason is related to the height of aspiration of the outlet. The height of aspiration calculated experimentally for the case of $\phi = 100\%$ on a horizontal bed is $h_L = 21.5$ cm (above and below the outlet's central axis). Since h_L depends on the outflow discharge and the density of the current approaching the outlet, the same value is valid for the different cases of vertical levels. For the outlets placed at $l_{outlet} = 0$ cm and $l_{outlet} = 12$ cm, the outlet's central axis is located at 6 cm and 18 cm above the bed level respectively. The height of aspiration $h_L > 6$ cm and 18 cm, therefore the turbidity currents reaching the outlet will be in the zone of aspiration. Contrarily, in the case of $l_{outlet} = 24$ cm, the central axis of the outlet is located at a height of 30 cm above the bed while the lower limit of the height of aspiration only reaches a height of 30-21.5 = 8.5 cm above the bed. Hence, the part of the turbidity currents comprised in the first 8.5 cm above the bed are not evacuated nor affected by the outlet.

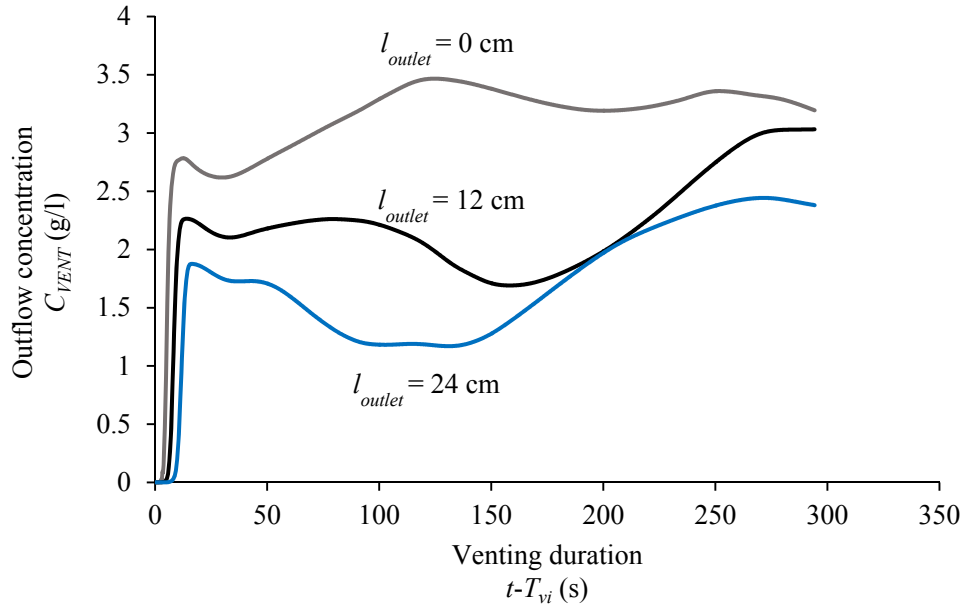

Figure 7.11: Outflow concentrations obtained with the different outlet levels with $\phi = 100\%$ (simulations N0.4, N0.8 and N0.9).

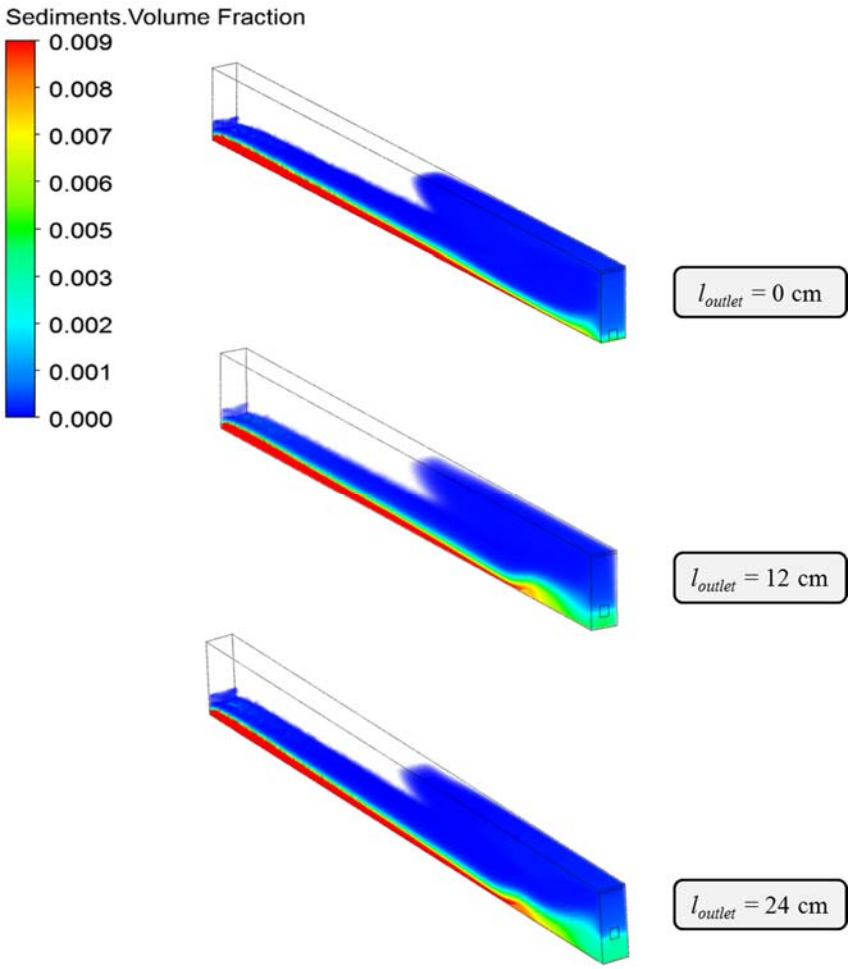

Figure 7.12: Volume rendered sediment volume fraction for the three different outlet levels tested with $\phi = 100\%$ (simulations N0.4, N0.8 and N0.9 at $t = 400$s).

7.5.2 Outlet height

The height of the outlet was varied while maintaining the same venting degree $\phi = 100\%$. A total of four outlet heights were tested: $h_{outlet} = 3$ cm, 6 cm; 12 cm and 24 cm. Figure 7.13 shows the upper limits of the different outlet heights tested, relatively to the turbidity current's height as well as a front view of the outlet and downstream wall. The ratio between the height of the outlet and the current's height (section 7.3) h_{outlet}/H_{num} is 0.1, 0.3, 0.5 and 1.1 respectively. The ratio between the level of the height of aspiration and the height of the current $[h_L + (h_{outlet}/2)]/H_{num}$ is 1.0, 1.1, 1.2 and 1.5 respectively.

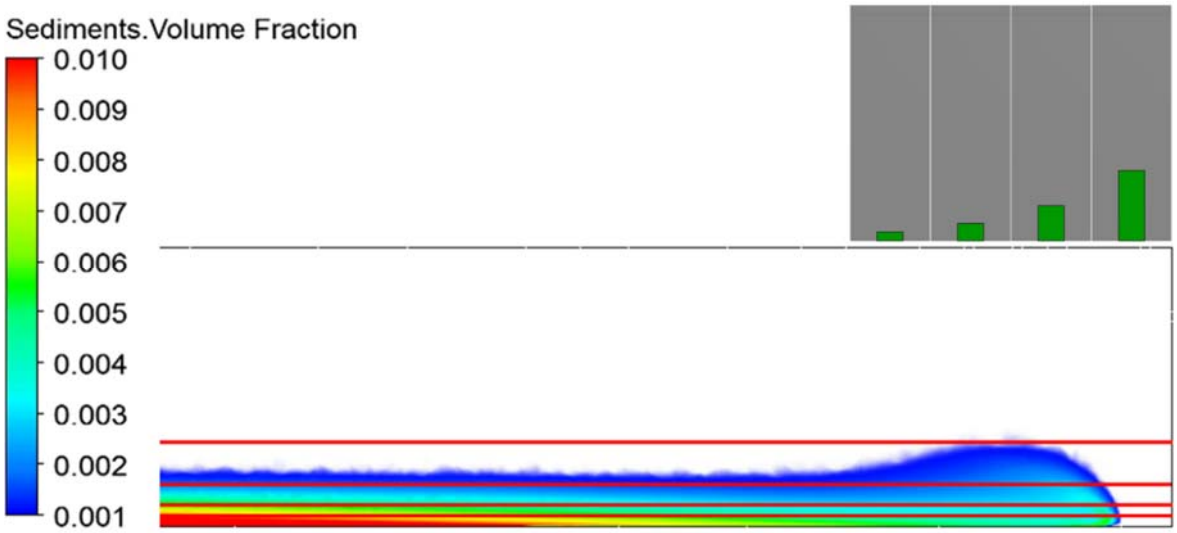

Figure 7.13: Upper limit of the different outlet heights compared with the turbidity current's height (simulations N0.1, N0.2, N0.3 and N0.4).

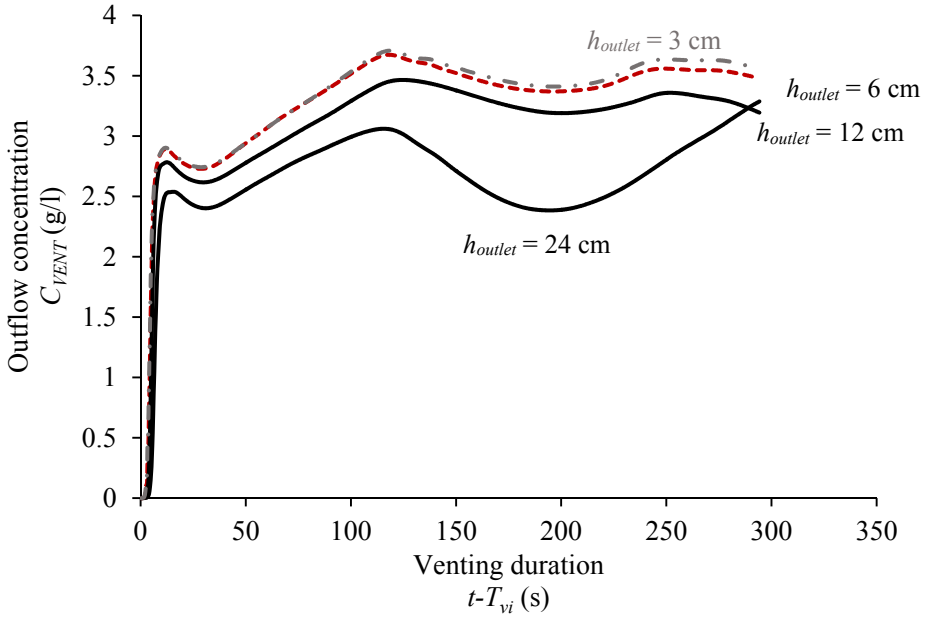

Figure 7.14: Outflow concentrations obtained with the different outlet heights h_{outlet} with $\phi = 100\%$ (simulations N0.1, N0.2, N0.3 and N0.4).

The height $h_{outlet} = 24$ cm results in the lowest outflow concentrations. The height $h_{outlet} = 12$ cm leads to relatively higher (compared with $h_{outlet} = 24$ cm) while $h_{outlet} = 6$ cm and 3 cm lead to highest and very similar concentrations (Figure 7.14). This is due to the fact that, when $h_{outlet} = 24$ cm, there is more clear water loss as $h_{outlet}/H_{num} > 1$ and $[h_L+(h_{outlet}/2)]/H_{num} >> 1$. Furthermore, small outlet heights induce higher velocity fields compared with larger outlet heights (for the same venting degree) in the close vicinity of the

outlet (Figure 7.15) and thus a better suction of the approaching current. Summarily, the height of the bottom outlet should be conditioned by the height of the potential turbidity current and fulfill $[h_L+(h_{outlet}/2)]/H_{num} \approx 1$.

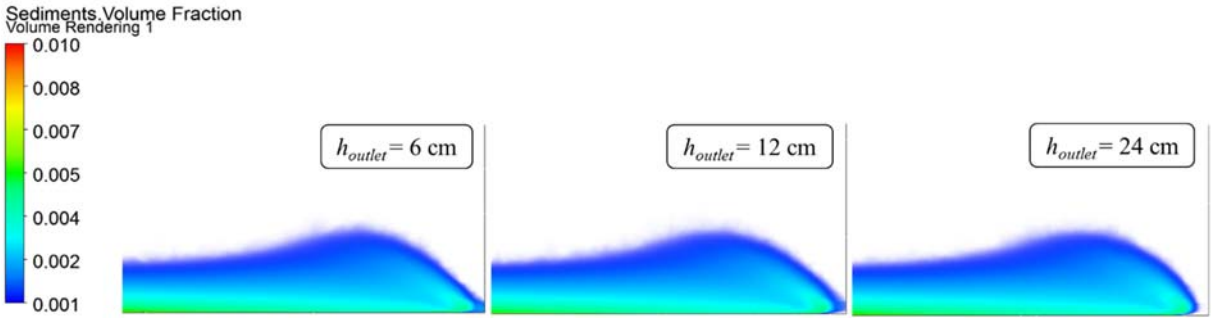

Figure 7.15: Sediment volume fraction contour lines in the vicinity of the outlet once venting has started for the different outlet heights with ϕ = 100% (simulations N0.1, N0.2, N0.3 and N0.4 at t = 180 s).

7.5.3 Outlet width

The width of the outlet was varied while keeping the height at 12 cm. Four different outlet widths were tested: w_{outlet} = 1 cm, 3 cm, 9 cm and 27 cm (on the whole width of the flume). A similar venting degree ϕ = 100% was used for all the cases. Figure 7.16 shows that outflow concentrations are closely similar for the three orifices tested and higher than the case when a whole-width outlet is used (w_{outlet} = 27 cm).

In fact, when using the orifices, the outlet's streamlines immediately reach the walls of the flume, creating similar conditions of aspiration than in the case where the outlet is placed on the whole width of the flume (Figure 7.17). Additionally, in the case of the orifices, outlet velocities are larger the smaller the orifice and thus the current is better drawn to the outlet when reaching it. The relatively stagnant zones on the sides of the orifices, unattained by the outlet's flow field are very limited and do not decrease the outflow concentrations. Hence, the outlet's width should be smaller than the turbidity current's width.

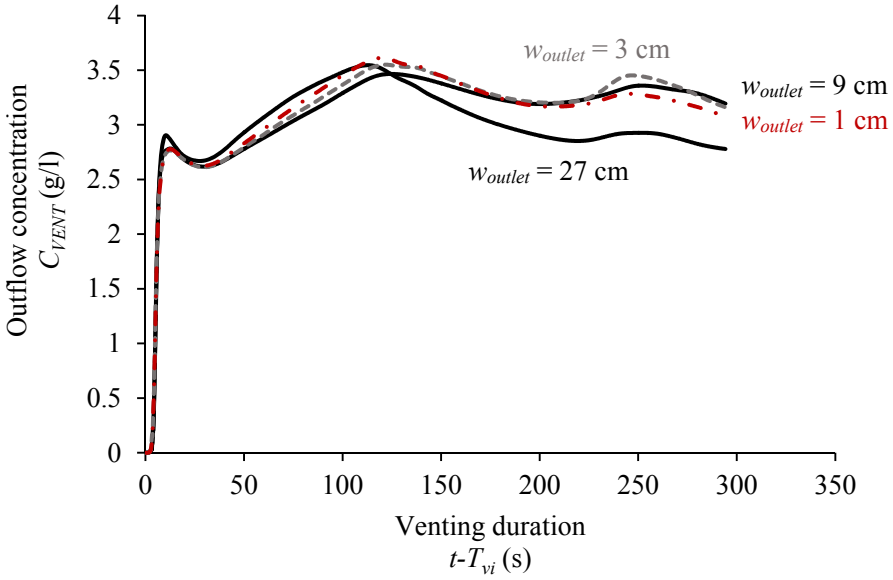

Figure 7.16: Outflow concentrations obtained with the orifice and the whole-width outlet for ϕ = 100% (simulations N0.4, N0.5, N0.6 and N0.7).

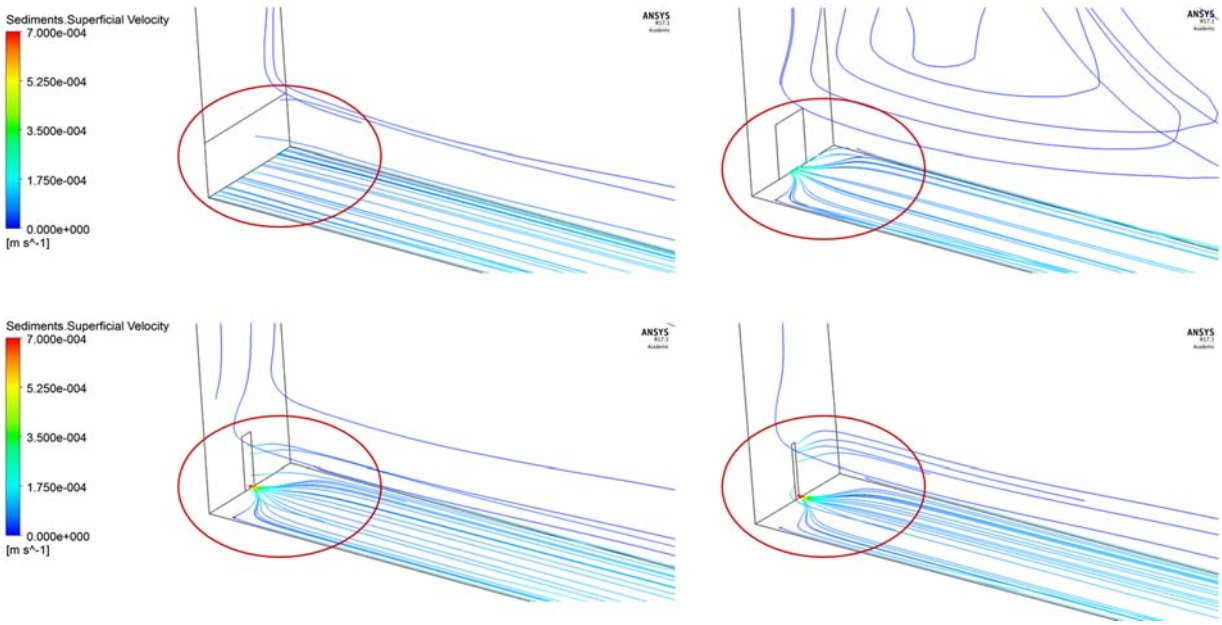

Figure 7.17: Streamlines of the velocities obtained with the four outlet widths tested (simulations N0.4, N0.5, N0.6 and N0.7 at t = 180 s).

7.5.4 Venting degree

As the experimental model using the horizontal bed had constraints on the venting degrees (i.e., the maximum value that could be reached was ϕ = 125%), additional venting degrees were numerically simulated. Namely, ϕ = 150%, 165%, 185%, 200%. The representative venting

efficiency *RVE* (defined in Chapter 4, section 4.3.7) obtained is shown in Figure 7.18 as a function of the venting degree. The results confirm that a change of trend (trendlines in dashed lines) occurs at $\phi = 100\%$. Therefore, the same conclusion concerning the optimal venting degree of $\phi = 100\%$ for the horizontal bed is also reached numerically. Nonetheless, the numerical *RVE* does not show a decrease for $\phi > 100\%$ but keeps increasing with a smaller rate than for $\phi < 100\%$.

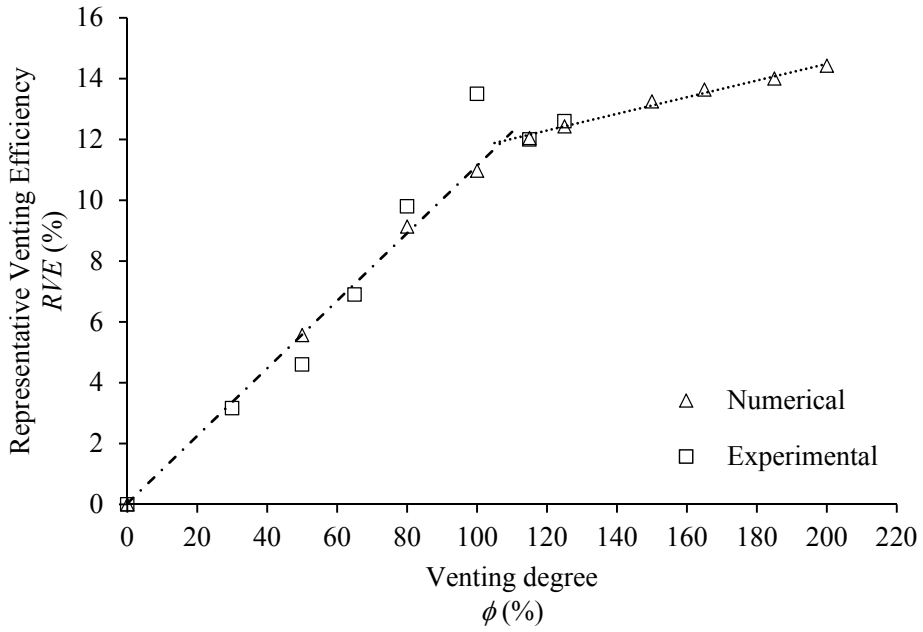

Figure 7.18: Representative venting efficiency *RVE* relatively to the venting degree ϕ for a horizontal bed and venting timing synchronized with the arrival of the current at the dam. The trend lines correspond to the numerical data (tests N0.4 and N.010 to N0.17).

7.5.5 Distance of influence

The influence of the outlet in terms of height has been previously discussed using the concept of height of aspiration h_L. At present, the upstream longitudinal distance at which the outlet's flow field starts accelerating the turbidity current is discussed. For this goal, a line called ''L1'' (Figure 7.19) was created and located between x = 1 m and x = 6.7 m from the inlet, on a fixed height $y = h_{outlet}/2 = 0.06$ m, and centered on the width of the flume at z = 0.135 m.

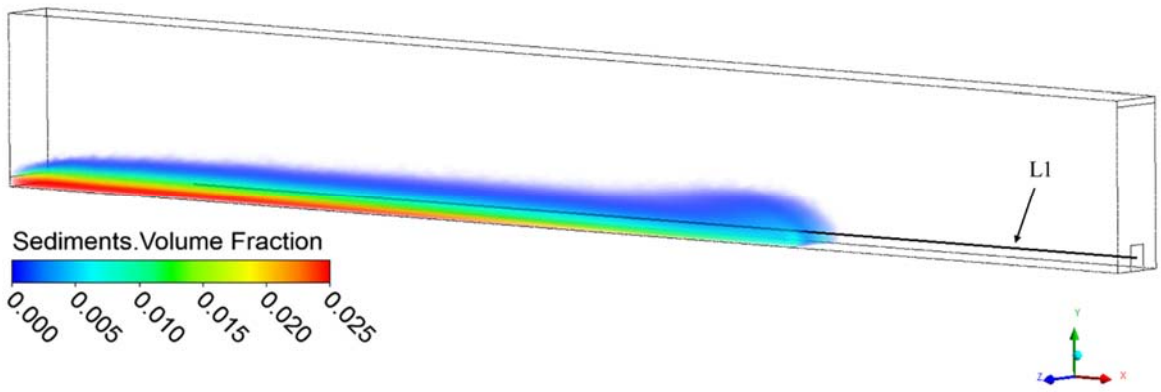

Figure 7.19: Location of the line L1 in the numerical model.

The longitudinal velocity of the turbidity current u was plotted along L1 and considered as a criterion to determine the distance at which the current is accelerated. Different time steps were considered starting from t = 110 s up to t = 180 s (time at which the current reaches the outlet). First of all, reference simulations were performed (Figure 7.20) where no venting is applied. The latter give the ‘’undisturbed’’ longitudinal velocity values of the turbidity current. In the remaining simulations, venting is applied at $t = T_{vi}$ = 115 s. Early venting is simulated in order to better evaluate the time starting which the current is drawn by the outlet's flow field. Several venting degrees were simulated, namely ϕ = 10%, 30%, 50%, 65%, 80%, 90% and 100%. For each case, the longitudinal velocity u is plotted as a function of the distance x from the inlet for the different time steps. Note that numerical simulations were also performed using the three different outlet heights discussed in section 7.5.2 (Appendix A4A5) and showed that the different outlet velocities corresponding to the different heights, using the same venting degree, did not affect the distance of influence of the outlet.

In the figures below, the dashed lines correspond to the reference simulations where no venting is applied. The solid lines correspond to the different venting cases. The reference simulation (Figure 7.20) and selected cases of venting (i.e., ϕ = 10%, 50%, 80% and 100%) are shown (Figure 7.21, Figure 7.22, Figure 7.23, Figure 7.24 respectively). Note that the results related to the remaining simulations (i.e., ϕ = 30%, 65%, 90%) are shown in Appendix A6.

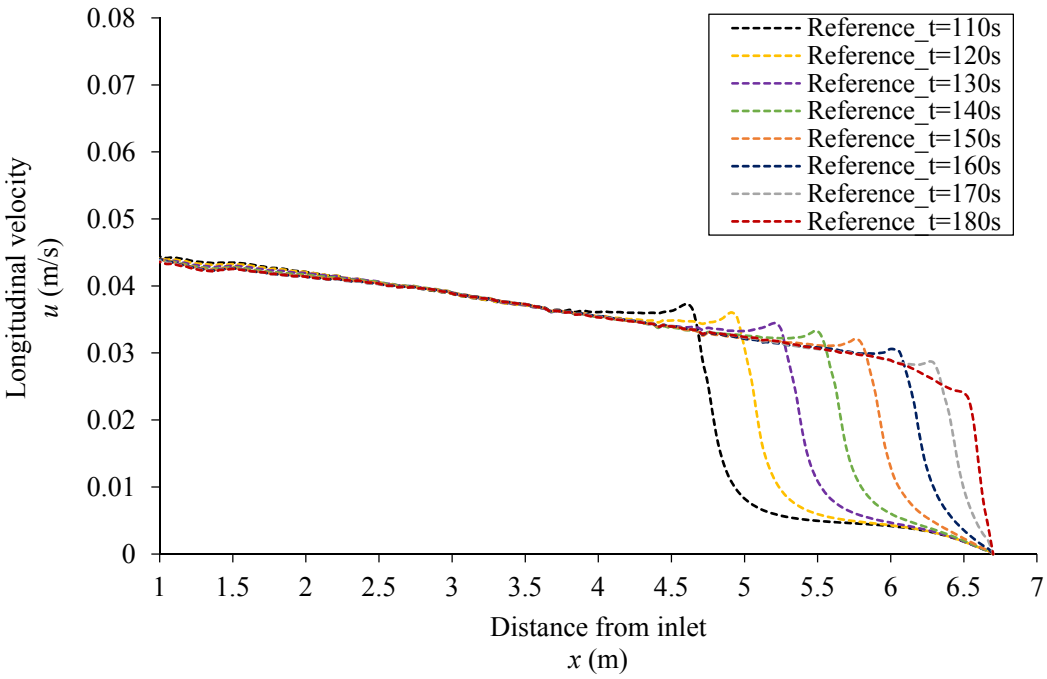

Figure 7.20: Longitudinal velocity u plotted on L1 for the reference simulation with no venting (simulation N0.18).

As expected based on the trend of front velocities (Figure 7.10), the velocity u decelerates going from the inlet to the outlet. In the cases where venting is applied, the acceleration is noted when the velocity reaches larger values than the reference simulation. This suggests that the head of the current is drawn to the outlet. The lowest venting degree $\phi = 10\%$ considered (Figure 7.21) shows that the acceleration (positive deviation between the solid line and the dashed line) of the current indicated by the arrow is barely noticeable even at $t = 170$ s and very low at $t = 180$ s which is the time at which the current reaches the outlet. The current is hardly affected before reaching the outlet and the maximum distance of influence $s_{max} = 10$ cm.

However, for the case of $\phi = 50\%$ (Figure 7.22), there is a more marked acceleration starting at $t = 150$ s. The corresponding maximum distance of influence is $s_{max} = 70$ cm upstream of the outlet. The deviation between the reference velocity and the velocity corresponding to $\phi = 50\%$ increases in time, the closer the current gets to the outlet. In the cases of venting with $\phi = 80\%$ and $\phi = 100\%$, the acceleration of the current starts at $t = 140$ s and thus at a distance $s_{max} = 1$ m upstream of the outlet as shown in Figure 7.23 and Figure 7.24.

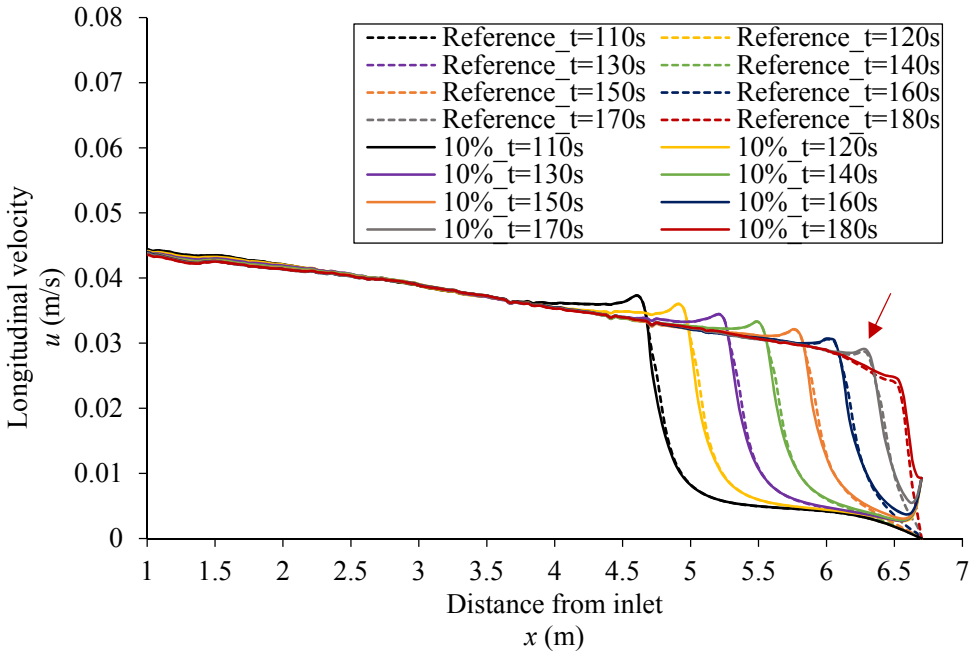

Figure 7.21: Longitudinal velocity u plotted on L1 for the reference simulation (dashed lines) and the case of venting with $\phi = 10\%$ (solid lines). The arrow indicates the time step at which the current starts being accelerated (simulation N0.19).

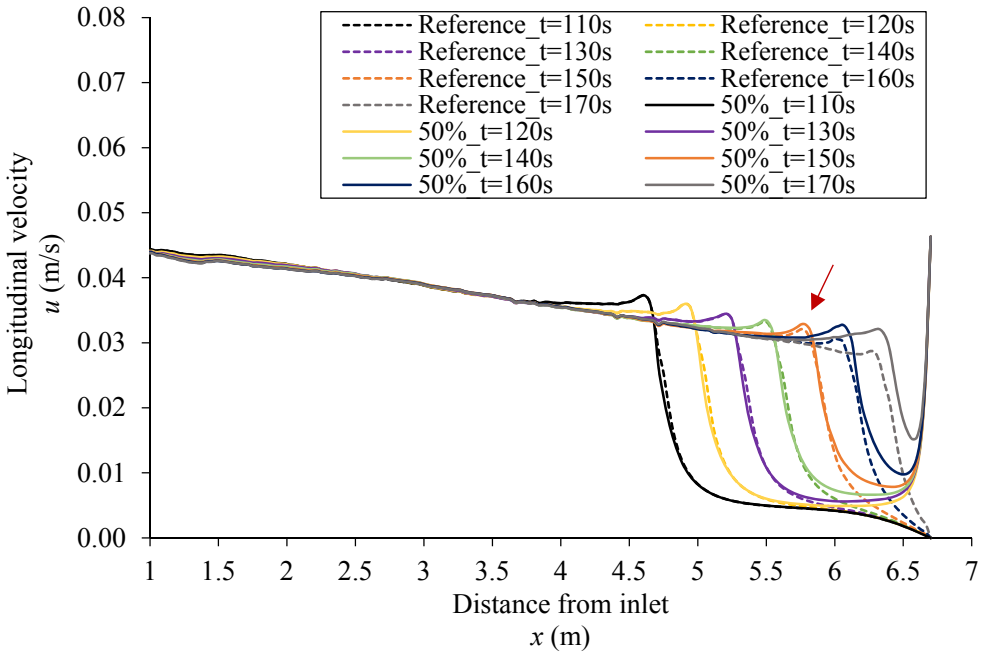

Figure 7.22: Longitudinal velocity u plotted on L1 for the reference simulation (dashed lines) and the case of venting with $\phi = 50\%$ (solid lines). The arrow indicates the time step at which the current starts being accelerated (simulation N0.21).

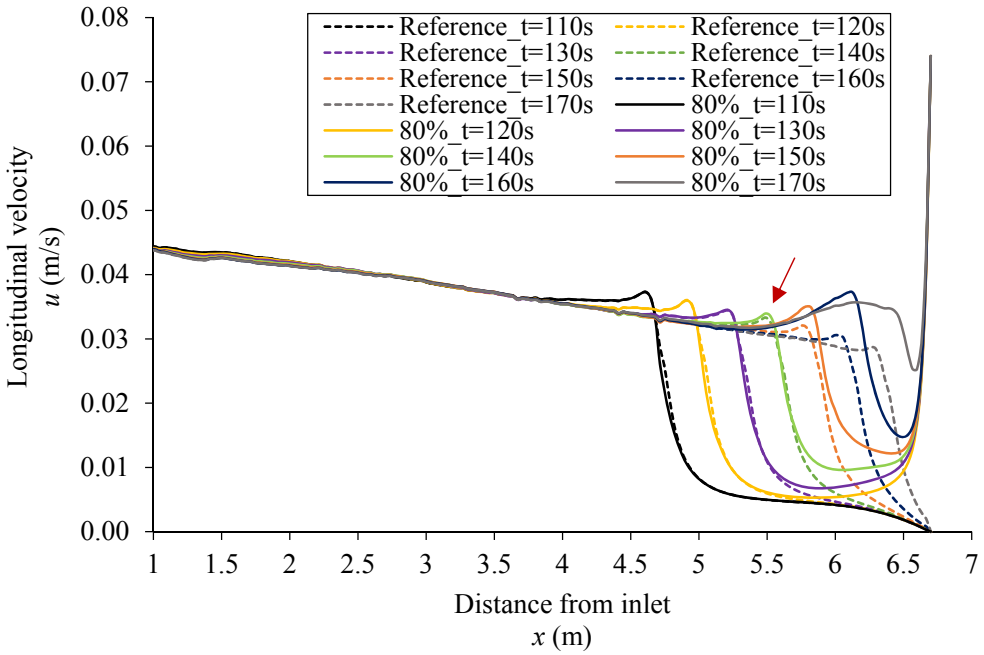

Figure 7.23: Longitudinal velocity u plotted on L1 for the reference simulation (dashed lines) and the case of venting with $\phi = 80\%$ (solid lines). The arrow indicates the time step at which the current starts being accelerated (simulation N0.23).

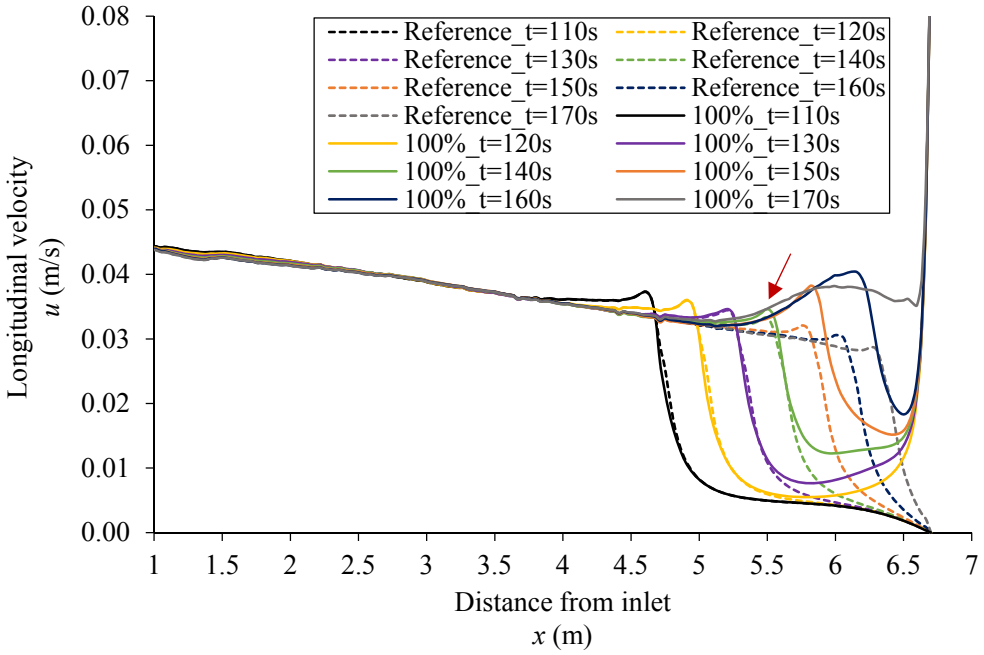

Figure 7.24: Longitudinal velocity u plotted on L1 for the reference simulation (dashed lines) and the case of venting with $\phi = 100\%$ (solid lines). The arrow indicates the time step at which the current starts being accelerated (simulation N0.25).

A similar analysis was performed for all the venting degrees simulated. Based on the results, the maximum distance of influence was plotted as a function of the venting degree ϕ (Figure 7.25). It shows that for $\phi > 80\%$, $s_{max} = 1$ m. Hence, the maximum distance of influence is $s_{max} = 1$ m obtained with a minimum venting degree of $\phi = 80\%$.

This analysis helps in defining the close vicinity of the outlet during venting. For instance, if early venting is performed, it is preferable to apply it when the turbidity current is at a distance $s_{max} < 1$ m in the case of the present model. In order to upscale the result, the height of aspiration $(h_L)_{\phi=80\%}$, which depends on the venting degree and the density difference between the turbidity current and the clear water is chosen. A relationship $s_{max}/(h_L)_{\phi=80\%} = 5$ was found. The latter relationship provides an estimation of the maximum distance (reached by the current) from the dam at which early venting can begin. At larger distances, the current is not even reached by the outlet's flow field.

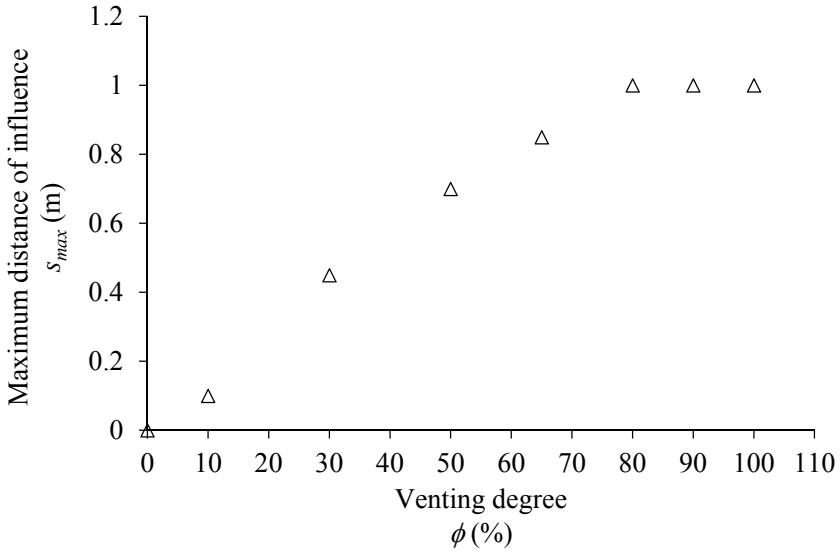

Figure 7.25: The maximum distance of influence s_{max} as a function of the venting degree ϕ (tests N0.18 to N0.25).

7.5.6 Geometrical variation

In reservoirs where sedimentation in the dead storage has already occurred, the part of the thalweg close to the dam tends to approach horizontal. This is due to the settling of fine sediments mostly because of turbidity currents that could not be evacuated during past flood events. Examples include Tsengwen Reservoir in Taiwan (Lee et al., 2014), Sautet Reservoir in France (Nizery et al., 1952), Steeg Reservoir in Algeria (Morris & Fan, 1997), Tarbela dam

in Pakistan (Khan & Tingsanchali, 2009) among others. Inspired by these cases, a geometrical variation combining two bed slopes was simulated. The first 3.5 m of the model now correspond to the thalweg having a slope of 5.0% and followed by a horizontal bed on the remaining 3.2 m leading to the outlet (Figure 7.26). The latter is placed at the bottom of the wall (12 × 9 cm^2). The water depth H_{water} = 80 cm is similar to the one used with the horizontal bed. Apart of the geometrical variation combining the two slopes, the characteristics of the numerical model were kept similar to the previous sections. The venting degree simulated is ϕ = 100%.

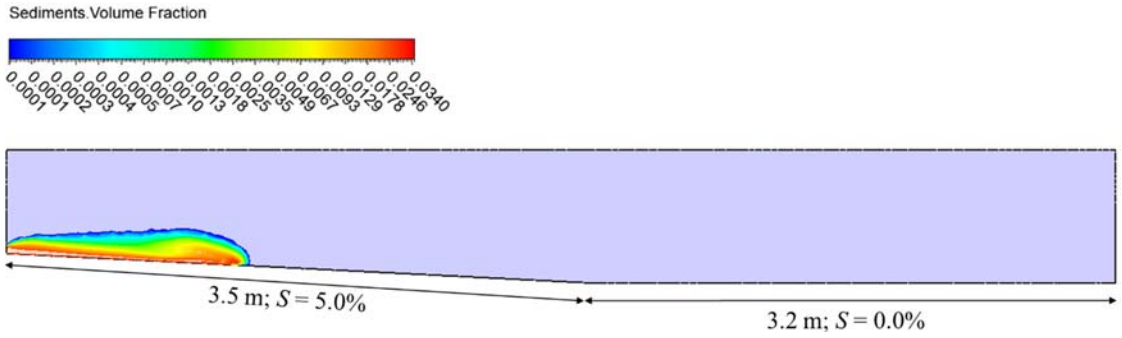

Figure 7.26: Longitudinal profile of the new geometry.

In Figure 7.27, the outflow concentrations corresponding to the cases of horizontal bed, slope of 5% and that of the new geometry with combined slopes are compared. As expected based on the experimental results, the slope of 5% produced higher outflow concentrations compared with the horizontal bed. By combining the two slopes within the new geometry, outflow concentration showed smaller values compared with S = 5% and larger values compared with the horizontal bed, particularly at the beginning of venting. However, concentrations then dropped below the ones obtained using the horizontal bed.

In order to understand the main difference between the case of the horizontal bed and the combined geometry, the bed deposition at t = 470 s is plotted for both cases (Figure 7.28). It shows that contrarily to the horizontal bed, the deposition with the combined slopes does not spread on the whole length of the flume but is rather ‘’trapped’’ in the zone of the horizontal bed only. The current is reflected but is not able to climb back the 5% slope.

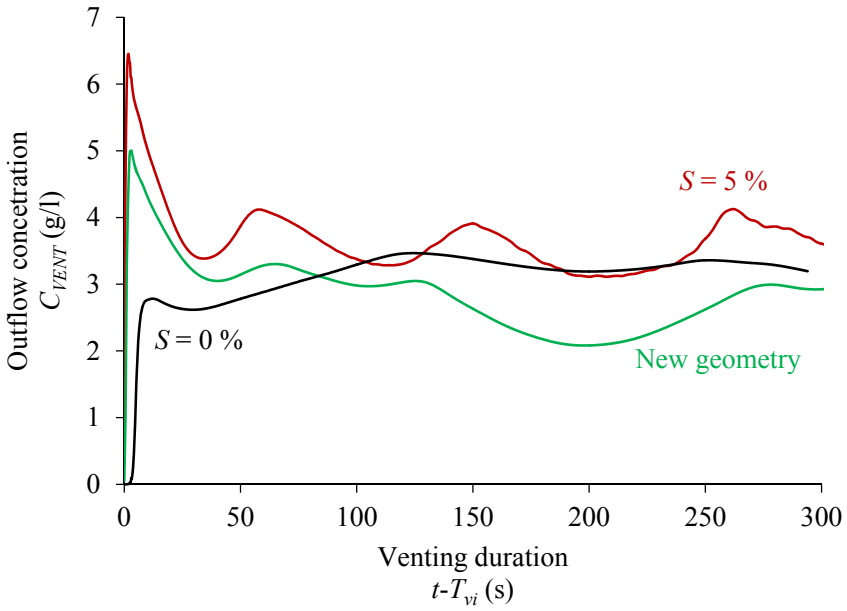

Figure 7.27: Outflow concentrations obtained with S = 0%, S = 5% and the combined geometry as a function of the duration of venting with ϕ = 100% (simulations N1.1, N 1.2 and N0.4).

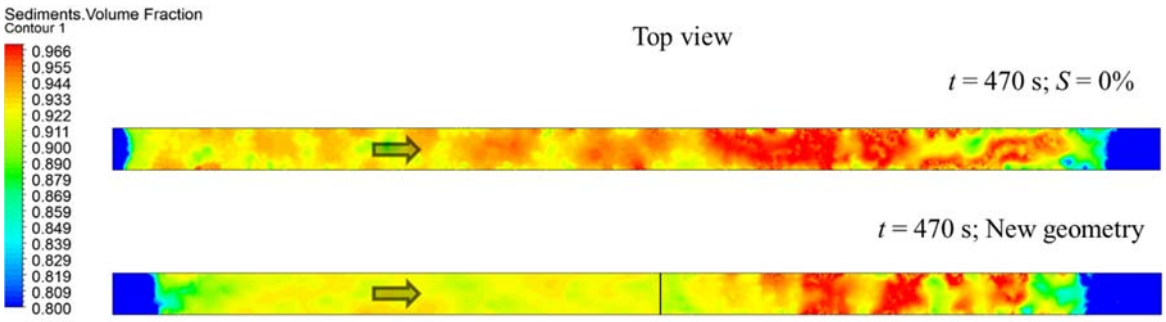

Figure 7.28: Top view of the flume in the case of the horizontal bed and the case of the combined geometry. The black line delimits the transition from the 5% slope to the horizontal bed. The concentration contours are plotted in the logarithmic scale with a minimum of 0.8 and a maximum of 0.97 at t = 470 s (simulations N1.1 and N0.4).

Nevertheless, a profile view of the concentration contours (Figure 7.29) shows that for t = 470 s, the amount of suspended sediments that propagates is larger for the case of the combined slopes than that of the horizontal bed. In fact, the currents reach the wall with slightly higher velocities imposed by the slope of 5% in the first part of the flume and are thus more reflected.

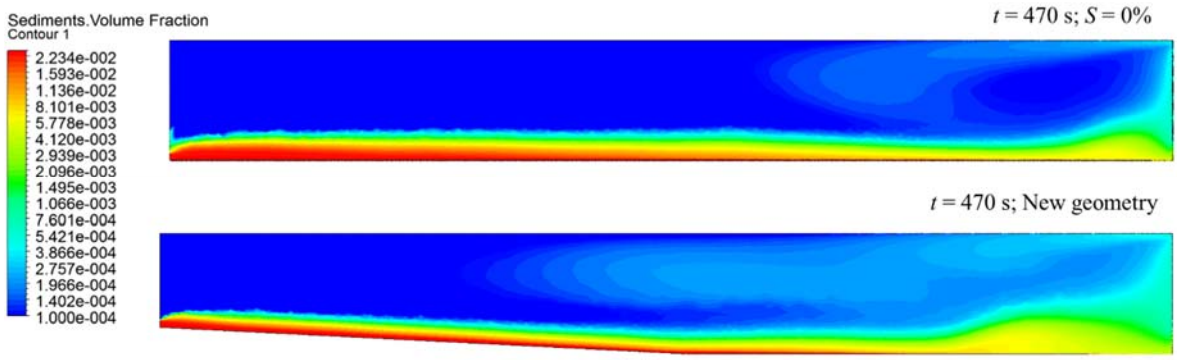

Figure 7.29: Profile view of the concentration contour lines at t = 470 s for the case of the horizontal bed compared with the case of the combined geometry. The minimum value of the volumetric concentration is 0.0001 and the maximum is 0.025 (simulations N1.1 and N0.2).

7.6 Conclusions

In order to extend the number of studied parameters and gain more insight of the operation of venting, a numerical model was built and calibrated using the experimental data.

The results were assessed by the help of the outflow concentration as a criterion since the numerical conditions ensured that the turbidity currents are similar. The variation of the outlet's height (total of four heights) showed that the largest height (while keeping the same venting degree) leads to the lowest outflow concentration. The height of the outlet should be fixed so that the height of aspiration englobes the turbidity current's body height. However, it should not exceed the current's height as clear water will be lost. Four outlet widths were simulated: three orifices and an outlet placed on the whole width of the flume. The orifices resulted in higher outflow concentrations leading to the conclusion that the width of the outlet should not be as the large as the current's width. It is mostly important that the lateral aspiration distance of the outlet englobes the turbidity current's width. Moreover, three different levels (vertical position of the lower sill) of the outlet were simulated. The outlet was placed at the bed level (bottom outlet), as well as 12 cm and 24 cm above the bed level. The higher the outlet's level, the lower the outflow concentration of the released current. In fact, when the outlet's level is above the bed, the current is partially reflected by the structure below the outlet. Furthermore, the higher the outlet, the smaller the zone reached by the height of aspiration below the outlet will be. Hence, the outlet should be placed at the lowest level possible.

Additionally, the venting degrees tested experimentally with the horizontal bed were extended using the numerical model. This allowed to verify that the optimal venting degree

$\phi = 100\%$ obtained by the experiments is valid on a larger range of values in the case of the horizontal bed.

Besides, the maximum upstream distance of influence s_{max} at which the turbidity current is affected by the outlet's flow field was evaluated. It was defined as the distance starting which the turbidity current is accelerated compared to a reference state where no venting was performed. This distance was shown to be influenced by the momentum of the outlet and thus the venting degree. The relationship between s_{max} and ϕ was shown to be linear up to $\phi = 80\%$, after which s_{max} is a constant. Therefore, a relationship was found and proposed a distance upstream of the wall, after which the turbidity currents remain undisturbed by the outlet's discharge: $s_{max}/(h_L)_{\phi=80\%} = 5$ where $(h_L)_{\phi=80\%}$ is the height of aspiration corresponding to a venting degree of 80%. In case of early venting, the operation should start the earliest when the turbidity current reaches s_{max}.

Finally, a different geometry was simulated which represents a realistic prototype geometry, characterized by the combination of a thalweg slope of 5% followed by a horizontal bed when approaching the dam. The combined geometry globally yielded smaller outflow concentrations compared with the cases using a single slope of 5% or a horizontal bed.

Chapter 8

CONCLUSIONS AND FUTURE WORK

8.1 Conclusions and practical relevance

Bottom outlets are vital release structures that can lower the reservoir's level in case of an emergency and thus ensure the safety of dams (Schleiss & Pougatsch 2011). If an outlet is clogged by sediments and its use is hindered, then the safety of the dam may be endangered. Turbidity currents are often the main cause for the blockage of outlets by sediments. Thus, venting turbidity currents is highly important in terms of safety. In addition, the loss of storage capacity induced by sedimentation leads to economic losses especially in the case of storage used for the purpose of power generation. Venting can preserve the storage capacity, and since no reservoir drawdown is usually caused, the water loss remains very limited. Concerning sediment transport and restoration of rivers downstream of dams, the technique of venting turbidity currents, if performed appropriately, can offer environmental benefits. If properly controlled, venting has the advantage of using relatively low outflow discharges and directly transiting the amount of fine sediments required by the river.

This study presents an unprecedented investigation of venting turbidity currents. This technique has not been systematically studied in the past despite the fact that reservoir operators require specific guidelines to improve outlet design and gate operation during venting. For the first time, several parameters known to be the most influential on the release efficiency of venting were studied. The novel contributions of this research are of practical relevance and help in increasing venting efficiency. The used approach was mainly experimental. A numerical model complemented the analysis by extending the studied parameters. The principal goal was to assess the influence of different parameters on the sediment release efficiency of venting, namely the outflow discharge during venting, the bed slope of the thalweg, the duration of venting, the timing of venting, the outlet's dimensions and its level relatively to the reservoir's bottom elevation. The maximum distance of influence of the operating outlet was also studied. The efficiency of venting was evaluated using three different criteria:

- The definition which is probably the most used on prototype due to its practicability is the Representative Venting Efficiency (*RVE*). The latter represents the ratio between the averaged outflow sediment mass and the averaged inflow sediment mass. It provides one representative value of the efficiency during the total duration of venting.
- The Global Venting Efficiency (*GVE*) adds a temporal dimension to the *RVE* by computing the ratio between the sum of vented sediment mass and that of inflow sediment mass at a given time. Thus, it allows to uncover the trend of the efficiency of venting in time.

- The Local Venting Efficiency (*LVE*) differs from the *GVE* by considering the deposited sediment mass. Due to the relatively low outflow discharges used during venting, the retrogressive erosion of deposited sediments upstream of the outlet is inexistent or very limited. Therefore, the cumulated mass of deposition is subtracted from that of the inflow. Despite the fact that this definition is hardly applicable in the field without continuous measurement of sediment deposition, it is however the most convenient for the investigation of the ‘’filtered’’ performance of the outlet during venting.

Additionally, in order to include water loss considerations in the definition of venting efficiency, a Venting Efficiency Indicator (*VEI*) was also introduced and was used, along with the *LVE*, to choose adequate conditions that maximize sediment release and minimize clear water loss.

The main scientific findings of the present work and their practical relevance can be summarized as follows:

The optimal venting degree depends on the reservoir slope in the vicinity of the outlet.

The venting degree is defined by the ratio between the outflow discharge applied during venting and the inflow discharge of the turbidity current. The optimal value of the venting degree revealed to be dependent on the slope of the reservoir thalweg in the vicinity of the dam. In the range of the slopes tested, a venting degree of 100% is optimal when the thalweg in front of the dam, on which the turbidity current flows, is horizontal. However, higher bed slopes (i.e., 2.4% and 5%) yielded an optimal venting degree of about 135% in case the outlet’s capacity can reach up to 155% of the turbidity current’s discharge. When the outlet’s capacity can reach 200% of the current’s discharge, the latter resulted in the highest venting efficiency. Nevertheless, a venting degree of 200% was shown to be unlikely since the capacity of the outlet is usually smaller or slightly larger than the discharge of the turbidity current reaching it.

The lowest level possible to place a bottom outlet is just above the foreseen dead storage. As long as the dead storage is not full, the slope of the thalweg in the vicinity of the outlet will be relatively steeper than at later stages (when the dead storage starts filling). Applying a venting degree of 135% will help in preserving the space for more sediments in the dead storage because the aspiration height of the outlet extends to lower levels than the outlet’s lower sill. If venting is applied after the dead storage has been filled, then the bed in the vicinity of the

outlet will be almost horizontal. In this case, venting with a degree of 100% is sufficient and leads to the most efficient sediment release compared to the water losses.

For application in prototype scale, numerical simulations would allow to estimate the discharge of typical turbidity currents that can potentially form in a specific reservoir. Then, the value of the outflow discharge corresponding to the venting degree leading to the highest release efficiencies can be determined.

Steeper thalweg slopes lead to higher venting efficiencies.

Within the range of slopes tested, it could be seen that the steeper the slope, the more efficient venting will be. The main reason is that for higher slopes the upstream reflection of the current by the dam decreases.

Therefore, when selected as sediment management technique, venting of turbidity currents should be started from the very beginning of the dam operation. This helps in maintaining a cone in the vicinity of the dam and avoids the filling of the dead storage and thus the development of a flatter bed. Furthermore, in the case where bottom outlets are already clogged by sediments and their capacity is not high enough to mobilize and release the sediments, the efficiency of venting will be reduced.

The timing or start of venting should be synchronized with the arrival of the turbidity current at the dam. In any case, an early venting is more efficient than a late venting.

The in-time venting which is synchronized with the arrival of the current at the dam is the most efficient in comparison with early and late venting. Water losses are minimized but sediment release maximized. If measurements are not available or not precise enough to predict the arrival time of the current at the dam, then, through a rough estimation of turbidity currents' velocity, an early venting should be performed rather than a late venting. In fact, early venting revealed to be more efficient than late venting and almost as efficient as the in-time venting. Nevertheless, venting should not be too early; the earlier the venting the higher the water loss. With the numerical simulations, a maximum distance of influence $s_{max} = (s_{max})_{\phi=80\%}$ of the bottom outlet's aspiration was obtained for a venting degree of 80%. A relationship $s_{max}/(h_L)_{\phi=80\%} = 5$ could be identified where $(h_L)_{\phi=80\%}$ is the height of aspiration corresponding to a venting degree of 80%. For distances larger than s_{max}, the turbidity current is not aspired by the outlet's flow field. It has to be noted that s_{max} is dependent on the momentum of the outflow rather than its velocity i.e., outlet size.

In practice, one of the most important conditions for a successful venting operation is to have measurements which allow to detect turbidity currents and estimate their arrival time. Based on the required time to open the gate and reach a stable flow (~ 5 – 10 minutes) and for typical velocities of turbidity currents (0.3 – 1 m/s), it is highly recommended to measure velocities and/or concentrations on the reservoir bed, at a location of about 200 – 300 m upstream of the outlet.

Venting should last as long as there is a turbidity current approaching the dam. Also, it should be maintained after the end of the flood event entering the reservoir.

The efficiency of venting reaches a quasi-steady value shortly after the beginning of venting, as long as the turbidity current's inflow is continuous. However, the turbidity current's inflow is directly linked to the flood inflow. At the end of the flood, the fine sediment supply diminishes rapidly and the turbidity current dies out. Nevertheless, a muddy lake in the vicinity of the dam has been formed by fine sediments. The settling of this muddy lake takes more time than that of the turbidity current in the reservoir. Therefore, once the inflow is interrupted, venting should be maintained for a certain time dependent on the venting degree. The higher the venting degree, the faster the evacuation of the muddy lake.

Nevertheless, in the downstream river, fine sediments in high concentrations may clog small interstices in the gravel bed needed for fish to place their eggs. Thus, venting should be extended if possible until outflow concentrations become low (< 0.5 g/l) in order to ''rinse'' the downstream river with clear water.

The duration of venting tested in the experiments can be related to prototype. Using the experimental height of the current $H = 23.9$ cm and the settling velocity $v_s = 0.15$ cm/s of the sediment material, an experimental ''settling time'' t_s of the particles can be calculated: $t_s = H/v_s = 23.9/0.15 = 159$ s. The duration of venting used in the numerical simulations $t = 300$ s is considered and a normalized venting duration can be found through $t/t_s = 300/159 \approx 2$. The turbidity currents found in prototype have typical heights around 5 – 15 m (Nizery et al., 1952; Sinniger et al., 1994; Xu et al., 2004). Considering an example of $H_{prot} = 10$ m with the same settling velocity v_s, the prototype $t_{sprot} = H_{prot}/v_s \approx 6667$ s. Therefore, the venting duration of 300 s in the experimental time correspond to more or less $t_{prot} = t_{sprot} \times 2 = 6667 \times 2 = 13334$ s ≈ 4 hours of venting in prototype conditions.

The width of the bottom outlet(s) should be smaller than the width of the turbidity current. The lateral aspiration should englobe the turbidity current.

The efficiency of venting is higher when using an orifice than an outlet placed on the whole width of the current. The width of the outlet(s) should not spread over the whole width of the current to avoid the evacuation of clear water from the reservoir. The lateral limit of the aspiration cone of the outlet should englobe the turbidity current. In order to fulfill this condition, placing several outlets that induce an aspiration cone which covers the width of the turbidity current could be an option. For a particular reservoir, it is highly recommended to perform numerical simulations in order to estimate the width of the currents and to study the possibilities on the number, position and width of the outlets. It should be noted that the outlet's flow field as well as the turbidity current could not freely develop and were limited by the width of the flume in the present study due to the narrow flume used.

The bottom outlet should be positioned in a way to minimize the dead storage.

A bottom outlet placed at the optimal level to minimize the dead storage is the most efficient for venting. In fact, the higher the level of the outlet, the higher will be the lower limit of its height of aspiration and the more significant the upstream reflection of the current will be. Thus, outlets placed at high levels will cause more deposition inside the useful storage of the reservoir. A low position of the outlet should be fixed provided that venting is frequently performed and starting the beginning of the dam operation in order to keep the cone in the vicinity of the outlet free. Keeping a free cone upstream of the outlet induces steep slopes close to the outlet and thus increases the efficiency of venting (based on the second recommendation).

The height of the outlet should be chosen in a way that the height of aspiration englobes the turbidity current.

The height of the outlet should not be too small to avoid its fast clogging. However, it should not largely exceed the height of the body of the turbidity current. In other words, if the height of aspiration englobes a large amount of the clear water above the turbidity current, water loss will increase and venting will not be efficient. In the opposite case where turbidity currents have very large heights compared to feasible outlet dimensions, increasing the number of outlets in the vertical direction should be considered. As a result, the height of aspiration of an

outlet operating with a certain venting degree and transiting a turbidity current having a specific density should optimally correspond to the height of the turbidity current's body.

General practical recommendations

- Implementing the above mentioned recommendations highly depends on the monitoring system of the reservoir. Concretely, an anchored raft can be implemented and used to perform the measurement of parameters such as temperature and turbidity between the surface of the reservoir and the bed. In the absence of any measurement, theoretical and numerical analysis should be an alternative. For instance, Fan (1986) proposed a method for computing turbidity currents occurring in reservoirs helping to predict when and where they plunge, what their concentrations and velocities would be, and whether they can reach the dam or not.
- Venting of turbidity currents can be combined when appropriate with drawdown flushing for delta mobilization. Venting releases mainly fine sediments such as silt and clay while the downstream river needs also coarse sediments for a healthy ecosystem. Fine material alone can harm fish habitats in the downstream river. Therefore, replenishment techniques that supply coarse sediments to the downstream environment should be considered along with venting.
- In reservoirs where turbidity currents form during floods, it is recommended to first open the bottom outlets before operating the spillway. This leads to the evacuation of possible turbidity currents reaching the dam or at least unblocks the outlets, freeing a cone upstream which might have been filled with sediments in past events.

8.2 Future work

In the present research, a single outlet was used for venting turbidity currents having similar inflow conditions in terms of discharge and concentration. The main focus was on operational parameters of venting. In future investigations on venting, a wider flume may be used and one or multiple outlets placed. The arrangement of outlets can be varied with respect to the width of the flume and the height of the dam. It would be of interest to understand the effect, on venting efficiency, of the number of outlets placed and their different configurations.

Three slopes were tested and turbidity currents were subcritical or slightly supercritical in the case of the highest slope. In the future, a larger range of slopes should be tested, particularly

inducing highly supercritical turbidity currents. The effect of the turbidity current's regime on its venting efficiency could then be studied.

In addition, in the goal of simplifying considerations on mass fluxes, a smooth bed was used in the present work. In the future, it is suggested to test erodible beds, created by the accumulation of sediment deposition resulting from consecutive tests of depositive turbidity currents, in order to assess its effect on the venting efficiency.

Finally, the effect of the width of the outlet should be further studied using three-dimensional turbidity currents. In the present study, two-dimensional turbidity currents were tested as they were confined by the width of the flume. Three-dimensional turbidity currents would lead to a better assessment of the effect of the width of bottom outlets on the venting efficiency. It would then be possible to determine a limit of the lateral distance of influence of the outlet. In particular, a narrow trapezoidal section of the flume would be the most representative of typical reservoirs' sections where turbidity currents occur.

BIBLIOGRAPHY

Abid, A. (1980). Transported sediments and drawing off at the Nebeur Dam on the Mellegue Wadi during the period 1 May 1954 to 30 April 1980. In *International Seminar of Experts on Reservoir Desiltation*. Tunis.

Althaus, J. (2011). *Sediment evacuation from reservoirs through intakes by jet induced flow*. PhD thesis, No. 4927 and Communication 45, Laboratory of Hydraulic Constructions (LCH), Ed. A. Schleiss, École Polytechnique Fédérale de Lausanne EPFL, Switzerland.

Althaus, J., & De Cesare, G. (2006). *Sustainable sediment management of Alpine reservoirs considering ecological and economical aspects*. Neubiberg: Institut für Wasserwesen.

Altinakar, M. S., Graf, W. H., & Hopfinger, E. J. (1996). Flow structure in turbidity currents. *Journal of Hydraulic Research*, *34*(5), 713–718.

Altinakar, S., Graf, W. H., & Hopfinger, E. J. (1990). Weakly depositing turbidity current on a small slope. *Journal of Hydraulic Research*, *28*(1), 55–80.

Annandale, G. W. (2005). *Reservoir sedimentation*. *Encyclopedia of Hydrological Sciences*. Chichester, U.K.: Wiley.

ANSYS® Academic Research (2013), Release 15.0.

Antoine, G., Jodeau, M., Camenen, B., Esteves, M., Nemery, J., & Lauters, F. (2013). Estimation des flux de matières en suspension lors des chasses hydrauliques de l'Arc de 2006 à 2011. *La Houille Blanche*, *99*(4), 43–49.

Attewill, L. J. S., White, W. R., Tariq, S. M., & Bilgi, A. (1998). Sediment management studies of Tarbela dam, Pakistan. "The prospect for reservoirs in the 21st century". In *Proc. 10th Conference of the British Dam Society* (pp. 212–225). 9-12 September 1998, University of Wales, Bangor.

AXPO Power, A., & Kraftwerke Sarganserland, A. (2013). Ergebnisse der Versuchsphase 2007-2012. *Ausgleichsbecken Mapragg - Durchleitung der Trübeströme*.

Baas, J. H., Van Kesteren, W., & Postma, G. (2004). Deposits of depletive high-density turbidity currents: a flume analogue of bed geometry, structure and texture. *Sedimentology*, *51*(5), 1053–1088.

Bagnold, R. A. (1962). Auto-suspension of transported sediment; turbidity currents. In

Proceedings of the Royal Society of London. Series A, Mathematical and Physical Sciences (pp. 315–319).

Basson, G., & Rooseboom, A. (1997). *Dealing with reservoir sedimentation: Prepared for the Water Research Commission*. Water Research Commission, South Africa.

Basson, G., & Rooseboom, A. (1999). *Dealing with reservoir sedimentation - Dredging*. Water Research Commission, South Africa.

Batuca, D., & Jordaan, J. (2000). *Silting and desilting of reservoirs*. Rotterdam: A.A.Balkema.

BAUMER. (2014). *UNAM 30 - Ultrasonic distance measuring sensors - Data sheet*.

Bell, H. S. (1942). *Stratified flow in reservoirs and its use in prevention of silting*. USDA, 491.

Beyer Portner, N., & Schleiss, A. (1998). *Erosion des bassins versants alpins par ruissellement de surface*. PhD thesis No. 1815 and Communication 6, Laboratory of Hydraulic Constructions (LCH), Ed. A. Schleiss, École Polytechnique Fédérale de Lausanne EPFL, Switzerland.

Boillat, J.-L., De Cesare, G., Schleiss, A. J., & Oehy, C. (2000). Successful sediment flushing conditions in Alpine reservoirs. In *Proceedings International Workshop and Symposium on Reservoir Sedimentation Management* (pp. 47–59). 26-27 October 2000, Tokyo, Japan.

Boillat, J.-L., Dubois, J., De Cesare, G., & Bollaert, E. (2000). Sediment management examples in Swiss Alpine reservoirs. In *Proceedings International Workshop and Symposium on Reservoir Sedimentation Management*. 26-27 October, Tokyo, Japan.

Boillat, J.-L., & Pougatsch, H. (2000). State of the art of sediment management in Switzerland. In *Proceedings International Workshop and Symposium on Reservoir Sedimentation Management* (pp. 143–153). 26-27 October, Tokyo, Japan.

Brandt, S. A. (2000). A review of reservoir desiltation. *International Journal of Sediment Research*, *15*(3), 321–342.

Britter, R. E., & Linden, P. F. (1980). The motion of the front of a gravity current travelling down an incline. *Journal of Fluid Mechanics*, *99*(3), 531–543.

Brown, C. B. (1950). *Sediment transportation*. (H. Rouse, Ed.)*Engineering hydraulics 12*. New York: Wiley.

Brune, G. M. (1953). Trap efficiency of reservoirs. *American Geophysical Union*, *34*(3), 417–418.

Cao, Z., Li, J., Pender, G., & Liu, Q. (2015). Whole-process modeling of reservoir turbidity currents by a double layer-averaged model. *Journal of Hydraulic Engineering*, *141*(2), 4014069.

Chamoun, S., Zordan, J., De Cesare, G., & Franca, M. J. (2016). Measurement of the deposition of fine sediments in a channel bed. *Flow Measurement and Instrumentation*, *50*, 49–56.

Chamoun, S., De Cesare, G., & Schleiss, A. J. (2016a). Experimental investigation on turbidity current venting under restrained outflow discharges. In Constantinescu, Gracia, & Hanes (Eds.), *Proceedings of River Flow* (pp. 1435–1441). Saint Louis, USA.

Chamoun, S., De Cesare, G., & Schleiss, A. J. (2016b). Managing reservoir sedimentation by venting turbidity currents: a review. *International Journal of Sediment Research*, *31*(3), 195–204.

Chamoun, S., De Cesare, G., & Schleiss, A. J. (2016c). Venting turbidity currents for the sustainable use of reservoirs. *International Journal on Hydropower and Dams*, *23*(5), 64–69.

Chamoun, S., De Cesare, G., & Schleiss, A. J. (2017a). Venting of turbidity currents approaching a rectangular opening on a horizontal bed. *Journal of Hydraulic Research* (Accepted for publication, available online).

Chamoun, S., De Cesare, G., & Schleiss, A. J. (2017b). Management of turbidity current venting in reservoirs under different thalweg slopes. *Journal of Environmental Management* (Under revision).

Chamoun, S., De Cesare, G., & Schleiss, A. J. (2017c). Influence of operational timing on the efficiency of venting turbidity currents. *Journal of Hydraulic Engineering* (Under review).

Chang, F. J., Lai, J. S., & Kao, L. S. (2003). Optimization of operation rule curves and flushing schedule in a reservoir. *Hydrological Processes*, *17*(8), 1623–1640.

Chen, J., & Zhao, K. (1992). Sediment Management in Nanqin Reservoir. *International Journal of Sediment Research*, *7*(3), 71–84.

Cheng, N. (1997). Simplified settling velocity formula for sediment particle. *Journal of Hydraulic Engineering*, *123*(2), 149–152.

Chien, N., & Wan, Z. (1999). *Mechanics of sediment transport*. Reston, Virginia: ASCE Press.

Craya, A. (1949). Recherches théoriques sur l'écoulement de couches superposées de fluides de densités différentes. *La Houille Blanche*, *35*(1), 44–55.

Crowder, B. M. (1987). Economic costs of reservoir sedimentation: A regional approach to estimating cropland erosion damage. *Journal of Soil and Water Conservation*, *42*(3), 194–197.

Czuba, J. A., Best, J. L., Oberg, K. A., Parsons, D. R., Jackson, P. R., Garcia, M. H., & Ashmore, P. (2011). Bed morphology, flow structure, and sediment transport at the outlet of Lake Huron and in the upper St. Clair River. *Journal of Great Lakes Research*, *37*(3), 480–493.

De Cesare, G. (1998). *Alluvionnement des retenues par courants de turbidité*. PhD thesis No. 1820 and Communication 7, Laboratory of Hydraulic Constructions (LCH), Ed. A. Schleiss, École Polytechnique Fédérale de Lausanne EPFL, Switzerland (in French).

De Cesare, G., Altenkirch, N., Schleiss, A., Roth, M., Molinari, P., & Michel, M. (2015). Störfall vom 30. März 2013 bei der Staumauer Punt dal Gall. *Wasser Energie Luft - Eau Energie Air*, *140*, 1–8.

De Cesare, G., Boillat, J., & Schleiss, A. J. (2006). Circulation in stratified lakes due to flood-induced turbidity currents. *Journal of Environmental Engineering*, *132*(11), 1508–1517.

De Cesare, G., & Lafitte, R. (2007). Outline of the historical development regarding reservoir sedimentation. In CORILA (Ed.), *32nd IAHR Congress, Harmonizing the Demands of Art and Nature in Hydraulics.* (p. 50). Vol. 1, 1-6 July. Venice, Italy.

De Cesare, G., Schleiss, A. J., & Hermann, F. (2001). Impact of turbidity currents on reservoir sedimentation. *Journal of Hydraulic Engineering*, *127*(1), 6–16.

De Rooij, F., Dalziel, S. B., & Linden, P. F. (1999). Electrical measurement of sediment layer thickness under suspension flows. *Experiments in Fluids*, *26*(5), 470–474.

Dinehart, R. L., & Burau, J. R. (2005). Repeated surveys by acoustic Doppler current profiler for flow and sediment dynamics in a tidal river. *Journal of Hydrology*, *314*(1), 1–21.

Ellison, T. H., & Turner, J. S. (1959). Turbulent entrainment in stratified flows. *Journal of Fluid Mechanics*, *6*(3), 423–448.

ENDRESS+HAUSER. (2005). *Proline Promag 50W, 53W, Technical information*.

Espa, P., Brignoli, M. L., Crosa, G., Gentili, G., & Quadroni, S. (2016). Controlled sediment

flushing at the Cancano Reservoir (Italian Alps): Management of the operation and downstream environmental impact. *Journal of Environmental Management*, *182*, 1–12.

Fan, J. (1960). Experimental studies on density currents. *Scientia Sinica*, *4*(2), 275–303.

Fan, J. (1986). Turbid density currents in reservoirs. *Water International*, *11*(3), 107–116.

Fan, J. (2008). Stratified flow through outlets. *Journal of Hydro-Environment Research*, *2*(1), 3–18.

Fan, J., & Morris, G. L. (1992a). Reservoir sedimentation I: Delta and density current deposits. *Journal of Hydraulic Engineering*, *18*(3), 354–369.

Fan, J., & Morris, G. L. (1992b). Reservoir Sedimentation II: Reservoir desiltation and long-term storage capacity. *Journal of Hydraulic Engineering*, *118*(3), 370–384.

Fan, S. S. (1999). An overview of three sedimentation studies in the U.S. In J. H. W. L. and Z. Y. W. A.W. Jayawardena (Ed.), *River sedimentation : theory and applications : Proceedings of the 7th International Symposium on River Sedimentation* (pp. 391–396). Balkema, Rotterdam.

Felix, D., Albayrak, I., & R.M., B. (2016). Continuous measurement of suspended sediment concentration: Discussion of four techniques. *Measurement*, *89*, 44–47.

Filatova, T. N., & Kalejarv, T. O. (1973). Some results of 20-year network observations on currents in Tchudsko-Pskovskoe lake. In *Man-made lakes: their problems and environmental effects* (pp. 316–319). Washington, D. C.: American Geophysical Union.

Fiock, L. R. (1934). Records of silt carried by the Rio Grande and its accumulation in Elephant Butte Reservoir. *Eos, Transactions American Geophysical Union*, *15*(2), 468–473.

Forel, F. A. (1885). Les ravins sous-lacustres des fleuves glaciaires. In *Comptes Rendus* (pp. 725–728). Gauthier-Villars, Paris.

Francou, J., & Rodier, J. (1967). *Essai de classification des crues maximales observées dans le monde*. ORSTOM.

Garcia, M. (1992). Turbidity currents. In *Encyclopedia of Earth System Science, Vol. 4* (pp. 399–408). Harcourt Brace Jovanovich.

Garcia, M., & Parker, G. (1993). Experiments on the entrainment of sediment into suspension by a dense bottom current. *Journal of Geophysical Research*, *98*(C3), 4793–4807.

Gariel, P. (1949). Recherches expérimentales sur l'écoulement de couches superposées de fluides de densités différentes. *La Houille Blanche*, *35*(1), 56–64.

Georgoulas, A. N., Angelidis, P. B., Panagiotidis, T. G., & Kotsovinos, N. E. (2010). 3D numerical modelling of turbidity currents. *Environmental Fluid Mechanics*, *10*(6), 603–635.

Gladstone, C., Phillips, J. C., & Sparks, R. S. J. (1998). Experiments on bidisperse, constant-volume gravity currents: propagation and sediment deposition. *Sedimentology*, *45*(5), 833–843.

Graf, W., & Altinakar, M. S. (1991). *Hydrodynamics* (Eyrolles).

Graf, W. H., & Altinakar, M. S. (1995). Courants de turbidité. *La Houille Blanche*, *81*(7), 28–37.

Graf, W. H., & Altinakar, M. S. (2000). *Hydraulique fluviale*. Presses Polytechniques et Universitaires Romandes.

Hage, S., Cartigny, M., Clare, M., & Talling, P. (2016). A multi-instrument approach to monitoring turbidity currents: Case study from the Squamish Delta, British Columbia (Canada). In *EGU General Assembly Conference Abstracts* (p. 13038).

Haun, S., & Lizano, L. (2016). Evaluation of a density current from ADCP backscatter data and LISST measurements. In *River Flow* (pp. 875–881). CRC Press.

Heidarnejad, M., Golmaee, S. H., Mosaedi, A., & Ahmadi, M. Z. (2006). Estimation of sediment volume in Karaj Dam Reservoir (Iran) by hydrometry method and a comparison with hydrography method. *Lake and Reservoir Management*, *22*(3), 233–239.

Huang, H. Q., Imran, J., & Pirmez, C. (2008). Numerical study of turbidity currents with sudden-release and sustained-inflow mechanisms. *Journal of Hydraulic Engineering*, *134*(9), 1199–1209.

Jiang, T., Zhang, Y., Tang, S., Zhang, D., Zuo, Q., Lin, W., … Wang, B. (2014). CFD simulation on the generation of turbidites in deepwater areas: a case study of turbidity current processes in Qiongdongnan Basin, northern South China Sea. *Acta Oceanologica Sinica*, *33*(12), 127–137.

Kantoush, S. A., & Sumi, T. (2010). River morphology and sediment management strategies for sustainable reservoir in Japan and European Alps. In *Annuals of Disaster Preventive*

Research Institute (pp. 821–839). Kyoto, Japan.

Khan, N. M., & Tingsanchali, T. (2009). Optimization and simulation of reservoir operation with sediment evacuation: a case study of the Tarbela Dam, Pakistan. *Hydrological Processes*, *23*(5), 730–747.

Khan, S. M., Imran, J., Bradford, S., & Syvitski, J. (2005). Numerical modeling of hyperpycnal plume. *Marine Geology*, *222*, 193–211.

Khripounoff, A., Vangriesheim, A., Babonneau, N., Crassous, P., Dennielou, B., & Savoye, B. (2003). Direct observation of intense turbidity current activity in the Zaire submarine valley at 4000 m water depth. *Marine Geology*, *194*(3), 151–158.

Kneller, B., & Buckee, C. (2000). The structure and fluid mechanics of turbidity currents : a review of some recent studies and their geological implications. *Sedimentology*, *47*(s1), 62–94.

Kondolf, G., Gao, Y., & Annandale, G. (2014). Sustainable sediment management in reservoirs and regulated rivers: Experiences from five continents. *Earth's Future*, *2*(5), 256–280.

Kondolf, G. M. (1997). PROFILE: hungry water: Effects of dams and gravel mining on river channels. *Environmental Management*, *21*(4), 533–551.

Lambert, A., & Giovanoli, F. (1988). Records of riverborne turbidity currents and indications of slope failures in the Rhone Delta of Lake Geneva. *Limnology and Oceanography*, *33*(3), 458–468. Retrieved from -

Lane, E. W., & Koelzer, V. A. (1943). *A study of methods used in measurement and analysis of sediment loads in streams*. Iowa University, Iowa.

Lara, J. M. (1960). *The 1957 sedimentation survey of elephant butte reservoir*. Bureau of Reclamation, U.S. Dept. of Interior, Denver.

Lee, F. Z., Lai, J. S., Tan, Y. C., & Sung, C. C. (2014). Turbid density current venting through reservoir outlets. *KSCE Journal of Civil Engineering*, *18*(2), 694–705.

Lowe, J., & Fox, I. (1995). Sediment management schemes for Tarbela reservoir. In *USCOLD annual meeting*.

Meiburg, E., & Kneller, B. (2010). Turbidity currents and their deposits. *Annual Review of Fluid Mechanics*, *42*(1), 135–156.

Meiburg, E., Radhakrishnan, S., & Nasr-Azadani, M. (2015). Modeling gravity and turbidity

currents: computational approaches and challenges. *Applied Mechanics Reviews*, *67*(4), 40802.

Metflow, S. (2014). UVP monitor - User's guide, Lausanne, Switzerland.

Middleton, G. (1993). Sediment deposition from turbidity currents. *Annual Review of Earth Planet*, *21*, 89–114.

Morris, G., & Fan, J. (1997). *Reservoir sedimentation handbook: Design and management of dams, reservoirs, and watersheds for sustainable use*. McGraw-Hill, New York.

Mulder, T., & Syvitski, J. (1995). Turbidity currents generated at river mouths during exceptional discharges to the world oceans. *The Journal of Geology*, *103*(3), 285–299.

Müller, M. (2012). *Influence of in- and outflow sequences on flow patterns and suspended sediment behavior in reservoirs*. PhD thesis No. 5471 and Communication 53, Laboratory of Hydraulic Constructions (LCH), Ed. A. Schleiss, École Polytechnique Fédérale de Lausanne EPFL, Switzerland.

Müller, P. J., & De Cesare, G. (2009). Sedimentation problems in the reservoirs of the Kraftwerke Sarganserland - Venting of turbidity currents as the essential part of the solution. General Report Q.89-R.21. In *Proc. of the 23rd Congress of the Int. Commission on Large Dams CIGB-ICOLD*. Brasilia: Vol. 2, Brasilia, Brazil, Q.89-R.21.

Nizery, A., Braudeau, G., & Bonnin, J. (1952). La station du Sautet pour l'étude de l'alluvionnement des réservoirs. In *Proc. Transport hydraulique et décantation des matériaux solides* (pp. 180–218). France.

Nogueira, H. I. S., Adduce, C., Alves, E., & Franca, M. J. (2014). Dynamics of the head of gravity currents. *Environmental Fluid Mechanics*, *14*(2), 519–540.

Oehy, C. (2003). *Effects of obstacles and jets on reservoir sedimentation due to turbidity currents*. PhD thesis No. 2684, Communication 15, Laboratory of Hydraulic Constructions (LCH), Ed. A. Schleiss, École Polytechnique Fédérale de Lausanne EPFL, Switzerland.

Oehy, C., De Cesare, G., & Schleiss, A. J. (2000). Parametric study on the influence of turbidity currents on the sedimentation of Alpine reservoirs. In *Hydro 2000 - Making Hydro more Competitive''* (pp. 137–146). Session III: Sediment Management, Berne, Switzerland.

Oehy, C., De Cesare, G., & Schleiss, A. J. (2010). Effects of inclined jet screen on turbidity

currents. *Journal of Hydraulic Research*, *48*(1), 81–90.

Oehy, C., & Schleiss, A. J. (2007). Control of turbidity currents in reservoirs by solid and permeable obstacles. *Journal of Hydraulic Engineering*, *133*(6), 637–648.

Palmieri, A., Shah, F., Annandale, G., & Dinar, A. (2003). *Reservoir conservation volume I: the RESCON approach economic and engineering evaluation of alternative strategies for managing sedimentation in storage reservoirs*. *A contribution to promote conservation of water storage assets worldwide* (Vol. 1). The International Bank for Reconstruction and Development/The World Bank, Washington, DC, USA.

Palmieri, A., Shah, F., & Dinar, A. (2001). Economics of reservoir sedimentation and sustainable management of dams. *Journal of Environmental Management*, *61*(2), 149–163.

Pan, J., & He, J. (2000). *Large Dams in China*. Beijing, China: China WaterPower Press.

Parker, G. (1982). Conditions for the ignition of catastrophically erosive turbidity currents. *Marine Geology*, *46*, 307–327.

Parker, G., Fukushima, Y., & Pantin, M, H. (1986). Self-accelerating turbidity currents. *Journal of Fluid Mechanics*, *171*, 145–181.

Parker, G., Garcia, M., Fukushima, Y., & Yu, W. (1987). Experiments on turbidity currents over an erodible bed. *Journal of Hydraulic Research*, *25*(1), 123–147.

Paull, C. K., Ussler, W., Greene, H. G., Keaten, R., Mitts, P., & Barry, J. (2003). Caught in the act: the 20 December 2001 gravity flow event in Monterey Canyon. *Geo-Marine Letters*, *22*(4), 227–232.

Pazwash, H. (1982). Sedimentation in reservoirs case of Sefidrud dam. In *Proc. 3rd Congress of the ADP, IAHR* (pp. 215–223). Bandung, Indonesia.

Rai, A. K., & Kumar, A. (2015). Continuous measurement of suspended sediment concentration: Technological advancement and future outlook. *Measurement*, *76*, 209–227.

Raud, J. (1958). Les soutirages de vases au barrage d'Iril Emda (Algérie). In *6th ICOLD*. Com. 31, New York.

Ren, Z., & Ning, Q. (1985). *Lecture notes of the training course on reservoir sedimentation*. Beijing, China: IRTCES.

Richardson, J. F., & Zaki, W. N. (1997). Sedimentation and Fluidisation: Part I. *Chemical Engineering Research and Design*, *75*, 82–100.

Rosca, D., Craciun, S., & Grumazescu, H. (1982). Cercetarea spectrelor de turbiditate din lacurile de acumulare cu ajutorul unor metode moderne de masurare [Research on turbidity spectra in the lakes using modern methods of measurement]. *Rev. Hidrotehnica*, *27*(4), (in Romanian).

Sahnaz, T., & Aras, T. (2012). Techniques for preventation of sediment deposition. *Reservoir Sedimentation Management*, 41–59.

Schlegel, B., & Dietler, T. (2010). Dez-Damm , Iran : Hohe - Sedimentationsraten in der Stauhaltung erfordern den Bau von Spülstollen. *Wasserwirtschaft*, *100*(4), 90–92.

Schleiss, A., De Cesare, G., & Althaus, J. J. (2010). Verlandung der Stauseen gefährdet die nachhaltige Nutzung der Wasserkraft. *Wasser, Energie, Luft - Eau, Energie, Air*, *102*(1), 31–40.

Schleiss, A. J. (2013). Sedimentation of reservoirs. In *Encyclopedia of Natural Hazards* (pp. 901–905). Springer Netherlands.

Schleiss, A. J., De Cesare, G., & Althaus, J. J. (2008). Reservoir sedimentation and sustainable development. In *International Conference on Erosion, Transport and Deposition of Sediments,* (pp. 23–28). April 28, Berne, Switzerland.

Schleiss, A. J., Franca, M. J., Juez, C., & De Cesare, G. (2016). Reservoir sedimentation. Vision paper. *Journal of Hydraulic Research*, *54*(6), 595–614.

Schleiss, A. J., & Pougatsch, H. (2011). *Les barrages: Du projet à la mise en service. Traité de Génie Civil de l'École Polytechnique Fédérale de Lausanne. Volume 17*. Lausanne: Presses polytechniques et universitaires romandes.

Schleiss, A., & Oehy, C. (2002). Verlandung von Stauseen und Nachhaltigkeit. *Wasser, Energie, Luft - Eau, Energie, Air*, *94*(7/8), 227–234.

Schneider, J., Badura, H., Troy, W., & Knoblauch, H. (2007). Determination of parameters for venting turbidity currents. In *IAHR Congress Vol. 32, No. 1* (p. 425). Venice, Italy.

Schock, S. G., LeBlanc, L. R., & Mayer, L. A. (1989). Chirp subbottom profiler for quantitative sediment analysis. *Geophysics*, *54*(4), 445–450.

Simpson, J. E., & Britter, R. E. (1979). The dynamics of the head of a gravity current advancing

over a horizontal surface. *Journal of Fluid Mechanics*, *94*(3), 477–495.

Sinniger, R. O., De Cesare, G., & Boillat, J.-L. (1999). Propriétés des alluvions récentes dans les retenues alpines. *Wasser, Energie, Luft - Eau, Energie, Air*, *89*(9/10), 255–258.

Sinniger, R. O., De Cesare, G., & Martini, O. (1994). Apports de sédiments dans une retenue par courant de fond, mesures in situ. In *XVIII ICOLD Congress Q.69, R.7* (pp. 85–98). Durban.

Sloff, C. J. (1991). *Communications on hydraulic and geotechnical engineering*. Faculty of Civil Engineering, Delft University of Technology.

Sloff, K., Commandeur, A., & Yang, J.-C. (2016). Models for effective sluicing of turbidity-currents in resevoirs. In G. Constantinescu, M. Gracia, & D. Hanes (Eds.), *River Flow Proceedings* (pp. 868–874). CRC Press.

Smith, W. O., Vetter, C. P., & Cummings, G. B. (1960). *Comprehensive survey of sedimentation in Lake Mead, 1948-49*. United States Government Printing Office, Washington.

Stow, D. A., & Bowen, A. J. (1980). A physical model for the transport and sorting of fine-grained sediment by turbidity currents. *Sedimentology*, *27*(1), 31–46.

Turner, J. S. (1973). *Buoyancy Effects in Fluids*. (C. U. Press, Ed.). Cambridge, GB.

Van Rijn, L. C. (1987). Mathematical modelling of morphological processes in the case of suspended sediment transport. *Delft Hydra. Communication*, (382).

Vanoni, V. A. (2006). *Sedimentation engineering*. American Society of Civil Engineers.

Wan, X. Y., Wang, G. Q., Yi, P., & Bao, W. M. (2010). Similarity-based optimal operation of water and sediment in a sediment-laden reservoir. *Water Resources Management*, *24*(15), 4381–4402.

Wang, Z., & Hu, C. (2009). Strategies for managing reservoir sedimentation. *International Journal of Sediment Research*, *24*(4), 369–384.

Wang, Z., & Lin, B. (2004). Sediment studies and management strategies in China. *International Journal of River Basin Management*, *2*(1), 39–50.

Wang, Z., Xia, J., Deng, S., Zhang, J., & Li, T. (2017). One-dimensional morphodynamic model coupling open-channel flow and turbidity current in reservoir. *Journal of Hydrology and Hydromechanics*, *65*(1), 68–79.

Wen Shen, H. (1999). Flushing sediment through reservoirs. *Journal of Hydraulic Research*, *37*(6), 743–757.

Wenxue, L. I., Zhang, Y., & Zhang, C. (2005). The operation mode of storing the clear water and discharging the muddy flow for reservoirs built on heavily silt-laden rivers - a case study of the Sanmenxia reservoir. *International Journal of Sediment Research*, *20*(2), 109–116.

Wüest, A. (2010). Downstream relevance of reservoir management. Alpine Waters. In *Handbook of Environmental Chemistry* (Vol. 6, pp. 235–246).

Xu, J. P. (2010). Normalized velocity profiles of field-measured turbidity currents. *Geology*, *38*(6), 563–566.

Xu, J. P., Noble, M. A., & Rosenfeld, L. K. (2004). In-situ measurements of velocity structure within turbidity currents. *Geophysical Research Letters*, *31*(9).

Yu, W.-S., Hsu, S. M., & Fan, K.-L. (2004). Experiments on selective withdrawal of a codirectional two-layer flow through a line sink. *Journal of Hydraulic Engineering*, *130*(12), 1156–1166.

Zhiyao, S., Tingting, W., Fumin, X., & Ruijie, L. (2008). A simple formula for predicting settling velocity of sediment particles. *Water Science and Engineering*, *1*(1), 37–43.

APPENDIX

A1. Typical turbidity currents for the different slopes

The time step between the different figures is Δt = 25 s.

Slope 0%

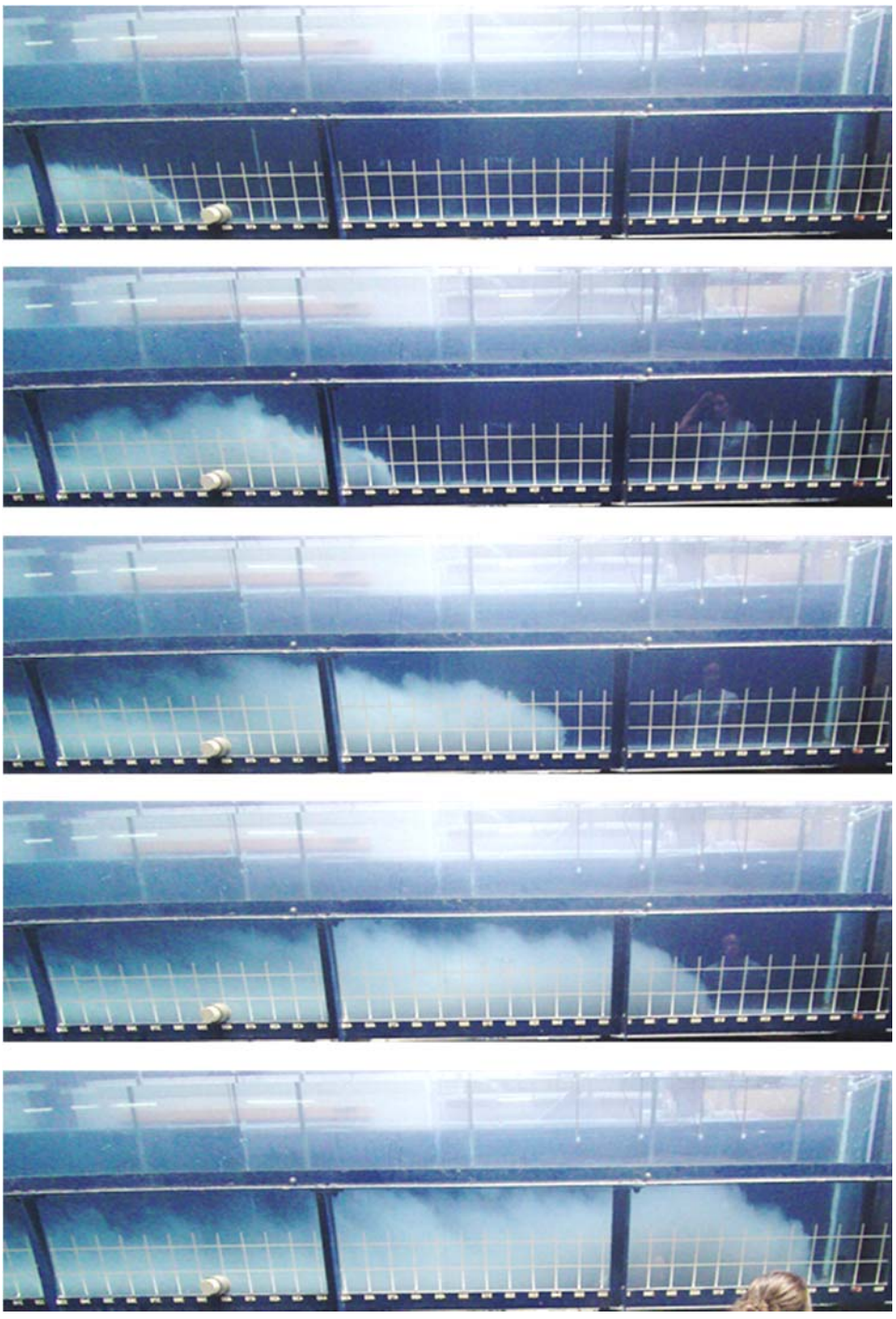

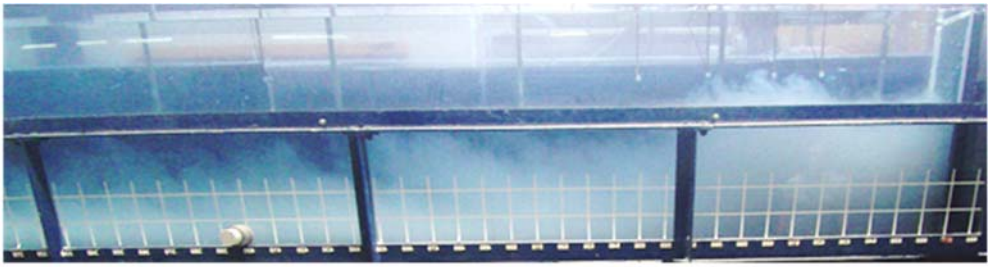

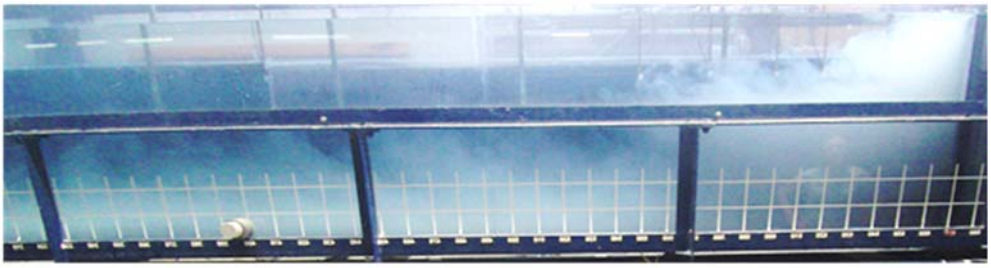

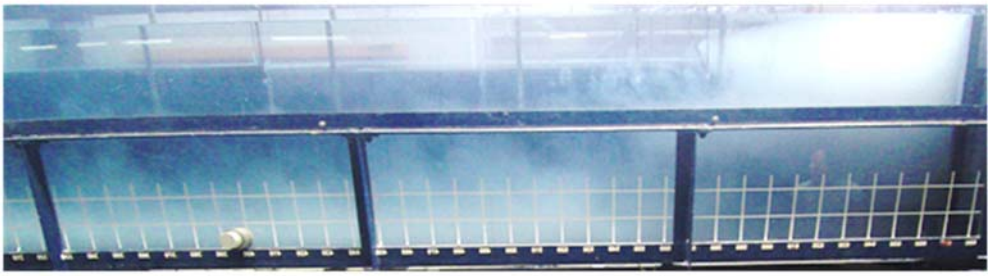

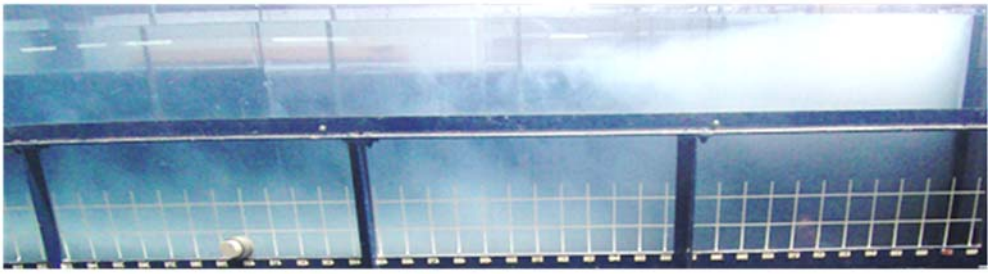

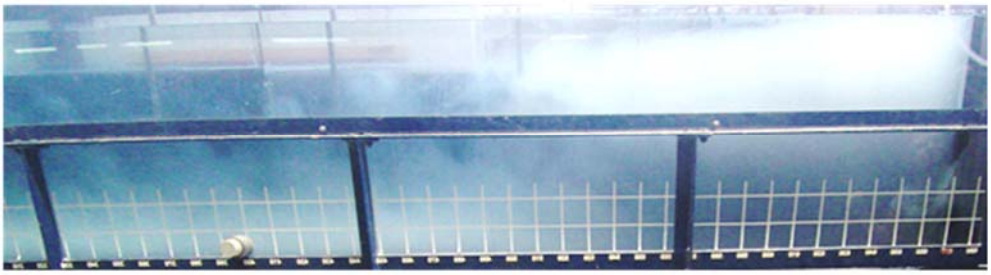

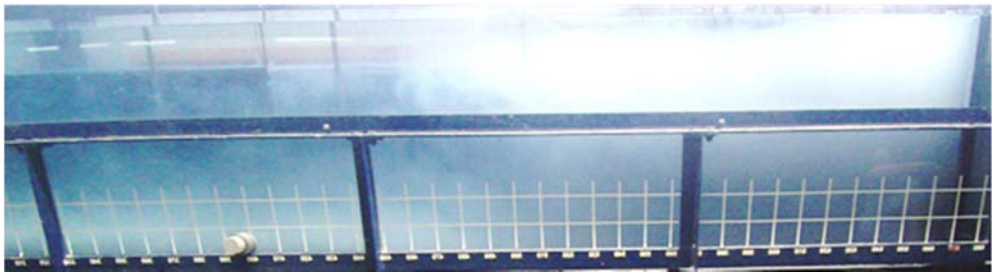

Figure A1.1: Typical behaviour of the turbidity currents for the experimental tests using a horizontal bed. Time step Δt = 25 s.

Slope 2.4%

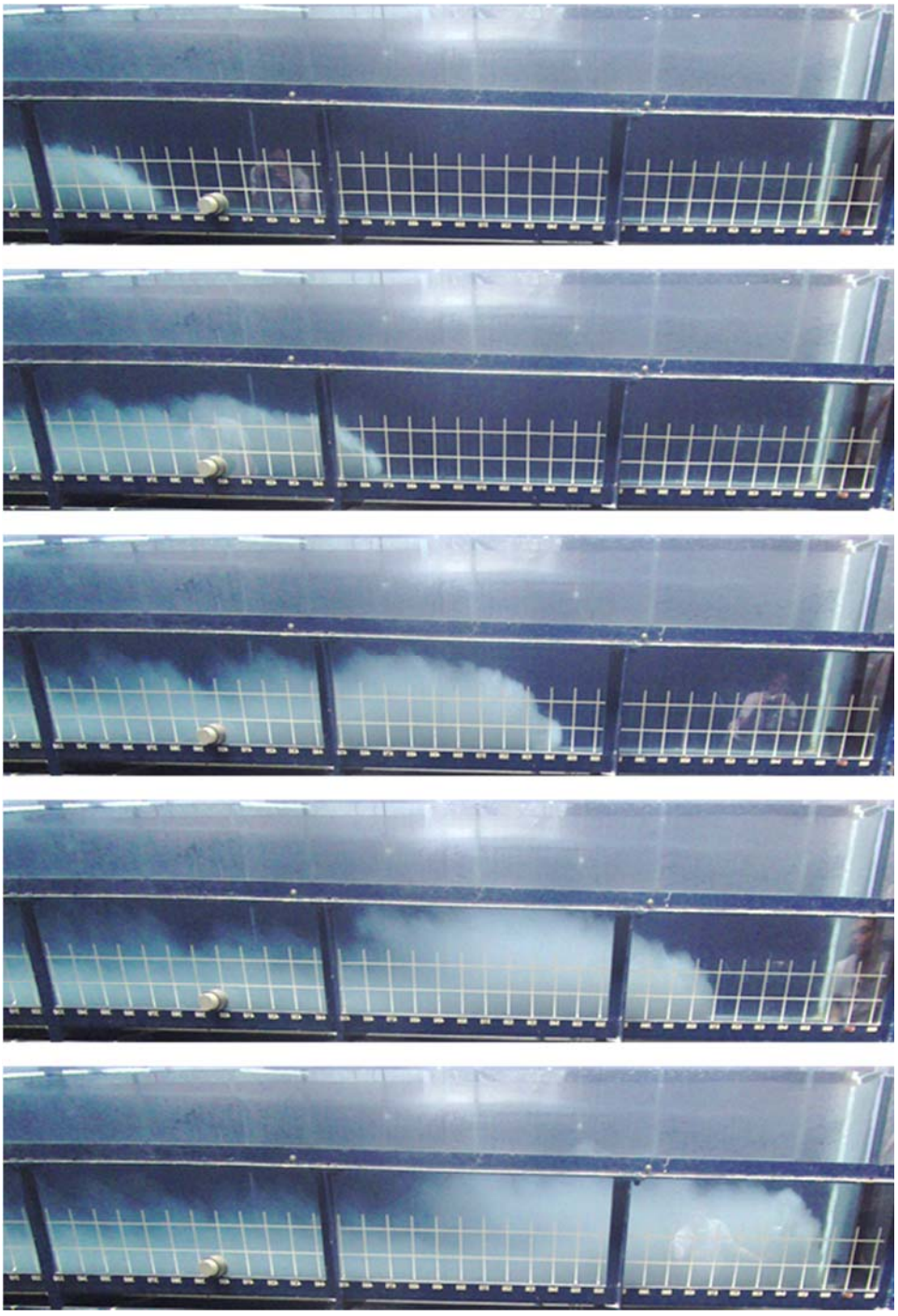

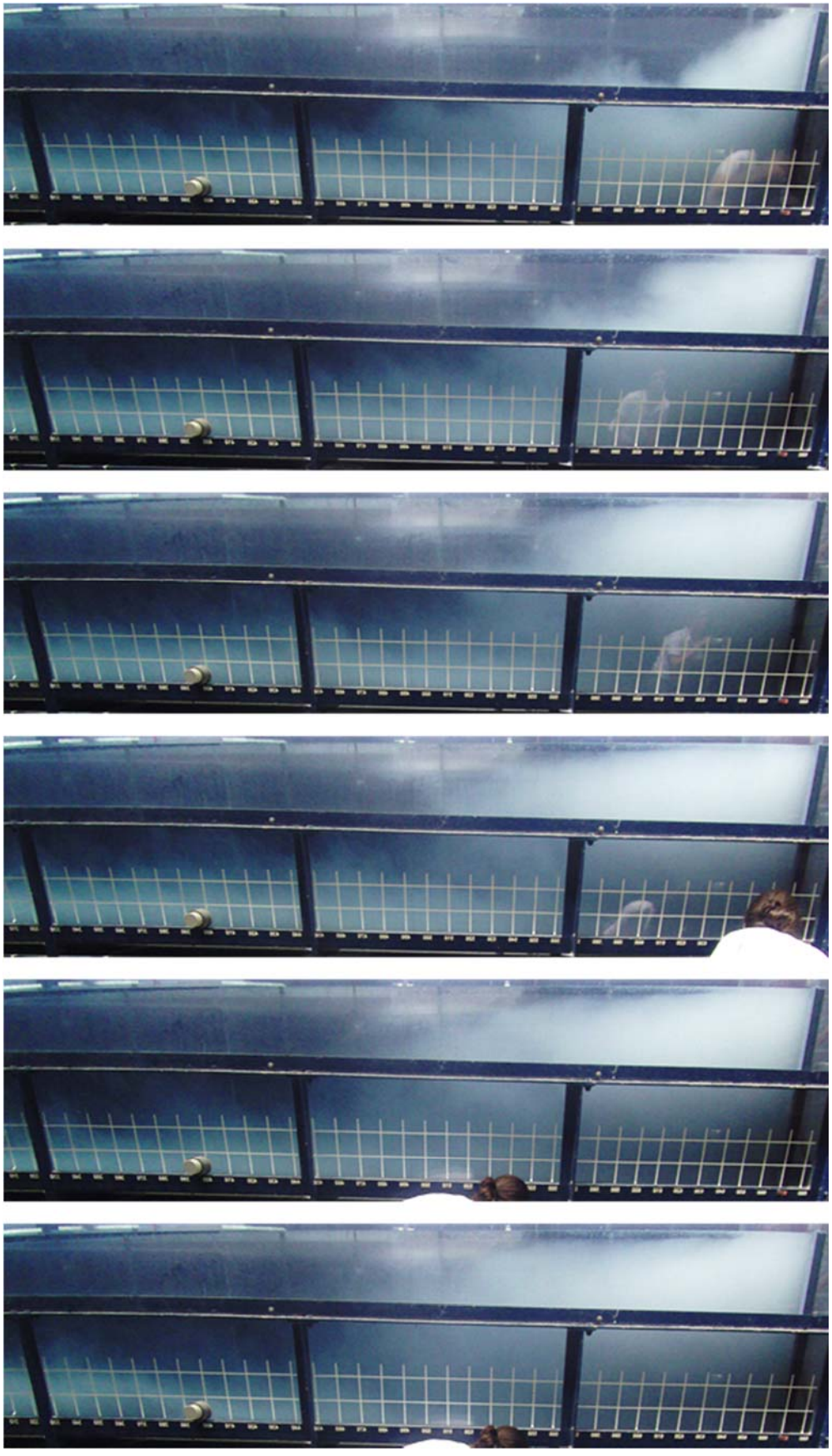

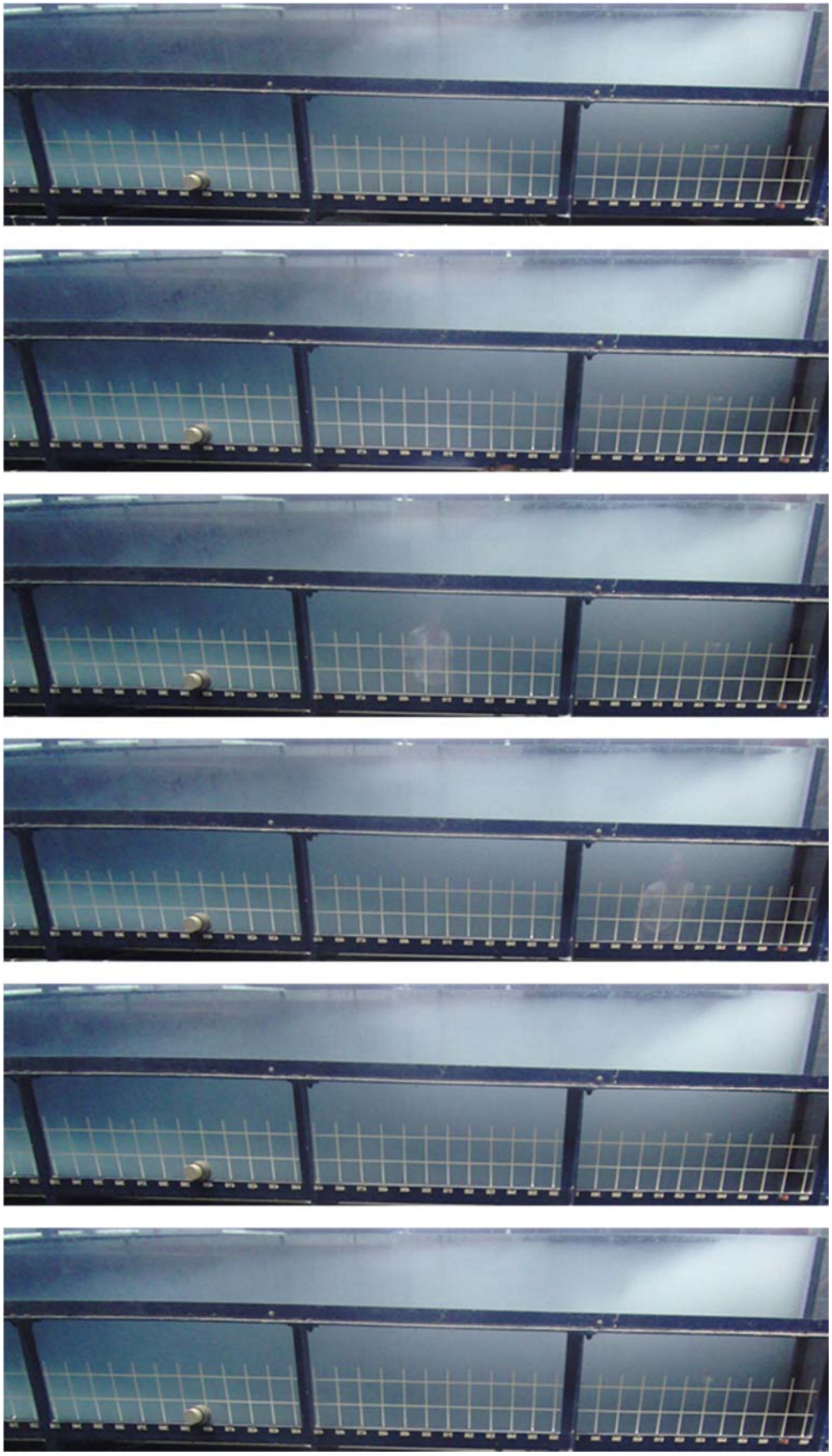

Figure A1.2: Typical behaviour of the turbidity currents for the experimental tests using a slope of 2.4%. Time step Δt = 25 s.

Slope 5.0%

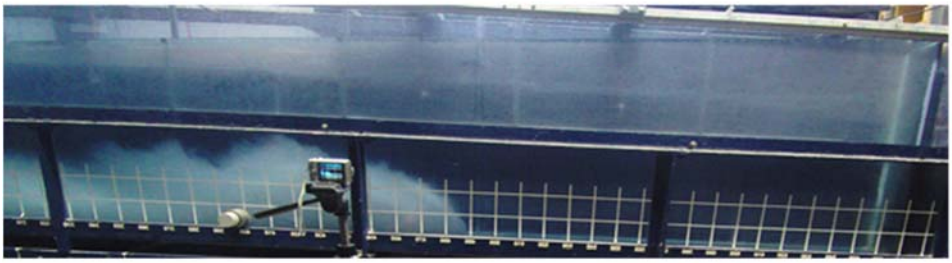

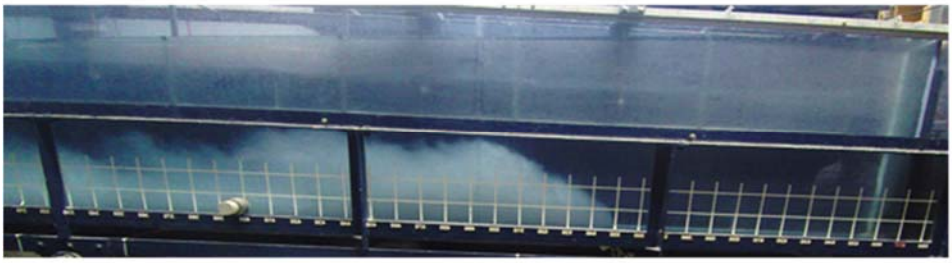

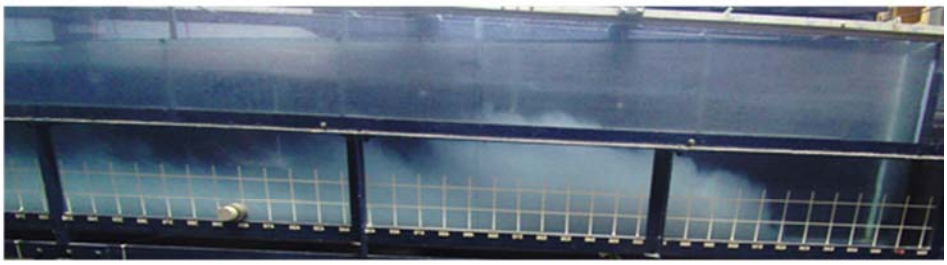

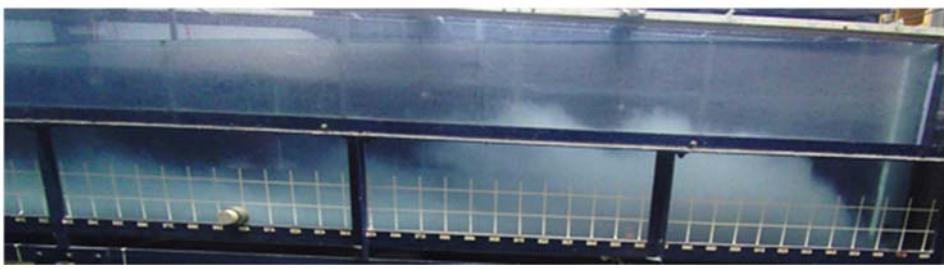

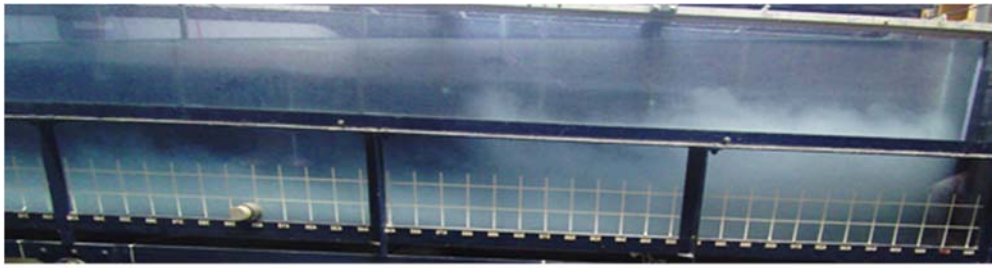

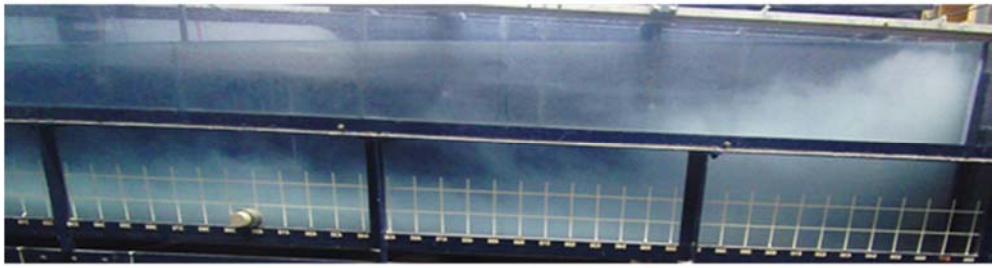

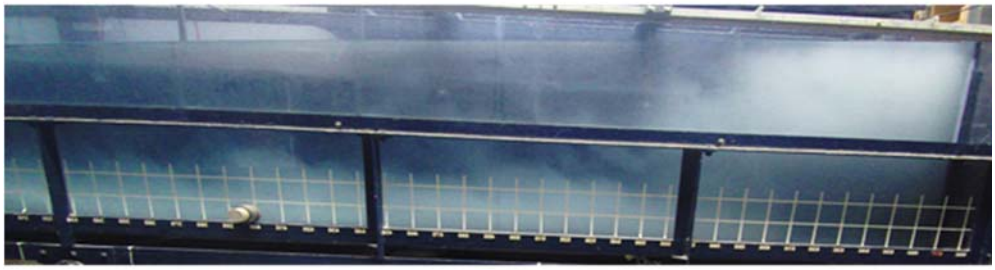

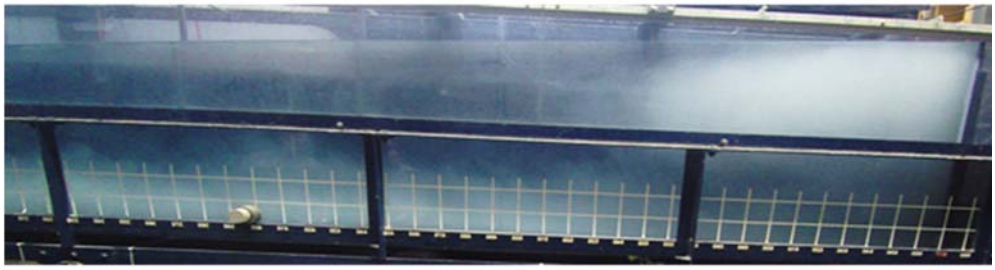

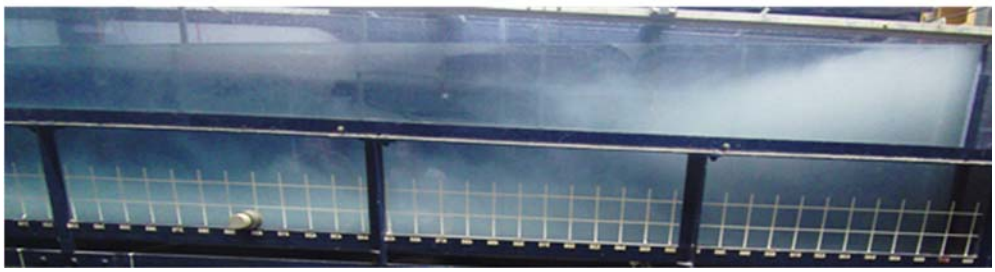

Figure A1.3: Typical behaviour of the turbidity currents for the experimental tests using a slope of 2.4%. Time step Δt = 25 s.

A2. Initial test conditions: temperatures and water depths

Table A2.1: Temperature and water depth in the main flume and in the head tank during the experimental tests.

Test No.	Temperature (°C)		Water depth (cm)	
	T_{head}	T_{flume}	H_{head}	H_{flume}
E0.1	12.0	9.1	83.0	82.6
E0.2	11.8	9.4	82.5	81.9
E0.3	11.8	10.2	81.3	81.1
E0.4	9.7	10.8	81.4	80.7
E0.5	13.3	10.7	81.0	80.8
E0.6	11.9	9.2	80.6	80.1
E0.7	12.5	9.7	81.8	80.8
E1.0	10.5	9.0	66.2	66.1
E1.1	11.5	9.5	69.9	66.0
E1.2	10.9	8.7	66.5	65.8
E1.3	11.5	8.4	66.6	65.7
E1.4	12.7	10.2	66.2	65.6
E1.5	12.4	10.3	65.6	65.3
E1.6	12.2	10.0	65.8	65.6
E1.7	12.1	9.0	64.0	63.9
E1.8	13.5	11.5	66.2	65.1
E1.9	11.5	10.7	65.4	65.3
E1.10	13.5	10.8	65.6	65.4
E2.0	14.2	10.5	62.1	61.5
E2.1	11.7	9.4	61.4	61.1
E2.2	11.8	9.2	60.7	60.4
E2.3	12.5	9.0	60.8	60.3
E2.4	14.1	11.0	61.3	60.3
E2.5	13.9	10.7	60.6	60.1
E2.6	13.0	9.9	60.7	60.1
E2.7	13.4	10.3	60.8	60.4
E2.8	13.3	11.6	60.9	60.6
E2.9	13.3	11.2	61.7	61.1
E2.10	13.9	10.5	61.5	60.9

A3. Normalized concentration of the outflow

Horizontal bed

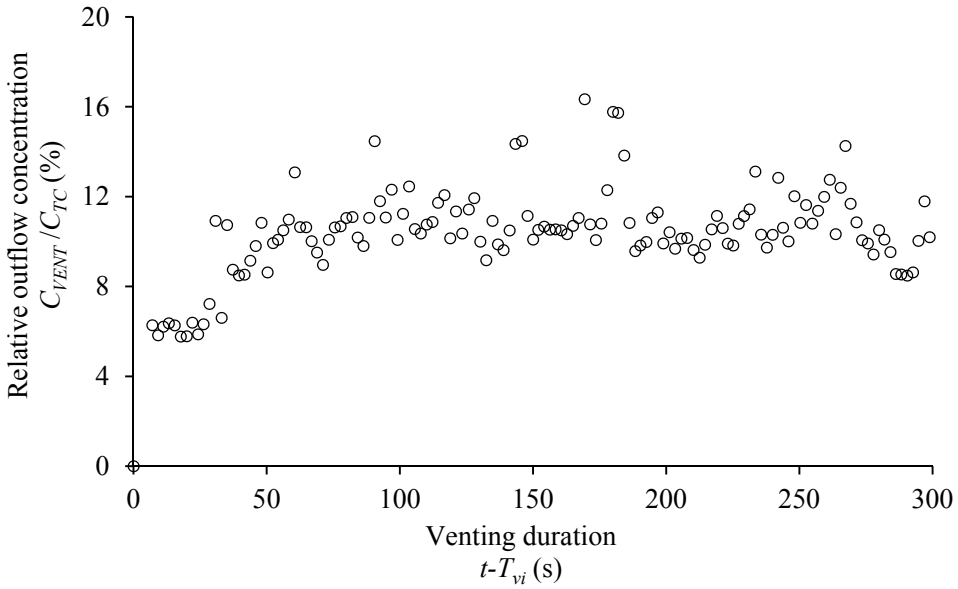

Figure A3.1: Normalized outflow concentration obtained with ϕ = 30% on the horizontal bed (test E0.1).

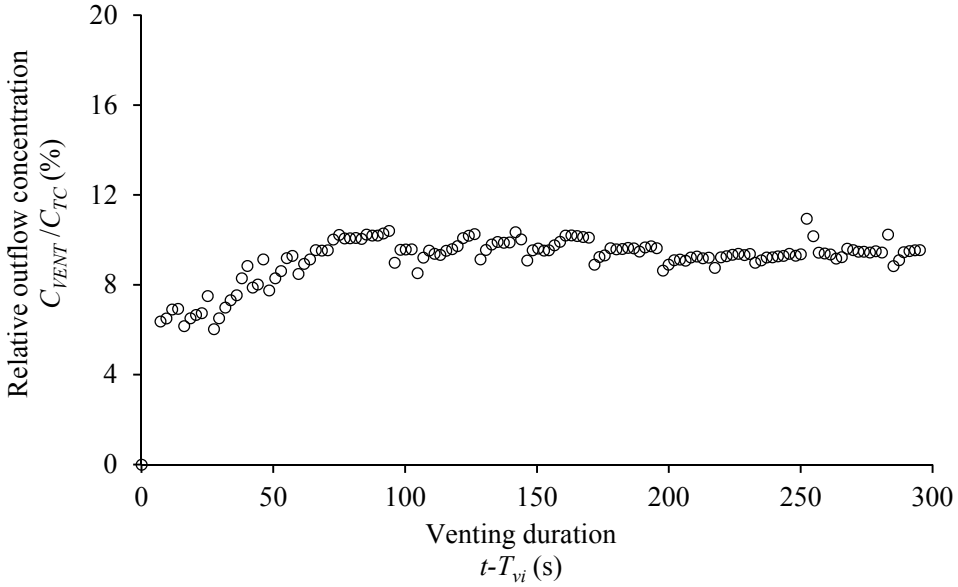

Figure A3.2: Normalized outflow concentration obtained with ϕ = 50% on the horizontal bed (test E0.2).

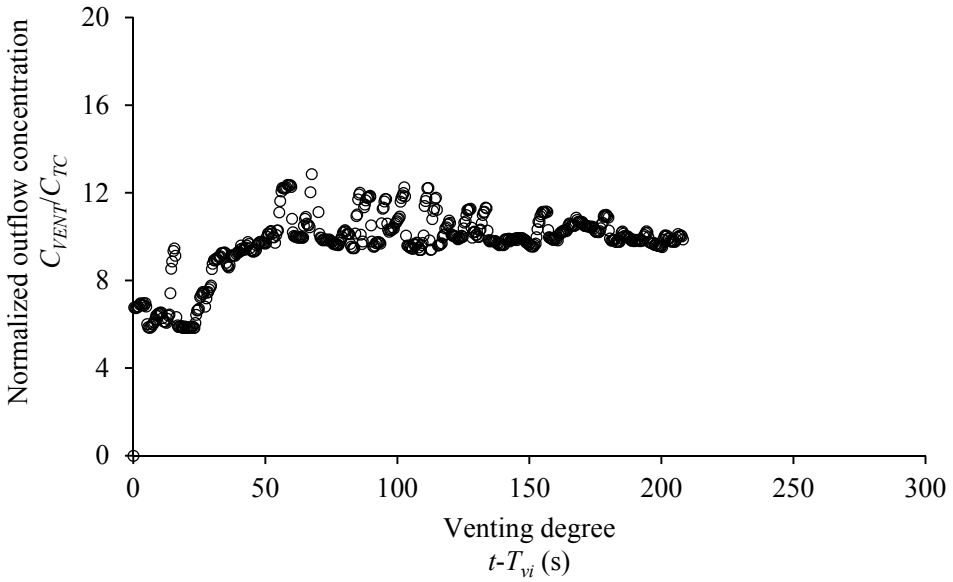

Figure A3.3: Normalized outflow concentration obtained with ϕ = 65% on the horizontal bed (test E.03).

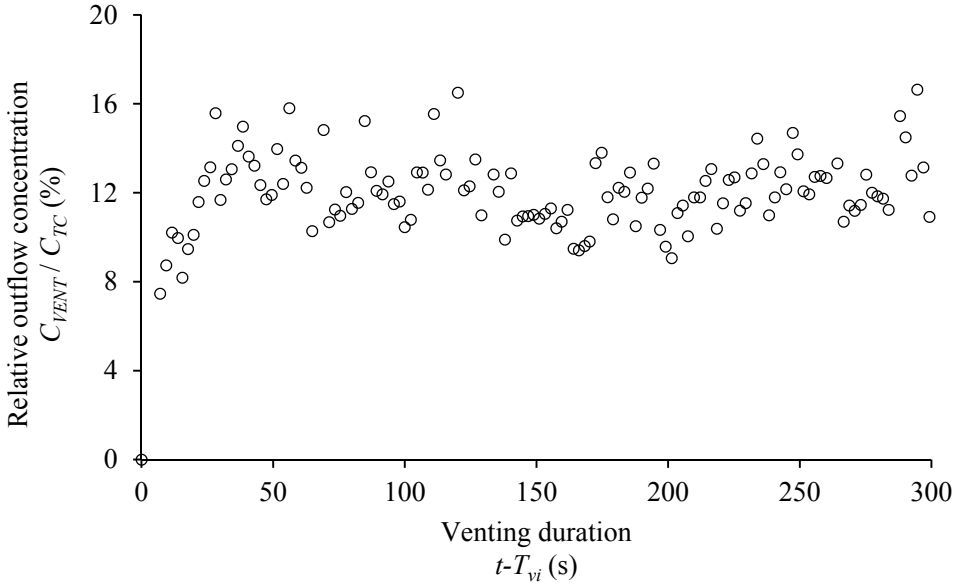

Figure A3.4: Normalized outflow concentration obtained with ϕ = 80% on the horizontal bed (test E0.4).

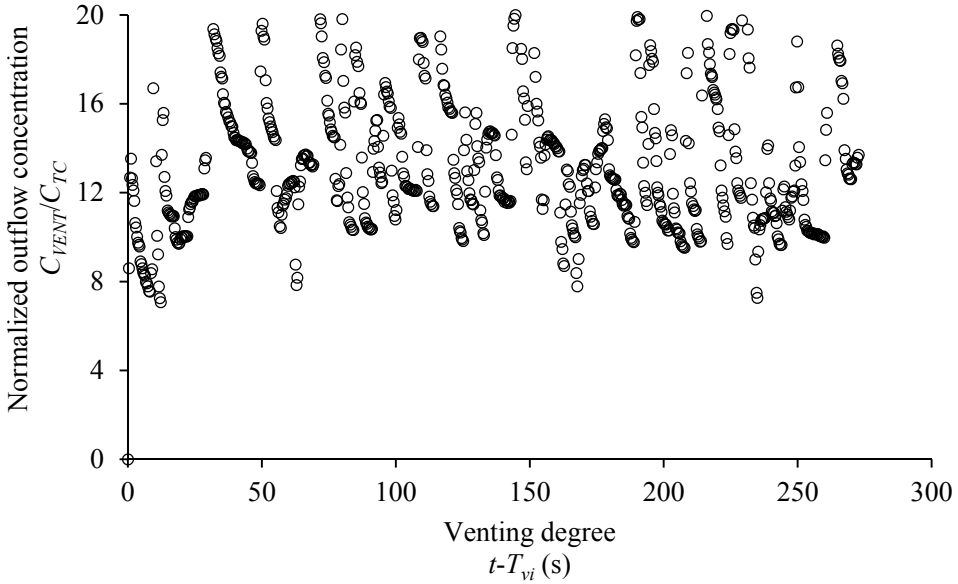

Figure A3.5: Normalized outflow concentration obtained with ϕ = 100% on the horizontal bed (test E0.5).

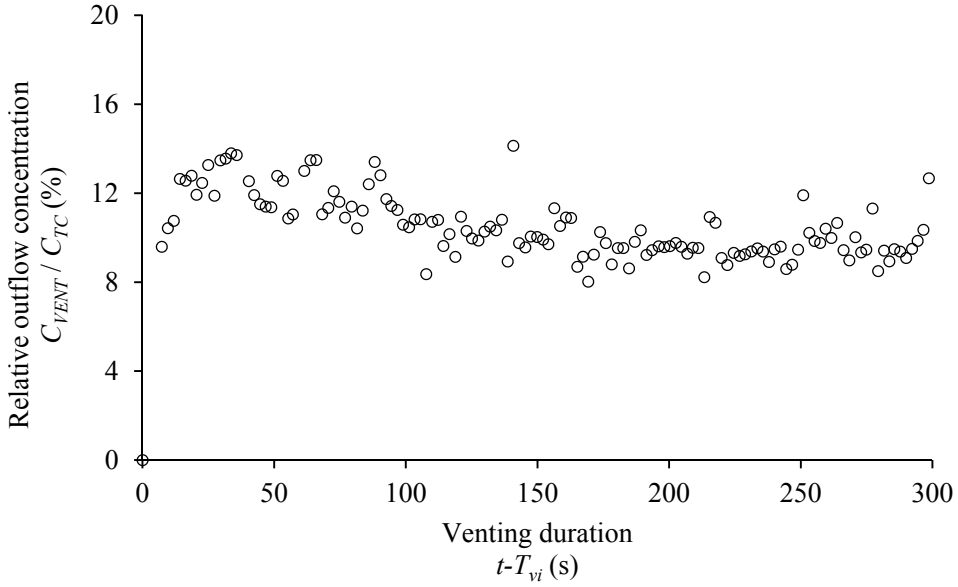

Figure A3.6: Normalized outflow concentration obtained with ϕ = 115% on the horizontal bed (test E0.6).

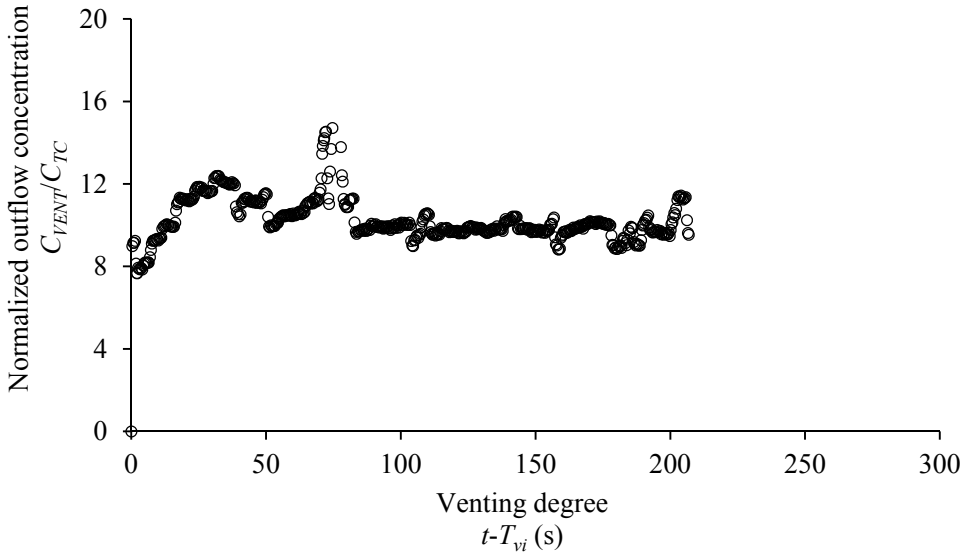

Figure A3.7: Normalized outflow concentration obtained with ϕ = 125% on the horizontal bed (test E0.7).

Slope S = 2.4%

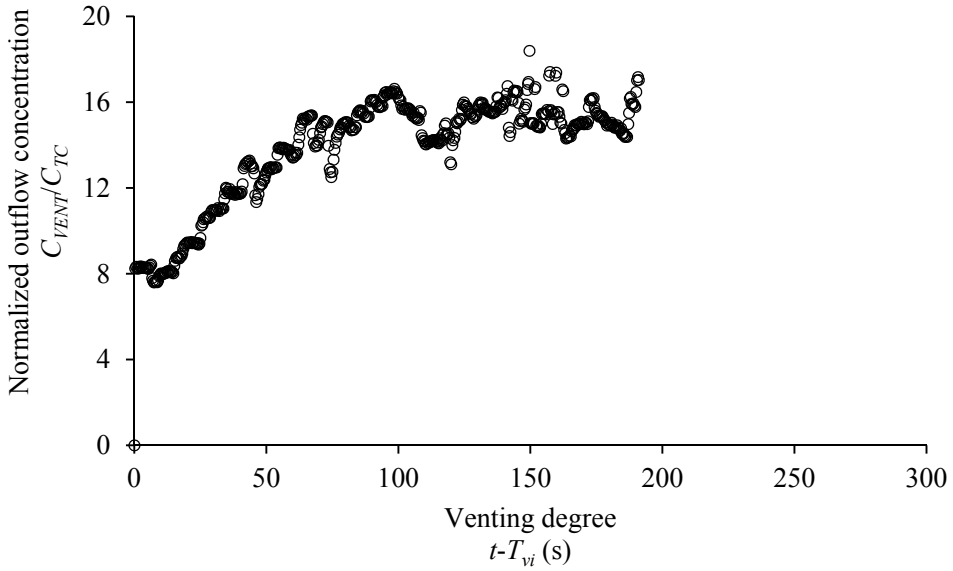

Figure A3.8: Normalized outflow concentration obtained with ϕ = 30% on the 2.4% slope (test E1.1).

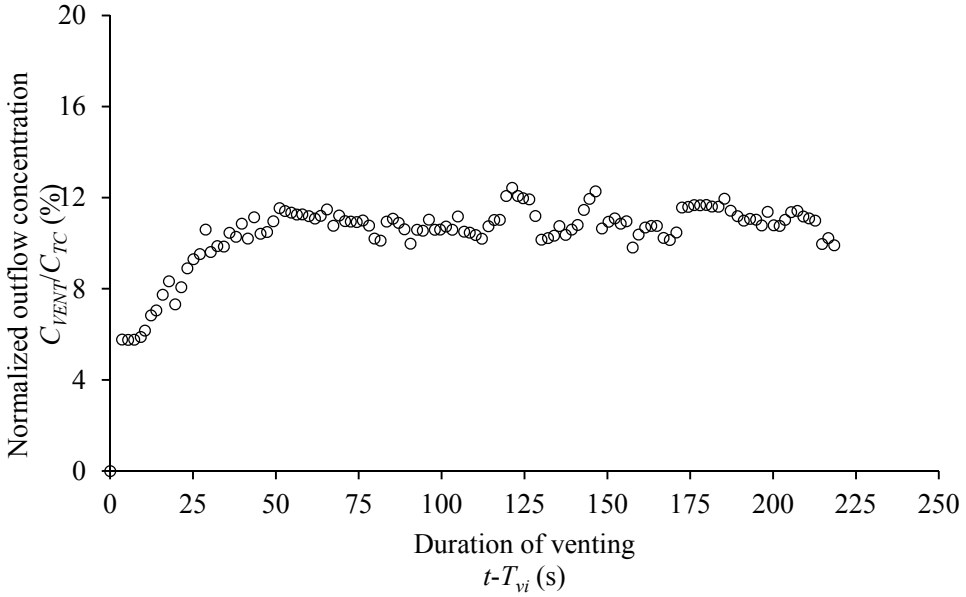

Figure A3.9: Normalized outflow concentration obtained with ϕ = 50% on the 2.4% slope (test E1.2).

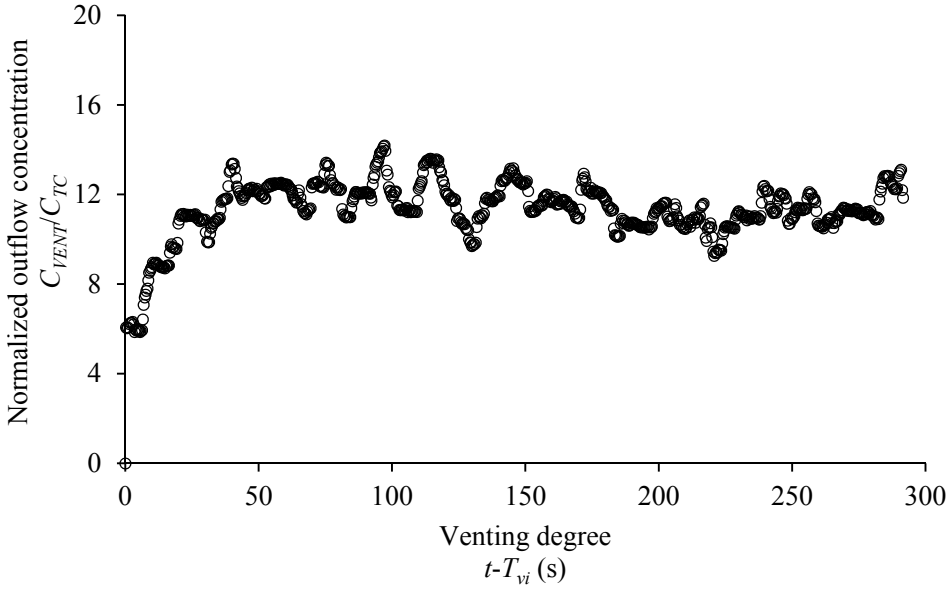

Figure A3.10: Normalized outflow concentration obtained with ϕ = 65% on the 2.4% slope (test E1.3).

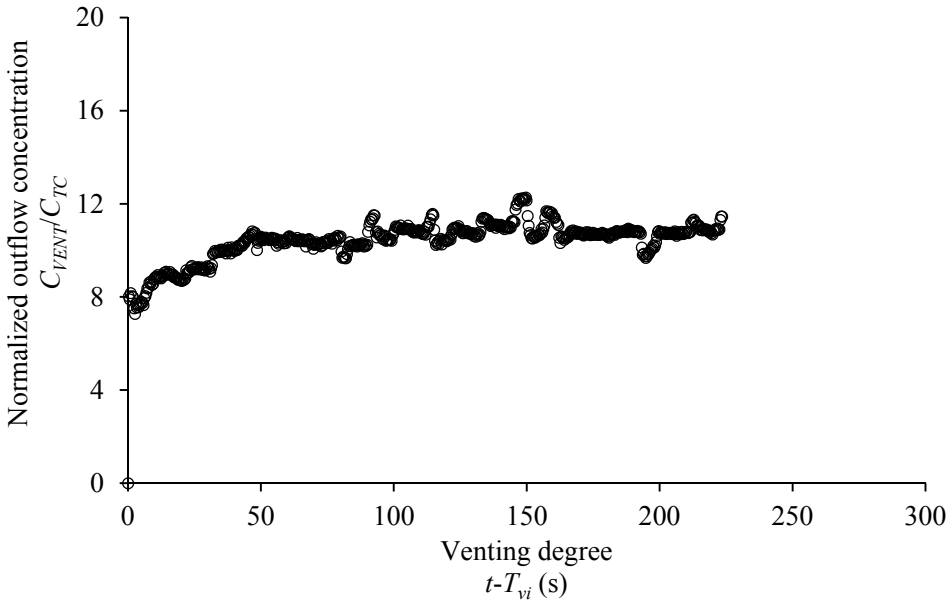

Figure A3.11: Normalized outflow concentration obtained with ϕ = 100% on the 2.4% slope (test E1.4).

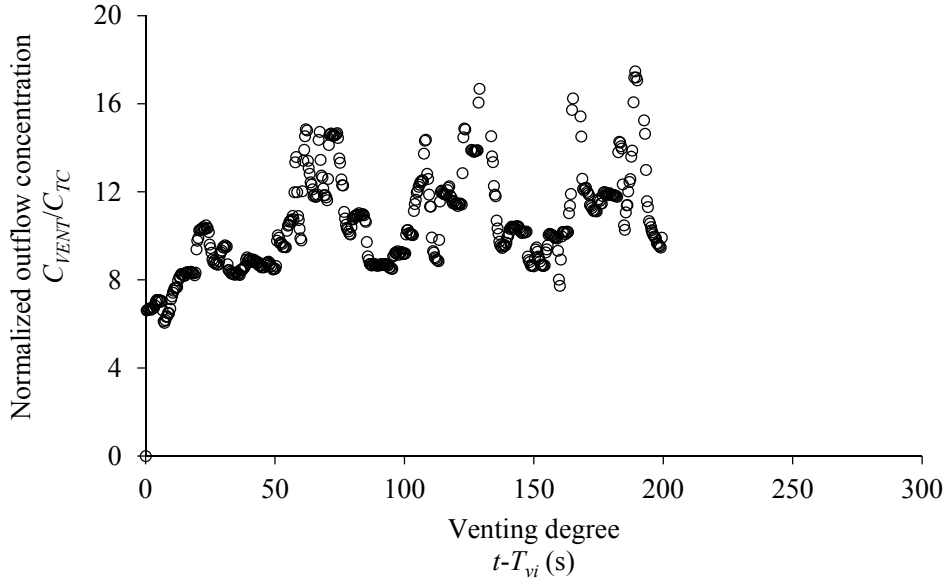

Figure A3.12: Normalized outflow concentration obtained with ϕ = 155% on the 2.4% slope (test E1.6).

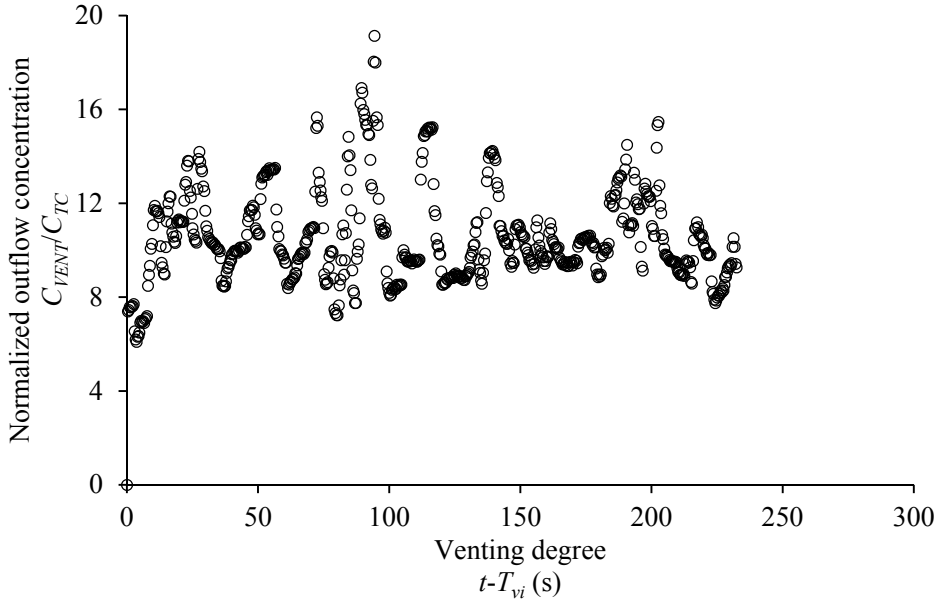

Figure A3.13: Normalized outflow concentration obtained with ϕ = 200% on the 2.4% slope (test E1.7).

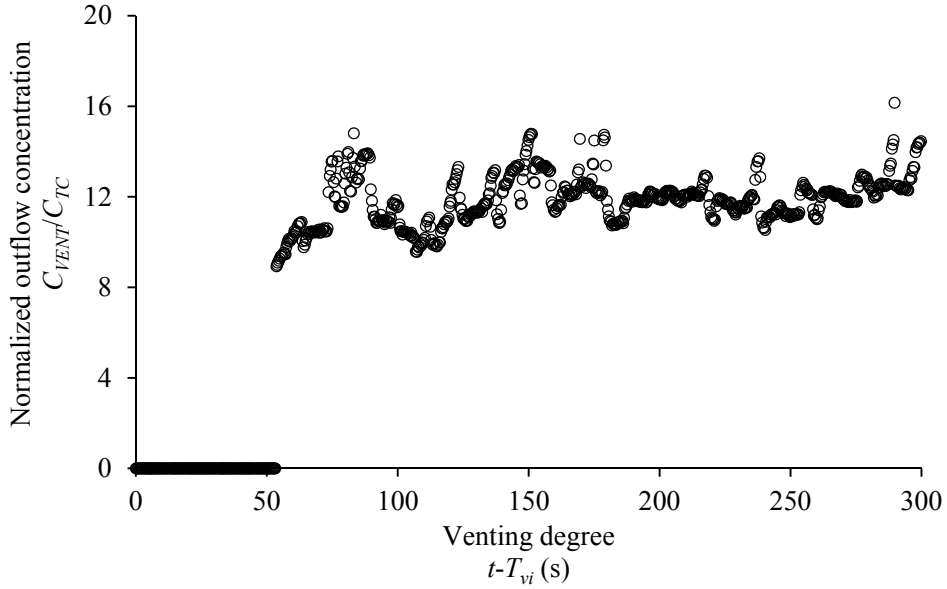

Figure A3.14: Normalized outflow concentration obtained with ϕ = 115% for the early venting at d/h_{outlet} = 5 on the 2.4% slope (test E1.8).

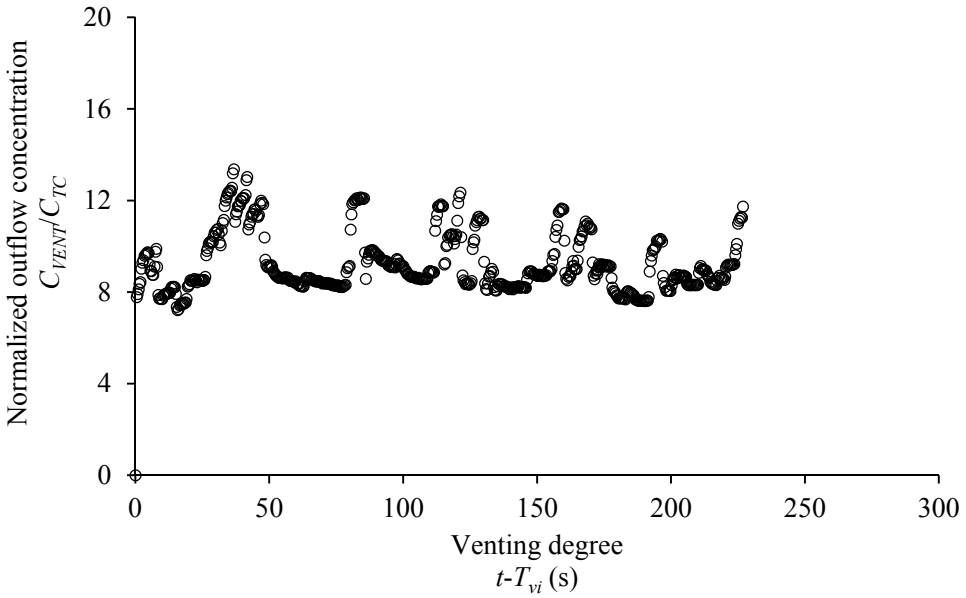

Figure A3.15: Normalized outflow concentration obtained with ϕ = 115% for the 30-s late venting on the 2.4% slope (test E1.9).

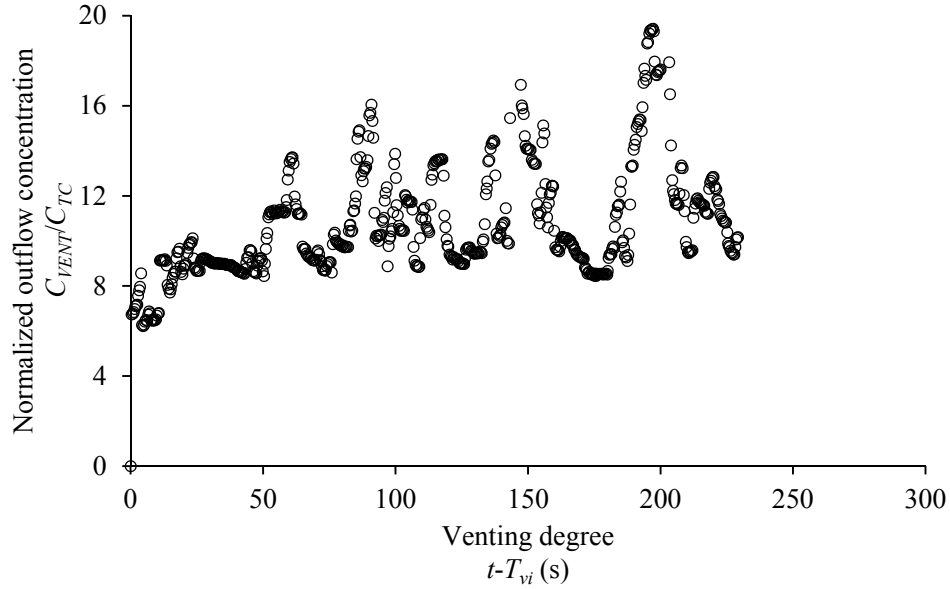

Figure A3.16: Normalized outflow concentration obtained with ϕ = 115% for the 60-s late venting on the 2.4% slope (test E1.10).

Slope S = 5.0%

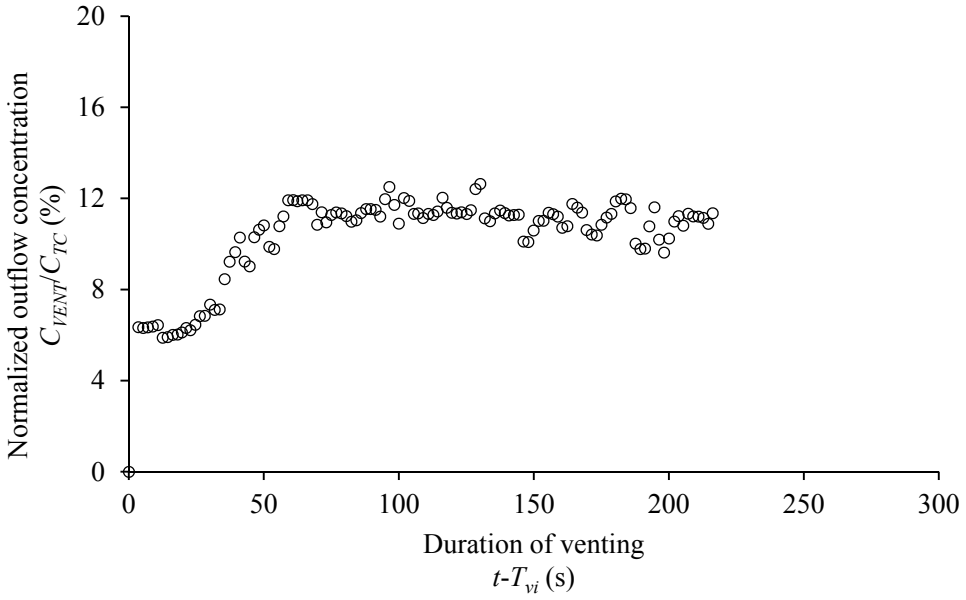

Figure A3.17: Normalized outflow concentration obtained with ϕ = 50% on the 5% slope (test E2.1).

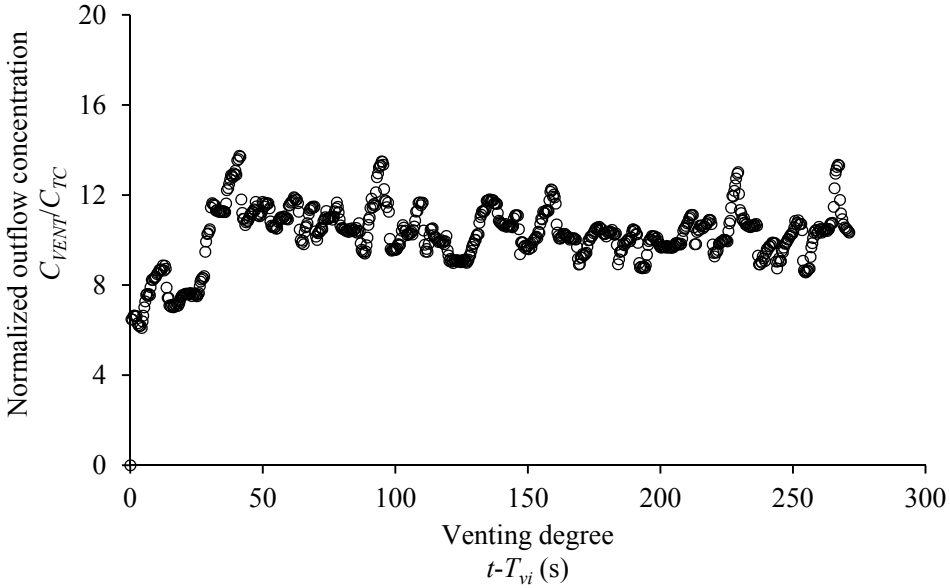

Figure A3.18: Normalized outflow concentration obtained with ϕ = 100% on the 5% slope (test E2.2).

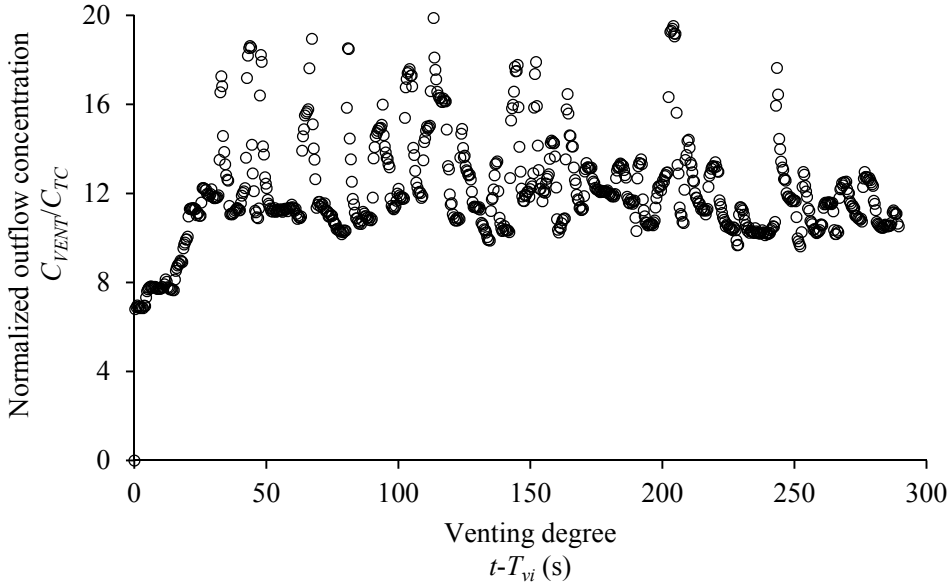

Figure A3.19: Normalized outflow concentration obtained with ϕ = 135% on the 5% slope (test E2.3).

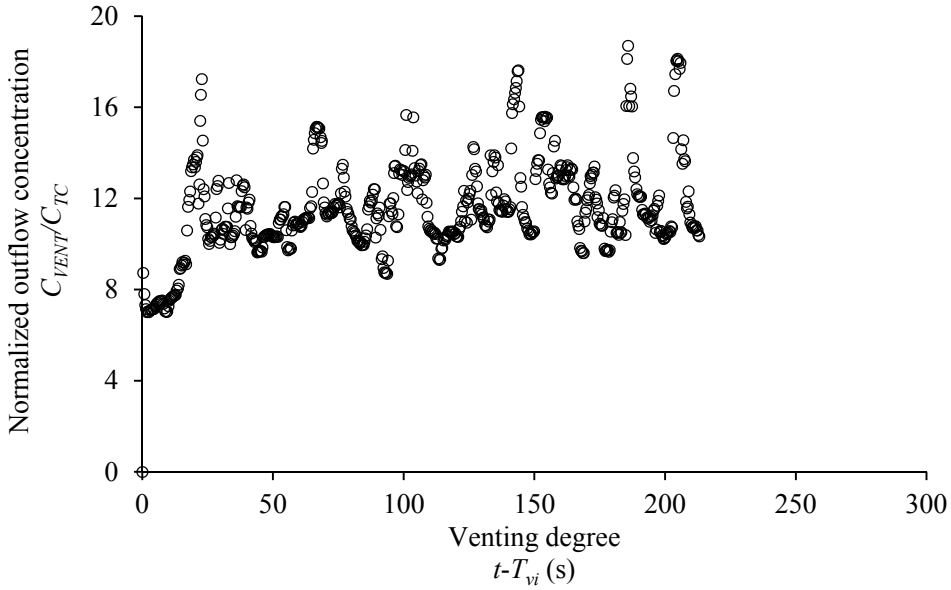

Figure A3.20: Normalized outflow concentration obtained with ϕ = 155% on the 5% slope (test E2.4).

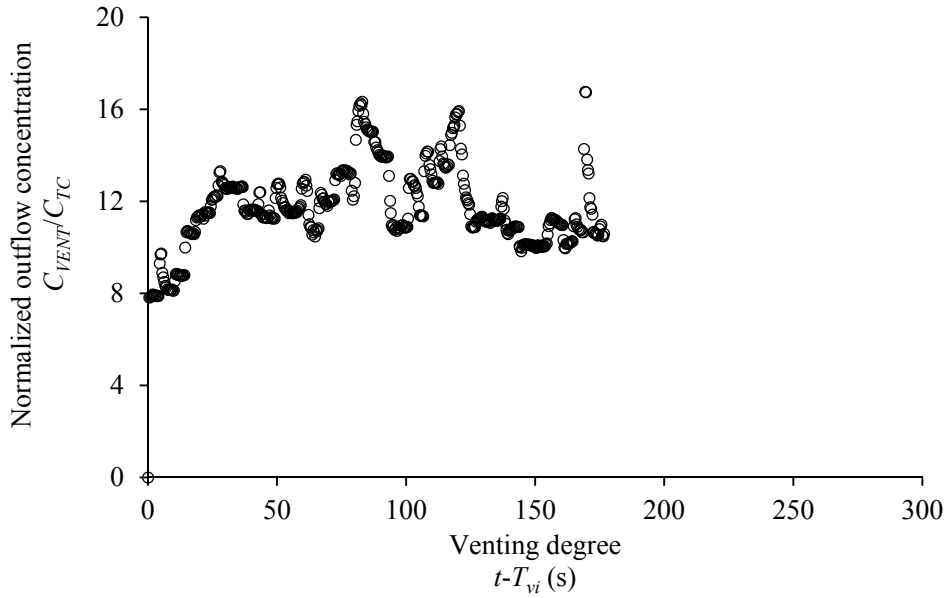

Figure A3.21: Normalized outflow concentration obtained with ϕ = 200% on the 5% slope (test E2.5).

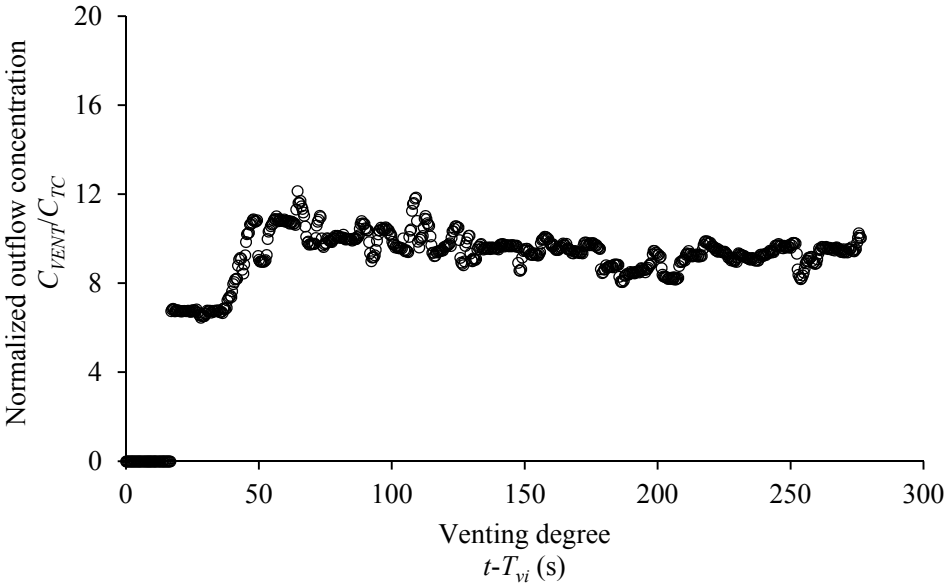

Figure A3.22: Normalized outflow concentration obtained with ϕ = 115% for the early venting at d/h_{outlet} = 5 on the 5% slope (test E2.6).

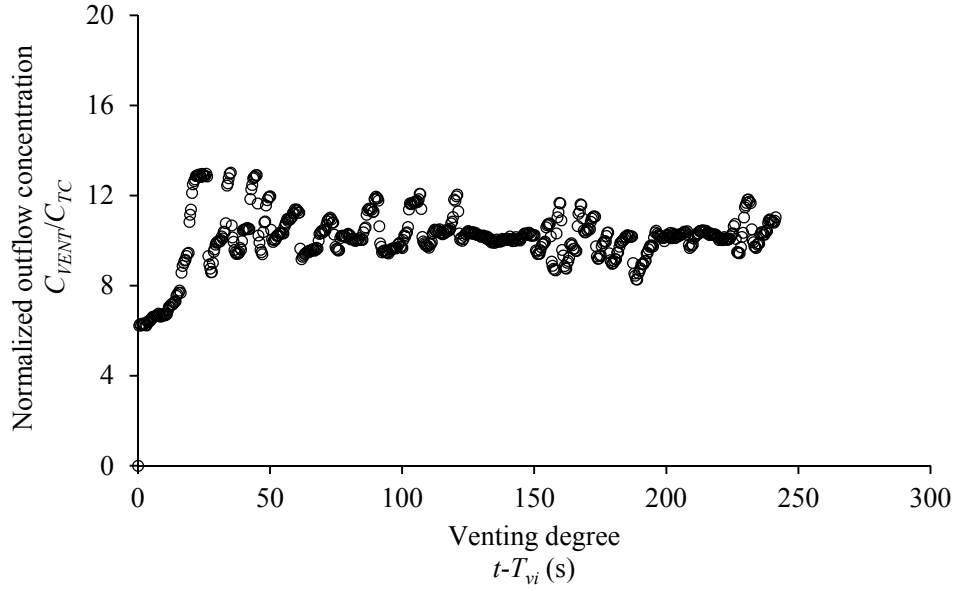

Figure A3.23: Normalized outflow concentration obtained with ϕ = 115% for the 30-s late venting on the 5% slope (test E2.7).

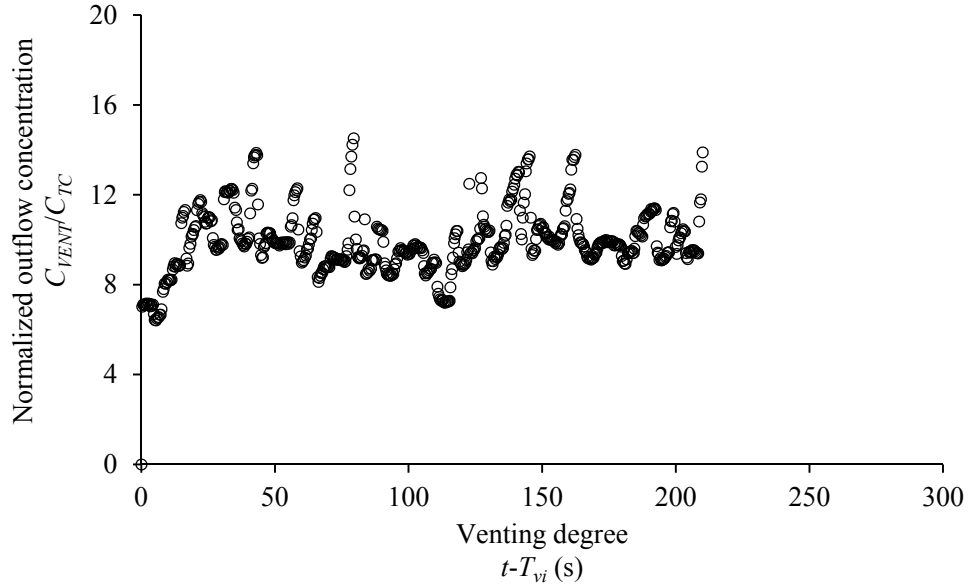

Figure A3.24: Normalized outflow concentration obtained with ϕ = 115% for the 60-s late venting on the 5% slope (test E2.8).

A4. Early versus late venting (Chamoun, S., (2017) ''Venting of turbidity currents: when to act?'', Proceedings of IAHR 2017, Kuala Lumpur, Malaysia)

The numerical model was used to make use of supplementary features that could not be observed/measured in the experimental model.

Table A4.1: Characteristics of the numerical simulations performed with early and late venting.

Simulation number No.	Outlet height h_{outlet} (cm)	Outlet width w_{outlet} (cm)	Outlet level l_{outlet} (cm)	Bed slope S (%)	Venting degree ϕ (%)	Timing
N1.3	12	9	0	5	115	Early
N1.4	12	9	0	5	115	60-s late

The early and 60-s late venting were numerically simulated using the 5.0% slope with similar conditions as the ones used in the experimental tests. Figure A4.1 shows the volume rendered sediment concentrations at t = 430 s (T_{vi} = 125 s for the early venting and 205 s for the 60-s late venting). The late venting leads to higher concentrations close to the outlet, while the early venting shows very low concentrations. In order to better assess the difference between the two cases, sediment concentrations of the early venting were subtracted from the sediment concentrations of the late venting. Positive values (Figure A4.2) were obtained in the vicinity of the wall, explaining the lower efficiencies obtained with the late venting (Chapter 6, section 6.2.1). In fact, in the latter case, the muddy lake is large and the flow field is complex in the vicinity of the outlet, rendering the suction of the current more complicated once venting starts. Moreover, an interflow (Figure A4.2) seems to form in the case of late venting due to the high reflection upstream.

Furthermore, the sediment velocity streamlines during venting were computed (Figure A4.3). In fact, the streamlines obtained with the late venting are not well developed between the current and the outlet compared with the early venting. Parts of the sediments are stuck close to the outlet in a sort of stagnant zone. This zone seems to force the continuously flowing turbidity current to bound over it and reach the outlet at higher levels. This renders the transit of the current more complicated and thus its venting less efficient. As concluded during the experimental investigation based on the values of the efficiency, opening before the current reaches the outlet ensures a better suction of the current once it reaches the dam and yields higher efficiencies than late venting.

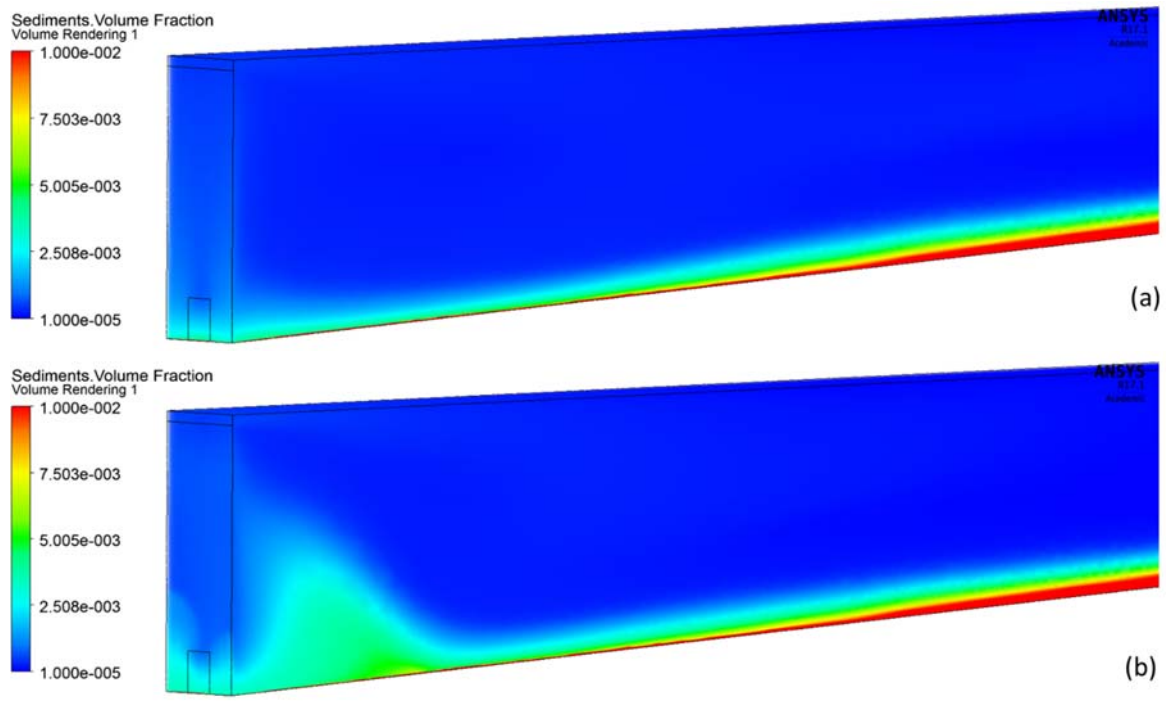

Figure A4.1: Rendered volumes showing the sediment concentration at t = 430s for the (a) early and (b) the 60-s late venting cases (simulations N1.3 and N1.4).

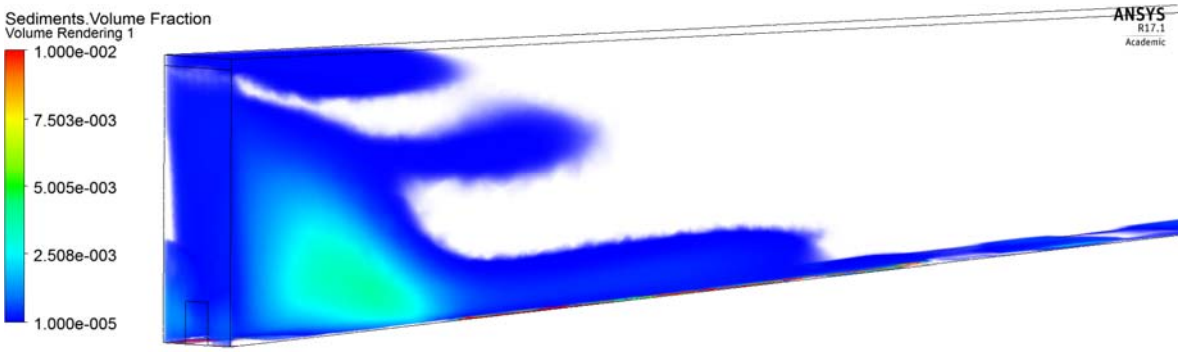

Figure A4.2: Difference between concentration values for the 60-s late and the early venting obtained numerically at t = 430s in the vicinity of the wall (slope 5%).

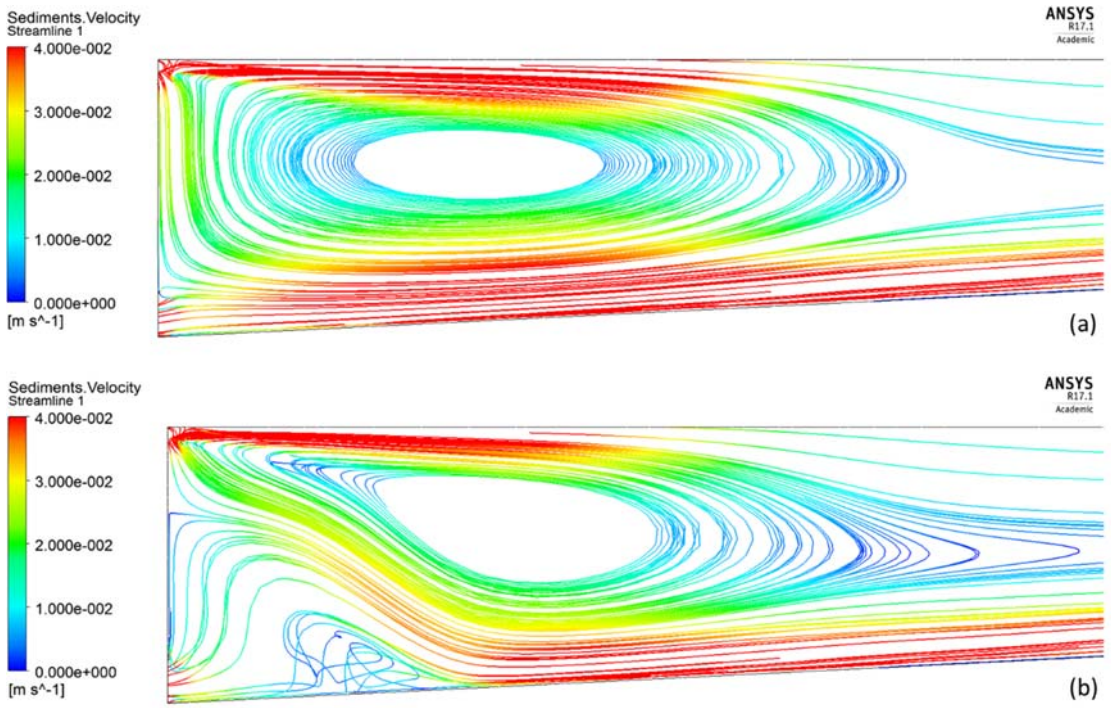

Figure A4.3: Streamlines in the vicinity of the outlet for the cases of (a) early and (b) the 60-s late venting.

A5. Effect of the outlet height (velocity) on distance of influence

The effect of the outlet's height on the maximum distance of influence s_{max} was numerically checked: It could be shown that s_{max} = 1 m is the same for the three cases and the size (consequently the velocity) of the outflow does not have a considerable effect on s_{max}.

Table A5.1: Characteristics of the numerical simulations used to test the effect of the outlets height on the distance of influence

Simulation number No.	**Outlet height h_{outlet} (cm)**	**Outlet width w_{outlet} (cm)**	**Outlet level l_{outlet} (cm)**	**Bed slope S (%)**	**Venting degree ϕ (%)**	**Timing**
N0.26	6	9	0	0	100	Early
N0.27	12	9	0	0	100	Early
N0.28	24	9	0	0	100	Early

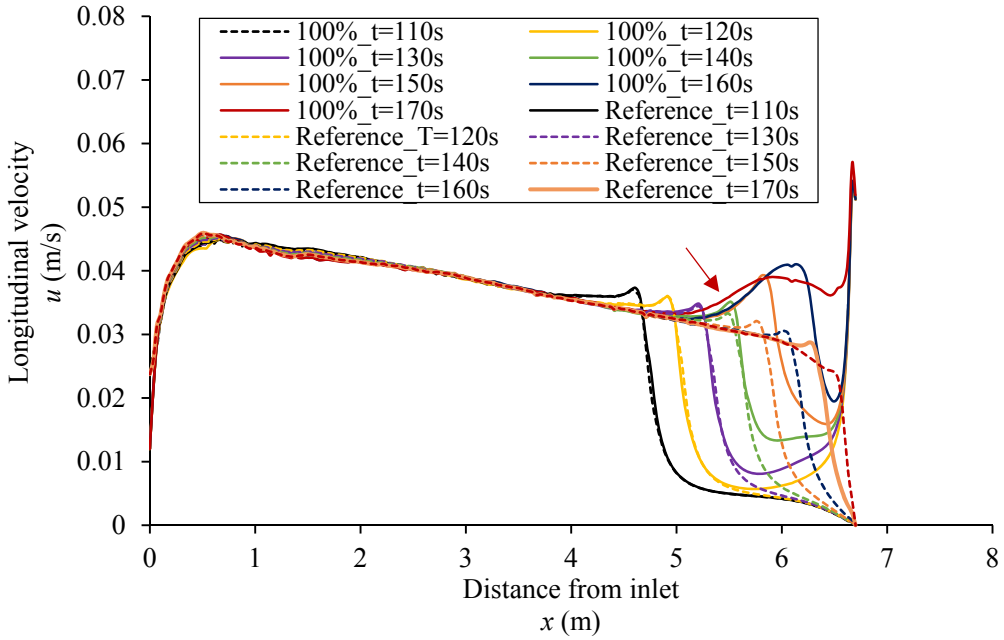

Figure A5.1: Longitudinal velocity u plotted on L1 for the reference simulation (dashed lines) and the case of venting with ϕ = 100% (solid lines) using the outlet height h_{outlet} = 6 cm. The arrow indicates the time step at which the current starts being accelerated (simulation N0.25).

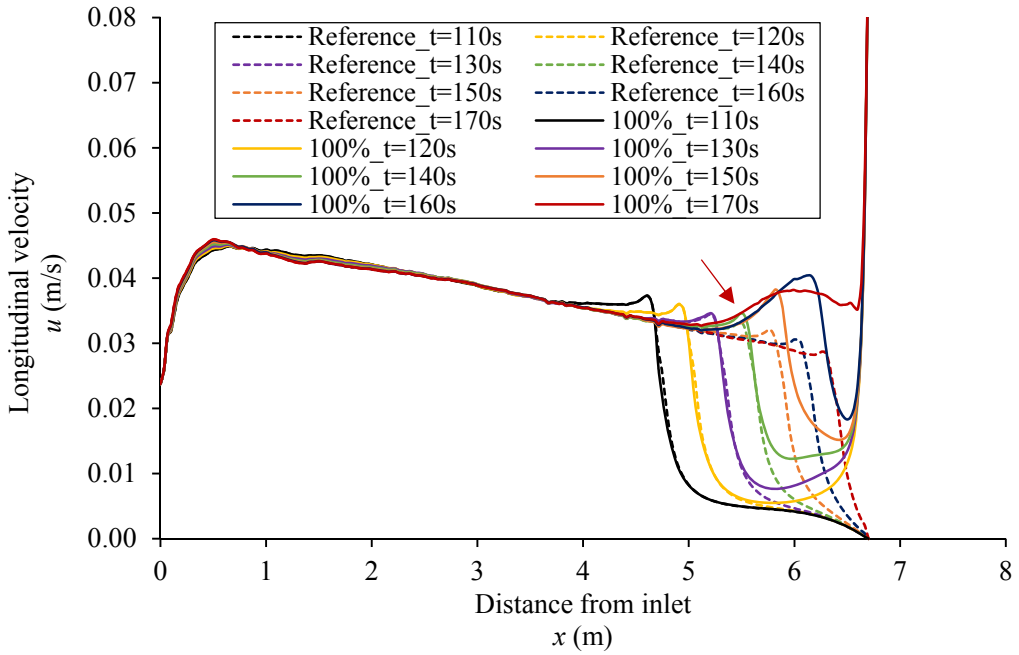

Figure A5.2: Longitudinal velocity u plotted on L1 for the reference simulation (dashed lines) and the case of venting with ϕ = 100% (solid lines) using the outlet height h_{outlet} = 12 cm. The arrow indicates the time step at which the current starts being accelerated (simulation N0.26).

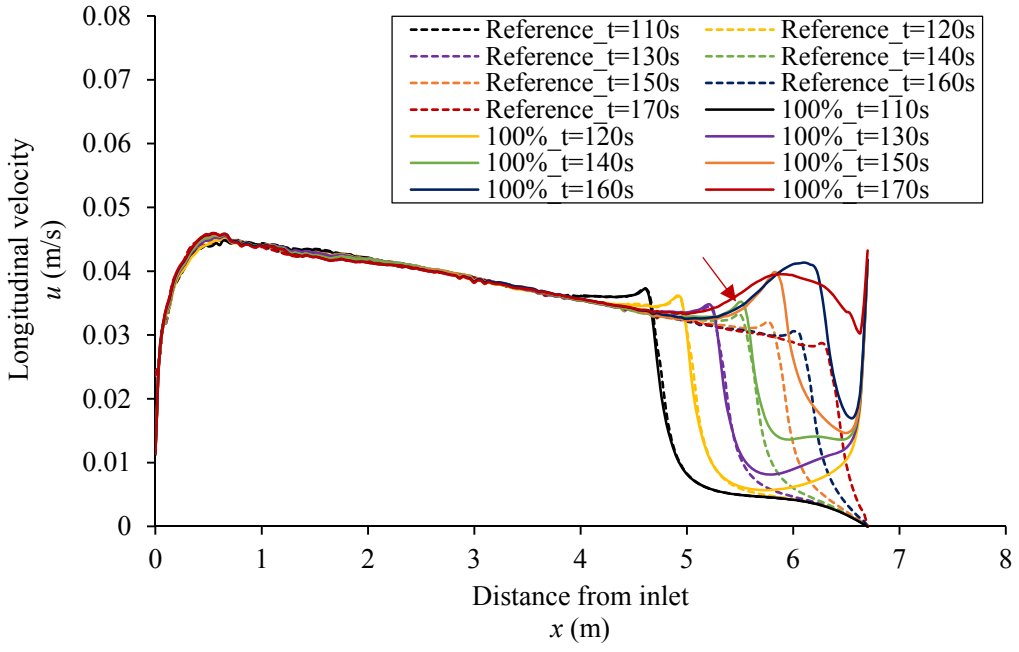

Figure A5.3: Longitudinal velocity u plotted on L1 for the reference simulations (dashed lines) and the case of venting with ϕ = 100% (solid lines) using the outlet height h_{outlet} = 24 cm. The arrow indicates the time step at which the current starts being accelerated (simulation N0.27).

A6. Distance of influence for venting degrees of 30%, 65% and 90%

Table A6.1: Characteristics of the numerical simulations used to investigate the effect of the outflow discharge on the distance of influence.

Simulation number No.	Outlet height h_{outlet} (cm)	Outlet width w_{outlet} (cm)	Outlet level l_{outlet} (cm)	Bed slope S (%)	Venting degree ϕ (%)	Timing
N0.20	12	9	0	0	30	Early
N0.22	12	9	0	0	65	Early
N0.24	12	9	0	0	90	Early

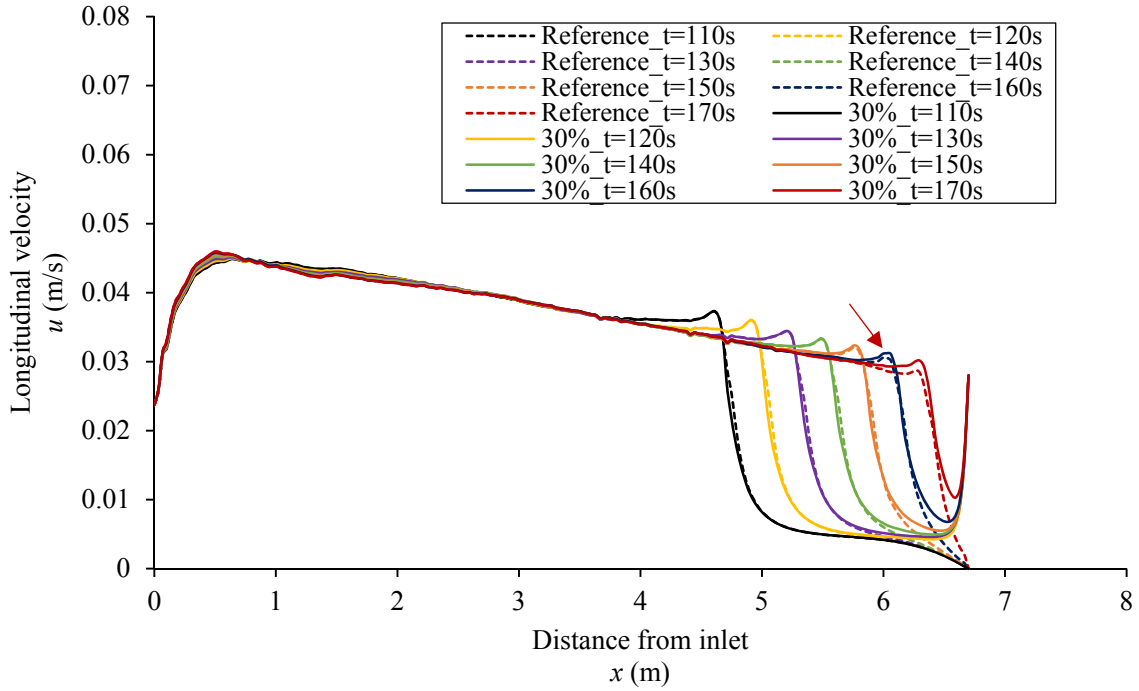

Figure A6.1: Longitudinal velocity u plotted on L1 for the reference simulation (dashed lines) and the case of venting with $\phi = 30\%$ (solid lines) using the outlet height $h_{outlet} = 12$ cm. The arrow indicates the time step at which the current starts being accelerated (simulation N0.19)

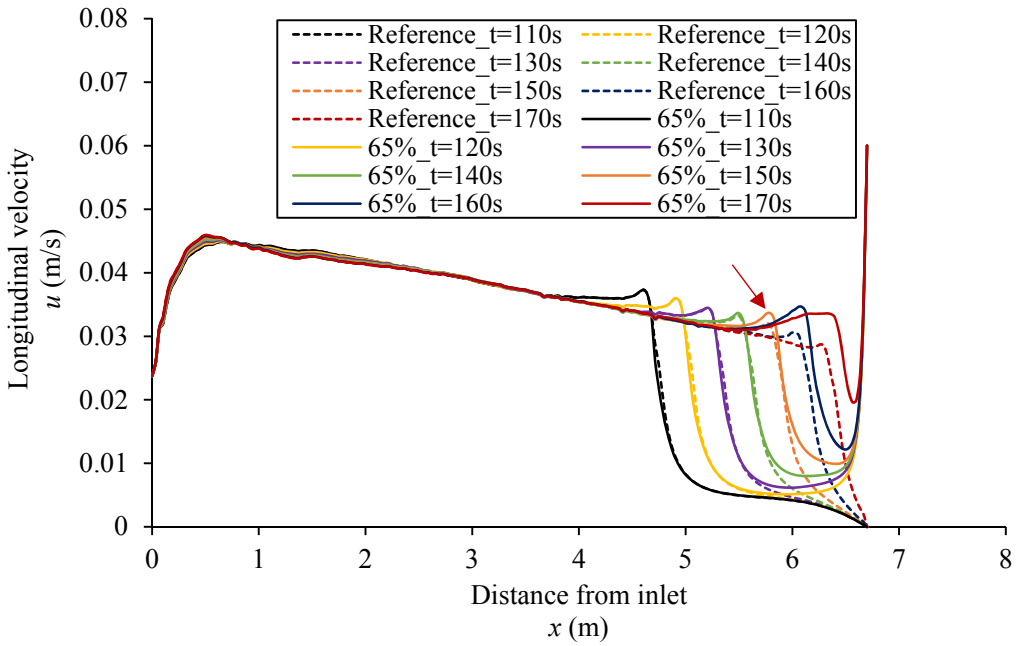

Figure A6.2: Longitudinal velocity u plotted on L1 for the reference simulation (dashed lines) and the case of venting with $\phi = 65\%$ (solid lines) using the outlet height $h_{outlet} = 12$ cm. The arrow indicates the time step at which the current starts being accelerated (simulation N0.21)

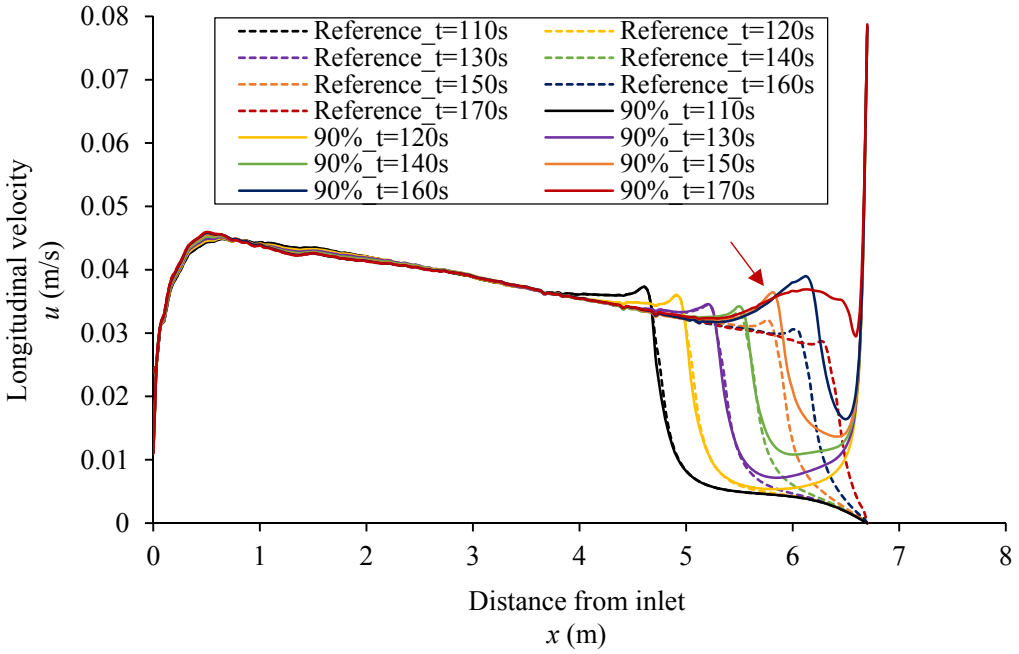

Figure A6.3: Longitudinal velocity u plotted on L1 for the reference simulation (dashed lines) and the case of venting with $\phi = 90\%$ (solid lines) using the outlet height $h_{outlet} = 12$ cm. The arrow indicates the time step at which the current starts being accelerated (simulation N0.23)

A7. Variation of wall height and weir conditions

The possible scale effect of the height of the wall representing the dam on the values of the outflow sediment concentration was checked. A height of 160 cm was simulated, double the height of the wall used. The deviation between the outflow concentrations corresponding to the two different cases is of 4.5% (Figure A7.1). Additionally, the effect of the weir conditions was checked. The weir condition was set to opening and two variations were simulated: a case where only water is allowed to flow out of the model and another case where both water and sediments are allowed to flow. The outflow concentration obtained is similar showing that the sediment flowing out of the weir, considered negligible, do not affect the amount of sediments vented (Figure A7.2).

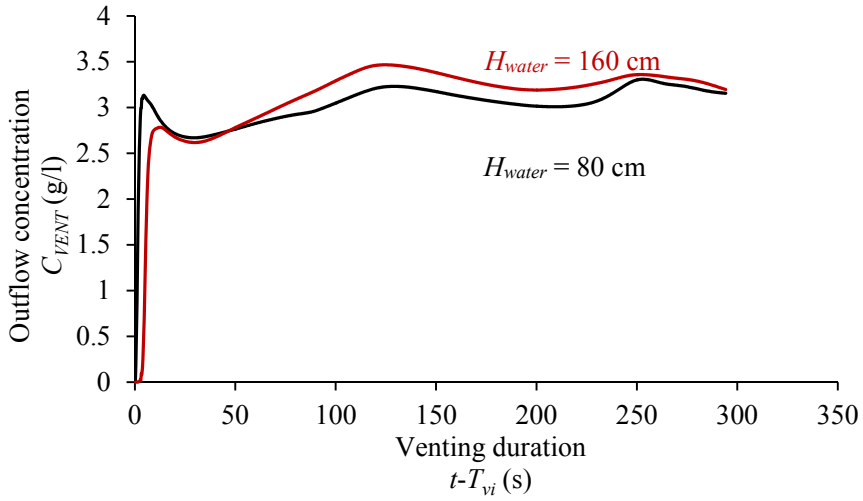

Figure A7.1: Outflow concentration obtained with two different wall heights.

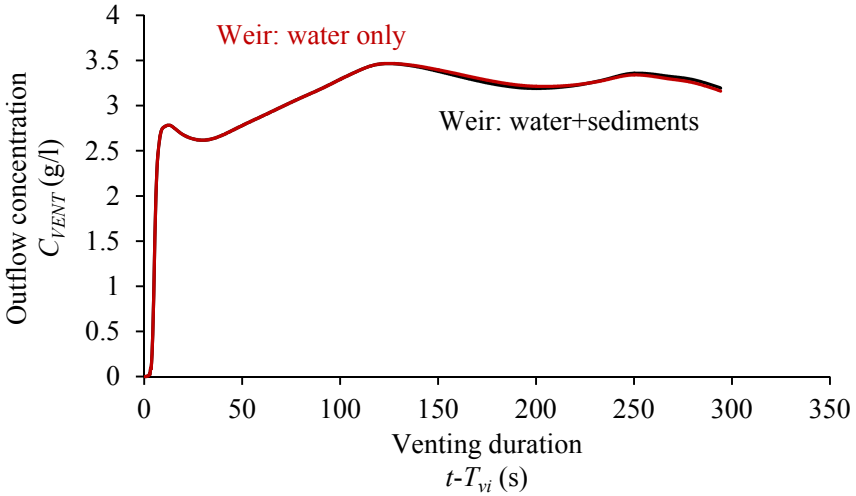

Figure A7.2: Outflow concentration obtained with two weir condition

Communications du Laboratoire de Constructions Hydrauliques ISSN 1661-1179
Ecole Polytechnique Fédérale de Lausanne
Editeur: Prof. Dr A. Schleiss

N°	59	2014	R. Duarte Influence of air entrainment on rock scour development and block stability in plunge pools
N°	60	2014	J. P. Matos Hydraulic-hydrologic model for the Zambezi River using satellite data and artificial intelligence techniques
N°	61	2015	S. Guillén Ludeña Hydro-morphodynamics of open-channel confluences with low discharge ratio and dominant tributary sediment supply
N°	62	2016	M. Jafarnejad Chaghooshi Time-dependent failure analysis of large block size riprap as bank protection in mountain rivers
N°	63	2016	S. Terrier Hydraulic performance of stepped spillway aerators and related downstream flow features
N°	64	2016	M. Ostad Mirza Experimental study on the influence of abrupt slope changes on flow characteristics over stepped spillways
N°	65	2016	I. Almeida Samora Optimization of low-head hydropower recovery in water supply networks
N°	66	2016	D. Ferràs Segura Fluid-structure interaction during hydraulic transients in pressurized pipes: experimental and numerical analyses
N°	67	2016	E. Battisacco Replenishment of sediment downstream of dams: Erosion and transport processes
N°	68	2017	F. Zeimetz Development of a methodology for extreme flood estimations in alpine catchments for the verification of dam safety
N°	69	2017	A. J. Pachoud Influence of geometrical imperfections and flaws at welds of steel liners on fatigue behavior of pressure tunnels and shafts in anisotropic rock
N°	70	2017	F. Oberrauch Hydropower design under uncertainties
N°	71	2017	S. Schwindt Hydro-morphological processes through permeable sediment traps at mountain rivers
N°	72	2017	S. Chamoun Influence of outlet discharge on the efficiency of turbidity current venting

ISSN 1661-1179

DOI: 10.5075/epfl-lchcomm-72

Prof. Dr A. Schleiss
Laboratoire de constructions hydrauliques - LCH
EPFL, Bât. GC, Station 18, CH-1015 Lausanne
http://lch.epfl.ch
e-mail: secretariat.lch@epfl.ch